

Exploration of uncertainty-aware energy transition pathways

Reinforcement learning and principal
component analysis-based methods

Doctoral dissertation presented by
Xavier RIXHON

in partial fulfillment of the requirements for
the degree of Doctor in Engineering Sciences

September 2024

Thesis committee

- Pr. Francesco CONTINO (UCLouvain, Supervisor)
- Pr. Hervé JEANMART (UCLouvain, Supervisor)
- Pr. Paul FISSETTE (UCLouvain, President)
- Pr. Christophe DE VLEESCHOUWER (UCLouvain, Secretary)
- Pr. Sylvain QUOILIN (ULiège)
- Dr. Stefano MORET (ETH Zurich)
- Pr. Stefan PFENNINGER (TU Delft)

© 2023
Xavier Rixhon
All Rights Reserved

Contents

| | |
|--|-----------|
| Symbols | v |
| Introduction | 1 |
| 1 Methodology: Through a variety of complementary tools | 11 |
| 1.1 EnergyScope Pathway | 13 |
| 1.1.1 Perfect foresight: One global optimisation of the transition | 14 |
| 1.1.2 Myopic: Sequential optimisation of the transition | 18 |
| 1.1.3 Discussion and guidelines for future researchers | 22 |
| 1.2 Uncertainty quantification | 22 |
| 1.2.1 Uncertainty characterisation | 23 |
| 1.2.2 Polynomial Chaos Expansion | 24 |
| 1.2.3 Preliminary screening and selection | 29 |
| 1.2.4 Discussion and guidelines for future researchers | 30 |
| 1.3 Agent-based reinforcement learning to support myopic energy transition | 30 |
| 1.3.1 Reinforcement Learning fundamentals | 32 |
| 1.3.2 Problem formulation and algorithm | 33 |
| 1.3.3 Discussion and guidelines for future researchers | 36 |
| 1.4 Robustness assessment via PCA | 37 |
| 1.4.1 Principal Component Analysis: General concept | 37 |
| 1.4.2 Principal components of the transition | 40 |
| 1.4.3 Discussion and guidelines for future researchers | 47 |
| 2 Case study: the Belgian energy system | 49 |
| 2.1 End-use demands | 51 |
| 2.1.1 Non-energy demand | 51 |
| 2.1.2 Forecast of the demands over the transition | 54 |

| | | |
|----------|--|------------|
| 2.2 | Resources | 56 |
| 2.3 | Conversion technologies | 58 |
| 2.3.1 | Small modular reactor | 58 |
| 2.3.2 | Technologies supplying the non-energy demand | 60 |
| 2.4 | Uncertainty ranges | 62 |
| 2.5 | CO ₂ budget for the transition | 63 |
| 2.6 | Conclusions | 65 |
| 3 | The atom-molecules dilemma: deterministic and uncertainty analyses | 67 |
| 3.1 | Deterministic impact of integrating SMR in 2040 | 69 |
| 3.1.1 | Power sector | 69 |
| 3.1.2 | System-level impacts | 73 |
| 3.1.3 | Non-power sectors | 74 |
| 3.2 | Uncertainty quantification on the cost, the atom and the molecules | 77 |
| 3.2.1 | Total transition cost | 77 |
| 3.2.2 | Atom and molecules | 79 |
| 3.2.3 | Local renewables | 86 |
| 3.3 | Conclusions | 86 |
| 4 | Reinforcement Learning CO₂-policy investigation | 89 |
| 4.1 | Definition of the actions, reward and states | 90 |
| 4.1.1 | Actions | 91 |
| 4.1.2 | Reward | 92 |
| 4.1.3 | States | 94 |
| 4.2 | Convergence and learning process | 95 |
| 4.2.1 | Reward and success | 96 |
| 4.2.2 | States | 97 |
| 4.2.3 | Actions | 102 |
| 4.2.4 | Discussion and guidelines for future researchers | 107 |
| 4.3 | Comparison with references | 108 |
| 4.4 | Conclusions | 110 |
| 5 | Robustness assessment of pathway roadmaps | 113 |
| 5.1 | Definition of the principal components of the transition | 114 |
| 5.1.1 | Principal components of each representative year | 115 |
| 5.1.2 | Principal components of the perfect foresight REF transitions | 118 |
| 5.2 | Robustness assessment of pathway roadmaps | 120 |
| 5.2.1 | A robust roadmap? | 121 |

| | | |
|--|---|------------|
| 5.2.2 | Projection on robustness metric | 124 |
| 5.2.3 | Principal components of myopic transitions | 125 |
| 5.2.4 | What about the costs over the transition? | 125 |
| 5.3 | Conclusions | 128 |
| Conclusions and perspectives | | 131 |
| Bibliography | | 139 |
| A Taxonomy of the fuels in a whole-energy system | | 159 |
| A.1 | Terminology used in the literature | 160 |
| A.2 | Classification and definition of the fuels | 162 |
| A.3 | Discussion | 165 |
| B EnergyScope Pathway: Its choice and its formulation | | 167 |
| B.1 | EnergyScope Pathway: The right model | 167 |
| B.2 | EnergyScope Pathway and its linear formulation | 173 |
| B.2.1 | The starting point: a scenario analysis model | 173 |
| B.2.2 | Extending the model for pathway optimisation | 177 |
| C Case study: the Belgian energy system | | 185 |
| C.1 | Belgian energy system in 2020 | 185 |
| C.2 | Belgian energy transition pathway towards carbon neutrality in 2050 | 185 |
| C.2.1 | Greenhouse gases and primary energy | 187 |
| C.2.2 | Electricity sector: Capacities and yearly balance | 190 |
| C.2.3 | Costs: Investments and operation | 192 |
| C.3 | Myopic versus perfect foresight pathway optimisation | 195 |
| C.4 | Assessment of different emissions-trajectories | 199 |
| C.4.1 | CO ₂ budget versus linear decrease of emissions | 199 |
| C.4.2 | Comparison without restriction on Greenhouse Gases (GHG) | 201 |
| C.5 | Monthly versus hourly pathway optimisation | 202 |
| D Pathway optimisation under uncertainties | | 207 |
| D.1 | Total transition cost | 207 |
| D.2 | Imported renewable electrofuels | 209 |
| D.3 | Installed capacities | 211 |
| E Reinforcement Learning on hourly and monthly models | | 219 |

Symbols

Acronyms

| | |
|--------------|---|
| API | Application Programming Interface |
| BECCS | Bioenergy with Carbon Capture and Storage |
| BEMS | Building Energy Management System |
| BEV | Battery Electric Vehicles |
| BTX | Benzene, Toluene and Xylene |
| CAPEX | Capital Expenditure |
| CCGT | Combined Cycle Gas Turbine |
| CCS | Carbon Capture and Storage |
| CHP | Combined Heat and Power |
| CNG | Compressed Natural Gas |
| DC | Direct Current |
| DHN | District Heating Network |
| DNN | Deep Neural Network |
| DRL | Deep Reinforcement Learning |
| ESOMs | Energy System Optimisation Models |
| ESTD | EnergyScope Typical Days |
| EUD | End-Use Demand |
| FC | Fuel Cell |
| FEC | Final Energy Consumed |
| GDP | Gross Domestic Product |
| GHG | Greenhouse Gases |
| GSA | Global Sensitivity Analysis |
| GWP | Global Warming Potential |
| HP | Heat Pump |
| HT | High-Temperature |

| | |
|-------------|---|
| HVC | High-Value Chemicals |
| IAMs | Integrated Assessment Models |
| ICE | Internal Combustion Engine |
| IEA | International Energy Agency |
| IPCC | Intergovernmental Panel on Climate Change |
| IQR | Interquartile Range |
| LCA | Life Cycle Assessment |
| LCOE | Levelised Cost of Energy |
| LFO | Light Fuel Oil |
| LOO | Leave-One-Out |
| LP | Linear Programming |
| LPG | Liquefied Petroleum Gas |
| LT | Low-Temperature |
| MDP | Markov Decision Process |
| MMSA | Methanol Market Services Asia |
| MTBE | Methyl Tert-butyl Ether |
| MTO | Methanol-to-olefins |
| NED | Non-energy Demand |
| NG | Fossil Gas |
| NN | Neural Network |
| NRE | Non-renewable Energy |
| NSC | Naphtha Steam Cracker |
| OPEX | Operational Expenditure |
| PC | Principal Component |
| PCs | Principal Components |
| PCA | Principal Component Analysis |
| PCE | Polynomial Chaos Expansion |
| PV | Photovoltaic |
| RE | Renewable Energy |
| RL | Reinforcement Learning |
| SAC | Soft Actor-Critic |
| SMR | Small Modular Reactor |
| SVD | Singular Value Decomposition |
| TRL | Technology Readiness Level |
| UQ | Uncertainty Quantification |
| VRES | Variable Renewable Energy Sources |

List of publications

Limpens, G., **Rixhon, X.**, Contino, F., & Jeanmart, H. (2024). “*EnergyScope Pathway: An open-source model to optimise the energy transition pathways of a regional whole-energy system.*” In Applied Energy, (Vol. 358). URL: <https://doi.org/10.1016/j.apenergy.2023.122501>

Rixhon, X., Limpens, G., Coppitters, D., Jeanmart, H.,& Contino, F.(2022). “*The role of electrofuels under uncertainties for the Belgian energy transition.*” In Energies (Vol. 14). URL: <https://doi.org/10.3390/en14134027>

Rixhon, X., Tonelli, D., Colla, M., Verleysen, K., Limpens, G., Jeanmart, H. ,& Contino, F.(2022). “*Integration of non-energy among the end-use demands of bottom-up whole-energy system models.*” In Frontiers in Energy Research, Sec. Process and Energy Systems Engineering, (Vol. 10). URL: <https://doi.org/10.3389/fenrg.2022.904777>

Rixhon, X., Colla, M., Tonelli, D., Verleysen, K., Limpens, G., Jeanmart, H., & Contino, F.(2021). “*Comprehensive integration of the non-energy demand within a whole-energy system: Towards a defossilisation of the chemical industry in Belgium.*” In proceedings of ECOS 2021 conference (Vol. 34, p. 154).

Rixhon, X., Limpens, G., Contino, F., & Jeanmart, H. (2021). “*Taxonomy of the fuels in a whole-energy system.*” In Frontiers in Energy Research, Sec. Sustainable Energy Systems, (Vol. 9). URL: <https://doi.org/10.3389/fenrg.2021.660073>

Limpens, G., Coppitters, D., **Rixhon, X.**, Contino, F., & Jeanmart, H. (2020). “*The impact of uncertainties on the Belgian energy system: application of the Polynomial Chaos Expansion to the EnergyScope model.*” In proceedings of ECOS 2020 conference (Vol. 33, p. 711).

Introduction

The rate at which climate changes today is mostly due to the concentration of anthropogenic GHG in the atmosphere [1]. Therefore, the GHG emissions from human activities must be mitigated to prevent further environmental damage. Energy consumption, mainly from fossil fuels, is the main contributor: it is responsible for 75% of GHG emissions, the remaining 25% originating from agriculture and industrial processes [2]. The Kaya identity is an economic formulation stating that the total emission level of the GHG can be expressed as the product of four factors: human population, Gross Domestic Product (GDP) per capita, energy intensity (per unit of GDP), and carbon intensity (emissions per unit of energy consumed) [3]. From an energy point of view, this identity can be adapted by replacing the economic metric, GDP, by the End-Use Demand (EUD), see Equation (1). EUD is the energy service required by the final consumer. In Equation (1), the first factor on the right-hand side represents the Global Warming Potential (GWP) of the primary energy mix, the second is the inverse of the efficiency and the third is the energy intensity per capita.

$$\text{GHG} = \frac{\text{GHG}}{\text{Primary energy}} \times \frac{\text{Primary energy}}{\text{EUD}} \times \frac{\text{EUD}}{\text{Population}} \times \text{Population} \quad (1)$$

Such an identity is criticized for the arbitrary choice of variables, the non-independence of them usually leading to the rebound effect and its encompassing approach that does not appropriately mirror the heterogeneity of the situation [4]. Considering the expected growing trend of the Population, Equation (1) highlights three levers of action that should be activated to reduce GHG emissions and favour the energy transition [5, 6]: renewables, efficiency and sufficiency.

Focusing on the levers that are within the grasp of engineering studies, this thesis addresses the two “technical” levers of the energy transition identified in Equation (1): renewables and efficiency. This focus is aligned with the current European policies binding the Member States of the European Union. For instance, the Renewable

Energy Directive (RED) III, published in October 2023 [7], states that “the Union’s climate neutrality objective (by 2050) requires a just energy transition which leaves no territory or citizen behind, an increase in energy efficiency and significantly higher shares of energy from renewable sources in an integrated energy system”.

Despite the growing echo it finds in the scientific community [8], sufficiency is lacking in the RED III. Explicitly mentioned by the IPCC for the first time in 2022 [9], it is defined as “*a strategy for reducing, in absolute terms, the consumption and production of end-use products and services through changes in social practices in order to comply with environmental sustainability while ensuring adequate social foundation for all people*” [10]. Due to its intrinsically political nature, studying sufficiency requires an interdisciplinary approach involving economy, sociology, psychology and political science, and is beyond the scope and knowledge of engineering research [11]. Among all the lenses through which it is necessary to assess sufficiency policies, one of the objectives of this work is to support these interdisciplinary projects by providing informed techno-economic guidelines.

To ensure the energy supply of a growing and more demanding population in the context of an environmental crisis, major transformations are needed (see Figure 1). Similarly to the RED III, the transformations identified by the International Energy Agency [12] focus on technical aspects, disregarding the sufficiency. The technical transformations that can be brought to the energy system concern both the primary energy sources and the technologies used to convert more efficiently these resources into the EUD [12, 13].

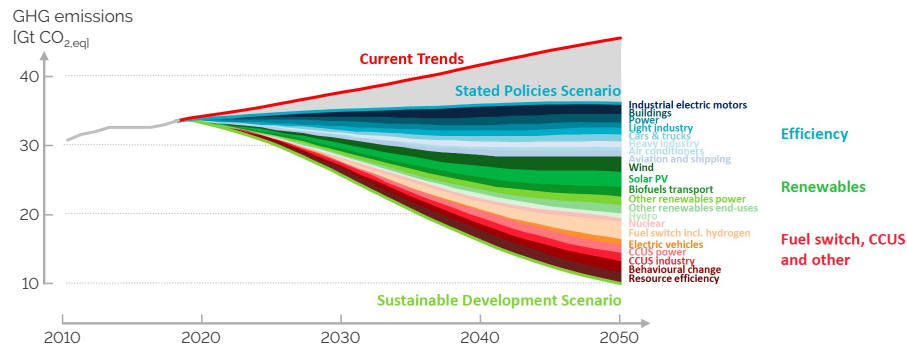


Figure 1. Energy-related CO₂ emissions and reductions by sources in the Sustainable Development Scenario of the International Energy Agency [12].

Changing primary energy sources corresponds to integrating more renewables. Variable Renewable Energy Sources (VRES) like wind and solar are the keystones to defossilise the energy system but they face challenges related to their intermittency and space disparity. With a growing share of VRES, sector coupling and electrification, with electrical heat pumps or Battery Electric Vehicles (BEV), are essential to absorb the surplus of electricity from these intermittent production means [14] and integrate them cost-effectively [15, 16].

However, direct electrification is not foreseen to be cost-competitive for some sectors such as marine, aviation and heavy-duty transport [17–19]. Moreover, transport and long-term storage of renewable electricity are not optimal with electricity-based solutions, e.g., DC lines or batteries. This is why, to reach the objective of sustainable development, after increasing the efficiency of the system, more renewables is associated with a “fuel switch” (see Figure 1).

The fuel switch consists in replacing fossil fuels with new energy carriers. Among them, *electrofuels* are promising solutions to tackle the challenges related to renewable electricity [20]. These fuels represent energy carriers where electricity has the major share in the energy balance of the fuel. In practice, this electricity is mainly converted into hydrogen through electrolysis and then potentially upgraded into more complex fuels such as methane, methanol or ammonia.

Electrofuels offer three main advantages: infrastructure compatibility, capacity to link sectors (i.e., from electricity to mobility, heat, or industry) and storage. Given their similar physicochemical properties, electrofuels could substitute fossil in technologies that are already in place today. An example is ammonia-hydrogen blends burned in spark ignition engines [21] or Combined Heat and Power (CHP) applications [22].

Electrofuels can also couple energy and non-energy sectors [23]. For instance, electricity from VRES can be converted into ammonia through the Haber-Bosch process and subsequently transformed into fertiliser, coupling the power and agro-industrial sectors [24].

Concerning storage, batteries exhibit limited storage capacity (up to 10 MWh) and self-discharge losses. On the contrary, electrofuels are promising solutions for high capacity (from 100 GWh) and long-term storage of energy [25, 26] (Figure 2). In their analysis of the German transport sector in 2050, Millinger et al. [27] highlighted that producing electrofuels can represent an efficient usage of the ambient CO₂ to supply hydrocarbon fuels while limiting the curtailment of VRES. Moreover, gas networks present much more storage potential than electrical networks: 50 times more in Germany and 300 times more in France [28].

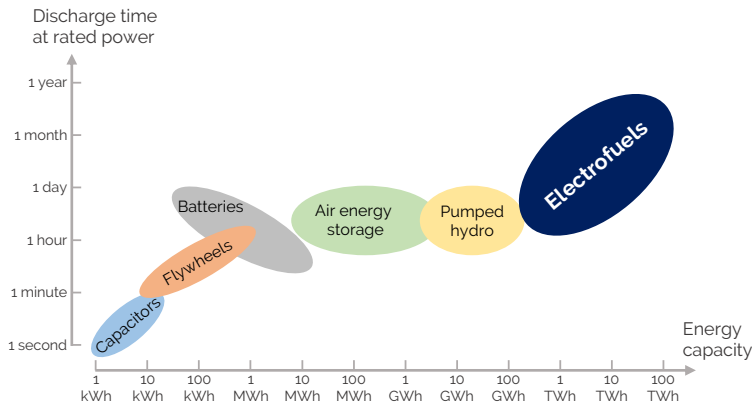


Figure 2. Energy carriers and technologies to store electricity. Electrofuels provide a solution for high-capacity and long-term storage of energy. Graph adapted from [29].

Even if the share of electricity will increase in the energy system through the electrification of the end-use demand, gaseous and liquid fuels will keep on being big players during, and after, the energy transition [30]. In other words, hydrocarbons, currently produced from fossil resources, will still be composed of carbon in a renewable world. This is why this thesis rather uses “defossilisation” rather than “decarbonisation” as carbon will still play a key role in the energy transition that aims at carbon neutrality where there is no additional, if no removal, of GHG emissions in the atmosphere [31].

Besides electrofuels, “*biofuels*”, “*synthetic fuels*”, “*renewable fuels*” or even “*sustainable fuels*” will play a key role in the transition. To avoid the confusion between all these “alternative” fuels and thereby reduce misunderstanding in political or academic discussions, we have developed a comprehensive and harmonised taxonomy (see Appendix A). In the rest of this thesis, the electro — and bio — fuels, imported from the exterior of the considered energy system, are regarded as renewable with no associated GWP.

To harvest the maximum potential of synthetic fuels in a sustainable transition and maximise the overall system efficiency [32], it is necessary to study the integration of these fuels within a whole-energy system which is multi-sector and accounts for multiple energy carriers [33]. To reach this goal, an energy system optimisation model (ESOM) can optimise the design and the operation of the system to minimise, for instance, its costs or its emissions [34].

In the field of energy system planning and scenario analysis, Yue et al. [35] highlighted that most ESOMs use a deterministic approach (75% of the 134 reviewed studies). However, the models and their numerous composing parameters are inherently uncertain especially when it comes to defining an energy transition strategy for a large-scale system such as a country. Given the lifetime of energy conversion technologies, such a strategy implies decisions with long-term impacts (20 to 50 years) where forecasts can be highly unreliable [36]. This long-term and large-system optimisation motivates the need to account for Uncertainty Quantification (UQ), which is considered a major challenge of such models in the literature [37].

On top of dealing with these uncertainties, the reality of decision-makers leads to a limited foresight into the future [38]. In a perfect foresight approach, decision-makers would be able to, from now on, see the “finish-line of the transition” in 2050 and accordingly make the planning decisions once and for all. On the contrary, they uncover the realisation of these uncertainties step-by-step, in a “myopic” way, and progressively act on them to, hopefully, meet the set target to reduce the anthropogenic GHG. In the objective to respect an overall CO₂ budget rather than to follow a prescribed CO₂-emissions trajectory, there is a need for a framework to explore these multiple transition pathways and provide insight into intermediate milestones not to miss. On top of the “what to do?”, this framework should aim at helping the policymakers to answer the question “how to do it?”.

The robustness of transition pathways provided by ESOMs is an essential question due to their sensitivity to uncertain factors. A variety of techniques are used to assess this robustness including Monte-Carlo analysis, stochastic programming or robust optimisation [35]. However, the robustness is commonly assessed to evaluate the sensitivity of the total cost (objective function) to input parameters. Given the complexity of whole-energy system models, the time scale of the transition and the large number of uncertainties, only considering the total cost does not give information on the sensitivity of the design strategy, i.e., the investment decisions. For instance, total cost might consist of excessive upfront investments and a better balance of Capital Expenditure (CAPEX) and Operational Expenditure (OPEX) might be preferable despite a slightly higher total cost. Moret et al. [39] proposed a method to assess the robustness of a design by investigating the potential overcapacity needed to face uncertainties. However, their work focused on the power sector only and on the target future year of 2035. Instead, an objective of this thesis is to tackle these two challenges: go beyond the total transition cost and provide more details on the sensitivity of the design to uncertainties while assessing a whole-energy system over

its whole transition.

“Our task is not to foresee the future, but to enable it”¹. Rather than trying to answer the question “What could happen in the future?”, this work addresses the “What could or should we do to make the future possible?”. This thesis aims at providing decision-makers with information and new methods considering the intrinsic uncertainties of the future. In that spirit, the research questions are described as follows:

- What can be the role of electrofuels in the transition pathways of a whole-energy system considering uncertainties, limited foresight, and a given CO₂ budget? What are the key uncertainties driving their local production or import?
- How to explore the multiple possible pathways through the optimisation of a sequence of actions to support an energy transition?
- How to assess the robustness of a transition roadmap whilst developing strategy and designing possible pathways?

To answer these questions, several tasks have been carried out on the whole-energy system model accounting for the uncertainties, the method to explore the myopic pathway of such a system and the approach to assess the robustness of a pathway roadmap.

The model developed and used in the context of this thesis is EnergyScope Pathway [40]. First introduced by Limpens in his PhD thesis [41], this model optimises the design and the operation of a whole-energy system over several decades and accounts for transition pathways from an existing system to a long-term target, i.e., 2050. Based on this model originally implemented for a perfect foresight approach, we have developed the myopic method in which the whole time horizon (30 years) is optimised through a sequence of 10-year time windows with 5-year overlaps.

To address the question of the role of electrofuels, they have been integrated into the pre-existing model, focusing on four molecules: hydrogen, methane, ammonia and methanol. Moreover, given their current and (expected) future role in the sector of the Non-energy Demand (NED), we have added this sector to the model with a similar level of detail as for the other sectors of the system, i.e., electricity, heat and transport.

To account for uncertainties, uncertainty characterisation and quantification have been applied by adapting the works of Moret [42] and Coppitters [43], respectively. In his thesis, Moret [42] developed a framework to obtain uncertainty ranges for a variety of parameters such as cost of purchasing and availability of resources or investment cost and efficiency of technologies. These ranges have then been sampled and

¹Saint-Exupéry in Citadelle, 1948

propagated through the EnergyScope Pathway via the RHEIA framework developed by Coppitters [43]. Using the surrogate modeling approach called Polynomial Chaos Expansion (PCE), this framework allows identifying the uncertain parameters with the biggest impact on the variation of total transition cost or other outputs of interest such as the imported amount of electrofuels.

To explore the different pathway trajectories in this myopic optimisation process, we have applied the Reinforcement Learning (RL) method. In this branch of machine learning, an “agent” is trained through its interactions with its environment, EnergyScope Pathway, to optimise its policy, i.e., the sequence of actions to take to support the transition.

Finally, in the objective to assess the sensitivity to uncertainties of different transition roadmaps, we have defined an approach to come up with a “robustness metric”. This approach is based on Principal Component Analysis (PCA) where directions capturing the widest design variations are identified and serve as a reference frame. Roadmaps resulting from perfect foresight optimisation have been tested in myopic and uncertain pathways. The results of these myopic runs have then been “projected” on the aforementioned frame to be able to compare the robustness of different roadmaps with each other.

All this work has been applied to the case of Belgium, a densely populated country with a limited potential of renewable energies, which represents roughly half of the forecast energy demand [44]. This makes it a challenging case to go from a highly fossil-dominated system in 2020 (73% of the primary energy mix [45]) to carbon neutrality by 2050.

This thesis is composed of five chapters to provide answers to the different research questions (see Figure 3). Chapter 1 details the tools and methods we used. It starts with the main constraints, parameters and variables of EnergyScope Pathway, the whole-energy system optimisation model. Then, it explains the Uncertainty Quantification (UQ) approach and the way it has been adapted to the case of Belgium and its transition pathway. Finally, general fundamentals and more case-specific considerations are brought up about the Reinforcement Learning (RL) and PCA-based robustness approaches.

Chapter 2 presents the case study of this work: Belgium and its energy transition. Without exhaustively detailing the data used from the work of Limpens [41], this chapter focuses on the main contributions of this work regarding the case study: the NED, the implementation of electrofuels and their respective routes of production and consumption, limiting the cumulative emissions of the transition to a certain CO₂ budget

rather than a prescribed emissions-trajectory and the data related to Small Modular Reactor (SMR) as an option to produce nuclear-based electricity in the future.

Chapter 3 details the results of the Global Sensitivity Analysis (GSA) carried out on the Belgian energy transition under uncertainties. On top of the impact of uncertainties on the total transition cost and the system design in general, we analyse the impact of having new nuclear (“atom”) capacities by 2040 onward and the driving parameters on the import of electrofuels (“molecules”): the so-called atom-molecules dilemma.

In Chapter 4, we detail the rules of the “RL game”. In other words, we define the action and state spaces as well as the reward function driving the agent’s behaviour in its quest to optimise its policy. Then, we analyse the results of the agent’s learning process and compare these results with the perfect foresight approach. Chapter 4 focuses on the robustness of a policy as its ability to maximise the chances to succeed a myopic transition under uncertainties to meet a CO₂ budget.

Chapter 5 assesses the robustness of different technological roadmaps as their ability to limit the investment into additional capacities when tested in myopic conditions. Three roadmaps resulting from different deterministic perfect foresight optimisation, are presented: REF, SMR and ROB. The first one, the reference case, considers nominal values for all the uncertain parameters. The SMR case is the one introduced in Chapter 3 where we allow the model to install SMR from 2040 onward. Eventually, the ROB case accounts for the highest values of uncertain parameters having the biggest impact on the total cost of transition (i.e., cost of purchasing fossil fuels and renewable electrofuels, industrial EUD, discount rate and variable OPEX of technologies).

Finally, we draw the main conclusions from this work: near-term actions are needed to respect the ambitious CO₂ budget and investing in electrofuels provides robustness to uncertainties and limited foresight into the future. Perspectives are suggested for future research on further developments and uses of the methodological tools.

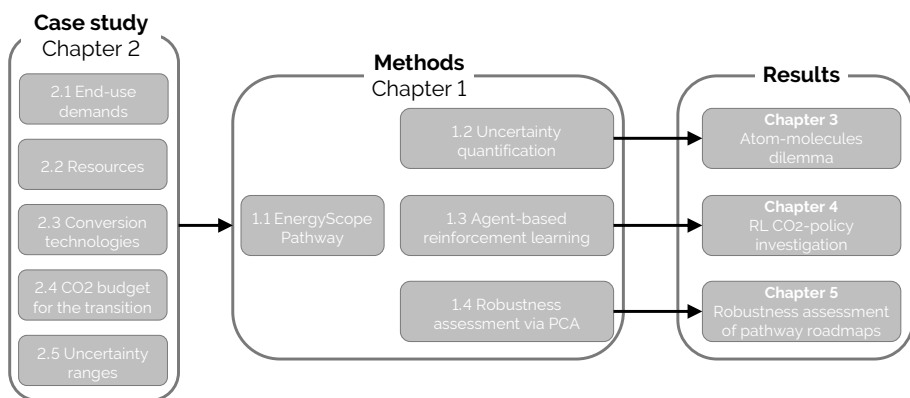


Figure 3. Structure of the thesis. Beyond Chapter 2 that describes the case study of Belgium, Chapters 3, 4 and 5 collect the analyses resulting from the application of the different methodologies developed in Chapter 1. Given the (quasi-)independence of the analyses presented in the last three chapters, they can be read separately.

Chapter 1

Methodology: Through a variety of complementary tools

“Technique aussi brûlante que les derniers bilans du GIEC.”
Primero (ft. Romeo), in *Deux deux*, 2022

Assessing the robustness of a whole-energy system transition pathway calls for a variety of methodological tools. First and foremost, such an extensive system needs to be represented, i.e., modelled, to further be optimised. This model requires some characteristics to capture the peculiarities of this system such as the intermittency of VRES, the coupling between the different energy and non-energy sectors and a pathway vision to pave the way from where we are to where we want to go. Then, as looking into the future (i.e., up to 2050 in this work) comes with a lot of uncertainties, these have to be assessed carefully in terms of characterisation and quantification. The former aims at defining the range over which the parameters of the model vary. The latter allows assessing the impact that such uncertainties can have on the output of the model. Finally, meeting the environmental objectives while minimising the cost of the system, accounting for this decision-making process, the uncertainties, and potential shocks/crises, require therefore a framework to assess the relevance and the timing of the decisions throughout the transition. This work encompasses the optimisation of the policy, i.e., a set of actions to take along the transition with a specific methodology to assess its robustness.

Detailing the different tools needed to answer the research questions, this chapter starts with the presentation of the whole-energy system optimization model, EnergyScope Pathway and its myopic formulation. Then, it focuses on the uncertainties,

their characterisation as well as their quantification. Finally, an agent-based Reinforcement Learning (RL) approach is detailed to address the robustness of a policy in the uncertain transition with limited vision in the future. This chapter ends with a PCA-based approach to draw a robustness metric and assess the ability of technological roadmaps to limit the investment into additional capacities. Each section of this chapter ends with some discussion and guidelines for researchers to further use and develop these methodologies.

Contributions

The main methodological contribution of this work is the implementation of the RL approach to simulate and optimise the behaviour of an artificial agent interacting with its environment, i.e., the whole-energy system through its transition. Given the uncertainties and potential shocks of the future, this approach allows the agent to play the transition in a sequential, i.e., myopic, way and optimise the choice and the timing of its actions. This optimization is done through trial and error where the agent repeats the transition with a new set of uncertainties.

Then, to support this step-by-step transition with limited foresight in the future, we have extended the EnergyScope Pathway model [41]. Originally developed to optimise the transition in one global optimisation up to 2050, i.e., perfect foresight, part of this thesis consisted in making this model able to optimise the same transition but with sequential more limited time windows, i.e., myopic approach. Besides its shorter computational time, this approach is more representative of an actual decision process with limited foresight in the future [46].

The third principal methodological contribution is the use of Principal Component Analysis (PCA) to assess the robustness of a technological roadmap. Given the uncertainties and the timespan of the transition, this approach allows highlighting the main “directions” of variation of the system design (i.e., the installed capacities). After this step of identification, strategies can be projected on these directions to see how robust they are to the need for additional capacities.

Finally, more minor methodological developments are part of this thesis. Following an approach similar to Guevara et al. [47], we have extended the ranges of uncertainty developed by Moret et al. [36] to pathway optimisation. After assessing the relevance of using Polynomial Chaos Expansion (PCE) on the optimisation of a whole-energy system [48], we have applied this uncertainty quantification method on the snapshot model, i.e., optimising the system in a target future year considering a green field approach, subject to different emission constraints [49] as well as the pathway

model (see Chapter 3). Eventually, starting from the initial investigation of Goffaux [50], this work has converged to the most relevant formulation of the salvage value for the model EnergyScope. This aims at considering the residual value of assets that would still be in place after the end of the optimisation. It avoids penalising capital-intensive and long-lasting asset. In this formulation, the capacities that have been anticipatively decommissioned are removed from the total installed capacities. Therefore, this penalises decisions that would lead to investments that are later decommissioned before having reached the end of their lifetime.

Other authors' main contribution statement

Novelty does not stand in the reinvention of the wheel. This thesis, instead, finds its fundamentals in great tools previously developed by other authors. As developers of the building blocks of the main contributions of this thesis, three main authors are to be mentioned for having brought a significant part of the methodological work. Based on Stefano Moret's monthly whole-energy system model (i.e., EnergyScope) [51], Gauthier Limpens has developed the hourly version of the snapshot model (i.e., EnergyScope TD) [52], as well as the perfect foresight pathway model [40], to which I personally contributed. Diederik Coppitters has developed the RHEIA framework that allows quantifying the impact of uncertainties and carry out robust optimisation of energy systems [43]. The current work used this framework for the first of these functionalities. Finally, Stefano Moret extensively assessed the uncertainty characterisation of the Swiss energy system [36]. This thesis follows the same methodology, updating the uncertainty ranges for the pathway model.

1.1 Whole-energy system transition model optimisation: EnergyScope Pathway

This work optimises the entire transition pathway from a known system in 2020 up to 2050 thanks to EnergyScope Pathway [40]. According to the pathway models review (see Appendix B.1), EnergyScope Pathway can be categorised as an investment and operation optimisation model that assesses the whole-energy system, has an hourly time resolution and is an open-source documented model. Moreover, it maintains a low computational cost (i.e., around 15 minutes for a 30-year pathway with an hourly discretisation)¹. From the perfect to the myopic foresight of the transition optimisation,

¹To keep this low computational time, crossover was disabled to solve the optimisation problem. This had no observed impact regarding the values of the objective function or the design variables at the optimum.

this section presents only the main constraints of the former approach to further dig into more details about the latter. The reader is invited to refer to Appendix B.2 for more details about the formulation of the model and its extension from EnergyScope TD, the snapshot model, optimising a target future year with a greenfield approach [53]. More extensive information about the formulation choices, for instance, can be found in [40] and the documentation [54].

1.1.1 Perfect foresight: One global optimisation of the transition

The whole-energy system model developed in this work originates from the perfect foresight (PF) formulation (Figure 1.1) of EnergyScope—the entire transition is computed in one optimisation, assuming a complete but uncertain knowledge of the different parameters until 2050 [40]. Each representative year is represented via the variables and constraints of the snapshot model, EnergyScope TD [52]. Then, to draw a consistent pathway between these years, additional constraints aim at linking them, e.g., limiting the modal shifts within some energy sectors.

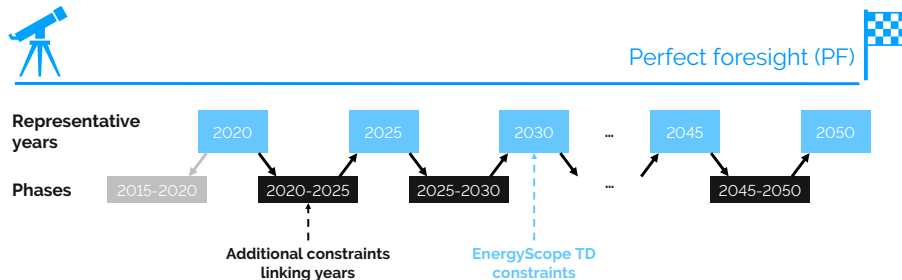


Figure 1.1. Illustration of the pathway methodology based on an existing energy system model, here EnergyScope TD [52]. The methodology spans from 2020 to 2050, with one representative year every five years. The model EnergyScope Typical Days (ESTD) is applied in 7 representative years (light blue boxes). The formulation includes additional constraints (black boxes) that link the years together. The initialisation of the pathway assumes that all capacities installed in 2020 were built during the pseudo-phase of 2015-2020 (grey box). The overall problem is defined as the pathway model.

The objective function of the pathway model, i.e., the total transition cost $C_{\text{tot,trans}}$, is computed as the sum of the total CAPEX, $C_{\text{tot,capex}}$, and the OPEX, $C_{\text{tot,opex}}$ (see Equation (1.1)).

$$\min C_{\text{tot,trans}} = C_{\text{tot,capex}} + C_{\text{tot,opex}} \quad (1.1)$$

The total CAPEX is the difference between the total investments done during the transition, $\mathbf{C}_{\text{inv},\text{phase}}$, and the residual value of the assets that would still be in place after the end of the transition, $\mathbf{C}_{\text{inv},\text{return}}$ (see Equation (1.2)).

$$\mathbf{C}_{\text{tot,capex}} = \sum_{p \in \text{PHASE} \cup \{2015_2020\}} \mathbf{C}_{\text{inv},\text{phase}}(p) - \sum_{j \in \text{TECH}} \mathbf{C}_{\text{inv},\text{return}}(j), \quad (1.2)$$

where $\mathbf{C}_{\text{inv},\text{phase}}$ is given as the sum over all the newly installed technologies at the phase p , $\mathbf{F}_{\text{new}}(p)$, multiplied by the average investment costs, c_{inv} , of the year starting and ending the corresponding phase, y_{start} and y_{stop} respectively (see Equation (1.3)).

$$\mathbf{C}_{\text{inv},\text{phase}}(p) = \sum_{j \in \text{TECH}} \mathbf{F}_{\text{new}}(p, j) \cdot \tau_{\text{phase}}(p) \cdot c_{\text{inv}}(p, j) \quad \forall p \in \text{PHASE}, \quad (1.3)$$

$$\tau_{\text{phase}}(p) = 1/(1 + i_{\text{rate}})^{\text{diff_2015_year}(p)}, \quad (1.4)$$

where τ_{phase} is the annualised phase factor and $c_{\text{inv}}(p, j)$ is the arithmetic average of the investment cost of the technology j at the beginning and the end of the phase, $c_{\text{inv}}(y_{\text{start}}, j)$ and $c_{\text{inv}}(y_{\text{stop}}, j)$.

In EnergyScope Pathway, τ_{phase} aims at depreciating the value of expenses done in the future (see Equation (1.4)). The discount rate accounted for in this annualisation factor, i_{rate} , is considered identical for all the technologies of the system. In line with Limpens [41], we set the nominal value to $i_{\text{rate}} = 1.5\%$ which is lower than values taken in other studies, between 7.5% and 12% [55–57]. Having a low-value discount rate favours less late expenses compared to a higher value of discount rate. In practice, the discount rate would vary depending on the technology investment risk. Depending on the technology readiness level, private investors would be more or less risk-averse. However, EnergyScope only considers the vision of a central planner where a single agent makes the investment decisions without differentiating the sources of the capital, i.e., private and public. Assuming a differentiated discount rate would require making assumptions about the private-public distribution of the capital. For this reason, we have decided to keep an identical value of discount rate for all the technologies.

Similarly, the salvage value is computed in the proportion of the remaining years of life versus the initial lifetime of an installed capacity of a technology from which the anticipatively decommissioned part, $\mathbf{F}_{\text{decom}}$, is removed. To cope with the end-of-time-horizon effects of multi-stage models, the salvage value avoids penalising the capital-intensive technologies towards the end of the transition [38]. After assessing the sensitivity of the formulation of the salvage value (see Appendix B.2.2), we have

kept the one given by Equation (1.5), being also similar to the expression used by Prina et al. [58].

$$\begin{aligned} \mathbf{C}_{\text{inv,return}}(j) = & \sum_{p \in \text{PHASE} \cup \{2015_2020\}} \tau_{\text{phase}}(p) \cdot c_{\text{inv}}(p, j) \cdot \\ & \frac{\text{remaining_years}(j, p)}{\text{lifetime}(y_{\text{start}}, j)} \left(\mathbf{F}_{\text{new}}(p, j) - \sum_{p2 \in \text{PHASE}} \mathbf{F}_{\text{decom}}(p2, p, j) \right) \quad \forall j \in \text{TECH}. \end{aligned} \quad (1.5)$$

About the total OPEX of the transition, $\mathbf{C}_{\text{tot,opex}}$, on top of the initial costs in 2020, we assume that the OPEX of a phase is equal to the average operational costs, \mathbf{C}_{opex} , of y_{start} and y_{stop} , multiplied by the duration of a phase t_{phase} equal to 5 years in our case (see Equation (1.6)).

$$\mathbf{C}_{\text{tot,opex}} = \mathbf{C}_{\text{opex}}(2020) + t_{\text{phase}} \cdot \tau_{\text{phase}}(p) \cdot \sum_{p \in \text{PHASE}} \mathbf{C}_{\text{opex}}(p), \quad (1.6)$$

where $\mathbf{C}_{\text{opex}}(p)$ is the arithmetic average of the operational cost at the beginning and the end of the phase p , $\mathbf{C}_{\text{opex}}(y_{\text{start}})$ and $\mathbf{C}_{\text{opex}}(y_{\text{stop}})$. The operational cost of a year, y , $\mathbf{C}_{\text{opex}}(y)$, is the sum of the costs related to the maintenance and operation of technologies, $\mathbf{C}_{\text{maint}}$, and the consumption of resources, \mathbf{C}_{op} (see Equation (1.7)).

$$\mathbf{C}_{\text{opex}}(y) = \sum_{j \in \text{TECH}} \mathbf{C}_{\text{maint}}(y, j) + \sum_{i \in \text{RES}} \mathbf{C}_{\text{op}}(y, i) \quad \forall y \in \text{YEARS}, \quad (1.7)$$

where the costs related to each representative year are:

$$\mathbf{C}_{\text{maint}}(y, j) = c_{\text{main}}(y, j) \mathbf{F}(y, j) \quad \forall y \in \text{YEARS}, \forall j \in \text{TECH} \quad (1.8)$$

$$\mathbf{C}_{\text{op}}(y, i) = \sum_{t \in T} c_{\text{op}}(y, i) \mathbf{F}_t(y, i, t) t_{\text{op}}(t) \quad \forall y \in \text{YEARS}, \forall i \in \text{RES}, \quad (1.9)$$

where the variable \mathbf{F} represents the size of the installed capacities (for all technologies j) and the variable \mathbf{F}_t is the hourly consumption of the resources; the parameter c_{main} is the OPEX of the technologies, and the parameter c_{op} is the cost of purchasing resources. For the sake of simplicity, as done by Limpens et al. [40], the sum over the 8760 hours of the year is written as the sum over $t \in T$.

The CO₂ budget for the transition, $\mathbf{GWP}_{\text{tot,trans}}$ is equal to the arithmetic average of the representative years at the beginning and the end of each phase (see Equation (1.10)). Similarly to initial operational costs to account for the system in place in 2020 (see Equation (1.6)), $\mathbf{GWP}_{\text{tot}}(2020)$ accounts for the entire operational emissions in

2020, as the initial cumulative emissions of the transition. Then, as detailed in Section 2.5, these cumulative emissions are constrained by a budget (see Equation (1.11)).

$$\mathbf{GWP}_{\text{tot,trans}} = \mathbf{GWP}_{\text{tot}}(2020) + t_{\text{phase}} \sum_{p \in \text{PHASE}} \mathbf{GWP}_{\text{tot}}(p) \quad (1.10)$$

$$\mathbf{GWP}_{\text{tot,trans}} \leq gwp_{lim,trans}, \quad (1.11)$$

where $\mathbf{GWP}_{\text{tot}}(p)$ is the arithmetic average of the yearly emissions at the beginning and the end of the phase p , $\mathbf{GWP}_{\text{tot}}(y_{\text{start}})$ and $\mathbf{GWP}_{\text{tot}}(y_{\text{stop}})$. The computation of these yearly emissions is based on the Global Warming Potential (GWP) of the resources:

$$\mathbf{GWP}_{\text{tot}}(y) = \sum_{i \in \text{RES}} \mathbf{GWP}_{\text{op}}(y, i) \quad \forall y \in \text{YEARS} \quad (1.12)$$

$$\mathbf{GWP}_{\text{op}}(y, i) = \sum_{t \in T} gwp_{op}(y, i, t) \mathbf{F}_t(y, i, t) t_{op}(t) \quad \forall y \in \text{YEARS}, \forall i \in \text{RES}, \quad (1.13)$$

where gwp_{op} is the specific emissions (i.e., in $\text{kt}_{\text{CO}_2,\text{eq}}/\text{GWh}$) of each resource. Based on an approach developed by the Intergovernmental Panel on Climate Change (IPCC) [59], this work considers the indicator “GWP100a - IPCC2013” to compute the emissions related to the use of resources. This includes the emissions due to the extraction, the transportation and the combustion of the energy carrier. EnergyScope proposes to account for the embodied emissions of the technologies based on a Life Cycle Assessment (LCA). These stand for extraction of materials, refining, construction and end of life [60] and can be one to three times higher than the direct emissions depending on the level of emission reduction [61]. However, this work is still in progress and the database is not yet complete. Consequently, it is not included in this work and is not accounted for.

Besides this constraint on the emissions, the main constraint to link years with each other is the one dictating the installed capacities at the end of each year:

$$\mathbf{F}(y_{\text{stop}}, j) = \mathbf{F}(y_{\text{start}}, j) + \mathbf{F}_{\text{new}}(p, j) - \mathbf{F}_{\text{old}}(p, j) - \sum_{p2 \in \text{PHASE} \cup \{2015_2020\}} \mathbf{F}_{\text{decom}}(p, p2, j) \quad (1.14)$$

$$\forall p \in \text{PHASE}, y_{\text{stop}} \in Y_STOP(p), y_{\text{start}} \in Y_START(p), j \in \text{TECH},$$

where the variables \mathbf{F}_{old} and $\mathbf{F}_{\text{decom}}$ are the capacities respectively having reached the end of their lifetime and prematurely decommissioned. Moreover, to account for the inertia of society and to prevent unrealistically fast modal share change, constraints limit this change for the sectors of the low-temperature, passenger mobility and freight mobility demands. The interested reader will find more information about the formulation choices related to it in the work of Limpens et al. [40].

1.1.2 Myopic: Sequential optimisation of the transition with limited foresight

One of the main methodological contributions of this work regarding the development of the whole-energy system model consists in giving it the possibility to optimise the transition pathway in a myopic approach. After introducing the general concept, this section details more the additions brought to the model in terms of implementation.

General concept of the myopic optimisation

Compared to perfect foresight, the myopic approach (Figure 1.2) has three main advantages: shorter computational time, more realistic representation of the short-sightedness of decision-makers and the ability to capture shocks and unexpected events [62]. For this reason, several studies are based on this approach [38, 46, 63, 64]. Babrowski et al. [46] analysed the benefit of the myopic approach to reduce the computational time. Poncelet et al. [38] use this approach to analyse the expansion planning of the power sector beyond 2050 to assess the realism of the decision-making process brought up by the myopic implementation. Nerini et al. [63] analysed the impact of the horizon windows and overlapping time. Overall these studies decided to choose the myopic approach to analyse the speed of change compared to a perfect foresight approach. Moreover, the myopic approach allows a sequential optimisation process that opens the doors to decision-making/policy-learning methodologies, like assessing shock events. This approach is used by Heuberger et al. [64] who assessed the speed of integration of technologies due to these events. In their analysis of the overcapacity in European power systems, Moret et al. [39] emphasised that such a “possibility of *recourse*” is very appropriate to address uncertainty gradually unfolding over time. Consequently, the development of the myopic approach with an overlap between two successive time windows has been implemented. This sequential optimisation framework also represents the foundations of the further implementation of the agent-based reinforcement learning framework (see Section 1.3).

After optimising, in design and operation, one time window (e.g., from 2020 to 2030), the intermediate system design (i.e., the installed capacities) is set as initial conditions for the start of the next time window (e.g., from 2025 to 2035) as well as the historical investment decisions (i.e., F_{new} , F_{old} and F_{decom}) (see Figure 1.3). Consequently, the solution obtained at the end of the first time window (e.g., 2030) as well as potential investment decisions between the start of the second time window and this end-year are discarded. In other words, they are not taken into account for the optimisation of the second time window since the new final year is further into the

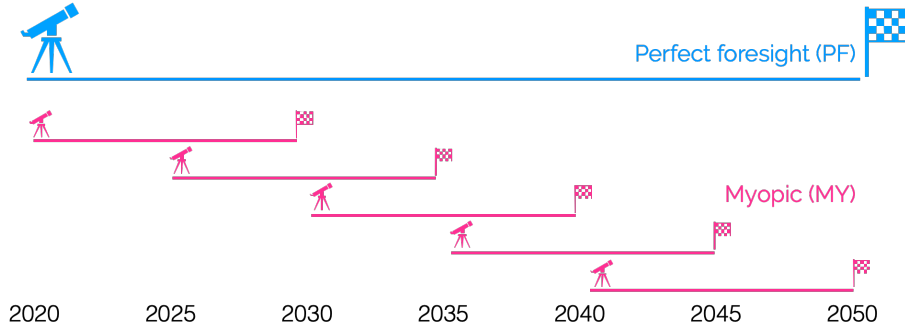


Figure 1.2. The myopic approach (in pink) uses several instances of the pathway model, illustrated in Figure 1.1, as a sequence of different and linked Linear Programming (LP) problems. In this example, the pathway instance has a time horizon of 10 years ($N_{\text{year,opti}} = 10$) with a 5 year-overlap ($N_{\text{year,overlap}} = 5$). As a comparison, the perfect foresight (in blue) has a time horizon of 30 years.

future. This process goes on until the stated end of the transition (i.e., 2050, in this case).

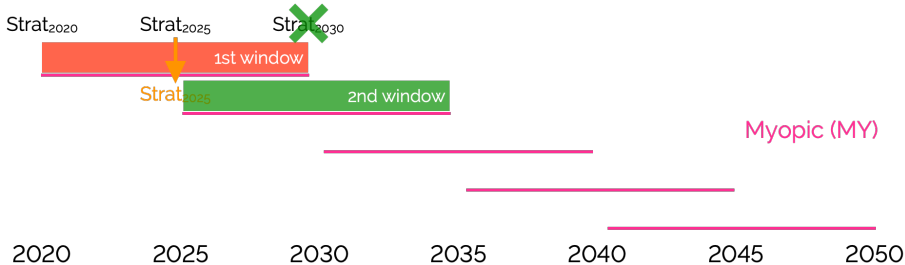


Figure 1.3. Sequential optimisation of the transition pathway in the myopic approach: (i) first time window optimisation, (ii) set-up of the initial conditions of the second time window, (iii) second time window optimisation discarding intermediate results from the first time window optimisation.

Additional sets, parameters and variables

The major add-on from the original EnergyScope Pathway model [41] to the myopic version developed in this thesis is the possibility to carry out the optimisation on a limited time window, of which the duration is defined by $N_{\text{year,opti}}$. Moreover, there is the possibility of having an overlap between two consecutive time windows. The period of this overlap is defined by the parameter $N_{\text{year,overlap}}$. The philosophy behind the development of the myopic approach was to add another layer on top of the per-

fect foresight model to make it more modular. For this reason, the already existing constraints are marginally adapted. This way, the newly developed model can easily be used to perform a perfect foresight optimisation by setting the time window to $N_{\text{year,opti}} = 30$ years (i.e., between 2020 and 2050) and the overlap between the time windows to $N_{\text{year,overlap}} = 0$. It is fundamental to define on the one hand, the actual time window on which the system is optimised, and on the other hand, the history, i.e., what has already been optimised earlier in the transition. Consequently, four new sets are implemented: $\text{YEARS}_{\text{WND}}$, $\text{YEARS}_{\text{UP TO}}$, $\text{PHASE}_{\text{WND}}$ and $\text{PHASE}_{\text{UP TO}}$ (see Table 1.1).

Table 1.1. New SETs for the myopic pathway formulation.

| Set | Index | Description |
|-------------------------------|-----------|---|
| $\text{YEARS}_{\text{WND}}$ | $y \in Y$ | Representative years of the time window to optimise |
| $\text{YEARS}_{\text{UP TO}}$ | $y \in Y$ | Representative years including the years already optimised, i.e., the history |
| $\text{PHASE}_{\text{WND}}$ | $p \in P$ | Phases of the time window to optimise |
| $\text{PHASE}_{\text{UP TO}}$ | $p \in P$ | Phases including the phases already optimised, i.e., the history |

$\text{YEARS}_{\text{WND}}$ and $\text{PHASE}_{\text{WND}}$ substitute YEARS and PHASE in the constraints defined in the pathway model in Section 1.1.1. These two sets aim to set the optimisation to a more limited time window. Progressing through the transition, $\text{YEARS}_{\text{UP TO}}$ and $\text{PHASE}_{\text{UP TO}}$ allow keeping track of the history of the investments (e.g., technology installations, decommissioning or retirement), the consumption of resources, the cumulative amount of emissions, etc.

On top of these four specific sets, some artefacts were also necessary to avoid computational rounding errors. For instance, the first year of a time window is the result of the optimisation of the previous one. Therefore, optimising again this first year could lead to rounding errors preventing the optimisation from converging. For this reason, the set YEAR_{ONE} accounts for the first representative year of the time window to optimise, which is excluded from $\text{YEARS}_{\text{WND}}$ to avoid these errors. This remark remains valid for any time window except the first one of the transition where the year 2020 is optimised even though its technological strategy is set according to the actual system presented in Appendix C.1. Finally, as the end of the time windows changes for each of them, the parameter *remaining_years* has to be updated accordingly to keep a meaningful definition of $\mathbf{C}_{\text{inv,return}}$ in Equation (1.5).

Myopic pathway implementation

Starting this work in 2017, AMPL Optimization Inc. has developed a Python Application Programming Interface (API) called `amplpy` [65]. In a nutshell, this API allows the pre/post-processing of an `ampl` optimisation problem by accessing its features (e.g., constraints, parameters, variables, objective function) from within Python. Using this API, this updated version of the model interacts with the AMPL problem representing the optimisation of the whole-energy system transition pathway as represented in Figure 1.4. The myopic optimisation of the pathway consists of a sequence of smaller LP problems limited to their respective 10-year time window, until eventually reaching 2050.

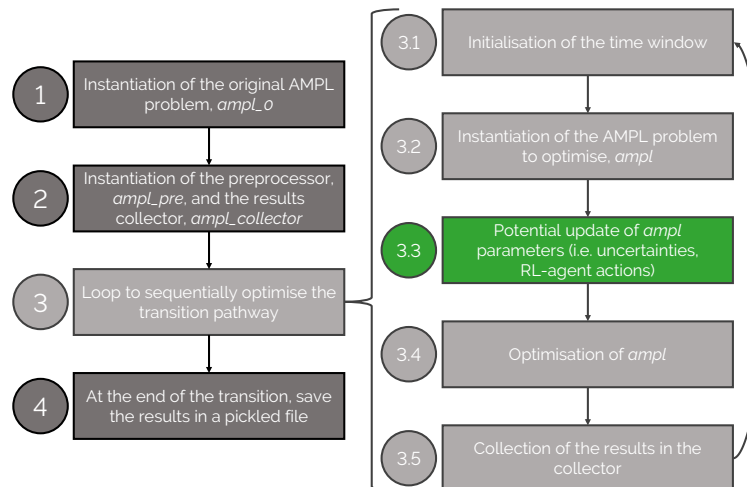


Figure 1.4. Diagram of the iterative optimisation of the whole-energy system transition pathway. Myopic optimisation of the pathway consists of a sequence of smaller LP problems limited to their respective 10-year time window. If the optimisation is not deterministic, step 3.3 is the one where the value of some parameters is changed due to uncertainties (see Section 1.2) or the actions taken by the Reinforcement Learning-agent (see Chapter 4)

Impact of the myopic formulation on the system

In line with the work of Babrowski et al. [46], the computational time is reduced drastically (i.e., by 55%). On top of this, we observed that the resulting design, i.e., the technological mix, remains similar. Given the continuous change of the input parameters over the considered time frame, the perfect foresight and myopic approaches results

are very similar, like in [66]: less than 1% cost difference over the transition, similar system designs by 2050 and slight shifts in time in terms of adoption of technologies.

The main difference lies in the myopic transition itself and especially in the earlier deployment of PVs and offshore wind turbines. These induce the reinforcement of the grid which is a capital-intensive and long-lifetime asset. This is mostly due to the impact of the salvage value, Equation (1.5), on the objective function. Since this is now the transition cost over a more limited time window (i.e., 10 years rather than 30 years), a bigger salvage value, deduced from the total investments, leads to a temporary better optimum at the early stages of the transition. A more detailed comparison between the myopic and perfect foresight approaches is available in Appendix C.3.

1.1.3 Discussion and guidelines for future researchers

Given the research questions targeted in this work, EnergyScope Pathway was the right model to choose for several reasons: its low computational burden, its hourly time resolution, its operation and design optimisation of a whole-energy system and the openness of the code and availability of the documentation (see Appendix B.1).

However, depending on the research questions to address, other pathway energy system models might be more appropriate given their better spatial resolution or higher techno-economical details, for instance. Such models can be used and combined with the other methodological tools presented in this chapter. Although, the main (and only) requirement is to keep a low computational time as getting relevant results from the following approaches usually requires $10^3 \sim 10^4$ runs. In our case, we have implemented the model to keep the time to run a pathway composed of 7 representative years below 15 minutes on a personal laptop.

1.2 Uncertainty quantification

In their systematic review, Yue et al. [35] highlighted that a wide majority of studies addressing the optimisation of energy systems (i.e., 75% out of the 134 reviewed studies) were not investigating the impact of uncertainties. However, disregarding these impacts can have drastic consequences on the system design. For instance, historical low Fossil Gas (NG) prices have led to overcapacity of Combined Cycle Gas Turbine (CCGT) in Europe [39]. This is why accounting for uncertainty in Energy System Optimisation Models (ESOMs) is crucial [67], especially when it comes to optimise several decades in an inherently uncertain future [68].

This section aims at briefly presenting the methods followed to first characterise these uncertainties, then to quantify their impact on different outputs of interest of the model (e.g., amount of molecules imported from abroad, the installed capacity of SMR or the total transition cost) and finally, the screening and selection of the parameters to analyse.

1.2.1 Uncertainty characterisation

Characterising precisely the uncertainty—ideally with their respective probability density functions (PDFs)—of the thousands of parameters in the model is daunting if not impossible because of the lack of data [69]. Therefore, we used a workaround developed by Moret et al. [36] that defines relative ranges of variation for different groups of parameters. These ranges have been adapted for the Belgian energy system and the pathway formulation. Moreover, some ranges have been added to account for new parameters coming from the pathway formulation described in Section 1.1 like the society inertia. Like other works [42, 70, 71] and given the scarcity of information, the uncertain parameters are assumed to be independent and uniformly distributed between their respective lower and upper bounds. Alternatives like PERT or Gaussian distributions could also have been considered [43].

Following the methodology defined by Moret et al. [36], uncertainties of types I (investment-type) and II (operation-type, constant uncertainty over time) keep the same range width for the whole transition. In other words, unlike type III parameters, this width is not expanding (nor narrowing) for the different representative years of the transition. However, parameters with an uncertainty increasing over time, type III, (i.e., end-use demands, in this case) will have a wider and wider range over the transition (see Figure 1.5). In this work, a +50% linear increase has been set between the width of the range of such parameters in 2025 and the same ranges in 2050. This choice leads to an industrial EUD that could be, in 2050, -30.8% compared to its nominal value. This potential drop compared to the reference is in line with the work of Climact and VITO [72]. In their work, the total energy demand in the industry sector in 2050 could be between -19% to -50% of the reference value, depending on the scenario. In Figure 1.5, this means that for type III uncertainties only, R_{2050}^+ is 50% bigger than R_{2025}^+ and R_{2050}^- is 50% smaller than R_{2025}^- . For uncertainties of types I and II, the relative variation versus the nominal value remain the same over the transition. Inspired by Guevara et al. [47], the values of the uncertain parameters are set at a fixed relative position from the nominal values for each sampled transition—the values do not zigzag from 2025 to 2050 within the bounds (Figure 1.5).

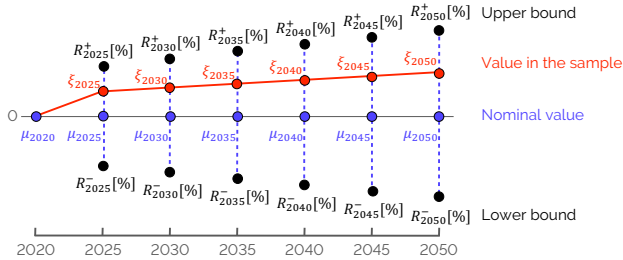


Figure 1.5. Expansion of the width of the uncertainty range for type III parameters. $\mu_{2020}, \mu_{2025}, \dots, \mu_{2050}$ are the nominal values equal to 0 as the uncertain parameters represent a relative increase/decrease of actual parameters of the model. R^+ and R^- are respectively the upper and lower bounds of the range and $\xi_{2025}, \xi_{2030}, \dots, \xi_{2050}$ are the values taken by one parameter for a specific sample of the GSA for each of the representative years of the transition, always starting from the nominal value in 2020, μ_{2020} . The graph has been adapted from [47].

Finally, the model accounts for thousands of parameters. The computational burden of considering all of them separately would be completely overwhelming ($\sim 10^7$ model runs). Similarly to other works [36, 48], the model parameters that would follow the same uncertainty have been grouped into one single uncertain parameter. On top of mitigating the computational burden, this aims at grouping parameters that are closely linked with each other. For instance, the uncertainty on the cost of purchasing renewable electrofuels, $c_{\text{op,electrofuels}}$, identically affects the cost of e-hydrogen, e-methane, e-ammonia and e-methanol. Indeed, besides their respective specificities, each of these fuels will be similarly affected by the variation in the cost of electricity or the electrolyser, which drive the majority of their cost of purchasing [73]. Similarly, the uncertainties impacting the industrial demand, *industry_EUD*, alters equally the industrial high- and low-temperature and electricity demands as well as the non-energy demand. Section 2.4 gathers the list of the uncertain parameters considered in this work.

1.2.2 Polynomial Chaos Expansion

To avoid the computational burden of well-known methods like Monte-Carlo analysis [35], we used PCE to carry out a GSA. PCE is an approach for surrogate-assisted UQ that propagates uncertainties in input parameters through the system model. This allowed us to assess statistical moments of the quantity of interest and determine Sobol' indices [74]. To construct a PCE of the EnergyScope Pathway model, we

employed the open-source Python framework RHEIA [75, 76]. Where the first part of this section is dedicated to the mathematical definition of this approach, the second details its choice and summarises the comparison made with another approach (i.e., the Morris method) in a previous work [48].

Definition

The PCE model (\hat{M}) is a representation of the relationship between the input parameters and the output variable of interest (i.e., the value of the objective function, see Equation (1.1)) in the EnergyScope Pathway model (M). This representation is constructed as a truncated series of multivariate orthonormal polynomials Ψ , weighted by coefficients u :

$$\hat{M}(\xi) = \sum_{\alpha \in \mathcal{A}^{d,p}} u_\alpha \Psi_\alpha(\xi) \approx M(\xi), \quad (1.15)$$

where the vector $\xi = (\xi_1, \xi_2, \dots, \xi_d)$ comprises the independent random input parameters (see Section 2.4), d corresponds to the number of input distributions and α is a multi-index, i.e., a vector of non-negative indices of length d , where each index corresponds to the degree of each univariate polynomial that forms the basis of the multivariate polynomial Ψ_α . The coefficients $(u_0, u_1, \dots, u_{P+1})$ are quantified using a regression method applied to orthonormal polynomials [77]. As uniform distributions are considered, the Legendre polynomials are adopted, as they are the associated family of polynomials that are orthogonal concerning standard uniform distributions [77].

A truncation scheme is implemented to restrict the number of multivariate polynomials in the series. This is done based on two factors: a specified limiting polynomial order (p) and the number of uncertain parameters (d) involved. The multivariate polynomial order $|\alpha|$ is the summation of the orders for each univariate polynomial in the multivariate polynomials space. Thus, only the multi-indices corresponding to an order that is less than or equal to the specified limiting order are retained and stored in the truncated series denoted as $\mathcal{A}^{d,p}$:

$$\mathcal{A}^{d,p} = \{\alpha \in \mathbb{N}^d : |\alpha| \leq p\}. \quad (1.16)$$

The number of multi-indices satisfying this condition is as the cardinality of \mathcal{A} , i.e., the number of its elements:

$$\text{card}(\mathcal{A}^{d,p}) = \binom{p+d}{p} = \frac{(d+p)!}{d!p!} = P + 1. \quad (1.17)$$

To ensure a well-posed least-square minimisation, it is recommended to have a number of training samples at least twice the number of coefficients [77]. Therefore, $2(P + 1)$ samples are evaluated in the system model, and the model response for each quantity of interest is recorded. To generate the training samples, the quasi-random Sobol' sampling technique is employed [78]. As a low-discrepancy sequence, this technique exhibits the main advantage of investigating efficiently and (almost) uniformly the hypercube of uncertainties, unlike uniformly distributed random numbers.

The process of defining the polynomial degree includes incrementally increasing it until a desired level of accuracy is achieved [75]. Starting with $p = 1$, a PCE is constructed and the Leave-One-Out (LOO) error is evaluated. If the LOO error is below a specified threshold ($\sim 1\%$), the corresponding polynomial order is considered sufficient for generating an accurate PCE. However, if the error exceeds the threshold, the order is increased, and additional samples are generated following the rule of Equation (1.17).

For the specific study of this work, a polynomial order of 2 is necessary (with 1260 training samples as per Equation (1.17)) to achieve a LOO error below 1% for the total transition cost. As second-order PCE is the minimum to ensure the accuracy of the surrogate model, selecting and grouping the parameters as presented in Section 1.2.3 is compulsory to alleviate the computational burden. Otherwise, considering thousands of independent uncertain parameters would lead to millions of EnergyScope Pathway runs, if not more. Another alternative to reduce the computational cost of the GSA would be to consider the monthly (instead of hourly) time resolution for the runs of EnergyScope Pathway. However, despite its shorter computation time (i.e., a couple of seconds), the main drawback of the monthly model is its poor representation of the integration of VRES [40].

Lastly, the statistical moments can be analytically derived from the PCE coefficients, eliminating the need for further model evaluations. The mean μ and standard deviation σ are obtained as follows:

$$\mu = u_0, \quad (1.18)$$

$$\sigma^2 = \sum_{i \neq 0} u_i^2. \quad (1.19)$$

Furthermore, the Sobol' indices can also be determined analytically. The total-order Sobol' indices (S_i^T) assess the overall influence of a stochastic input parameter on the performance indicator, encompassing all possible interactions:

$$S_i^T = \sum_{\alpha \in A_i^T} u_\alpha^2 / \sum_{i=1}^P u_i^2 \quad A_i^T = \{\alpha \in A | \alpha_i > 0\}. \quad (1.20)$$

Here, A denotes the collection of all PCE coefficients and α_i corresponds to the coefficient associated with the uncertain parameter i .

Qualitative ranking based on Sobol' indices

When a LOO error of 1% cannot be achieved, Sobol' indices can still provide a qualitative ranking to identify the most impacting parameters on the output of interest (see Table 1.2). A first-order PCE to assess the uncertainties on the total transition cost has a LOO error of 16%. However, it has the main advantage of requiring significantly fewer runs than more accurate second-order PCE (70 versus 1260) while computing similar Sobol' indices for the most impacting parameters, and consequently giving a similar ranking.

Table 1.2. Total Sobol' indices of the uncertain parameters over the total transition cost via PCE of orders 2 and 1 having a LOO error of 1% and 16%, respectively. The similar rankings (and indices) show the validity of using the faster (even though less accurate) lower-order PCE to rank the most impacting uncertain parameters.

| Parameter | Ranking (Sobol' index) | | | |
|-------------------------------|------------------------|--|---------------|--|
| | PCE order 2 | | PCE order 1 | |
| | LOO error 1% | | LOO error 16% | |
| Purchase electrofuels | 1 (46.8%) | | 1 (43.5%) | |
| Industry EUD | 2 (23.2%) | | 2 (18.3%) | |
| Discount rate | 3 (12.0%) | | 3 (12.1%) | |
| Purchase fossil fuels | 4 (5.7%) | | 5 (3.5%) | |
| Variable OPEX of technologies | 5 (3.1%) | | 6 (2.4%) | |
| Purchase biofuels | 6 (2.6%) | | 4 (4.1%) | |

Comparison with a proven method

Besides being an in-house method, an early step of this thesis consisted in assessing PCE with a similar approach used in the literature [48].

After characterising the uncertainty ranges, Moret et al. [36] quantified the impact of these uncertainties on the snapshot model of EnergyScope, i.e., ranking them, using the Morris method [79]. This method, as a statistical analysis, relies on individually randomised one-factor-at-a-time designs. Given the d model parameters $\vec{\xi} = (\xi_1, \xi_2, \dots, \xi_d)$, the first step of the method consists in generating independent ran-

dom samples of $\vec{\xi}$ in a standardised and discretised p -level *region of experimentation*, ω . In this *region of experimentation*, each ξ_i , varying in the interval $[\xi_{i,\min}, \xi_{i,\max}]$, can take a random discrete value as follows :

$$\xi_i = \xi_{i,\min} + j \cdot \frac{1}{p-1} (\xi_{i,\max} - \xi_{i,\min}) \quad \text{with } j \in \{0, 1, \dots, p-1\} \quad (1.21)$$

Then, given these random one-factor-at-a-time samples, the Morris method defines, for a given set of $\vec{\xi}$, the elementary effect of the i th parameter (EE_i) as :

$$EE_i = \frac{M(\xi_1, \xi_2, \dots, \xi_i + \Delta, \dots, \xi_d) - M(\vec{\xi})}{\Delta}, \quad (1.22)$$

where M is the objective function, $\vec{\xi} \in \omega$, except $\xi_i \leq 1 - \Delta$ and Δ is a set multiple of $1/(p-1)(\xi_{i,\max} - \xi_{i,\min})$. As in other studies [36, 42, 80], we consider p as even and $\Delta = p/[2(p-1)](\xi_{i,\max} - \xi_{i,\min})$.

Finally, to evaluate the importance of the i th parameter over an output, the Morris method relies on F_i , the distribution of r elementary effects. Computing the mean, $\mu_i = \mu(F_i)$, and the standard deviation, $\sigma_i = \sigma(F_i)$, of the F_i distribution, allows ranking the parameters based on their influence on the concerned output. Usually, in the Morris method, p and r respectively get values as follows: $p \in \{4, 6, 8\}$ and $r \in [15; 100]$ depending on, d , the number of uncertain parameters. The higher this number is, the higher shall be, simultaneously, p and r . In the following comparative analysis, we set p and r to their maximum values, respectively 8 and 100 to get the most reliable parameters ranking.

Beyond the original Morris method, we used the standardised elementary effects, SEE_i , formulation [80], given by

$$SEE_i = EE_i \cdot \frac{\sigma(\xi_i)}{\sigma(M)}. \quad (1.23)$$

Among other things, the SEE allows comparing the influence of different inputs on the same output or compare the influence of the same parameter on different outputs, even if these parameters or outputs are significantly different in terms of variation range or average amplitude. Moreover, this standardised analysis does not require any additional model evaluations.

Therefore, in the following results, we rather use

$$\mu_i^* = \mu(|SF_i|) \quad (1.24)$$

to rank parameters among each other. In Equation (1.24), SF_i is the distribution formed by the r standardised elementary effects, as done in Moret [42].

In [48], we have assessed the PCE approach on the cost-optimum Belgian energy system in 2035, using EnergyScope TD. To do so, we compared the Top-14 most impacting parameters obtained from this approach with the one provided by the improved Morris method based on μ_i^* . Even if the output of each method does not have the same physical meaning, both methods can rank the parameters by their impact on the total annual cost of the energy system. Both rankings were very similar which validated the use of PCE in the rest of this work (see Table 1.3).

Table 1.3. Comparison of the Top-14 rankings for the improved Morris method (left) and total-order PCE method (right). We used the DTU’s implementation of the Morris method [81] (with $p = 8$, $r = 100$).

| Parameter | Morris Ranking (μ_i^*) | PCE Ranking (S_i^T) |
|----------------------------------|------------------------------|-------------------------|
| Prices of hydrocarbons | 1 (0.7141) | 1 (0.6434) |
| Cost of increased efficiency | 2 (0.3046) | 2 (0.1014) |
| Cost of maintenance | 3 (0.2371) | 4 (0.0534) |
| Discount rate | 4 (0.2019) | 5 (0.0467) |
| Price of imported electricity | 5 (0.1974) | 3 (0.0809) |
| CAPEX of the grid | 6 (0.1498) | 6 (0.0252) |
| CAPEX of PV | 7 (0.1270) | 7 (0.0187) |
| Increase of electricity demand | 8 (0.1168) | 8 (0.0154) |
| CAPEX of nuclear power plant | 9 (0.0963) | 9 (0.0119) |
| Increase of space heating demand | 10 (0.0856) | 11 (0.0088) |
| Price of coal | 11 (0.0856) | 12 (0.0087) |
| Price of renewable fuels | 12 (0.0794) | 10 (0.0104) |
| Price of uranium | 13 (0.0607) | 13 (0.0047) |
| Onshore wind load factor | 14 (0.0600) | 14 (0.0046) |

1.2.3 Preliminary screening and selection

After the initial phase of grouping (Section 1.2.1), a preliminary screening was necessary to identify the key parameters to account for in this GSA. Rixhon et al. [49] performed a similar sensitivity analysis on the 2050 Belgian whole-energy system under different CO₂ limits using the snapshot model, EnergyScope TD [52]. Screening the results of this work, we have discarded some parameters with negligible impact such as CAPEX of electrolyzers or variation of the freight demand. Parameters are considered “negligible” if their Sobol’ index is below the threshold = $1/d$, d being

the total number of uncertain parameters [82]. On top of this selection, we have added others that were intrinsic to the pathway formulation, e.g., modal share changes, or related to the integration of SMR, $f_{\max, \text{SMR}}$. The exhaustive list of these 34 parameters is presented in Section 2.4.

1.2.4 Discussion and guidelines for future researchers

Carrying out a Global Sensitivity Analysis (GSA) requires two steps: uncertainty characterisation and uncertainty quantification. Characterising the distribution followed by uncertain parameters requires a lot of data that are either seldom available or poorly documented in the literature. Consequently, once lower and upper bounds are computed following a method like the one developed by Moret et al. [36], a good practice is to consider uniform distribution. Preliminary analyses revealing key parameters impacting the most the feature of interest could direct further research to refine the characterisation of these parameters.

About the method to quantify the uncertainty, PCE has the advantage to provide Sobol' indices as the impact indicators of the uncertain parameters and extract statistical moments of the output of interest. Based on our experience, considering a second-order PCE is the minimum to get a reasonably low LOO error (below 1%) and reliable results. However, as presented in Section 1.2.2, starting with a first-order PCE is a good proxy to get an initial insight into the impact of the parameters and discard the negligible ones before moving to a higher-order PCE to increase the accuracy of the results.

1.3 Agent-based reinforcement learning to support myopic energy transition

The transition towards carbon neutrality of a whole-energy system (i.e., including all streams of energy carriers and demands) is uncertain. Therefore, instead of establishing single-shot definitive plans towards 2050 (and beyond), policymakers rather go through multiple rolling-horizon short-term decisions. Yet, these decisions can have long-term impacts, 20 to 50 years. The long-term future is intrinsically uncertain and could be the place for potentially sudden unexpected events. Meeting the environmental objectives without a prescribed CO₂ pathway while minimising the cost of the system, accounting for this decision-making process, the uncertainties, and potential shocks/crises, requires a framework to assess the relevance and the timing of the decisions throughout the transition.

To address this issue, several approaches have already been used. Among them, multi-stage stochastic programming is often put forward as a promising method. Stochastic programming formulates the problem as a mathematical program with probabilistic constraints or objective functions. These models explicitly consider the uncertainty by incorporating probability distributions for the uncertain parameters. The goal is to find an optimal decision that minimises/maximises the expected value of the objective function while satisfying the probabilistic constraints, modelled as a scenario tree. At each stage of the problem, here the transition pathway of a whole-energy system, the model has the possibility of recourse, i.e., to adapt the decisions made at earlier stages, in the response to unveiled uncertainties [83]. Using MARKAL model [84], Kanudia and Loulou [85] assessed a multi-stage stochastic optimisation of the transition of Quebec between 1995 and 2035 accounting for high/low mitigation action plans and high/low growth scenarios. The authors found that hedging strategies, adapting to future uncertainties, were outperforming the perfect foresight and deterministic optimisation of the different scenarios. However, stochastic programming is usually applied to a limited number of uncertainties, i.e., up to 10, and relies on probability distributions that are often difficult to define properly. Increasing the number of these uncertainties in stochastic programming increases exponentially the computational burden that limits the use of such a method in Integrated Assessment Models (IAMs) [86]. Based on the approach of Bertsimas and Sim [87], and similarly to Moret [42], Nicolas et al. [86] rather opted for the robust optimisation of the global pathway up to 2200 given different temperature deviation targets, i.e., 2 or 3°C by 2200 via the use of uncertainty budget, Γ , in the TIAM-World model [88]. Considering 9 climate parameters and their respective lower and upper bounds, the idea behind the uncertainty budget stems from the improbability of all parameters simultaneously reaching one of their two extreme values. However, robust optimisation fails to provide a comprehensive hedging strategy, that can help guide near-term actions, like stochastic programming.

To keep the best of both worlds, i.e., stochastic programming and robust optimisation, we decided to investigate the RL approach, and its policy optimisation mechanism, to explore myopic transition pathways under uncertainties. Indeed, policy-making to transition a whole-energy system can be viewed as an iterative process of learning from policy implementation efforts, involving ongoing analysis of energy policy challenges and experimenting with various solutions [89]. RL exhibits two main advantages: its effectiveness in handling uncertainties and the model-free approach where an accurate representation of the real world is not needed to optimise the policy [90].

This section aims at presenting the general concepts of this approach. Then, its application to the myopic optimisation of a whole-energy system is introduced as well as the policy optimisation algorithm. Chapter 2 presents the input of the case study and Chapter 3 details the results of the GSA on the pathway model, the reader interested by the results of the RL-method is invited to go to Chapter 4.

1.3.1 Reinforcement Learning fundamentals and application to energy systems

RL is a subfield of machine learning focused on training an agent to make sequential decisions by interacting with an environment to achieve specific goals (see Figure 1.6). Unlike supervised learning, where data is labelled, and unsupervised learning, where patterns are inferred from unlabelled data, reinforcement learning deals with learning from interaction, typically through trial and error. This way, RL is considered as active learning [91]. Starting from an initial state, the agent takes an action that impacts its environment. The latter feeds back the agent with a reward and the new state. This goes on until the end of the episode. When the episode is done, the agent starts again from an initial state, takes an action and so on.

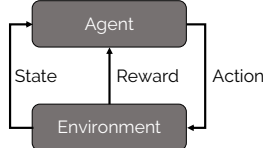


Figure 1.6. General concept of Reinforcement Learning (RL) as the interactions between the agent and its environment. The agent takes some action that has an impact on the environment which feeds back the agent with a reward and the new state. The objective of the agent is to optimise its policy, i.e., the mapping between the state it is at and the action to take, by maximising its cumulative reward.

The agent learns to optimise its policy by maximising the cumulative reward over time. This policy refers to the strategy or mapping from states to actions that the agent employs to make decisions. Essentially, it defines the behaviour of the agent in the environment. The ultimate goal of the agent is often to find an optimal policy, which maximises the expected cumulative reward over time. All these concepts and interactions between the agent and its environment are formalised as a Markov Decision Process (MDP) [92], represented by the tuple $\langle s, a, T, r, \pi, \gamma \rangle$. The Markov property of such a decision process states that a decision is made only based on this tuple and not on the history/path that has led to it. In this tuple, $s \in S$ is the state defined

in a certain state space, S , that represents the observable parts of the environment that the agent uses to make decisions; $a \in A$ is the action among the action space, A ; T is the probability of transitioning from one state s to another state s' given a specific action, a : $T(s, a, s') : \Pr(s'|s, a)$; r is the reward received by the agent when taking the action a from state s , $r(s, a)$; π is the policy telling the action to take depending on the current state and; γ is the discount factor that controls the importance of future rewards versus immediate rewards. During the learning/optimisation process, the agent acts according to the exploitation-exploration trade-off. In the exploitation, the action a is directly given by the mapping provided by the current policy π , depending on the state s . In the exploration, the action is randomly picked within the action space. For further information, the interested reader is invited to refer to the work of Sutton and Barto [92] or the course given by David Silver [93] available online.

Due to the increasing complexity of the systems and the integration of uncertainties, the last decades have seen the emergence of publications where RL is applied to energy systems [90, 91]. In their respective reviews, Cao et al. [91] and Perera and Kamalaruban [90] highlighted groups of problems addressed with RL in the research field of energy systems: building energy management system (BEMS), optimisation of dispatch and operational control closely linked with the energy market and the optimal power flow problem in the grid, micro-grid management, electro-mobility or even demand-side management or optimal control of energy system devices like maximum power point tracking (MPPT) of wind turbines and Photovoltaic (PV) panels. The major novelty of this thesis is the application of RL to a new kind of energy system problem: the optimisation of the transition pathway of a whole-energy system. In this sense, the objective is to optimise a policy to support this transition subject to uncertainties.

1.3.2 Problem formulation and algorithm

Before starting an episode, a sample of uncertain parameters is drawn and affects the environment, EnergyScope Pathway, according to the methodology detailed in Section 1.2.1. At the initial state, i.e., the energy system in 2020, the agent gets an initial observation, o_0 . An observation represents a set of the characteristics of the environment accessible to the agent for it to take the next action. The state, though, is the exhaustive list of these characteristics. Even though an observation is a subset of the state, this work uses these two words interchangeably. From this state, the agent takes a step: action, reward, and new state. The action, a_0 , impacts the environment, i.e., the energy system limited transition over the first decision window (2020-2030). Through this

interaction with its environment, the agent is given a reward, $r_1 = r(a_0|o_0)$, and ends up in a new state, i.e., the energy system in 2025, characterised by a new observation, o_1 , and so on (see Figure 1.7).

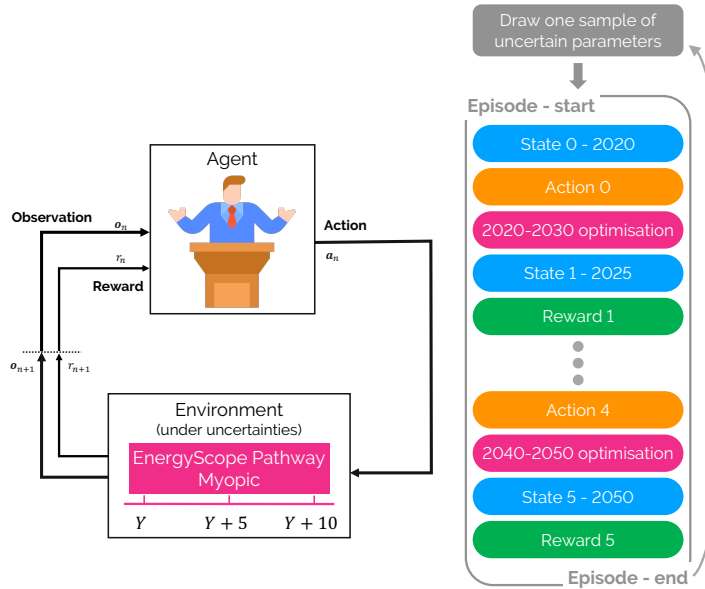


Figure 1.7. The Reinforcement Learning (RL) framework applied to the myopic optimisation of the energy transition pathway between 2020 and 2050. Here, the agent interacts with its environment, i.e., the energy-system model on a limited decision window of 10 years. At the beginning of each episode, one different sample of uncertain parameters is drawn and affects the environment, EnergyScope Pathway, according to the methodology detailed in Section 1.2.1.

A learning episode is a succession of such learning steps. In the context of the transition pathway between 2020 and 2050, an episode can come to an end for different reasons. First, if the actions taken by the agent make the optimisation infeasible, the episode is prematurely stopped before reaching 2050. Similarly, cumulative emissions of the system over the predefined CO₂ budget (see Section 2.5) lead to an anticipated end of the episode. Finally, the “natural” end is the prescribed end of the transition, i.e., 2050. Consequently, the maximum value of steps for an episode is equal to $N = 5$.

Before jumping to the choice of the learning algorithm, it is worth noting that we opted for the combination of RL with Deep Neural Network (DNN), called Deep Reinforcement Learning (DRL). Among others, one of the main drawbacks of traditional RL algorithms, i.e., without the use of Neural Network (NN), is that it suffers from the “curse of dimensionality” when facing problems with continuous action and state spaces (see Chapter 4). By approximating the state-action function with its parameters (i.e., weights and biases), DNN can address this difficulty.

Given the assumed absence of knowledge of the agent about the dynamics of the environment, i.e., its transition or reward functions, we needed a so-called “model-free” learning algorithm. In practice, in a model-free approach, the agent estimates the optimal policy directly from experience and without estimating the dynamics of the environment. However, model-free methods suffer from two major drawbacks: their sample inefficiency and their sensitivity concerning their hyper-parameters (e.g., learning rates, exploration constants) [94]. The former leads to a too-expensive computational burden while the second requires meticulous settings to get good results. To overcome these two challenges, we needed to choose between an “on-policy” or “off-policy” algorithm. In a nutshell, in on-policy learning, the agent learns the value function or policy based on the data it generates by following its current policy whereas, in off-policy, the agent can learn from data collected by any policy, not just the one it is currently following, which provides greater flexibility and potential for reusing data stored in the so-called replay buffer. This makes off-policy algorithms more data efficient and ensures better exploration by reusing past experiences or even following random exploration [94].

To optimise the mapping between the observations and the actions, the policy $\pi(a_n|o_n)$, an objective function, $J(\pi)$, is built on the cumulative rewards collected during each episode. Finally, a back-propagation process updates the weights and biases of the NN during the learning of the agent. Among the wide variety of RL algorithms applied in energy systems [90], this work opted for Soft Actor-Critic (SAC) [94] to train and update the NN. Like other actor-critic-based algorithms, SAC works with two NN in parallel: the actor learning the control policy and the critic judging the actor (see Figure 1.8).

SAC is a model-free and off-policy actor-critic deep RL algorithm based on the entropy-augmented objective function (see Equation (1.25)). The word “augmented” here is in opposition to the conventional RL objective function that is only based on the cumulative reward, i.e., the first term of Equation (1.25). In the RL context, entropy, also called “Shannon entropy”, stands for the randomness or stochasticity of the policy.

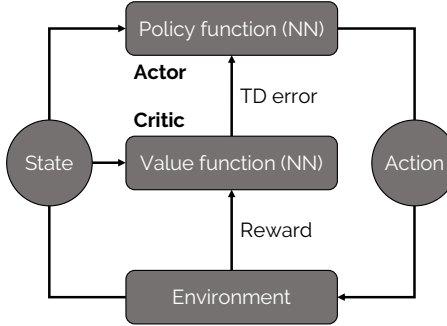


Figure 1.8. General concept of actor-critic-based algorithms. The two NN are trained against each other for the actor to improve the control policy and for the critic to provide a better judgement of the actor’s action via the temporal-difference (TD) error. Graph adapted from [91].

$$J(\pi) = \mathbb{E}_{\pi} \left[\sum_{n=0}^{N_{ep}} \gamma^n r_n(o_n, a_n) - \zeta \log(\pi(a_n|o_n)) \right], \quad (1.25)$$

where γ is the discount factor and ζ the temperature parameter. γ determines how much importance we want to give to future rewards within an episode. ζ balances the trade-off between the exploitation of proven actions via the return maximisation, i.e., $\sum_{n=0}^{N_{ep}} \gamma^n r_n(o_n, a_n)$, and the exploration through the entropy term, i.e., $\log(\pi(a_n|o_n))$. This way, SAC ensures sample efficiency while improving exploration [95] and robustness [96]. In their work, Haarnoja et al. [95] showed a lower sensitivity of SAC to hyper-parameters. These make SAC a state-of-the-art algorithm and one of the most efficient model-free deep RL methods nowadays [95]. In this thesis, we used the open-source SAC package developed by STABLE-BASELINES3 [97] where the policy NN is a fully connected multilayer perceptron (MLP) built with TENSORFLOW [98]. For further information on RL and the SAC algorithm, the interested reader is invited to refer to the works of Sutton and Barto [92] and Haarnoja et al. [94], respectively.

1.3.3 Discussion and guidelines for future researchers

Reinforcement Learning (RL) was found to be an appropriate approach to explore myopic transition pathways under uncertainties and assess the robustness of policies to support such pathways. As a novice user of a RL framework considering continuous action and state spaces, we would recommend opting for SAC as it is sample efficient,

ensures a wide exploration and has a low sensitivity to hyper-parameters [94]. Using the SAC package developed by STABLE-BASELINES3 allows a handy introduction to apply RL.

Besides the choice of the algorithm, most of the work when using a RL framework consists in properly defining the rules of the games following which the agent interacts with its environment: action, state and reward. These are defined and discussed in Chapter 4.

1.4 Robustness assessment via PCA

When optimising a transition pathway of a whole-energy system, including its uncertainties, capturing the variance of design (i.e., installed capacities of each technology) can become overwhelming due to the curse of dimensionality. For the case study detailed in Chapter 2, this consists of 113 possible technologies over 7 representative years. To tackle this challenge, we have developed a methodology based on the Principal Component Analysis (PCA). The philosophy behind this approach is to identify key combinations of design variables capturing most of the system variance, beyond the sole objective function, i.e., total transition cost, but without having to compare each design variable individually. This methodology provides two main outputs. First and foremost, using the model runs necessary to quantify the impact of the uncertain parameters on the total cost of the transition (see Section 1.2), it gives a metric on which to assess the robustness of different energy transition technological roadmaps. Where the total transition cost is a single value representing the entire system and analysing individually all technologies would be overwhelming, this metric gives the happy medium. Second, these “directions of variation” can highlight key modal shifts or highly varying design strategies over the transition. After introducing the general concept of PCA, this section aims to detail the methodology proposed to obtain these “directions of variation” and to assess the robustness of roadmaps. The reader interested in the results of the PCA-based method is invited to go to Chapter 5.

1.4.1 Principal Component Analysis: General concept

Born in the early 20th century, the Principal Component Analysis (PCA) finds its fundamentals in the Singular Value Decomposition (SVD) [99, 100]. SVD is a generalisation, to an arbitrary (i.e., not necessarily square) matrix, of the spectral theorem stating that a normal matrix can be diagonalised by an orthonormal basis of eigenvectors. The core concept of principal component analysis (PCA) involves simplifying the original

dataset with numerous interconnected variables by reducing its dimensionality while preserving as much variability within the data. This is accomplished by transforming the p -dimension data, \mathbf{x} , into a new set of variables called principal components (PCs), \mathbf{z} . These components are uncorrelated and arranged in such a way that the first ones retain the majority of the variability found in the original dataset. On the other hand, the final PCs pinpoint directions where there is minimal variation, indicating nearly constant linear relationships among the original variables [101].

The PCs are computed based on the covariance matrix of \mathbf{x} , Σ , where the diagonal of this matrix gives the variance of the i^{th} variable and the other elements give the covariance between the i^{th} and the j^{th} variables where $i \neq j$. Out of this matrix, α_k is the eigenvector of Σ corresponding to its k^{th} highest eigenvalue λ_k . These eigenvectors are orthogonal to each other so that they represent independent directions in the original feature space. These eigenvectors are also normalised such that $\alpha_k^T \alpha_k = 1$ [101], where T means the transpose vector. This makes it easier to interpret the relative importance of each principal component in explaining the variability of the data. Finally, this ensures a fair comparison between the original features. Without normalisation, variables with larger scales would dominate the principal components, potentially skewing the results and leading to misinterpretation of the principal components. In other words, given this normalisation, $\text{var}(z_k) = \lambda_k$, where $\text{var}(z_k)$ is the variance of z_k . Moreover, this means that the coefficient α_{ki} , i.e., the component of α_k related to the i^{th} original variable, x_i , gives its weight in the k^{th} PC, i.e., z_k . This PC captures λ_k variance of the original data. In other words, a high absolute value of α_{ki} means that x_i has a significant impact on the direction given by the k^{th} PC [102].

Easier to represent in two dimensions, let us consider a vector \mathbf{x} composed of the variables x_1 and x_2 , $p = 2$, and 25 realisations of them (See Figure 1.9).

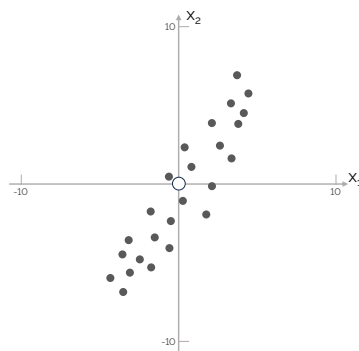


Figure 1.9. Original observations of a two-dimension dataset, x_1 and x_2 .

From these observations, the main objective of PCA is to find the linear combination, i.e., projection, of the original variables that maximise their spread, i.e., variance (see Figure 1.10). Another way to understand this is to look at the other side of the same coin. Indeed, PCA also looks for properties that allow reconstructing the original features as accurately as possible. In practice, it aims at minimising the total reconstruction error which is the average squared distance between the original observations and their respective projection.

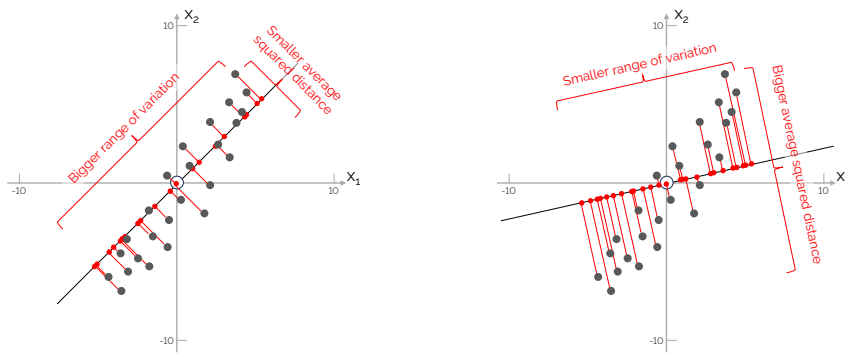


Figure 1.10. Two different projections (red dots) of the original observations (grey dots). The projection on the left captures a bigger variance than the projection on the right. At the same time, the average squared distance between the original observations and their respective projection is smaller for the projection on the left. Consequently, the left projection is closer than the right projection to be the first PC.

Mathematically, the first Principal Component (PC), z_1 , is a linear function, $\alpha_1^T \mathbf{x}$, of the different variables of \mathbf{x} with maximum variance:

$$z_1 = \sum_{j=1}^p \alpha_{1j} x_j = \alpha_1^T \mathbf{x} = \alpha_{11} x_1 + \alpha_{12} x_2. \quad (1.26)$$

Then, $z_2 = \alpha_2^T \mathbf{x}$, is another linear function of \mathbf{x} , uncorrelated with z_1 and capturing the remaining variance. These linear transformations can be seen as projection of the original data on the principal direction, i.e., PCs (see Figure 1.11).

In the general cases of p original variable, one can write $z_k = \alpha_k^T \mathbf{x}$ as the k^{th} PC. There can be up to p PCs even though, usually, most of the variance of the original data can be captured by m PCs where $m \ll p$. The interested reader is invited to refer to the work of Jolliffe [101] for further mathematical demonstrations, information and examples.

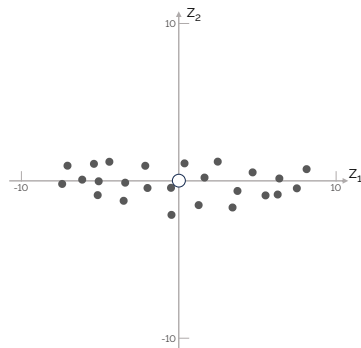


Figure 1.11. Projection of the original observations with respect to their PCs. The variation of the realisations was more significant in the direction of x_2 than x_1 . Once projected with respect to their PCs, the variation is even more significant in the direction of z_1 than in either of the original variables, as it captures most of their variance.

1.4.2 Principal components of the transition

As introduced, the objective is to define the main technological drivers of the variation through the transition to 2050 subject to uncertainties. To do so, before calculating the PCs of the transition, three preliminary steps are necessary: (i) selection of the right data, (ii) data scaling and, (iii) outliers management. Like any other dimension-reduction process, PCA has to be supplied with relevant data to reach the stated objective. Like the normalisation of the eigenvectors (see Section 1.4.1), data scaling is fundamental to compare features having potentially different units and/or orders of magnitude. Then, properly handling the outliers allows for reaching the relevant level of metric between the too-vague information of the sole total transition cost and too many details hidden in the peculiar/outlying cases. After this preprocessing, PCs can be computed for each of the representative years of the transition. Finally, PCs that indicate similar directions in different years are averaged into one single PC of transition. The different PCs of transition give a bigger picture over the whole transition.

Data selection

To characterise the variations of design within the transition under uncertainties, we have focused on the installed capacities, $\mathbf{F}(y, j)$ for all $y \in \text{YEARS}$ and $j \in \text{TECH}$ (see Equation (1.14)). Even though these represent only the design part of the result of the optimisation, focusing on the installed capacities gives direct information regarding

the required capital investments (see Equation (1.2)) and, more indirectly, the operation. In other words, it captures the technological landscape of the transition. Having defined the type of variable to consider, we need to assemble a relevant dataset. This is given by the runs to quantify the impact of the uncertain parameters on the total cost of transition required by the method described in Section 1.2. Overall, the original dataset is $\mathbf{x}(y, j, s)$ where, on top of y and j previously defined, $s \in [1, 2, \dots, S]$ stands for the sample number of the uncertainty quantification method. For the investigated case detailed in Chapter 3, this represents $S = 1260$ samples resulting from the perfect foresight optimisation of the transition pathway under uncertainties. Appendix D.3 gives the distribution of the installed capacities among the different end-use sectors from the GSA. Finally, among the seven representative years of the transition, we do not consider 2020 as it is the initialisation year for which the design of the system is fixed, to be representative of the actual design that was in place in Belgium in 2020 (see Appendix C.1). In other words, we focus here only on the years 2025, 2030, 2035, 2040, 2045 and 2050. This gives the whole dataset considered in this PCA (see Figure 1.12).

| Sample _s | TECH ₁ | TECH ₂ | TECH ₃ | ... | TECH _p |
|---------------------|---------------------|---------------------|---------------------|-----|---------------------|
| 2025 | | | | | |
| 2030 | | | | | |
| Sample ₂ | TECH ₁ | TECH ₂ | TECH ₃ | ... | TECH _p |
| Sample ₁ | TECH ₁ | TECH ₂ | TECH ₃ | ... | TECH _p |
| 2025 | F _{1,2025} | F _{2,2025} | F _{3,2025} | ... | F _{p,2025} |
| 2030 | F _{1,2030} | F _{2,2030} | F _{3,2030} | ... | F _{p,2030} |
| 2035 | F _{1,2035} | F _{2,2035} | F _{3,2035} | ... | F _{p,2035} |
| 2040 | F _{1,2040} | F _{2,2040} | F _{3,2040} | ... | F _{p,2040} |
| 2045 | F _{1,2045} | F _{2,2045} | F _{3,2045} | ... | F _{p,2045} |
| 2050 | F _{1,2050} | F _{2,2050} | F _{3,2050} | ... | F _{p,2050} |

Figure 1.12. Original raw data considered in the Principal Component Analysis (PCA) of the variation of the design strategy through the transition, $\mathbf{x}(y, j, s)$, accounting for the p possible technologies to install.

Data scaling

Preprocessing the dataset before employing a method to reduce dimensionality, like PCA, can greatly affect the structure of the simplified representation and the characteristics of the features extracted from the dataset [103, 104]. Scaling the original raw data via normalisation, i.e., reducing data to $[0, 1]$ interval has a double purpose: to

assess variables (i) representing different sorts of features, with different units (e.g., installed capacity of electricity and mobility technologies) and, (ii) ranging over the different orders of magnitude (e.g., installed capacity of private and public mobility) (see Appendix C.1). Consequently, the first part of this data preprocessing consists in scaling the installed capacities versus their respective sector and representative year (see Equation (1.27)). The sectors, as defined in EnergyScope, are the electricity, High-Temperature (HT) heat, Low-Temperature (LT) heat, passenger mobility, freight mobility, NED, storage and infrastructures. For instance, the installed capacity of PV panels in the year y of the sample s is scaled by the maximum installed capacity in the electricity sector in the year y among all the samples.

$$\mathbf{x}^*(y, j, s) = \frac{\mathbf{x}(y, j, s)}{\max_{sec, y}(\mathbf{x}(y, j, s))} \quad \forall y \in YEARS, sec \in SECTORS \quad (1.27)$$

Then, to give “directions/metrics” representative of the size of each sector within the energy system, we added another weight based on the relative share of commodities produced by each sector. For the case study of Belgium detailed in Chapter 2, this gives a higher weight to electricity and low-temperature heat sectors (see Figure 1.13).

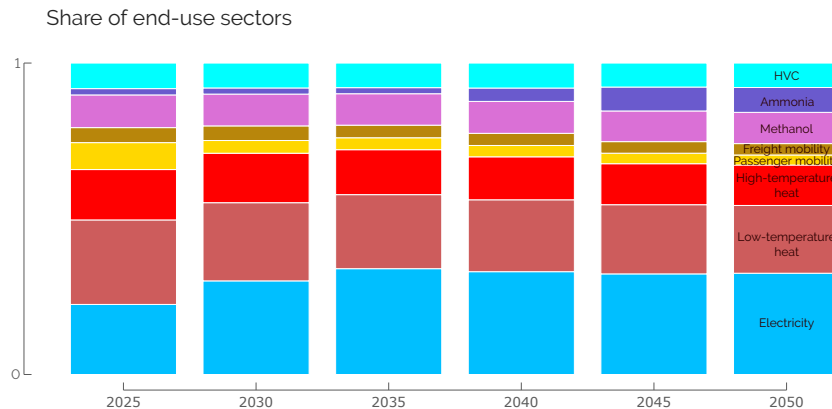


Figure 1.13. Multiplying factors for each of the end-use sectors in the case of the Belgian energy transition. These shares are based on the results of the reference scenario (REF) where nominal values are considered for the uncertain parameters and the transition is optimised through the perfect foresight approach. Over the transition, sectors like electricity (i.e., from 22% in 2025 to 33% in 2050) or ammonia (i.e., from 2% to 8%) become more important due to sector coupling, e.g., e-mobility or ammonia-CCGT.

To do so, we have arbitrarily considered these shares from the REF case, where the pathway is optimised according to the perfect foresight approach and considering all the uncertain parameters to their nominal values (see Chapter 3). The end-use-demands as well as the commodity produced for the sector coupling are based on the results of this deterministic REF case. For instance, the share of the electricity sector accounts for its EUD and the electricity produced to supply other sectors (e.g., heat, mobility). Finally, to compare apples with apples, we converted the EUD in the mobility sectors, i.e., passenger and freight, into the Final Energy Consumed (FEC) they require in the REF case. This gives the second weighing factors to scale data, on top of the ones of Equation (1.27), see Equation (1.28).

$$\mathbf{x}^{**}(y, j, s) = \mathbf{x}^*(y, j, s) \cdot \text{share}_{\text{EUD}}(y, sec) \quad \forall y \in \text{YEARS}, sec \in \text{SECTORS} \quad (1.28)$$

One can notice that this second scaling factor omits the infrastructure and storage technologies. In the process of defining “metrics” to assess the robustness of a roadmap for the case of Belgium, this has a negligible impact. Indeed, the variation of the installed capacity of these technologies is either limited compared to end-use-type (EUT) technologies, i.e., limiting their influence in the definition of PCs, or directly linked to these EUT technologies. For instance, District Heating Network (DHN) installed capacity is directly proportional to technologies producing LT heat in DHN or the additional capacity of the grid is caused by additional capacities of VRES.

Outliers management

Handling outliers is one of the biggest challenges in data science [105]. These are defined as data points differing significantly from the rest of the data set. Being extreme values, outliers influence the overall dataset variance and, consequently, rotate the PC directions towards them [106]. In the context of PCA, outliers could be defined as “model fit outliers” as their presence influences the fit of the model. There are several techniques to detect/define and handle the outliers [105]. In this work, detection is performed via the box plot technique, as outliers are identified as those points lying beyond the plot’s whiskers, or fences. These whiskers are themselves constructed as being 1.5 times the Interquartile Range (IQR) ($Q_3 - Q_1$) higher or lower than the third (Q_3) or first quartile (Q_1), respectively (see Figure 1.14). Therefore, the installed capacity of a technology in the

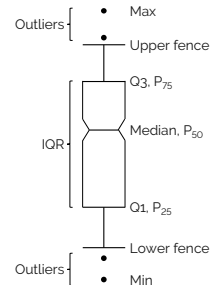


Figure 1.14

year y of the sample s is defined as an outlier if it falls out of this range compared to the dataset for this specific technology and year. There exist several techniques to handle these outliers depending on their nature or the method used to identify them. Since all the data points correspond to a result provided by the optimisation, we have decided to keep these points but carry out a “modification” of them [105]. In practice, the value of “high outliers” or “low outliers” is set to the upper or lower fence, respectively. In practice, this modification narrows the variation range of features presenting outliers and, consequently, reduces their weight in the different PCs.

Principal components of each representative year

Now that data are selected and preprocessed, principal components are first computed for each representative year separately, using the Python package PCA from SKLEARN.DECOMPOSITION. As explained in Section 1.4.1, the number of PCs per year to retain can go up to the number of considered variables (i.e., 73 in our case study²) which is intractable. Moreover, the first PCs keep track of most of the variance of the system whereas the last ones present a smaller interest. Choosing the appropriate threshold involves a trade-off. Retaining too few principal components may result in loss of important information, while retaining too many may lead to unclear analysis. For each of the representative years of the transition (except 2020), we compute the PCs that capture 90% of the total variance of this year [101]. At the end of this step, a list of m PCs is obtained, i.e., $\text{PC}_{y,i}$ where y stands for the representative year between 2025 and 2050 and

$$\sum_{i=0}^m \text{var}(\text{PC}_{y,i}) \geq 90\% \sum_{i=0}^p \text{var}(\text{PC}_{y,i}) \quad \forall y \in \text{YEARS}, \quad (1.29)$$

where m is presumably different for each representative year and p is the total number of variables, hence the maximum number of PCs. For the entire transition, it gives a total of $M = 34$ $\text{PC}_{y,i}$.

Principal components of the transition

The final step consists in defining metrics on the whole transition based on the $\text{PC}_{y,i}$ computed for each representative year, separately. To do so, all the $\text{PC}_{y,i}$ from every year are sorted together in a descending order based on their respective variance. Then, starting with the one with the highest absolute variance, all the other $\text{PC}_{y,i}$ similar to

²73 technologies out of the 113 in total as we do not consider the 15 infrastructure technologies or the 25 storage technologies.

it are clustered together. The similarity between two PCs is defined according to the cosine similarity approach, especially appropriate in high-dimensional positive spaces [107]. Indeed, as detailed in Section 1.4.1, a PC represents a vector for which the components are related to each variable of interest. Therefore, in this work, PCs are considered similar if their cosine similarity, $S_C(A, B)$, is either greater or equal to 90% or lower or equal to -90% (see Equation (1.30)). It is important to consider the second case as PCA gives the magnitude of variation within the original feature space via the components of the eigenvectors, regardless of the direction of these vectors. For instance, in a two-dimension original space, if the first PC has $(\sqrt{2}/2; \sqrt{2}/2)$ as an eigenvector, this could also be $(-\sqrt{2}/2; -\sqrt{2}/2)$. The second vector being the opposite of the first, they are considered PCA-wise equivalent.

$$S_C(A, B) := \cos(\theta) = \frac{\mathbf{A} \cdot \mathbf{B}}{\|\mathbf{A}\| \|\mathbf{B}\|} = \frac{\sum_{i=1}^n A_i B_i}{\sqrt{\sum_{i=1}^n A_i^2} \cdot \sqrt{\sum_{i=1}^n B_i^2}} \geq 90\% \text{ or } \leq -90\%, \quad (1.30)$$

where A and B represent two different PCs. The components of these similar PCs are then averaged to form the first PC of the transition, $\text{PC}_{\text{transition},1}$. Then, the process repeats with the next $\text{PC}_{y,i}$ with the highest absolute variance but that has not been integrated in the construction of $\text{PC}_{\text{transition},1}$, to form $\text{PC}_{\text{transition},2}$. This goes on until the sum of the absolute variance of the N $\text{PC}_{y,i}$ used to construct these $\text{PC}_{\text{transition}}$ is greater or equal to $\alpha\%$ of the sum of the absolute variance of all the M $\text{PC}_{y,i}$, i.e., the “total transition variance”, generated at the previous step:

$$\sum_{i=0}^N \text{var}(\text{PC}_{y,i}) \geq \alpha \% \sum_{i=0}^M \text{var}(\text{PC}_{y,i}) \quad (1.31)$$

In our case, we have decided to set the value of α to 85% as, beyond this value, the marginal gain of captured variance becomes too “costly” in terms of the number of $\text{PC}_{\text{transition}}$, i.e., the level of details, to account for (see Figure 1.15). Besides being the metrics to assess the robustness of roadmaps, these $\text{PC}_{\text{transition}}$ also point out the technologies that are more sensitive to uncertainties and are more likely to impact the overall variance of the transition design.

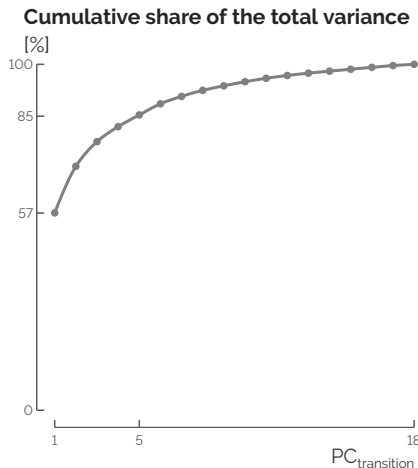


Figure 1.15. Cumulative share of the sum of the transition variance versus the number of $PC_{\text{transition}}$. Passing a certain threshold, here 85%, the number of $PC_{\text{transition}}$ to consider increases significantly compared to the share of transition variance that they capture.

Robustness assessment of roadmaps

In their analysis, Moret et al. [39] assessed the additional capacities after the realisation of uncertainties, the so-called *possibility of recourse* [83]. These adaptations from the initial investments lead to overcapacity where assets are built but not used because the values taken by uncertain parameters make them cost-inefficient. To address the same question of overcapacity in the context of the energy transition pathway with progressively revealed uncertainties, we have adapted the method of Moret et al. [39] (see Figure 1.16). Roadmaps are defined by setting minimal installed capacities based on the results of different transition pathway optimisations. The $PC_{\text{transition}}$ are the metrics on which the results from the myopic pathway optimisation subject to minimal installed capacities set by these roadmaps are projected.

In conclusion, a roadmap would be defined as more robust than another one if the projection of its myopic runs on the different $PC_{\text{transition}}$ spans on a more narrow range (see Figure 1.17). The bounds of this “range of projection” are computed as the mean, μ , of the projected data \pm a 95% confidence level, CL, on the margin of error, MOE:

$$\text{range of projection} = [\mu - \text{MOE}; \mu + \text{MOE}],$$

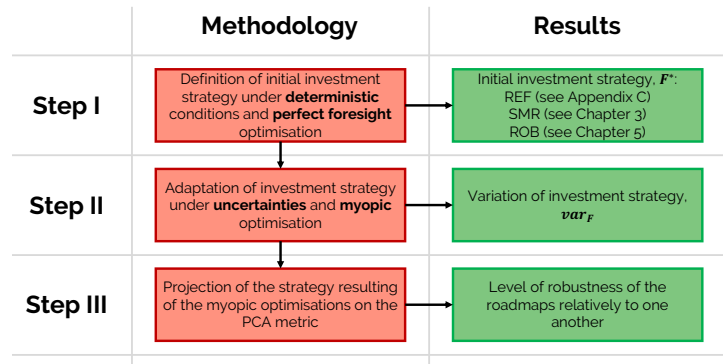


Figure 1.16. Overview of the three-step methodology to assess the robustness of roadmaps. Schematic adapted from [39].

where the margin of error, MOE, is computed thanks to the standard error of the mean, SEM, and assuming a Student's, distribution, t, of the N projected data:

$$\text{MOE} = \text{SEM} \cdot \text{PPF}_t((1 + \text{CL})/2, N - 1),$$

where PPF_t is the per cent point function (i.e., the inverse of cumulative distribution function) of the Student's distribution. It is the range over which the distribution spans, $2 \cdot \text{MOE}$, that matters to characterise the variability of the projections of a roadmap. Indeed, as $\mathbf{PC}_{\text{transition}}$ are vectors composed of positive and negative coefficients, the average position of the distribution, μ , does not bring insight into the robustness of a roadmap.

1.4.3 Discussion and guidelines for future researchers

Principal Component Analysis (PCA) was found to be an appropriate method to provide a metric that captures a major part of the system design variance through the transition while keeping the amount of information to a “graspable” level of detail. Besides selecting the installed capacities of end-use-type categories (electricity, heat, mobility and non-energy), one could discuss the scaling of these data and the management of the outliers. Where scaling the data is fundamental before computing the PCs, future researchers could adapt the scaling factor. To avoid singularities in our PCs, we have decided *a posteriori* to put high and low outliers to the upper and lower fences, respectively. However, before managing the outliers, we would recommend to keep them and assess the provided results in terms of the number of PCs and the key technologies that characterise them.

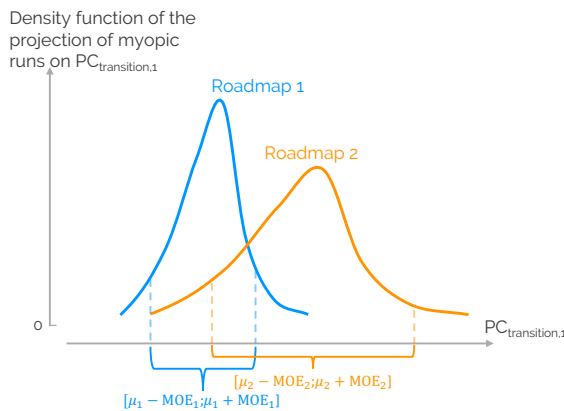


Figure 1.17. Projection on the first PC of the transition, $PC_{transition,1}$, of the different myopic runs under uncertainties based on different roadmaps. Given that the distribution resulting from roadmap 1 spans over a more narrow range of this PC of the transition, we conclude that this roadmap is more robust than roadmap 2 according to the direction of variation described by $PC_{transition,1}$.

Finally, we have assumed thresholds to limit the number of principal components of each representative year, PC_y (90%), the similarity between two of these PC_y (90%) and to limit the number of $PC_{texttransition}$ (85%). These thresholds have been defined based on good practices discussed in the literature and *a posteriori* observations specific to our case study. We would recommend starting with these values and adapting them in a second time if needed to increase or decrease the level of detail captured by the PCs.

Chapter 2

Case study: the Belgian energy system

“Ils vont le faire!”

Philippe Albert, during Belgium-Japan FIFA World Cup round of 16, 2018

As detailed by Limpens et al. [40], the analysis carried out in this work can be applied to any regional whole-energy system. As a densely-populated and highly-industrialised country with limited local renewable potentials (i.e., mainly solar and wind representing up to 50% of the primary mix by 2050), the transition of Belgium from a fossil-dominated system in 2020 (Appendix C.1) to carbon neutrality in 2050 makes it an intricate case study. Moreover, this case study and the subsequent analyses can be transferred - to some extent - to other industrialised countries highly dependent on fossil fuels with limited local renewable potentials (e.g., the Netherlands or Germany) [108]. This chapter presents the different demands to satisfy, with a particular focus on the non-energy demand, as well as the resources available and the conversion technologies to supply these demands. For a comprehensive understanding and detailed descriptions of the technologies, please refer to the documentation [54]. Then, the uncertainty ranges considered for some of the parameters are detailed. Finally, the CO₂ budget over the 2020-2050 transition is presented.

Contributions

First, as pointed out by Rixhon et al. [109], where most of the studies assessing whole-energy systems integrate energy demands (i.e., electricity, heat and mobility), the Non-energy Demand (NED) is often not considered. The latter is defined as ‘*energy products used as raw materials in the different sectors; that is not consumed as a fuel or*

transformed into another fuel [110]. The previous analyses carried out with EnergyScope Typical Days (ESTD) considered the non-energy demand as the related primary energy needs, i.e., either natural gas or Light Fuel Oil (LFO). To minimise the total cost of the system, the model simply selected the cheapest between the two resources (i.e., natural gas). This work goes one step further and accounts for the NED as a demand for three commodities (i.e., High-Value Chemicals (HVC), ammonia and methanol) as well as the associated production technologies. This allows bringing the non-energy sector to a similar level of detail as the other sectors. Keeping the same methodology to define EUD in EnergyScope as Limpens et al. [44], this work considers updated values given the latest release of the “EU reference scenario 2020: energy, transport and GHG emissions: Trends to 2050” by the European Commission [111].

Second, given the focus of this work on the electrofuels, the case study includes a more detailed representation of them: where the previous definition of the case study considered only renewable hydrogen and methane [41], now, e-ammonia and e-methanol (as well as their fossil-based equivalents), are implemented in the case study. As detailed later on, these electrofuels are considered renewable in the sense that their GWP is zero. This more detailed representation of the molecules themselves also comes with a more exhaustive integration of the ways to produce and use them in the system. For instance, considering the case of ammonia, on the top of the import routes, on the one hand, the Haber-Bosch process is accounted for to supply this molecule. On the other hand, ammonia-driven CCGT or ammonia-cracking-to-hydrogen are included as ways to consume it.

Third, where previous works considered a prescribed CO₂ trajectory to reach carbon neutrality by 2050 [40, 41], the case study analysed in this thesis is subject to a CO₂ budget for the transition, i.e., limiting the total amount of emissions over the transition. Based on the estimated world budget provided by the Intergovernmental Panel on Climate Change (IPCC) to limit the global warming to +1.5°C above pre-industrial levels by the end of the century, the grandfathering approach has been used to allocate part of this budget to the Belgian energy transition.

Fourth, as nuclear energy could be a real game-changer in the energy transition worldwide [112], and especially in Belgium, this thesis has integrated the uncertain decision to install SMR from 2040 onward.

Finally, this work includes updated values for some parameters compared to the work of Limpens [41]. The main change concerns the cost and performance of private mobility vehicles, which is a key component in the European [113] and Belgian [114] energy transitions. Based on the work of the National Research Council [115], Limpens [41] excessively favoured Fuel Cell (FC) car versus Battery Electric Vehicles

(BEV). In previous works [41, 49], despite their lower efficiencies (i.e., about 50% less efficient), FC cars had the bigger share of private mobility compared to battery electric vehicles(BEV) given the higher CAPEX (i.e., up to 10% more expensive) and limited range (i.e., 24kWh battery) of the latter. In these works, the more limited potential to import electricity from abroad and to produce it locally via VRES forced the model to electrify the low-temperature heat sector rather than the private mobility running on supposedly infinitely available renewable hydrogen. To align with other similar works on the modelling of whole-energy systems [111, 116], the CAPEX and efficiency of fuel cell cars have been increased. Regarding BEV, while the CAPEX has been kept unchanged, the efficiency and the battery capacity have been increased. As seen in the results, this change of data made BEV often more competitive than its hydrogen-based equivalent.

2.1 End-use demands

End-use demands, exogenously imposed as inputs to the model, are characterised by yearly quantities to satisfy and are also distributed over the different hours of each representative year of the transition, to account for their daily or seasonal variability [41, 44]. In this work, the yearly end-use demands (EUD) for all sectors are calculated from the forecast proposed by the European Commission for Belgium (Appendix 2 in report [111]).

2.1.1 Non-energy demand

The NED currently represents around 20% of the final energy consumption in Belgium [117]. This section summarises the rationale for adding a higher level of detail to the NED compared to what was done in the previous version of the case study [41]. Then, it explains the methodology used to quantify this demand.

Definition and historical trend

The NED can be split into four main categories of final molecules [118]: (i) HVC (worldwide production of $\sim 365\text{Mt/year}$, equivalent to $\sim 4770\text{TWh/year}$); (ii) ammonia ($\sim 185\text{Mt/year}$, equivalent to $\sim 964\text{TWh/year}$); (iii) methanol ($\sim 100\text{Mt/year}$, equivalent to $\sim 540\text{TWh/year}$) and (iv) the other products. HVC gather the light olefins (e.g. ethylene, propylene) and aromatics (benzene, toluene, xylene – BTX), mainly for the production of plastics, synthetic fibres or rubber. Their production today relies mainly on petroleum products such as naphtha, ethane or liquified petroleum gas. Ammonia is

mainly used for the production of fertilizers (~80% of global ammonia consumption). Its production is dominated by fossil gas via steam methane reforming to produce hydrogen, used as feedstock in the Haber-Bosch process. Methanol is mainly converted to formaldehyde (resin) but is also used for the production of other chemicals (e.g. solvents and gasoline-blends). Currently, its synthesis, like ammonia, is mainly relying on natural gas via steam methane reforming. Finally, the other products gather all chemicals not mentioned in the other categories such as bitumen, lubricants and other heavy products from oil refineries [119].

Over the recent history, there has been a relatively constant share of three main categories of the final consumption for non-energy use in Belgium [120] (see Figure 2.1): (i) naphtha and Liquefied Petroleum Gas (LPG) (between 59% and 67% of the total final consumption, around 59.4 TWh in 2019), (ii) fossil gas (between 9% and 14%, 11.8 TWh in 2019), and (iii) others (i.e., bitumen, coal tar and other oil products) (between 21% and 28%).

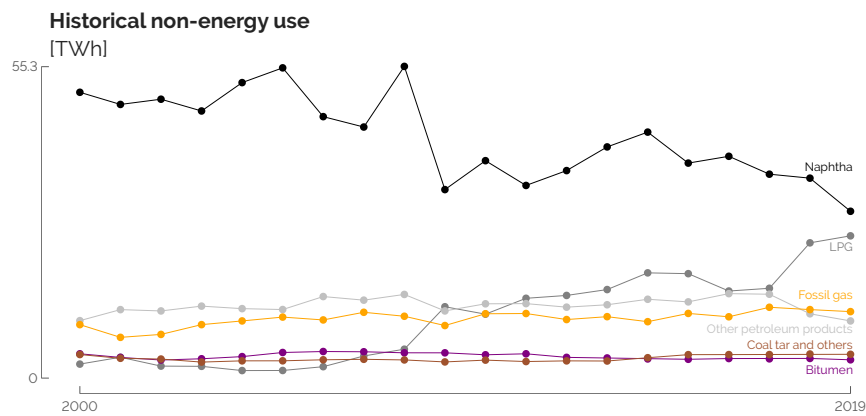


Figure 2.1. Historical data for the non-energy use in Belgium [120]. “Other oil products” account for tar and sulphur. This group also includes by-products of the oil-refining industry like aromatics (e.g., Benzene, Toluene and Xylene (BTX)) and olefins (e.g., propylene). Graph adapted from [121].

Naphtha and LPG are consumed in a naphtha cracker, which results in ethylene and propylene, which will be considered as HVC in the rest of this work. Similarly, fossil gas, as a non-energy carrier, is used in steam methane reformers to produce the required hydrogen for the synthesis of ammonia. The small shares of bitumen and coal tar are used for roadworks and to produce synthetic gas through gasification, respectively. Finally “other oil products” take into account, indistinguishably, tar and

sulphur as well as by-products of the refineries (e.g., Benzene, Toluene and Xylene (BTX)). About methanol, there is currently no production plant in Belgium even if the country plays a role in trading this commodity between its neighbouring countries and consumes part of what it imports.

Methodology of quantification

The non-energy demand studied in this work focuses on the chemical industry (more than 90% of the non-energy use in Belgium) and, similarly to other studies [118, 119], is split between the three aforementioned main groups of products (i.e., HVC, ammonia and methanol). Before describing these three demands, this study excludes bitumen, coal tar and “other oil products”. The first two represent marginal shares of the current non-energy use (i.e., 4% and 5% respectively) in such a way that they should not affect the conclusions. As described previously, the latest are mostly by-products from refineries that the system uses because they are available. However, in a perspective of defossilisation, since the future of fossil-based refineries is unclear, they have not been implemented in this study nor their by-products.

Regarding HVC, the future of their production is highly uncertain. Because of the new regulations and strategies promoting recycling and limitation of single-use plastics [122]. Besides this uncertainty, Belgium remains a major exporter as approximately 2/3 of plastic raw materials produced locally are exported abroad [123]. Even if a significant part of HVC produced in Belgium is not locally consumed, this demand has been set based on the assumption that Belgium will keep its industrial activity in this sector. In other words, we do not deduce the part of local production of HVC being then exported (and not consumed locally), unlike ammonia and methanol, which will be more traded commodities in the future (as energy carriers and non-energy products). Therefore, the actual demand for HVC is inferred from the consumption of naphtha and LPG as non-energy use as well as energy carriers in the chemical and petrochemical industries [120]. This assumption is based on the fact that, in the conversion processes to produce HVC from naphtha or LPG, these fuels also serve as energy carrier to supply the processes themselves. Then, given the respective efficiencies ($1.83t_{naphtha}/t_{HVC}$ and $1.67t_{LPG}/t_{HVC}$) [118], the current yearly demand of HVC is estimated equal to 3069 kt, without making distinctions between the different chemicals (i.e., ethylene, propylene and BTX).

The ammonia sector in Belgium is quite different: the country locally produces and imports ammonia much more than it exports it. Thanks to a database from the United Nations [124] and the National Bank of Belgium, it has been identified that, over the last ten years, Belgium, on average, has imported 1010 kt of ammonia, exported 105 kt

and locally produced 990 kt per year. Therefore, on top of the local production, the net import (i.e., import minus export) is also included in this non-energy demand. This gives a current yearly demand of 1895 kt of ammonia.

Concerning the demand for methanol, similarly to ammonia, this work solely considers the net imports as there is no local production in Belgium. To define the actual non-energy demand for methanol, only a 51%-share of this net import is kept since, according to the Methanol Institute and Methanol Market Services Asia (MMSA), this share is used for formaldehyde production in Belgium [125]. Currently, the rest of the methanol is used for energy purposes, mostly as Methyl Tert-butyl Ether (MTBE) in gasoline blending. This methodology gives a current yearly non-energy demand of methanol of 269 kt.

Eventually, after converting these masses of products into energy contents (i.e., LHV: HVC - 47 MJ/kg, ammonia - 18.8 MJ/kg and methanol - 19.9 MJ/kg), we assume that the current shares of each of the three commodities (i.e., 77.9%, 19.2% and 2.9% for HVC, ammonia and methanol, respectively) are supposed to remain unchanged over the transition.

2.1.2 Forecast of the demands over the transition

In its latest report [111], the European Commission forecasts a significant and abrupt increase of the NED compared to their previous report [57], i.e., +80% over the 2020-2030 time window. Given this discrepancy that is unsubstantiated and specific to the case of Belgium, the evolution trend of the NED of the current work has been inferred from the previous edition, published in 2016, [57]. Between 2020 and 2050, one observes a noteworthy increase in the electricity (+40%), passenger (+45%) and freight mobility (+35%) demands (see Figure 2.2). The rise of the non-energy demand is more limited, i.e., +6%, whereas the heating demands is forecast to decrease: -11% for the low-temperature heat demand and -3% for the high-temperature heat demand. This is explained by a better insulation of buildings and an improved efficiency of industrial processes. The top-right graph of Figure 2.2 is the aggregation of the same data as in the top-left graph but per economic sector, rather than per energy sector, with the non-energy demand being associated with the industry. This illustrates how industrialised Belgium is, compared to households and services, and, consequently, highly energy-intensive. The bottom graph of Figure 2.2 gives the passenger and the freight mobility. The sharp increase from 2020 to 2025 is due to the COVID-crisis that led to significantly reduced demands in 2020. As far as the hourly discretisation of these demands is concerned, time series are based on historical values of 2015 for the fluc-

tuating parts of electricity and low-temperature heating demands [44]. A daily time series is used for passenger mobility and applied similarly to every day of the year. Finally, for the other demands (i.e., high-temperature heat, freight mobility, NED and the share of electricity and low-temperature heat demands that are considered constant over the year), the yearly demand is distributed uniformly over the different hours of the year.

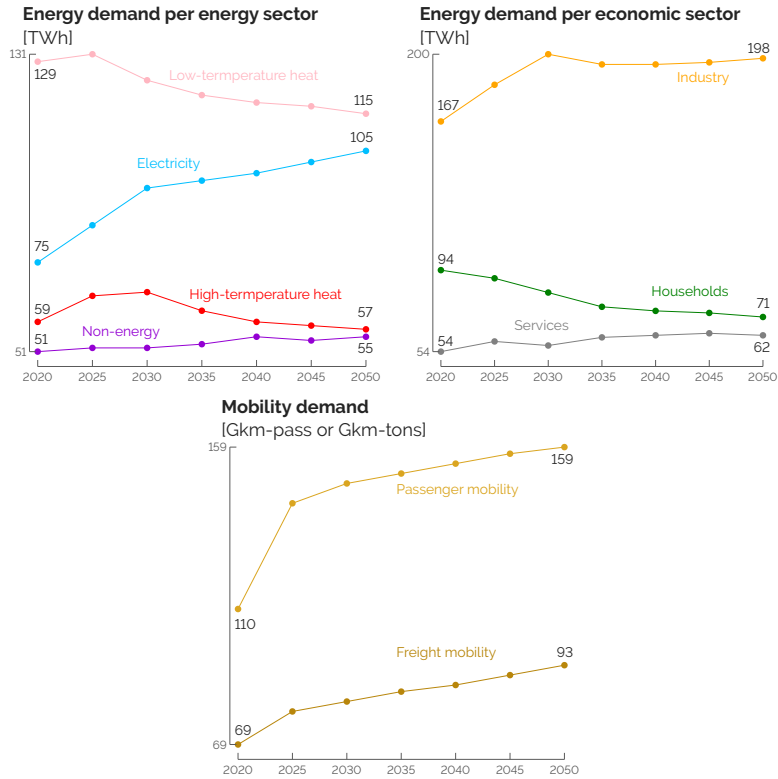


Figure 2.2. EnergyScope splits the whole-energy system end-use demands (EUD) into two sets: (non)-energy and transport-related. This figure presents the yearly values of each of these demands. In the top-right graph, the non-energy demand has been fully associated with the industrial demand. This highlights the significant level of industrialisation of Belgium compared to the other sectors.

2.2 Resources

To supply the aforementioned demands, EnergyScope Pathway implements a variety of resources defined by their cost of purchasing, c_{op} (see Figure 2.3), their availability, as well as their global warming potential, gwp_{op} , as detailed by Limpens et al. [40]. Regarding the cost of “renewable electrofuels”, they are in line with the recent study of Genge et al. [126] who carried out an extensive review and “meta-analysis [127, 128] of 30 studies on the supply costs of chemical energy carriers”.

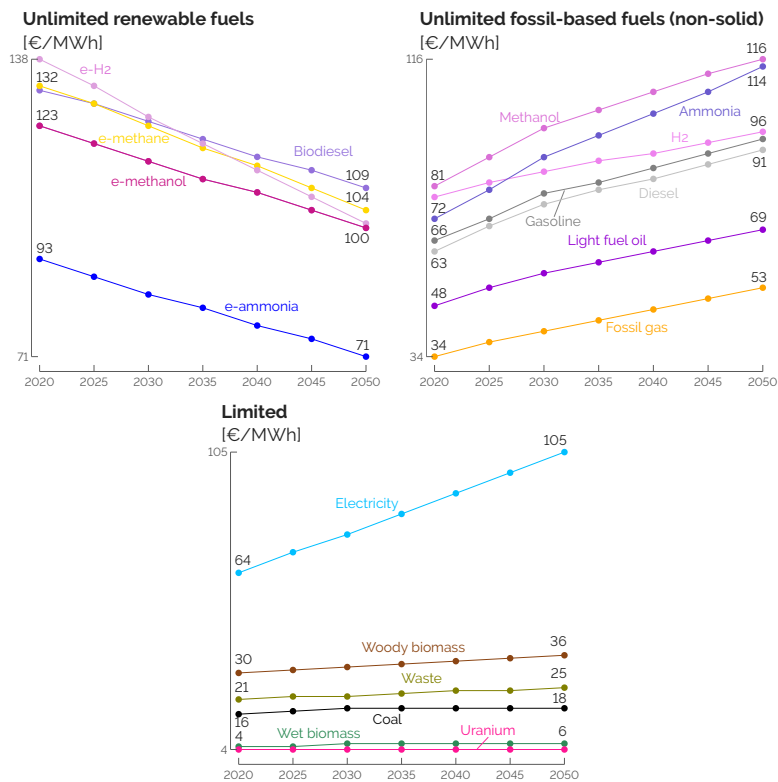


Figure 2.3. Cost of purchasing the different resources. Besides the free local renewables (i.e., sun, wind and hydro) limited by technical potentials, EnergyScope accounts for renewable energy carriers and their respective fossil counterparts (top-left and top-right). These fuels can be imported from abroad without limitation on their availability. Other carriers are limited either by their local potentials (i.e., biomass and waste) or other considerations like the power grid interconnections or the capacity of nuclear power plants.

Regarding the imported renewable electrofuels, the Hydrogen Import Coalition [73] has carried out an extensive techno-economic analysis to estimate their respective cost of purchasing, after having identified some key locations from which importing these energy carriers (e.g., Chile, Australia or Morocco). As the amount to import from each of these locations is hard to forecast, the current work considers the average cost between the different locations.

Besides the costs, the resources are either limited or unlimited in terms of availability and either renewable or not. The limitation in terms of availability can be direct or indirect. On the one hand, woody (23.4 TWh) and wet biomass (38.9 TWh) are directly limited by their local potentials and the consumption of waste (17.8 TWh) and coal (33.4 TWh) is assumed not to exceed the current use. Similarly to Limpens [41], we constrained the endogenous non-renewable wastes to be consumed locally. The local potential of biomass, i.e., about 60 TWh in total, could be considered as optimistic given the work of Colla et al. [129] limiting this potential to about 40 TWh. On the other hand, wind, solar, hydro and uranium are limited by the technical potentials of rooftop PV panels (59.2 GW), onshore (10 GW) and offshore (6 GW) wind turbines, run-of-the-river power plants (0.1 GW) and the choice to limit nuclear power plants to 6 GW, respectively. In line with the work of EnergyVille [130] and the maximum capacity of conventional nuclear reactors that have been installed in Belgium, the same 6 GW are assumed to be the maximum capacity for SMR. Imported electricity is limited in two ways: the potential of instantaneous capacity of interconnection with neighbouring countries (i.e., 11.9 GW by 2050 [131]) and a limitation to 30% of the yearly electricity end-use demand (i.e., 32.4 TWh by 2050) [41].

Regarding the power grid interconnections with the neighbouring countries, similarly to the import of other energy carriers, there is no representation of those physical routes. The imported energy commodities are available “at the front door” of the system. In terms of spatial resolution of the country itself, it is modelled as a single node. This is similar to the copper plate model of a power grid. In other words, the infrastructures to transport the energy carriers within the country are not considered. It is assumed that the demands have to be supplied by the production, regardless of the flows between the producers and the consumers. Yet, adapting the networks is accounted for in terms of the required investments. For instance, a high share of VRES requires an investment to reinforce the power grid (i.e., 368 M€/GW of additional installed capacity of VRES).

In the current work, imported electrofuels (i.e., e-methane, e-hydrogen, e-methanol and e-ammonia) are assumed to be “renewable” in the sense that they do not increase the concentration of CO₂ in the atmosphere [132]. In practice, it means that their

GWP is assumed to be zero in the model. Compared to equivalent electrofuels that would be locally produced, this assumption does not account for the emissions related to the transport of imported electrofuels from abroad to Belgium. However, the share of these emissions is limited (between 5 and 10%) compared to the whole cycle of production and use of imported electrofuels [133]. Therefore, the conclusions drawn in this thesis are not affected by this assumption. Besides these, every other resource has its specific GWP like coal ($gwp_{op,coal} = 0.40 \text{ kt}_{CO_2,eq}/\text{GWh}$), natural gas ($gwp_{op,NG} = 0.27 \text{ kt}_{CO_2,eq}/\text{GWh}$) or the fossil-based molecules equivalent to the electrofuels (e.g., $gwp_{op,ammonia} = 0.46 \text{ kt}_{CO_2,eq}/\text{GWh}$ or $gwp_{op,methanol} = 0.41 \text{ kt}_{CO_2,eq}/\text{GWh}$).

2.3 Conversion technologies

As the end-use demands are defined as energy (and non-energy with the NED) services rather than a certain quantity of oil or solar irradiance, for instance, technologies are implemented to convert these resources into end-use demands. Besides their CAPEX, OPEX and lifetime defined in Section 1.1, production and conversion technologies (i.e., CCGT, car or boiler) have a conversion efficiency whereas storage technologies (i.e., thermal storage, battery or molecule storage) have charge/discharge losses. There are also infrastructure technologies. They encompass, for instance, the power grid, the DHN or technologies to produce intermediate energy carriers (e.g., wood pyrolysis, biomethanolation or steam methane reforming to produce hydrogen).

Not digging into too many more details about the exhaustive list of these technologies presented in previous work [41], this section rather focuses on the implementation of Small Modular Reactor (SMR) and the technologies to supply the Non-energy Demand (NED).

2.3.1 Small modular reactor

Specific attention is put on the implementation of SMR as the 6 GW of conventional nuclear are assumed to drop to 2 GW in 2025 and total phase-out by 2035. Similarly to the analysis of EnergyVille [130], a Belgian consortium for energy research, and in line with the Belgian Nuclear Research Centre (SCK-CEN) [134], SMR is implemented with the features listed in Table 2.1. Where most of the features are similar to conventional nuclear power plants, they differ from these on two main points: their potential year start, 2040, and their flexibility. Indeed, unlike the current nuclear power plants, constrained in the model to produce a constant power output at every hour of the year (i.e., baseload production as it is actually the case in Belgium), SMRs, are

flexible in the sense that their production can vary between 0 and their full capacity at any hour of each representative year. Here, we simplify SMRs as only producing electricity and we disregard the heat produced by the nuclear reaction. This is considered lost to the atmosphere.

Table 2.1. Nominal features of the SMRs in EnergyScope. SMR exhibits the advantage to have a fully flexible production (i.e., between 0 to the full capacity) unlike conventional nuclear that is constrained to produce a constant baseload at every hour of the year.

| Feature | Value | Unit |
|----------------------------|-------------------|-----------|
| CAPEX | 4850 | €/kW |
| Annual OPEX | 103 ^a | €/kW/year |
| Lifetime | 60 | year |
| Cost of purchasing uranium | 4 | €/MWh |
| Efficiency | 40% | - |
| Maximum capacity | 6 | GW |
| Annual availability | 85% ^b | - |
| Operational year | 2040 ^c | - |
| Flexibility | Full | - |

^aThis value is in line with Caron et al. [135] that evaluate annual opex of 0.015\$/kWh, which makes 112\$/kW/year assuming a 85% full-load availability, and EnergyVille [130] that accounts for 83.3€/kW/year

^bThis annual availability accounts for yearly maintenance where the reactors might not operate or, at least, not at their maximum capacity.

^c2040 is the soonest year at which SMR could be available, optimistically assuming industrial prototypes being completed by 2035 and 5 additional years for their commercial installation.

For the sake of comparison, the Levelised Cost of Energy (LCOE) of the principal technologies to produce electricity, based on the computation used by Limpens [41], is detailed (see Figure 2.4). Not included here is the cost of integrating a technology in the system (e.g., reinforcement of the grid and storage capacities for VRES), the LCOE aims at aggregating and normalizing the CAPEX and OPEX of technologies providing a common commodity, i.e., electricity. Compared to the other flexible generation units, SMR is significantly more cost-effective. Besides being about six times more capital-intensive in €/kW, the investment is amortized over a longer expected lifetime (i.e., 60 years). Moreover, the cost of purchasing uranium driving SMR is expected to remain stable and low whereas the expected increase of the cost of purchasing fossil fuels dominates the LCOE of CCGT. In addition, one sees that CCGT supplied by e-ammonia outcompetes its e-methane equivalent, unlike their respective fossil-based equivalent. This is because e-ammonia, not requiring carbon capture, is expected to

be more cost-effective to produce versus e-methane [73]. On the contrary, fossil-based ammonia, mostly relying on steam methane reforming, requires additional steps in the production process compared to fossil gas, as introduced in Section 2.1.1.

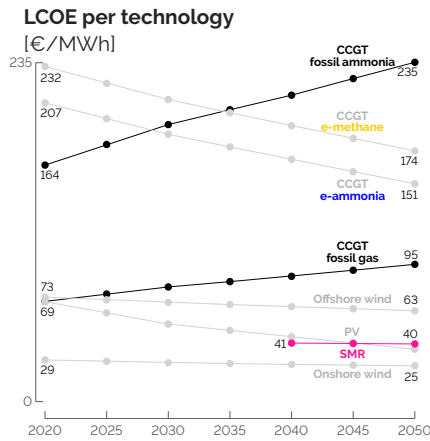


Figure 2.4. Levelised cost of energy (LCOE) for the main technologies in the power sector. Grey and black curves are related to technologies running on renewable and fossil resources, respectively. SMR is cheaper than the other flexible options. CCGT running on e-ammonia is cheaper than its e-methane alternative.

2.3.2 Technologies supplying the non-energy demand

Different paths are implemented to produce the final molecules of the NED (see Figure 2.5). Similarly to Tsipopoulos et al. [136], naphtha, here considered as LFO, resulting from refinery operation is modelled as an imported commodity. Presented here for the specific year of 2035, all data and related references can be found in [137]. To keep the same level of detail as other sectors of the model, the implementation of the conversion technologies consists of a single kind of technology per type of resource to produce a certain product. For instance, in the model, there is only one technology to produce HVC either from naphtha or from LPG, two liquid fossil hydrocarbons, i.e., Naphtha Steam Cracker (NSC). For ammonia and methanol, the molecules can either be produced locally from other resources or directly imported (with distinction between non-renewable and renewable molecules).

Works of Rixhon et al. [109, 121] assessed the impact of the integration of the NED in the case of Belgium in 2050, using EnergyScope TD (see Appendix B.2.1). To analyse the whole-energy system at different “climate targets”, the model forced

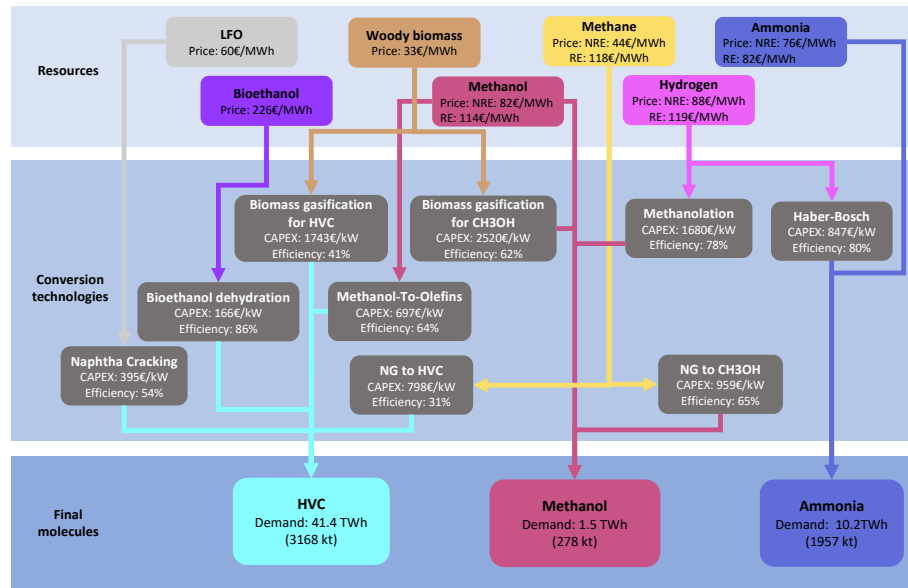


Figure 2.5. Schematic view of the different resources able to produce HVC, ammonia and methanol with their related conversion technologies (including energy efficiency and their CAPEX - in €/kW of final molecules). The efficiencies account for the potential consumption/production of heat and/or electricity within each conversion process. Values stand for 2035. Graph from [121].

the total emissions to decrease by reducing their upper limit while optimising the total cost. In practice, 10% steps of GWP reduction were made from the “reference scenario - 100%”. This strategy gave the following points of analysis: 100% (i.e., cost-optimum with no limitation on the total GWP), 90%, 80%, ..., down to 0% (i.e., carbon neutrality).

First and foremost, when the NED is implemented with this higher level of detail, we highlighted that woody biomass was “cannibalised” to produce methanol, instead of high-temperature heat, in the cost-optimum situation. At more ambitious “climate targets”, e-methanol rises as the keystone to defossilise the NED sector as Methanol-to-olefins (MTO) becomes the favoured option to produce HVC, representing the major share of the NED. Then, including the NED affects the selection of the technologies for the satisfaction of the heat and electricity demands. The additional high-temperature demand required by the NED forces the system to invest in more efficient technologies like CHP instead of CCGT. This additional heat demand mostly supplies naphtha-cracking substituted by MTO at more ambitious “climate targets” to produce HVC.

To a lesser extent, to respect the emissions caps, integrating the NED leads to a higher integration of solar PV to support the electrification of the low-temperature heat sector.

For further details on these analyses, the interested reader is invited to refer to previously published works [109, 121].

2.4 Uncertainty ranges

As detailed in Section 1.2, accounting for uncertainty in ESOMs is crucial [67], especially when it comes to optimising several decades in an inherently uncertain future. The fundamental step in this ambition is to characterise these uncertainties.

In this work, following the approach of Moret [42], we have defined ranges of uncertainties for the model parameters. For the operation-type parameters (types II and III), a scaling factor needs to be considered to avoid assuming that the uncertainty for the last year of the planning horizon (N) is representative for all years in the planning horizon Moret [42]. In EnergyScope Pathway, as the model optimises the system every 5 years, $N = 5$ has been selected to get the final ranges of uncertainties of type II and III. For type III uncertainties (i.e., uncertainty ranges increasing with time), a 50% increase has been set arbitrarily between the ranges for 2025 and these same ranges for 2050. In other words, for these specific uncertainties, the ranges for 2050 are 50% larger than for 2025. Like other works [70, 71], the uncertain parameters are assumed to be independent and uniformly distributed between their respective lower and upper bounds.

Rixhon et al. [49] analysed the impact of these parameters on the total cost of the snapshot Belgian whole-energy system in 2050 subject to different GWP limits. Based on this work, we have selected a subset of impacting uncertainties, added others due to the pathway formulation (e.g., $\Delta_{\text{change,pass}}$), and listed them in Table 2.2.

This work considers nine groups of uncertain parameters: (i) the cost of purchasing imported energy carriers; (ii) the investment cost (i.e., CAPEX) of some technologies, mostly related to the mobility sector and the integration of renewables; (iii) the maintenance cost (i.e., OPEX) of every technology; (iv) the consumption of electric and fuel cells vehicles in the mobility sector; (v) the potential installed capacity of renewables; (vi) the hourly load factor of renewables accounting for the variability of solar irradiance or wind speed; (vii) the availability of resources considered limited (i.e., biomass and electricity); (viii) the end-use-demands split per sector of activities (i.e., households, services, passenger mobility and industry) and (ix) other parameters like the discount rate or the exogenous modal share change in different key sectors. A particular attention is to pay to the potential installation of SMR, at the bottom of Table 2.2.

As detailed before, the commercial availability of such a technology is uncertain but would not be before 2040. Consequently, for SMR, the parameter $f_{\max, \text{SMR}}$ influences the maximum capacity to install to translate somehow the readiness of this technology. Arbitrarily, we have then assumed the following probability of availability of such a technology: 10% chance to be installable from 2040, 20% from 2045 and 40% from 2050¹. Based on the local sensitivity analysis carried out by EnergyVille [130], the current work also considers a [-40%; +44%] range on the CAPEX of SMR, on top of the uncertainty about its availability. Finally, the cost of purchasing renewable electro-fuels presents a wide range, [-64.3%; +179.8%], like the other imported commodities.

Table 2.2 summarises the uncertainty ranges for the different groups of technologies and resources, for the year 2025.

2.5 CO₂ budget for the transition

In most studies carried out on the pathway optimisation of a whole-energy system, a CO₂-trajectory is *a priori* set to reach carbon neutrality by 2050. Nerini et al. [63] used the emission trajectory indicated by the UK's Committee on Climate Change in their analysis of the impact of limited foresight to achieve the target of 80% reduction of GHG by 2050 in the United Kingdom. In their assessment of the impacts of economy-wide emission policies in the water-energy-land nexus, Licandeo et al. [138] analysed different CO₂ trajectories considering more or less severe water scarcity for the US. Poncelet et al. [38] with LUSYM (Leuven University SYstem Model) and EnergyVille [130] with TIMES-BE also set decreasing emission trajectories in their analysis of respectively the Belgian power sector and whole-energy system. Others only set the objective of carbon neutrality by 2050. For instance, Heuberger et al. [64] investigated the impact of different factors (e.g., limit of the foresight in the future, availability of “unicorn technologies” or committed versus market-driven decarbonisation strategies) to reach this ultimate objective in the UK system. In their “near-term to net zero” (NT2NZ) approach to estimate CO₂ prices, Kaufman et al. [139] emphasises the need to select, *a priori*, an emissions pathway to the net-zero target. Some authors suggest limiting near-term technological disruptions and, consequently, the initial rate of emission reductions [140] whereas others, to avoid technology lock-in and to benefit from early investments in the transition, encourage a sharper decrease of the emissions at an earlier stage [141].

¹In other words, if this parameter, ranging between 0 and 1, is (i) smaller than 0.6, there is no possibility to install SMR during the transition; (ii) between 0.6 and 0.8, these 6 GW can be installed only in 2050; (iii) between 0.8 and 0.9, these can be installed from 2045 onward and; (iv) higher than 0.9, the prescribed maximum capacity can be installed from 2040 onward.

Table 2.2. Application of the uncertainty characterization method of Moret [42] to the EnergyScope Pathway model for the year 2025.

| Category | Parameter | Meaning | Type ^a | Relative variation ^b | |
|-------------------------------------|----------------------------|---------------------------------------|-------------------|---------------------------------|--------|
| | | | | min | max |
| Cost of purchasing | $c_{op,fossil}$ | Purchase fossil fuels | II | -64.3% | 179.8% |
| | $c_{op,elec}$ | Purchase electricity | II | -64.3% | 179.8% |
| | $c_{op,electrofuels}$ | Purchase electrofuels | II | -64.3% | 179.8% |
| | $c_{op,biofuels}$ | Purchase biofuels | II | -64.3% | 179.8% |
| Investment cost | $c_{inv,car}$ | CAPEX car | I | -21.6% | 25.0% |
| | $c_{inv,bus}$ | CAPEX bus | I | -21.6% | 25.0% |
| | c_{inv,ic_prop} | CAPEX ICE | I | -21.6% | 25.0% |
| | c_{inv,e_prop} | CAPEX electric motor | I | -39.6% | 39.6% |
| | c_{inv,fc_prop} | CAPEX fuel cell engine | I | -39.6% | 39.6% |
| | $c_{inv,efficiency}$ | CAPEX efficiency measures | I | -39.3% | 39.3% |
| | $c_{inv,PV}$ | CAPEX PV | I | -39.6% | 39.6% |
| | $c_{inv,grid}$ | CAPEX power grid | I | -39.3% | 39.3% |
| | $c_{inv,grid_enforce}$ | CAPEX grid reinforcement | I | -39.3% | 39.3% |
| | $c_{inv,nuclear_SMR}$ | CAPEX SMR ^c | I | -40.0% | 44.0% |
| Maintenance cost | $c_{maint,var}$ | Variable OPEX of technologies | I | -48.2% | 35.7% |
| Consumption | η_{e_prop} | Consumption electric vehicles | I | -28.7% | 28.7% |
| | η_{fc_prop} | Consumption fuel cell vehicles | I | -28.7% | 28.7% |
| Potential installed capacity | $f_{max,PV}$ | Max capacity PV | I | -24.1% | 24.1% |
| | $f_{max,windon}$ | Max capacity onshore wind | I | -24.1% | 24.1% |
| | $f_{max,windoff}$ | Max capacity offshore wind | I | -24.1% | 24.1% |
| | $f_{max,SMR}$ | Potential capacity SMR | - | 0 | 1 |
| Hourly load factor | $c_{pt,PV}$ | Hourly load factor PV | II | -22.1% | 22.1% |
| | $c_{pt,winds}$ | Hourly load factor wind turbines | II | -22.1% | 22.1% |
| Resource availability | $avail_{elec}$ | Available electricity import | I | -32.1% | 32.1% |
| | $avail_{biomass}$ | Available local biomass | I | -32.1% | 32.1% |
| End-use demand | HH_EUD | Households EUD | III | -13.8% | 11.2% |
| | $services_EUD$ | Services EUD | III | -14.3% | 11% |
| | $pass_EUD$ | Passenger mobility EUD | III | -7.5% | 7.5% |
| | $industry_EUD$ | Industry EUD | III | -20.5% | 16.0% |
| Miscellaneous | i_{rate} | Discount rate | I | -46.2% | 46.2% |
| | $\%_{pub,max}$ | Max share of public transport | I | -10% | 10% |
| | $\Delta_{change,freight}$ | Modal share change freight mobility | - | -30% | 30% |
| | $\Delta_{change,pass}$ | Modal share change passenger mobility | - | -30% | 30% |
| | Δ_{change,LT_heat} | Modal share change LT-heat | - | -30% | 30% |

^aPer Moret [42], “I: investment-type, II: operation-type (constant uncertainty over time), III: operation-type (uncertainty increasing over time)”.

^bThe nominal values of each of the parameters is 0, meaning no variation compared to the nominal values of the impacted parameter in the model.

^cThis range has been inferred from the local sensitivity analysis performed by EnergyVille [130].

In this work, the effect of greenhouse gases is cumulative over time and a constraint is set on the overall emissions of the transition—a CO₂ budget for the transition. This approach is in line with the works defining safe operating spaces within the nine different global planetary boundaries (i.e., (i) novel entities, (ii) stratospheric ozone depletion, (iii) atmospheric aerosol loading, (iv) ocean acidification, (v) biogeochemical flows, (vi) freshwater change, (vii) land system change, (viii) biosphere integrity, and, (ix) climate change) [142–144]. This “systemic framework for addressing global anthropogenic impacts on Earth system” gives quantitative recommendations about the CO₂ concentration, among others, to maintain “the stability and resilience of Earth system as a whole” [142]. In their review, Ryberg et al. [145] identified three main sharing principle categories when considering these safe spaces: i.e., *utilitarian*, *egalitarian* and *acquired rights* principles. In a nutshell, the former, mostly applied to the industry sector [146, 147], aims at maximising the sum of welfare. The second shares the so-called “budget” equally among the total population, allocating the same share to each individual [8, 148]. Finally, in *acquired rights* principles, also called “grandfathering”, the sharing is based on “maintaining that prior emissions increase future emission entitlements”[149]. In this thesis, we have chosen the latter principle to allocate the CO₂ budget to the Belgian transition. This budget (1.2 Gt_{CO₂,eq}) corresponds to the proportion of Belgium’s emissions in the world energy-related emissions in 2020 (34.8 Gt_{CO₂,eq} [2]) applied to the global budget to have a 66% chance of limiting warming to 1.5°C of 420 Gt_{CO₂,eq} [1]. Therefore, in this work, a limit has been put on $gwp_{lim,trans} = 1.2 \text{ Gt}_{\text{CO}_2,\text{eq}}$ in Equation (1.11). This is another sign of the urgency to act to mitigate climate change as this 30-year budget represents only 10 years of the current emissions. In this approach, the residual emissions in 2050 are not explicitly constrained down to zero. This carbon neutrality is rather implicit given the ambitious CO₂ budget.

Compared to a linear decrease from the current emissions, as done by Limpens et al. [40], this budget represents a 60% reduction of the cumulative emissions over the transition. Appendix C.4.1 compares the emissions trajectory between the REF case and a case (without SMR) where the linear decrease is imposed between 2020 and carbon neutrality in 2050.

2.6 Conclusions

Mainly based on data collected during previous works [41, 42], this thesis has developed the case study along different axes. First, the non-energy demand, which currently represents about 20% of the final energy consumed in Belgium, has been brought to a

level of detail similar to the other energy sectors of the system. Previously considered as a fixed demand supplied by fossil gas, it has been detailed to account for final-use products (i.e., High-Value Chemicals (HVC), ammonia and methanol) and their respective production routes. Second, electrofuels are now more detailed in the model as well as their different supply and consumption routes. Third, instead of defining *a priori* the CO₂-trajectory through the transition, this work sets a limit on the overall CO₂ budget. Then, based on the methodology of Moret et al. [36], uncertainty ranges are defined for the 5-year step transition from 2020 to 2050. Finally, on top of adding the possibility to install small modular reactors (SMR), this thesis accounts for updated values for the EUD as well as adjusted assumptions regarding the two key drivers of the transition in private mobility, i.e., battery electric vehicles (BEV) and Fuel Cell (FC) cars.

Chapter 3

The atom-molecules dilemma: deterministic and uncertainty analyses

“It is difficult to make predictions, especially about the future.”
Niels Bohr, in *Bulletin of the Atomic Scientists*, 1971

On top of scenarios with more profound behavioural changes, a variety of technological pathways are often investigated to meet the ambitions of climate change mitigation. For instance, in their work, Climact and VITO [72] assessed different scenarios for a climate-neutral Belgium by 2050. Depending on the scenarios, the emphasis is put on a higher electrification of the whole-energy system, a higher consumption of hydrogen or more complex molecules (i.e., electrofuels) or a bigger reliance on biomass and the related Bioenergy with Carbon Capture and Storage (BECCS). Besides these, “unicorn” technologies are also investigated [64]. These technologies have not (yet) reached a high enough maturity, i.e., Technology Readiness Level (TRL) 3 to 7, or they face hurdles such as social acceptance. Therefore, they are currently not deployed on a large scale. Among others, nuclear energy finds an interest in the literature [130, 150]. In the form of Small Modular Reactor (SMR), nuclear energy is also discussed in actual current investments (in Belgium for instance [151]).

In the future, deeper integration of VRES will come with the bigger electrification of sectors like mobility, low-temperature and industry [152]. In such a context, there is a case for nuclear energy to produce reliable low-CO₂ emission electricity [153]. This is also in line with the willingness to phase out imported Russian fossil fuels anchored in the European REPowerEU Plan [154]. Unlike the consumption of fossil gas which represents about 80% of the LCOE from CCGT, the price of uranium accounts for 25-

30% of LCOE from nuclear power plants. This favours nuclear energy against price volatility and for the security of electricity supply, in case of a conflict like the invasion of Ukraine, for instance.

In a country like Belgium, reaching the goal of energy transition will not be a “winner-takes-all” situation but rather a combination of solutions [41, 44]. However, this chapter focuses on this atom-molecules dilemma. Often compared, if not opposed, to local renewables like wind and solar [155, 156], this chapter rather assesses the integration of nuclear energy in the future versus the need to import renewable molecules from abroad, in a country where the local potential of VRES is limited compared to its EUD. Relying on nuclear energy for some is highly controversial. On top of purely techno-economic aspects, non-exhaustively mentioned beforehand, there are other ethical, societal or even political considerations to account for when addressing this question [157]. In the same sense, on top of ethical or geopolitical aspects, one could question the availability of the imported electrofuels, assumed to be unlimited in this work (see Chapter 2). In their work, Lefebvre and Van Brussel [158] investigated this topic for the case of Belgium considering lower and upper bounds in terms of availability based on, on the one hand, the already signed agreements with the exporting countries and, on the other hand, their maximal technological potential of VRES, respectively. Their lower bound resulted in a total availability of electrofuels that is one order of magnitude lower than the needs provided by the cost-optimum carbon-neutral Belgium in 2050. Like the rest of this thesis, the purpose here is only to expose the impact of integrating SMR as well as the need to import electrofuels in the Belgian energy landscape, from a strictly techno-economical point of view with a cost-based optimisation. This is why, for the sake of transparency, the model and the data are documented and openly available online [54] and in Appendices B and C.

Section 3.1 targets the impact of integrating SMR from 2040 onward on the whole-energy system, in a deterministic way (i.e., considering only nominal values of the parameters). Accounting for uncertainties presented in Section 1.2, Section 3.2 will identify the key factors driving higher or lower imports of electrofuels as well as the installation of SMR, by the end of the transition, i.e., 2050.

Contributions

In their review, Yue et al. [35] pointed out that uncertainties were accounted for either snapshot models (i.e., optimizing a single target future year), to assess a single energy sector (i.e., the power sector, most of the time) or with a limited number of uncertain parameters, i.e., about ten, in a stochastic programming approach to optimise a transition

pathway with a small number of time stages, i.e., two or three. Here, the uncertainty quantification addresses the total transition pathway of the whole-energy system, with 34 uncertain parameters (see Section 2.4). This GSA applied to a model optimising the transition pathway of a whole-energy system with these many uncertain parameters is the main contribution of this chapter. Through this analysis, we also managed to point out the impact of integrating SMR in the Belgian energy system as well as the main drivers of the import of e-hydrogen, e-methane, e-ammonia and e-methanol by 2050.

3.1 Deterministic impact of integrating SMR in 2040

In this section, like in the rest of the thesis, the **REF** case is without any deployment of SMR anytime during the transition whereas in the **SMR** case, this technology is available, up to 6 GW (see Chapter 2), from 2040 onward. After investigating the deployment of SMR through the power sector, the first part of this section focuses on this impact on the whole-system level considerations (i.e., overall transition costs, primary energy mix and yearly emissions per sector). The second part will address the impact of SMR on each of the other sectors of the system.

3.1.1 Power sector

SMR is deployed as soon as available, i.e., 2040, to its maximum capacity, 6 GW, substituting other flexible power generation units (see Figure 3.1). There is no ammonia-CCGT at the end of the transition and an anticipatory reduction of methane CCGT (i.e., 2.1 GW in 2040 versus 3.7 GW for the REF case). To a lesser extent, the last 2% deployment of solar-PV is slightly delayed as the capacity in 2025 is 1.3 GW smaller than in the REF case. Overall, given the restriction on yearly availability and the slightly higher electrification (Figure 3.2), the total power capacity installed by 2050 is 3.5% higher for the SMR case. In their work, EnergyVille [130] also showed that SMR first substitutes “e-fuels/hydrogen” turbines before reducing the need for PV. However, in their “Central” scenario where no SMR is installed by 2050, they rely on 96.6 GW of PV, 63% more than the 59.2 GW potential considered in our work and about 15 times more than the current installed capacity, i.e., 6.5 GW.

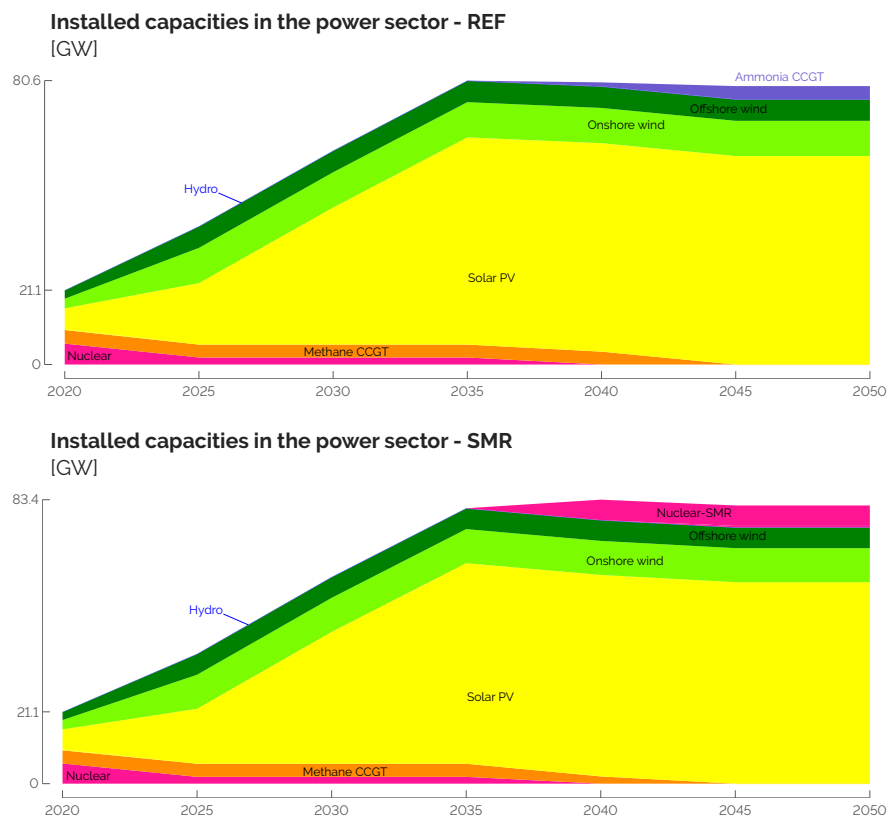


Figure 3.1. Installed capacities in the power sector in the REF (top) and SMR (down) scenarios. As soon as available (i.e., 2040), Small Modular Reactor (SMR) is deployed to its maximum potential (i.e., 6 GW) to substitute more expensive flexible generation units (i.e., methane and ammonia CCGT).

When assessing the electricity production-versus-consumption-balance (Figure 3.2), SMR, as a cheaper, flexible and low-emitting power generation system, produces to its full capacity. Given the 15% maintenance off-time assumed in this work, this represents 44.6 TWh by 2050. In comparison, in 2020, conventional nuclear power plants produced 34.4 TWh in Belgium. This resurgence of nuclear electricity occurs at the expense of other, although more efficient, technologies: CCGT and industrial CHP. Besides the unchanged end-use-demand compared with the REF case, we observe a slight increase in the electrification of the rest of the system: +9.4% which corresponds to +5.8 TWh, mostly consumed by electric heaters in industry (+48%) to produce industrial high-temperature heat.

72 Chapter 3. The atom-molecules dilemma: deterministic and uncertainty analyses

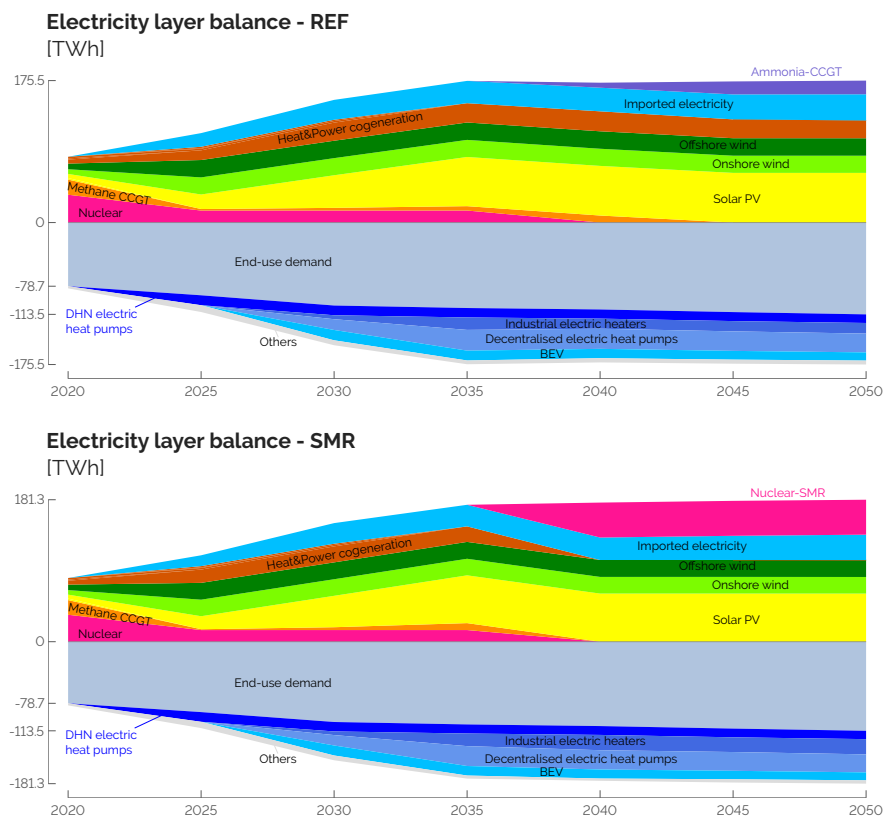


Figure 3.2. Balance between the production and the consumption of electricity in the REF (top) and SMR (down) scenarios. The production of electricity from SMR substitutes more efficient technologies (i.e., CCGT and CHP) and boosts the electrification of the rest of the system, mostly the industrial high-temperature heat sector.

3.1.2 System-level impacts

First of all, the 6 GW SMR installed from 2040 allow reaching a 3.3% (-36.9 b€) cheaper overall transition (Figure 3.3). Over the 30-year transition, this represents an annual cost saving equal to 0.2% of the Belgian GDP. Thanks to the perfect foresight approach, the model knows ahead that cheaper and low-emitting SMR will be available in the future. As the model can freely spend the constrained CO₂ budget over the transition, cost-savings also occur before 2040. These early-stage cost-savings are equally shared between the extended use of cheaper LFO to produce HVC and the delayed deployment of PV. Then, the capital-intensive investments in SMR, mostly recovered by the end of the transition as salvage value, are widely compensated by the smaller resource-related OPEX. This leads, at the end, aggregating the OPEX and the annualised CAPEX, to a system that is yearly 4.4 b€ (8.8%) cheaper by 2050 than in the REF case (Figure 3.3).

Extending the use of naphtha-crackers and, to a lesser extent, postponing the deployment of PV, lead to higher CO₂ emissions at the beginning of the transition that are then compensated by the deployment of SMR (Figure 3.4).

Then, considering the primary energy mix shown in Figure 3.5, three phases in the transition can be identified. Before 2040, thanks to the perfect foresight approach, the model finds it more economical in 2025 to keep on using 33.2 TWh of LFO to produce HVC through naphtha/LPG-cracking. In 2040, uranium-driven SMR substitutes the electricity originally produced from industrial CHP and CCGT running respectively on fossil gas and renewable ammonia. Finally, from 2045 onward, the significant drop in the consumption of electrofuels comes from the same industrial CHP. This is the illustration of the atom-molecules dilemma where the consumption of local renewables is, on its side, not much affected. In other words, SMR competes with importing electrofuels while both support the integration of local solar and wind energies. Then, like the power sector, the SMR case ends up in a less efficient whole-energy system by 2050 at it consumes 47 TWh (+12.7%) primary energy more to supply an unchanged EUD. Interestingly, in both cases, given the assumptions made on the GWP of the resources (i.e., $gwp_{op,electrofuels} = 0 \text{ ktCO}_2,\text{eq}/\text{GWh}$ and $gwp_{op,uranium} = 0.004 \text{ ktCO}_2,\text{eq}/\text{GWh}$), the constraint on the CO₂ budget leads to “carbon neutrality” by 2050¹.

¹The model being constrained to keep on using all the waste that would keep on being locally produced, the system in 2050 reaches a $\sim 3.5 \text{ MtCO}_2,\text{eq}/\text{year}$.

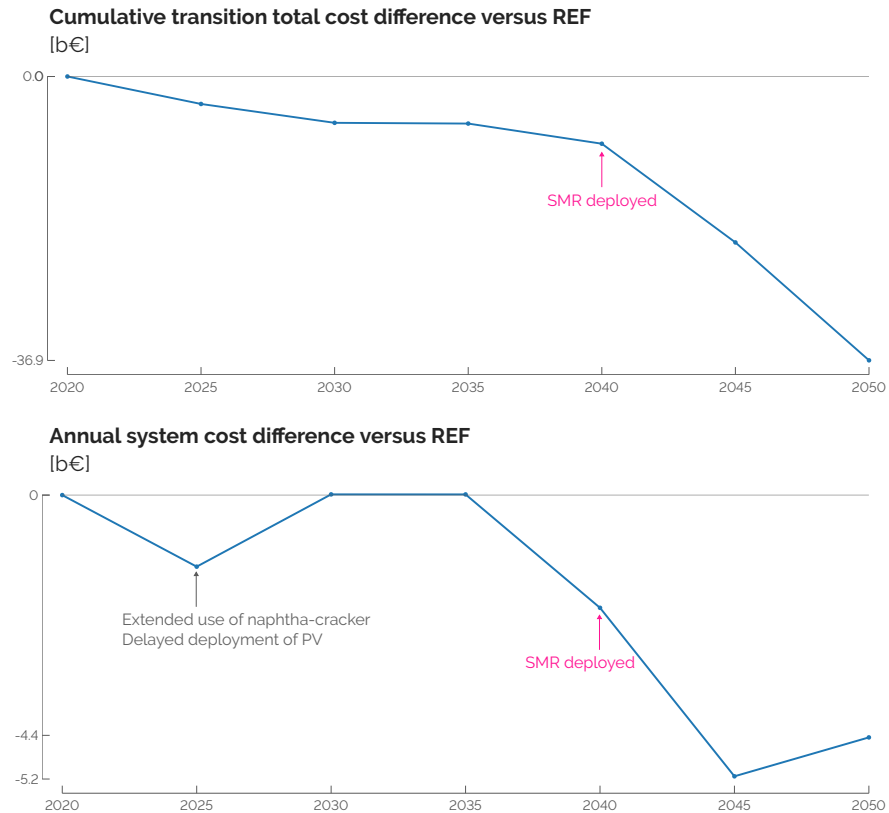


Figure 3.3. (Top) Cumulative transition cost and (down) annual system cost differences between the SMR and the REF cases. Including SMR ends up in a cheaper overall transition (-36.9 b€) and cheaper whole-energy system by 2050 (-4.4 b€).

3.1.3 Non-power sectors

Beyond the direct impact that SMR has on the power sector, it also affects the other sectors. This is due to the sector-coupling typical of a whole-energy system optimisation [33].

High-temperature heat

The main impact of including SMR from 2040 onward on the high-temperature heat sector is (i) its higher direct electrification and (ii) the reduction of more efficient heat-and-power co-generation in the benefit of single-output industrial boilers. In the

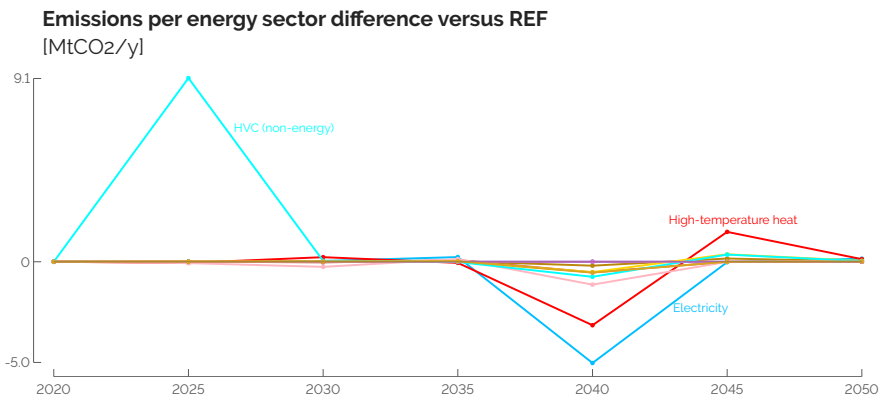


Figure 3.4. Emissions per energy sector difference between the SMR and the REF cases. The deployment of SMR from 2040 onward allows maintaining longer the use of Light Fuel Oil (LFO) for the production of High-Value Chemicals (HVC).

REF case, industrial electric heaters are mainly used to absorb the “over-production” of the 59 GW solar-PV when fully deployed, on sunny days, and limit the yearly curtailment to a maximum of 0.3 TWh, 0.5% of the yearly 61 TWh produced by solar-PV. With SMR, by 2050, an additional 1.7 GW (+13%) of these heaters can rely on a more constant supply of defossilised electricity. This increases the load factor (31%) and yearly production (48%) of these industrial electric heaters. Then, given the 44.6 TWh of electricity produced by SMR, cogeneration units are less relevant and, by 2050, 2.6 GW industrial gas boilers completely substitute CHP to produce 16.6 TWh (i.e., 23%) of the total production of high-temperature heat.

Low-temperature heat

This sector is marginally impacted. In both cases, the major shift of supply from decentralised to centralised productions operates early in the transition, to hit the constraint that DHN cannot supply more than 37% of the LT-heat production. Then, from a mix of oil (53%), gas (43%) and wood (4%) boilers for the decentralised production of LT-heat in 2020, the system shifts towards electric Heat Pump (HP) only by 2035. Similarly, for the centralised production of LT-heat, electric HP remains the most efficient and economical option.

Mobility

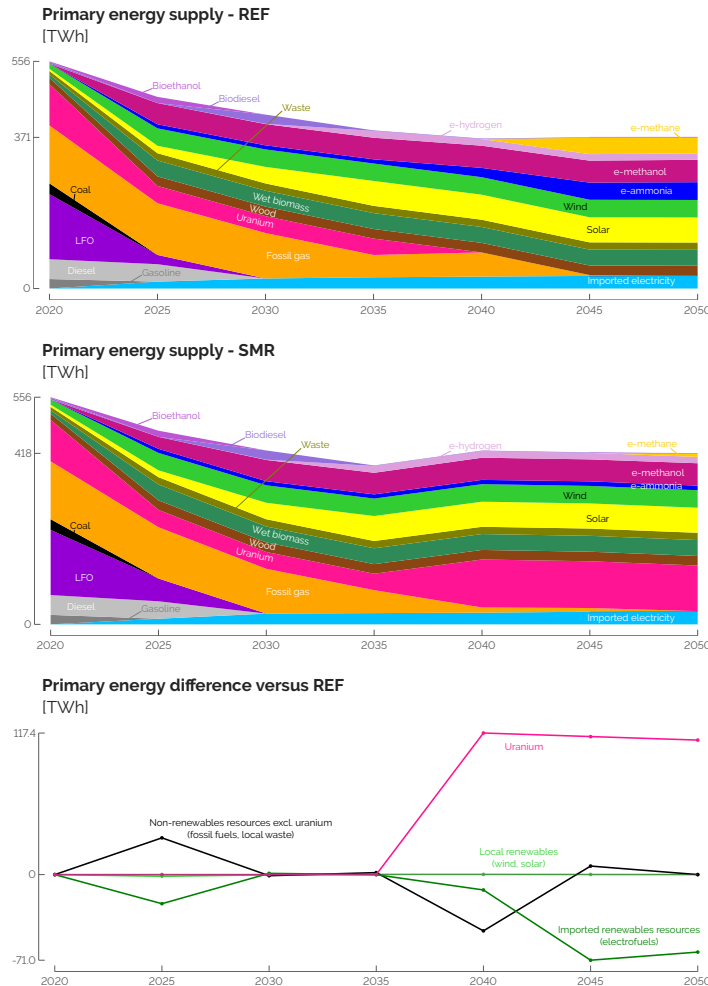


Figure 3.5. (Top) Primary energy mix over the transition for the REF and SMR cases. (Down) Difference of the mix between the two cases after aggregation per category. In line with Rixhon et al. [132], uranium is considered as a non-renewable resource. It is nevertheless dissociated from other non-renewable resources for the sake of clarity. The imported electricity is split between imported non-renewable and renewable resources between the current share of renewables, i.e., 37.41% [159], and an assumed 100%-renewable European electricity mix by 2050.

Passenger mobility is not affected either as the electrification of the system is preferentially done in this sector with BEV substituting Internal Combustion Engine (ICE) cars for the private sector by 2030. Regarding public mobility, trains and tramways supply their *a priori* set maximum share, respectively, 50% and 30% complemented by Compressed Natural Gas (CNG) buses substituting diesel-driven buses. Similarly, considering the freight transport, technology shifts (i.e., from diesel to FC trucks) or modal shares (i.e., 53%-47% split between NG and (bio)-diesel boats) are identical between the two cases.

Non-energy demand

The supply of ammonia (i.e., from Haber-Bosch to direct import of renewable ammonia) and methanol (i.e., import of renewable methanol) are unchanged between the two cases. However, as introduced previously, to produce HVC, the full substitution of naphtha/LPG-cracking by MTO is delayed as the emissions of the former are compensated by the later integration of SMR.

3.2 Uncertainty quantification on the cost, the atom and the molecules

Besides the detailed understanding of the deterministic results, it is important to challenge these conclusions accounting for the uncertainty of the parameters [160]. After briefly assessing the Global Sensitivity Analysis (GSA) on the total transition cost (Section 3.2.1), this section investigates more deeply the atom-molecules dilemma (Section 3.2.2). The Sobol' indices are computed for the import of renewable molecules and installed capacities of SMR.

3.2.1 Total transition cost

Exhaustively listed in Appendix D.1, Table 3.1 gathers the most impacting parameters on the total transition cost. Per Turati et al. [82], parameters are considered as “impacting” if their Sobol’ index is above the threshold = $1/d$, d being the total number of uncertain parameters after the pre-selection phase. In this case, $d = 34$, and, consequently, the threshold is equal to 2.9%. Table 3.1 shows that the cost of purchasing electrofuels is the most impacting parameter. On the contrary, the potentiality to install SMR and its CAPEX have a much lower influence on the variation of the total transition cost. Given the uncertainty characterisation presented in Section 2.4, there are 60% chance that no SMR could be installed. When $f_{\max, \text{SMR}}$ takes a value below

0.6, the variation of the total transition cost is only due to the variation of the other parameters. Then, in perspective with the scenario analysis of Section 3.1, the 3.3% reduction has been observed when SMR is installed from 2040 onward. This represents only 10% of the samples. Moreover, when it is possible, SMR is always installed thanks to its characteristics: cheap and low-emitting fuel, a long lifetime leading to lower annualised CAPEX and higher salvage value. However, given its limited deployment, up to 6 GW, SMR-related parameters have a lower impact on the variation of the total transition cost. On the contrary, more expensive renewable electrofuels are always imported, to a smaller or larger extent depending on the sample. For instance, in the REF case (Section 3.1.2), the imported electrofuels represent, by 2050, 152.9 TWh (i.e., 41% of the primary energy mix) with an average 93€/MWh cost of purchasing and, over the entire transition, a 273 b€ cumulative OPEX (i.e., 25% of the total transition cost).

Table 3.1. Total Sobol' indices of the uncertain parameters over the total transition cost. Where the cost of purchasing electrofuels is the top-1 parameter, SMR-related parameters have a negligible impact on this cost.

| Parameter | Ranking | Sobol' index |
|-------------------------------|---------|--------------|
| Purchase electrofuels | 1 | 46.8% |
| Industry EUD | 2 | 23.2% |
| Discount rate | 3 | 12.0% |
| Purchase fossil fuels | 4 | 5.7% |
| : | : | : |
| Potential capacity SMR | 11 | 0.9% |
| : | : | : |
| CAPEX SMR | 33 | <0.1% |

Given the relatively wide uncertainty range (i.e., up to [-30.8%; +24.0%] by 2050) and, above all, the major share of the total demand, between 53% and 60%, the industrial EUD is the second most impacting parameter.

As the driving factor for the annualisation and the salvage value of the assets, the discount rate has a 12% Sobol' index. As detailed in Chapter 1, the model considers an overall discount rate for the entire system (i.e., 1.5% as a nominal value). In practice, the discount rate would vary depending on the technology investment risk. This variation would have, for instance, a major impact on the LCOE of technologies like nuclear power plants [161], given the important capital needs and long time horizons [150].

The cost of purchasing fossil fuels is also a key parameter in terms of variation of the total transition cost. However, due to the ambitious CO₂ budget, phasing out of fossil fuels is urgent and makes their impact smaller than their renewable alternatives.

Figure 3.6 shows the distribution of the total transition cost given the 1260 samples. Stretching between 660 b€ and 2050 b€, the mean, the median and the nominal value (i.e., REF case) are close to each other, respectively 1180 b€, 1160 b€ and 1080 b€. Similarly to the analysis carried out by Coppitters and Contino [162], one observes here that the distribution is right-skewed. It could then be qualified as “fragile” as the top 50% of the samples cover a bigger range (i.e., between 1160 and 2050) than the bottom 50% of the samples (i.e., between 660 and 1160). In other words, the bad scenarios, resulting in a total transition cost higher than the median, have a bigger effect on this cost.

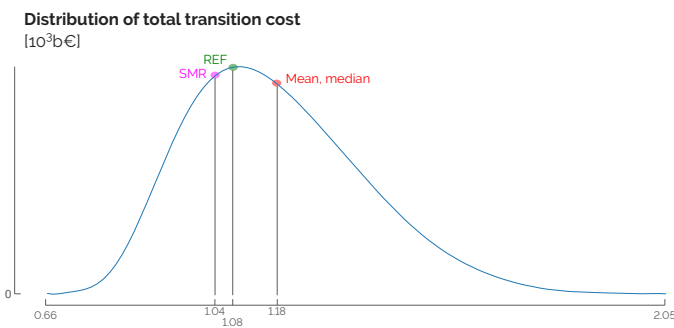


Figure 3.6. Distribution of the total transition cost over the 1260 runs of the Global Sensitivity Analysis (GSA). The mean, $\mu = 1.18 \cdot 10^3$ b€, is slightly higher than the median ($P_{50} = 1.16 \cdot 10^3$ b€) and the nominal cases cost, $1.08 \cdot 10^3$ b€ and $1.04 \cdot 10^3$ b€ respectively for the REF and SMR cases. Also, with a standard deviation, $\sigma = 197$ b€, a 95%-confidence interval would be about $[0.8; 1.6] \cdot 10^3$ b€.

3.2.2 Atom and molecules

The samples used to carry out the GSA on the total transition cost, also provide the distribution of other outputs of the model like the import of renewable electrofuels over the transition. As the general trends are increasing, discrepancies exist between the different energy carriers (see Figure 3.7).

E-methane, as the renewable alternative to fossil methane, substitutes it, sometimes at a very early stage of the transition, 2025, and large extent, 163 TWh, which is more than 6% more than the total import of electrofuels in the REF case. The necessity to

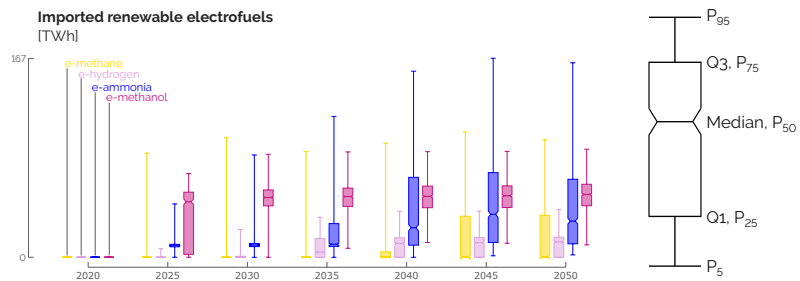


Figure 3.7. Distribution of the imported renewable electrofuels over the transition. Starting from no electrofuel in 2020, their respective import rises progressively along the transition at different growth rates and with different ranges of values.

import this molecule is progressive through the transition to supply mostly industrial CHP and boilers.

E-hydrogen becomes rapidly the main stream of hydrogen in the system, reaching median and maximum values of 13.0 TWh and 42.1 TWh in 2050, respectively. Hydrogen is more frequently used in the mobility sector. Like in the REF case, fuel cell trucks are often the first option but, in some outlying cases, fuel cell cars and buses appear to completely substitute respectively BEV cars and CNG buses by 2050. Moreover, some samples lead to local production of methanol via the methanolation process, to produce up to 17.8 TWh of methanol (i.e., 33% of the total supply of methanol of the nominal REF and SMR cases).

Then, the imported e-ammonia rapidly becomes cost-competitive against its fossil alternative (see Chapter 2). At the early stage of the transition, e-ammonia substitutes fossil ammonia and the Haber-Bosch process. Where the initial purpose of ammonia is to satisfy a relatively limited Non-energy Demand (NED) (i.e., 10 ± 3 TWh by 2050), the variation of its import is mostly due to the higher or lower need for ammonia-CCGT as a flexible option to produce electricity. From 2035, out of the four considered electrofuels, the imported e-ammonia is the one exhibiting the largest uncertainty with, for instance, an interquartile range (IQR)² of about 50 TWh. In some extreme cases, e-ammonia is the most imported molecule, i.e., up to 167 TWh or 45% of the total primary mix.

Likewise, e-methanol early becomes the selected option to supply methanol even though alternatives like biomass-to-methanol are selected to supply, on average, 5% of the demand for methanol. Its NED represents, on average, 3% of the total

²The interquartile range is the difference between the third quartile (Q_3 or P_{75}) and the first (Q_1 or P_{25}). It is an indicator of statistical dispersion around the median, Q_2 or P_{50} .

consumption of methanol. The variation of imported e-methanol is due to its role in the industrial production of HVC through the Methanol-to-olefins (MTO) process as it represents 95% of the total consumption. For the remaining 2%, methanol is also used to supply the freight transport sector via boats or trucks. More detailed statistics including the different sources of supply and consumption of gas, hydrogen, ammonia and methanol are provided in Appendix D.2.

This part assesses the space of uncertainties, like Pickering et al. [163] who investigated the space of feasibility to reach carbon neutrality in Europe. The trend lines of the key parameters can be drawn for these imports and the installed capacities of SMR in 2050. We picked 2050 as it is the time of the transition where electrofuels, if imported, are imported in the largest amount compared to the other years of the transition. Next to the name of a parameter, one can read its Sobol' index versus the output of interest. For these outputs of interest, different from the total transition cost, the LOO error is around 20%. Even though this is higher than the threshold of 1 %, the Sobol' indices allow ranking the most impacting parameters (see Section 1.2.2). Box plots also point out the distribution of this output for the extreme low or high values of some parameters.

For the import of e-methanol, industrial EUD is, by far (i.e., ~80% Sobol' index), the key factor (Figure 3.8). Due to its own NED but, above all, since it is the low-emitting alternative picked by the model to supply the significant NED of HVC, the lower this demand, the lower the need to import e-methanol, and vice versa.

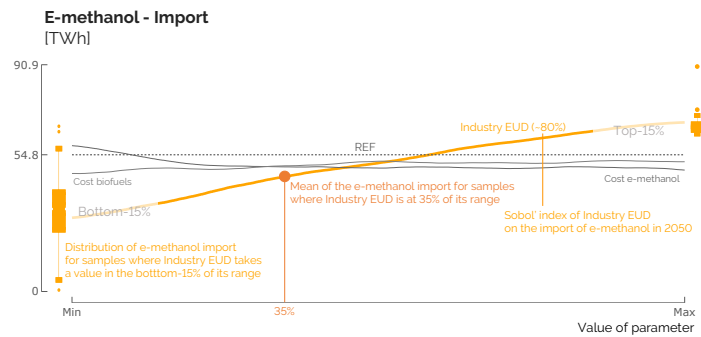


Figure 3.8. Trend lines of the key parameters (and their Sobol' index) on the import of e-methanol in 2050. Around these lines, box plots point out the distribution of the output of interest for the extreme values (either bottom-15% or top-15%) of some parameters. The grey dashed line gives the value of the output of interest in the REF case.

About e-hydrogen, the sensitivity analysis highlights its dependence on various driving parameters, particularly those linked to the transport sector (Figure 3.9). The utilisation of e-hydrogen is most prevalent in FC trucks, followed by FC cars and buses to a lesser extent (Appendix D.2). The adoption of fuel cell engines in trucks contributes, on average, to 63.5% of the total road freight transport, thereby affecting the level of e-hydrogen imports. Consequently, the smaller the CAPEX of fuel cell engines, the more the system imports e-hydrogen. Similarly, the cost of purchasing electrofuels influences e-hydrogen imports. Subsequently, the cost of purchasing biofuels emerges as the third most influential parameter. Indeed, biodiesel trucks are the most picked alternative to FC trucks to provide, on average, 27.6% of the total. Additionally, CNG buses are preferred in public road transport (34.9%), followed by FC buses (11.2%) competing with biodiesel and hybrid biodiesel buses, accounting for 27.8% and 26.1%, respectively. Finally, the last noticeable parameter at stake is the CAPEX of electric vehicles. In competition with BEV that stand for 83.4% on average of the private mobility sector, the cheaper these cars are, the more cost-competitive are these vehicles, and vice versa, versus FC cars (i.e., 13.7% of the total passenger mobility, on average).

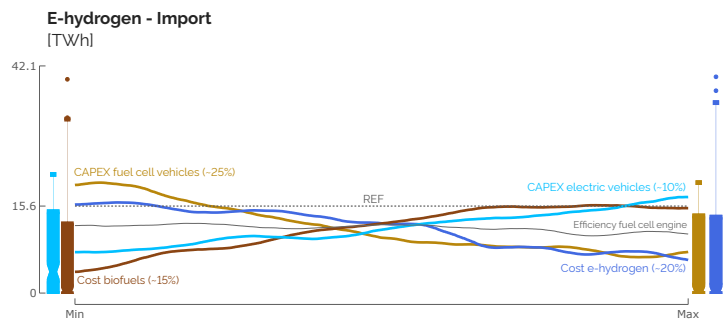


Figure 3.9. Trend lines of the key parameters (and their Sobol' index) on the import of e-hydrogen in 2050. Around these lines, box plots point out the distribution of the output of interest for the extreme values (either bottom-15% or top-15%) of some parameters. The grey dashed line gives the value of the output of interest in the REF case.

As aforementioned, the industrial EUD impacts the most the import of e-methane (Figure 3.10). This parameter directly dictates the demand of industrial high-temperature heat for which industrial gas CHP, and industrial gas boilers to a lower extent, represent, on average over all the samples, respectively 25.6% and 6.1% of the total production. Then, considering the smaller-impact parameters, we notice that SMR

plays a non-negligible role. Indeed, if deployed, SMR produces abundant low-emitting electricity for industrial electric heaters that substitute, even completely in some cases, gas alternatives. This confirms the observation made in Section 3.1.3. Highly available local biomass also leads to smaller imports of e-methane to supply bio-hydrolysis and produce methane-equivalent gas. Finally, and surprisingly, the costs of purchasing electrofuels and fossil fuels have a positive and negative correlation with the amount of e-methane, respectively. In other words, by 2050, more expensive electrofuels result in more e-methane imports. On the contrary, cheaper electrofuels result in higher imports of fossil methane. Given the techno-economic optimum sought by EnergyScope, if electrofuels are more expensive, the system will, overall, import less of them, especially e-ammonia, mainly used by CCGT. Subject to the CO₂ budget for the transition, the system goes towards more efficient technologies, like industrial methane-CHP to substitute e-ammonia-CCGT in the production of electricity. First running on fossil gas, these CHP consume more e-methane by 2050. On the contrary, if electrofuels are cheaper, there is more import of them, especially of e-ammonia. This leaves room for more emitting and cheaper resources to be used while respecting the CO₂ budget, i.e., coal in industrial boilers that produce, in these cases, on average 24% of the high-temperature (HT) heat in 2050. In these cases, the use of coal in 2050 highlights that, with a sharper decrease of the emissions at early stages in the transition, the model finds a solution including highly-emitting resources (e.g., coal) while respecting the CO₂ budget. Consequently, there are smaller investments in methane CHP, and consequently import of e-methane as more abundant renewable electricity is produced via e-ammonia-CCGT and more HT-heat is supplied by industrial coal boilers. Even though we might expect that no more coal will be consumed in Belgium by 2050, the model still has the opportunity to use it if the CO₂ budget allows it. Regarding the cost of purchasing fossil fuels, the parameter has mainly an impact on the import of fossil NG as the most versatile energy carrier in the whole-energy system. If NG is more expensive, the system will import less of it. Subsequently, the investments in methane-CHP and boilers are more limited. This ends up in a smaller need for e-methane by 2050.

As already pointed out in Section 3.1.1, the installation of SMR drastically reduces the import of e-ammonia (Figure 3.11). As ammonia CCGT is the biggest consumer of ammonia by the end of the transition, low-emitting and cheaper electricity produced by SMR (40 versus 151 €/MWh_{elec}) substitutes these CCGT. With a higher cost of purchasing electrofuels, this import of e-ammonia drops down to 2.0 TWh, 95.4% less than in the REF case. Then, with a 12%-Sobol' index, the cost of purchasing electricity from abroad, considered as renewable by 2050 and, therefore, a direct competitor to

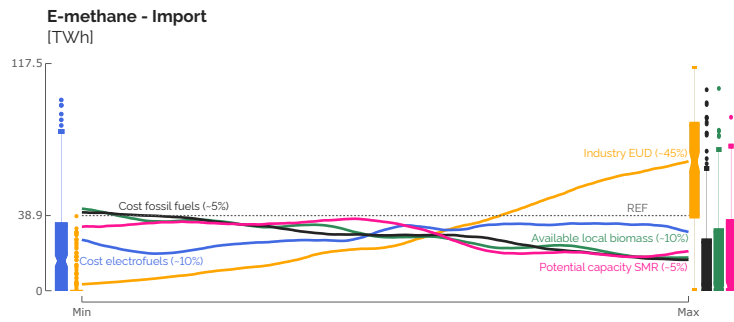


Figure 3.10. Trend lines of the key parameters (and their Sobol' index) on the import of e-methane in 2050. Around these lines, box plots point out the distribution of the output of interest for the extreme values (either bottom-15% or top-15%) of some parameters. The grey dashed line gives the value of the output of interest in the REF case.

e-ammonia CCGT, also affects the need of this molecule, especially when this cost is low.

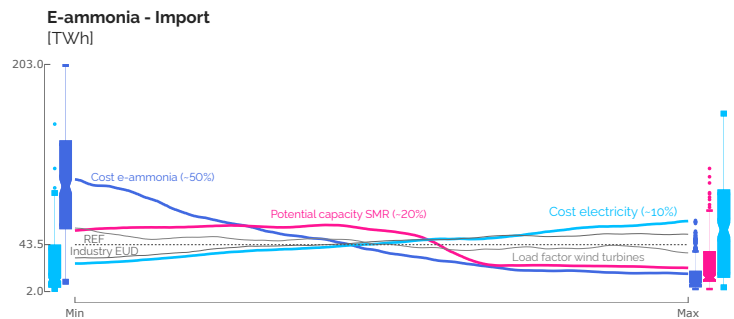


Figure 3.11. Trend lines of the key parameters (and their Sobol' index) on the import of e-ammonia in 2050. Around these lines, box plots point out the distribution of the output of interest for the extreme values (either bottom-15% or top-15%) of some parameters. The grey dashed line gives the value of the output of interest in the REF case.

For the installed capacity of SMR, it is the availability of the technology that drives its installation (Figure 3.12). Not shown here but all the samples of the GSA highlight that SMR is installed to its maximum capacity, i.e., 6 GW, as soon as possible. In other words, the only parameter “Potential capacity SMR” dictates the installation of

this technology. In practice, we observe that as soon as this parameter is equal or higher than 0.9, 0.8 and 0.6, 6 GW SMR is installed from 2040, 2045 and 2050, respectively. The large range of uncertainty of its CAPEX (-40%; +44%) has a negligible impact on the installed capacity, with a Sobol' index of 0.9%. This is explained by the long lifetime of the technology (60 years) and the salvage value recovered by 2050.

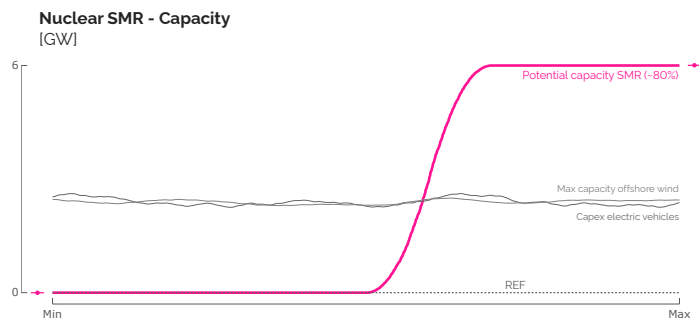


Figure 3.12. Trend lines of the key parameters (and their Sobol' index) on the installed capacity of SMR in 2050. Around these lines, box plots point out the distribution of the output of interest for the extreme values (either bottom-15% or top-15%) of some parameters. The grey dashed line gives the value of the output of interest in the REF case.

3.2.3 Local renewables

In line with the results given in Section 3.1, the GSA shows that SMR has a negligible impact on the deployment of local VRES (i.e., PV, onshore and offshore wind turbines). Whereas the installed capacities of onshore wind is totally driven by the uncertainty on its maximum potential, Sobol' indices change for the most impacting parameters on the deployment of PV and offshore wind (see Figure 3.13). The key factor that drives the installed capacities of these two technologies is mostly their respective maximum potential, especially at the end of the transition, much more than their CAPEX. Given its higher LCOE (Figure 2.4), PV is more impacted in the short term by the variation in the cost of purchasing electrofuels supplying e-methane (and e-ammonia to a lesser extent) CCGT. However, this impact becomes negligible by 2050.

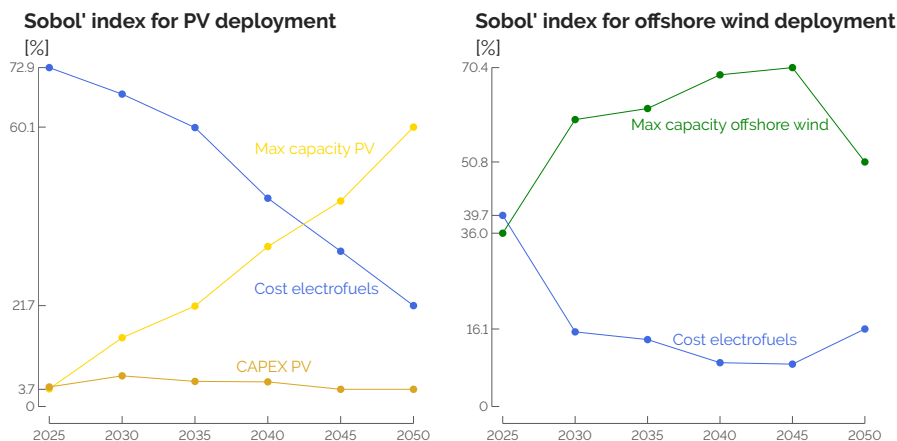


Figure 3.13. Parameters impacting the deployment of PV and offshore wind over the transition. Progressively, the impact of the uncertainty on the maximum potential increases, unlike the one on the cost of purchasing electrofuels.

3.3 Conclusions

Given its lower LCOE ($40 \text{ €}/\text{MWh}_{\text{elec}}$) and the important share of the investment recovered via its salvage value (between 79% and 96%), SMR is installed as soon as available. It directly substitutes other flexible power generation units (i.e., CCGT) and provides, by 2050, 44.6 TWh, 25% of the total electricity production. Consequently, this reduces the need to produce electricity via CHP and allows increasing by 48%

the high-temperature heat produced by electric heaters. Besides these two sectors, the others (i.e., low-temperature heat, mobility and non-energy demand) are marginally or not impacted by the integration of SMR.

Given the ambitious CO₂ budget (i.e., a 30-year budget representing 10 years of the current emissions), the global sensitivity analysis highlights the need for radical changes. Assumed to be carbon-neutral and directly available to a large amount, one of the “unicorn” solutions for the case of Belgium is the import of renewable electrofuels, even at the early stages of the transition. This is why the most impacting parameter on the variability of the total transition cost (around 45%) is the cost of purchasing these energy carriers. On the contrary, parameters directly related to SMR (i.e., its availability and its CAPEX) have a limited impact, below 1%. This GSA also points out the key drivers for the import of renewable electrofuels and the installation of SMR by 2050. Besides the cost of purchasing electrofuels (i.e., the lower this cost, the bigger the imports), it shows that available SMR would have mainly a direct impact on e-ammonia, by substituting the ammonia CCGT which is the biggest consumer of this molecule. Indirectly, this parameter will also reduce the import of e-methane by reducing the need for gas CHP and gas boilers. About e-hydrogen and e-methanol, their imports are impacted by the other technologies in competition in the transport sector and the industrial demand, respectively.

In conclusion, this work puts under the spotlight the “competition” between SMR and imported electrofuels while both of them support the integration of local VRES. Betting on SMR means letting the emissions go up at the early stages of the transition (i.e., LFO still used in 2025 to produce HVC) to end up with an overall transition and a system by 2050 that are 3.3% and 8.8% cheaper than in the REF case, respectively. However, given the need to import molecules at earlier stages of the transition, with or without SMR, it seems reasonable to keep on investing in the transport and the infrastructure to support these imports. In practice, Fluxys, the manager of the gas network in Belgium, already presents significant investments by 2032 (i.e., 1.3 b€) to support this transition in the near future [164]. The investments into the molecules would allow covering ourselves against the risk of eventually not having SMR available by the end of the first half of this century. The perfect foresight approach does not model this risk as the possibility to install or not SMR is known in advance. In the EnergyScope Pathway model, assuming the same technology mix as in the SMR case up to 2040 but without installing SMR for the rest of the transition, i.e., between 2040 and 2050, would require drastic (and quick) changes to still meet the CO₂ budget: around 44 b€ of additional cumulative OPEX in purchasing electrofuels, mostly e-ammonia (+32 TWh by 2050) and e-methane (+31 TWh) to supply CCGT and industrial CHP.

Chapter 4

Reinforcement Learning CO₂-policy investigation

“For the things we have to learn before we can do them, we learn by doing them.”
Aristotle, in *The Nicomachean Ethics*, IVth century BC

Uncertainties about the future along with a large variety of IAMs yield an even larger variety of GHG emissions reduction pathways [86]. For instance, several studies [1, 165] advocate for actions to take in the near future, especially to keep on track within the 1.5°C (if not, 2°C) increase of global temperature above pre-industrial levels by the end of the century. On the contrary, using his top-down model DICE, Nordhaus [166] states that immediate and drastic actions are not compulsory to meet the ambition of climate change mitigation.

To navigate through the myopic transitions not constrained by a prescribed CO₂-trajectory and investigate the efficiency of different policies, we apply the reinforcement learning approach detailed in Section 1.3 on the case study of Belgium. Besides the environment, i.e., the myopic transition pathway of the whole-energy system via EnergyScope Pathway (see Chapter 1), the first part of this chapter presents the three key features of interaction between the agent, optimizing its policy, and the environment: actions, states and reward. Then, the results of this policy optimisation point out strategies to follow, i.e., *sweet spots*, in the transitions under uncertainties as well as *no-go zones* where the chances of succeeding the transition, i.e., respecting the CO₂ budget, are very limited. Finally, these results are compared with references, i.e., the perfect foresight and the myopic optimisation of the transition under the same uncer-

tainties but without the trained RL-agent that can support this transition thanks to its learned policy.

Contributions

Applying the RL approach to the optimization of the myopic transition pathway of a whole-energy system presents several novelties. First of all, as introduced in Section 1.3.1, when applied to energy systems, RL is more dedicated either to smaller scale systems (e.g., Building Energy Management System (BEMS), vehicles and energy devices) or to sector-specific, often the power sector, problems (e.g., dispatch problems, energy markets and grid) [90]. In our case, the sector-coupling, the long-term goal at the end of a multiple-steps transition and the number of uncertain parameters make this application new for RL.

Applying RL to the optimisation environment of EnergyScope Pathway myopic, rather than a simulation environment, allows building a hierarchical multi-objective optimisation framework: while the objective of the environment remains the minimisation of the total “transition” cost (on the concerned limited time window), the agent optimises its strategy to respect the CO₂ budget.

Comparing the RL-based results with more conventional approaches, i.e., perfect foresight optimisation, highlights the added-value brought by this approach in the exploration of myopic transition pathways.

Usually, applications of RL focus more on the result of the learning process, the optimised policy, for optimising the control of a system [90]. This thesis also investigates the learning episodes themselves to explore the field of possibilities to succeed the transition.

4.1 Definition of the actions, reward and states

As already introduced in Section 1.3.2, the environment with which the RL-agent interacts is the optimisation of the transition pathway of a whole-energy system on a specific time window, e.g., 2020-2030 then 2025-2035 and so on, until 2040-2050 (see Figure 1.7). In a nutshell, starting from the initial state of the environment (i.e., the whole-energy system in 2020), the agent takes a set of actions that influence the environment, i.e., that affects parameters of the Linear Programming in EnergyScope Pathway. Then, the window 2020-2030 is optimised via EnergyScope. Some of the outputs of this optimisation feed the agent with either the new state of the system or the reward, i.e., telling the agent how good the actions were at the state the agent took

it. Based on the new state and the reward, the agent takes another set of actions and the window 2025-2035 is optimised. This goes on until 2050.

4.1.1 Actions

Defining the levers of action, the core of the policy, to support the transition of a country-size whole-energy system is challenging, especially when accounting for political and socio-technical aspects [167]. In our work, focusing only on the techno-economic aspect, we assume that the actions taken by the agent are directly implemented and impacting the environment. In other words, considering only the techno-economic lens, there is no moderation nor contest towards the agent's actions, as the objective is to assess how far and when within the transition to push the different levers of action. Given the overall objective of the agent to succeed the transition, i.e., respecting the CO₂ budget by 2050, we have defined the actions in this sense. The first action, $\text{act}_{\text{gwp}} \in [0, 1]$, aims at limiting the emissions at the representative year ending the concerned time window, $\mathbf{GWP}_{\text{tot}}(y_{\text{end of the window}})$, between the level of emissions in 2020, i.e., $\mathbf{GWP}_{\text{tot}}(2020) = 123 \text{ Mt}_{\text{CO}_2,\text{eq}}$, and carbon neutrality:

$$\mathbf{GWP}_{\text{tot}}(y_{\text{end of the window}}) \leq \text{act}_{\text{gwp}} \cdot \mathbf{GWP}_{\text{tot}}(2020). \quad (4.1)$$

This action is equivalent to setting a national CO₂-quota.

Three additional actions support the strict limitation of yearly emissions: limiting the consumption of oil, fossil gas and coal. Out of the total GHG emissions in Belgium in 2020, oil (i.e., so-called “LFO” in the model) and fossil gas account for roughly 40% and 31%, respectively. In 2020, solid fossil fuels (i.e., so-called “coal” in the model) is much less consumed than oil and gas: i.e., 28 TWh of solid fossil fuels versus 159 and 142 TWh for oil and fossil gas, respectively. Even though its cost (17€/MWh) makes coal cost-competitive, it is a highly-emitting resource, 0.40 kt_{CO₂,eq}/GWh. For these reasons, three independent actions limit the consumption of these three fossil resources up to the level of consumption in 2020, $\mathbf{Cons}_{\text{fossil gas}}(2020)$, $\mathbf{Cons}_{\text{LFO}}(2020)$ and $\mathbf{Cons}_{\text{coal}}(2020)$, over the entire concerned time window, except the first one as this year is the initial condition of the time window and cannot be optimised any more:

$$\mathbf{Cons}_{\text{fossil gas}}(y) \leq \text{act}_{\text{fossil gas}} \cdot \mathbf{Cons}_{\text{fossil gas}}(2020) \quad \forall y \in \text{time window} \quad (4.2)$$

$$\mathbf{Cons}_{\text{LFO}}(y) \leq \text{act}_{\text{LFO}} \cdot \mathbf{Cons}_{\text{LFO}}(2020) \quad \forall y \in \text{time window} \quad (4.3)$$

$$\mathbf{Cons}_{\text{coal}}(y) \leq \text{act}_{\text{coal}} \cdot \mathbf{Cons}_{\text{coal}}(2020) \quad \forall y \in \text{time window} \quad (4.4)$$

where $\text{act}_{\text{fossil gas}}$, act_{LFO} and act_{coal} can take values between 0 and 1. These complete the action space of the agent, $A \in \mathbb{R}_{[0,1]}^4$ (see Figure 4.1).

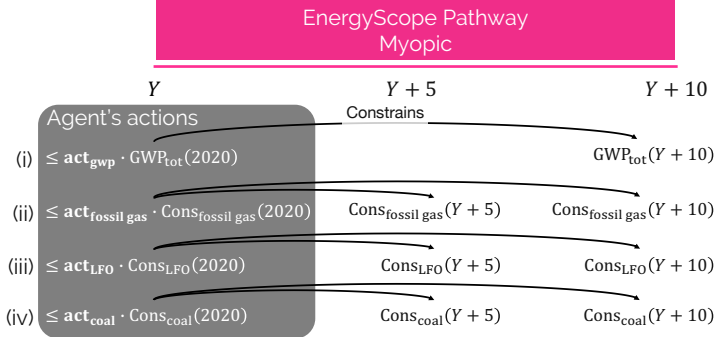


Figure 4.1. Actions available to the decision-maker. Taken at the beginning of the time window to optimise (year Y), the four actions impact (i) the emissions of the system at the end of the time window (year $Y + 10$) and, (ii-iv) the consumption of fossil gas, LFO and coal at years $Y + 5$ and $Y + 10$. Unlike the first action that sets a target for the end of the time window, the last three aim at limiting the consumption of these fossil resources over the whole time window.

4.1.2 Reward

When the reward is not properly defined, the agent may optimise its policy for an unintended objective, leading to undesired or suboptimal behavior, i.e., the so-called misalignment of the learning objective [168]. Even worse, it can lead to reward hacking (or reward tampering) where the agent exploits loopholes in the reward function to achieve higher rewards without actually performing the desired task [169]. On the contrary, a proper definition of the reward function increases the sample efficiency, i.e., requiring less episode to converge to the optimal policy. It also makes the policy more stable and able to withstand variations and uncertainties in the environment [170].

Through its maximisation of the expected return (see Section 1.3.2), a RL-agent is as sensitive to positive reward, i.e., the carrot, as negative reward, i.e., the stick. When the former encourages desired behaviours, the latter can be seen as a penalty or a punishment and discourages the undesirable behaviours [92]. In our case, we have decided to combine these two approaches (see Figure 4.2).

The reward function is defined in three steps. First of all, taking a set of actions at a certain state might lead to an infeasible optimisation problem. In other words, as actions have a direct impact on some constraints of the problem, they might limit too

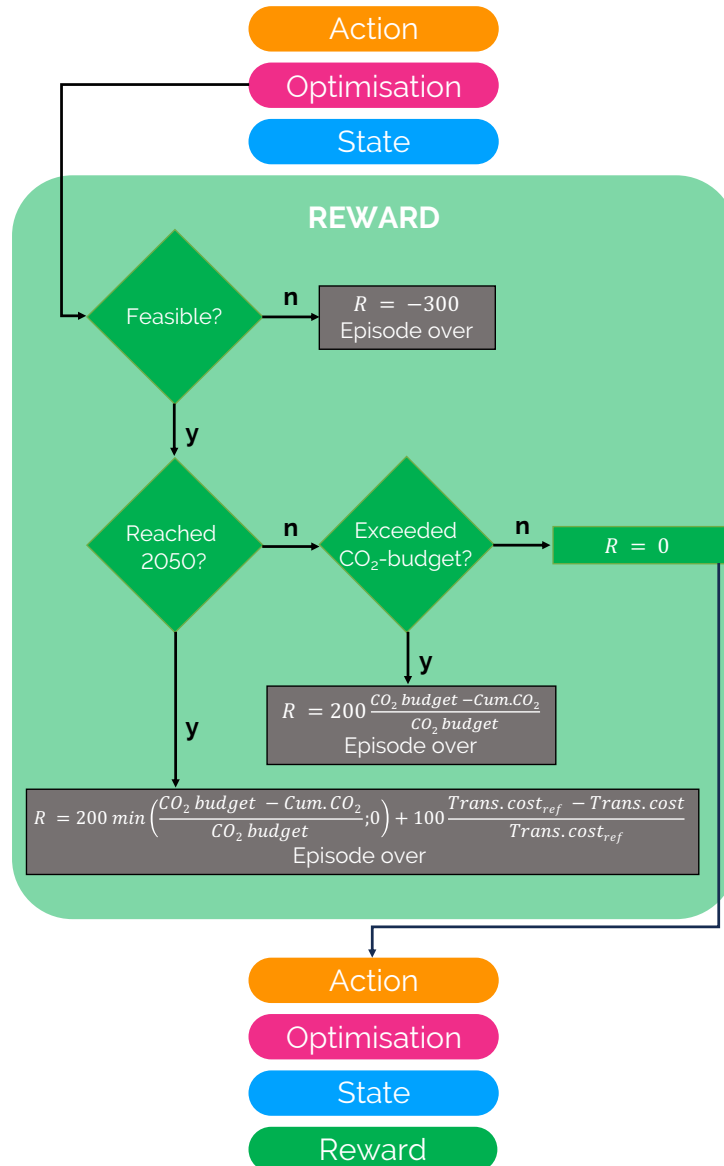


Figure 4.2. Reward function, R . Before reaching 2050, the episode is prematurely ended and a negative reward is given if the optimisation is infeasible or if the CO_2 budget is exceeded. If the optimisation provides a solution and the CO_2 budget is not exceeded, the episode continues. Finally, if the episode goes until 2050, the reward is a weighted sum between the capped cumulative emissions and the total transition cost, and the episode terminates. After terminating an episode, the process starts over at the initial state, i.e., 2020.

much the feasible domain to the point where no solution can be found. For instance, the extreme case of aiming at carbon neutrality, i.e., $\text{act}_{\text{gwp}} = 0$, and forbidding the use of the three aforementioned fossil fuels, i.e., $\text{act}_{\text{fossil gas}} = \text{act}_{\text{LFO}} = \text{act}_{\text{coal}} = 0$, from the beginning of the transition makes the optimisation impossible to solve. In this case, the episode is prematurely ended and the reward is “highly” negative, -300. If the optimisation is feasible and the end of the transition, i.e., 2050, is not reached, the cumulative emissions so far are evaluated. On the one hand, if these cumulative emissions exceed the CO₂ budget, 1.2 GtCO_{2,eq} (see Section 2.5), the episode is also ended and a penalisation is given to the agent. This penalisation is proportional to the difference between the CO₂ budget and the actual cumulative emissions. On the other hand, the episode continues with a zero reward if the CO₂ budget is not exceeded. Eventually, when reaching 2050, given the main objective of the agent to respect the CO₂ budget and not to be more “CO₂-ambitious”, we cut short the contribution of the cumulative emissions as soon as they are lower or equal to the CO₂ budget. On top of that, the reward function includes a secondary objective: the cumulative transition cost. To make the agent sensitive to the cost-impact of its policy, we added the total transition cost in the reward function where the *Trans. cost_{ref}* on Figure 4.2 is equal to $1.1 \cdot 10^3$ b€. This value comes from the mean of the total transition costs obtained through the GSA performed on the perfect foresight transition pathway optimisation (see Section 3.2.1). In this final form of the reward, one will notice that overshooting cumulative emissions are more penalising than an overshooting transition cost, i.e., weight of 200 for the emissions versus 100 for the cost. The values of these weights are the results of a trial and error to fine-tune the balance between more expensive successes and cheaper failures. This way, we observed that the agent first targeted the respect of the CO₂ budget and then, to a lesser scale, avoided reaching over-costly transitions.

4.1.3 States

Besides the reward, states are the other piece of information provided by the environment to the agent. In RL, the purpose of states are to represent the current situation or configuration of the environment in which the agent operates. The primary function of states in RL is to provide the necessary context for the agent to choose appropriate actions based on its current observations and goals [92]. The challenge in the definition of the states is to provide enough information but not too much to avoid overwhelming the agent with non-informative features.

Consequently, after testing several state spaces and observing the convergence of the reward, we have converged to a four-dimension state space characterizing the energy system at the end of the optimised time window. The first dimension is directly related to the main objective of the agent: respecting the CO₂ budget until 2050. Therefore, the cumulative emissions emitted so far up to the current step of the transition is the first dimension of the states. Similarly, the cumulative cost of the transition so far constitutes the second dimension of the states to inform the agent about the cost-impact of its actions on the environment. Finally, to enrich the level of details, we have added two other dimensions representative of the key-to-the-transition indicators identified in the Renewable Energy Directive (RED) III of the European Commission [7]: the share of renewables in the primary energy mix and, the energy efficiency. The former is computed as the share of local renewables (i.e., wind, solar, hydro and biomass) and imported renewable energy carriers (i.e., biofuels and electrofuels) in the total consumption of primary energy. Electricity imported from abroad is not considered in the set of renewable energy carriers even if it can be assumed to be fully renewable by 2050. Finally, even though energy efficiency is usually defined as the ratio between the FEC and the primary energy mix, we decided to define this efficiency with a focus on the EUD, like in the rest of this thesis. Where electricity, heat and non-energy EUD are expressed in terms of energy content, we needed to convert passenger and freight transports into their respective FEC to integrate them in the ratio. The information of efficiency fed back by the environment to the agent is the ratio between a “hybrid” EUD and the consumption of primary energy resources.

4.2 Convergence and learning process

Before comparing the agent’s optimised policy with references, the first step consists in assessing the learning of the NN, also called “training”. For this, numerous episodes are played through the myopic optimisation of the transition pathway of Belgium. During the learning process, the algorithm explored numerous transition pathways: 2,037 successful transitions out of 10,751 attempts. 2% of the total attempts led to an infeasible optimisation of the initial time window. On top of that, each pathway provides valuable insight into the possible alternatives — the primary goal of reinforcement learning. As a side benefit, the collection of all explored pathways also identifies the intermediate milestones to reach and the range of actions that must be avoided or must be taken. Yet, the exploration during this learning process is not exhaustive. The trends provided below are therefore not proven. The randomness of the process and the num-

ber of explored transition pathways still give high confidence in the conclusions drawn from these analyses.

We end this section with justifications of actions, reward and states implemented in this work as well as guidelines for researchers that would like to apply the RL approach on their own case study with their own model.

4.2.1 Reward and success

The learning phase has been split into batches of 500 steps, i.e., 500 sequences of state-action-reward-new state. At the end of each batch, the up-to-date policy, i.e., the NN, is saved. This way, we can assess the progress in the learning process and its convergence (see Figure 4.3). The mean reward increases rapidly at the beginning of the learning process before reaching a plateau where the optimisation of the policy becomes more marginal. As these successes indirectly drive the agent's optimisation, it shows that the reward function (see Figure 4.2) leads towards more and more successes. However, given the wide range of uncertainty of some parameters and the agent's levers of action, this success rate stays limited at the end of the learning process. In other words, there are conditions where it is impossible for the agent to succeed the transition.

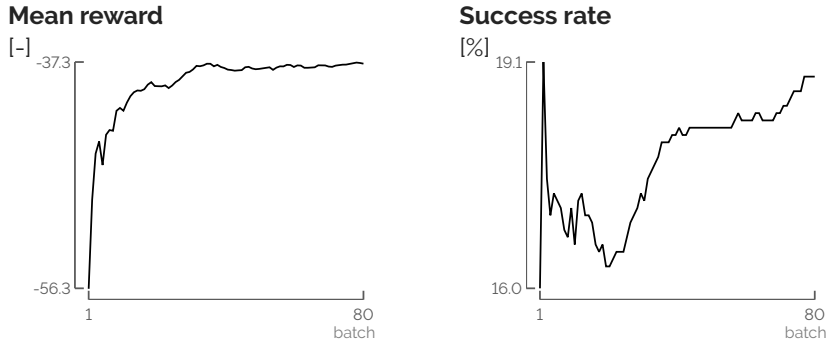


Figure 4.3. Mean reward and success rate of the different learning batches. The stabilisation of the reward curve shows a convergence of the learning process for the agent's point of view. The evolution of the success rate also shows that the reward function aims at more and more successful transitions.

When assessing the distributions of the values of reward in the failure and success cases, one notices a range where these distributions overlap (see left hand side of Figure 4.4). This area corresponds to either transitions that exceed the CO₂ budget in 2050 but are cheaper than the total transition cost of reference (see Section 4.1) or successful transitions that are more expensive. Besides this overlap, we observe that successes account for the majority of the cases with higher reward. This is another indication that the reward function is appropriate in this exploration of successful transition pathways. More indirectly, in case of applying this methodology to another case study, this substantiates that the weights between emissions and cost defined in Section 4.1.2 could be used as an initial step and fine-tuned afterwards.

Considering the end of the time window where the CO₂ budget is exceeded, the right hand side of Figure 4.4 shows that 2040 is the “tipping year” for the agent. Beyond this point, through this learning process, the chances to succeed the transition were 38%. In other words, near-term (2025-2030) actions are necessary to hope succeeding the transition.

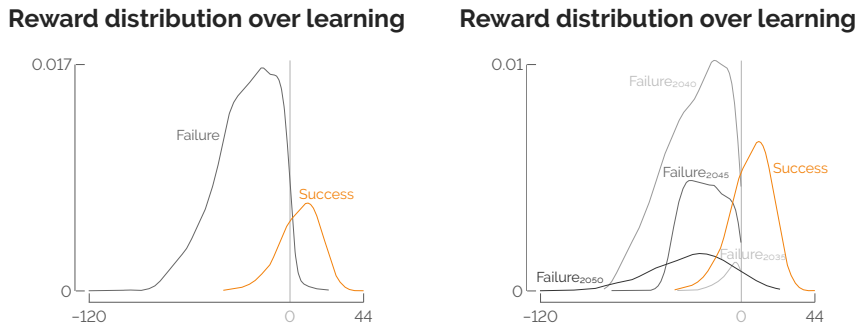


Figure 4.4. Reward distribution between successes and failures. Graph on the right hand side details at the end of which time window the failure occurred. The “tipping year” is 2040 as failing the transition by 2040 represents 57% of all the failures. Beyond this point, through this learning process, succeeding the transition represents 38% of the episodes.

4.2.2 States

The first two dimensions of the state space are the cumulative emissions and costs. They drive the value of the reward and, consequently, the optimisation of the agent’s policy. Per definition, the threshold of 1.2 GtCO_{2,eq} splits the episodes reaching 2050

into successes and failures (see Figure 4.5). Since infeasible cases or those that overshoot the CO₂ budget are discarded before reaching 2050 (see Section 4.1.2), the number of attempts that reach further steps in the transition progressively decreases. Consequently, the share of successful transitions compared to failures progressively increases with time. In the successful transitions, the median cumulative emissions, P₅₀, are about 0.9 Gt_{CO₂,eq}. Reaching cumulative emissions significantly lower than the CO₂ budget are possible thanks to efforts made at earlier stages of the transition and the potential to install SMR later on. Considering the failures in 2050, half of these episodes ended up with cumulative emissions lower or equal to 1.4 Gt_{CO₂,eq}. As illustrated in Figure 4.4, 2040 is identified as the tipping year. Where 98% of the failures were below the CO₂ budget in 2035, only 37% passed this threshold in 2040. This reminds the importance of near-term, 2025-2030, actions to hope for a successful transition.

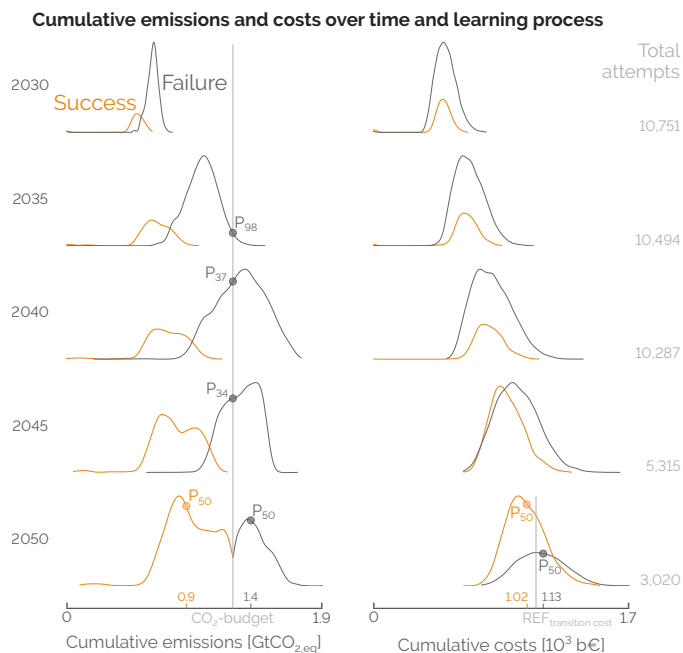


Figure 4.5. Exploration of the state space over the learning process: distribution of occurrence of cumulative emissions (left) and costs (right). Number of remaining attempts decrease with time since infeasible problem and solutions overshooting the CO₂ budget are discarded prematurely, i.e., before reaching 2050. Besides infeasible problems, distributions labelled as “Failure” represent the attempts that overshot the CO₂ budget by 2050 at the latest. The majority of successful transitions have cumulative emissions much lower than the CO₂ budget and are cheaper than the REF case.

Given the reward function (see Figure 4.2), the agent optimises its policy by aiming at lowering the total transition cost as soon as it meets the CO₂ budget. The skewness of the cumulative emissions and costs in 2050 are indications of this reward function (see Table 4.1). When succeeding the transitions, the cumulative emissions have a negative skewness: the agent successfully stayed within the budget and most of the cases were close to that budget (median at 0.9 GtCO_{2,eq}). On the contrary, the cumulative cost of successful transitions has a positive skewness: the agent successfully reduces the cost of the system as a secondary objective with 30% of the cases above the reference transition cost. This hierarchy of agent's objectives is verified with the failures. When it failed the transition, the agent aimed at reducing the emissions (skewness of 0.61) before minimising the total transition cost (skewness of 0.24).

Table 4.1. Skewness of cumulative emissions and costs in 2050. Cumulative emissions are skewed to the left and to the right for the successes and failures, respectively. The skewness of the cumulative costs for successful transitions is higher compared to failures. On top of being the results of the optimisation through EnergyScope, these are influenced by the agent's policy that aims only at lowering the total transition cost as soon as it meets the CO₂ budget.

| Status of episode in 2050 | Skewness of cumulative emissions | Skewness of cumulative costs |
|---------------------------|----------------------------------|------------------------------|
| Success | -0.52 | 0.50 |
| Failure | 0.61 | 0.24 |

Finally, we observe that the majority of the successful transitions are cheaper than the reference transition cost, 1.1 b€. Among the parameters impacting the most the total transition cost, we observe that success occurs when, on average, the cost of purchasing fossil fuels is increased more than the one of electrofuels (see Table 4.2). In other words, to have higher chances to succeed a myopic transition, the key factor is to reduce the uncertainty on the cost of purchasing electrofuels or to increase the cost of fossil fuels. Given the skewness that is positive and negative for the electrofuels and the fossil fuels, respectively, these cases represent more than the majority of the successful cases. On top of this, total transition costs of successful episodes are lower due to lower industrial EUD and discount rate. These favourable conditions combined with the right agent's actions led to transitions respecting the CO₂ budget.

Table 4.2. Uncertain parameters impacting the most the total transition cost and, for the successful transitions, the mean of their values between 0 and 100%, μ , and their skewness, γ . On top of being supported by the agent's actions, successful transitions occur when the cost of purchasing fossil fuels is more increased than the one of electrofuels.

| Parameter | μ | γ |
|-----------------------|-------|----------|
| Purchase electrofuels | 50.4% | 0.004 |
| Industry EUD | 49.8% | 0.026 |
| Discount rate | 48.4% | 0.089 |
| Purchase fossil fuels | 55.0% | -0.068 |

Besides the cumulative emissions and costs, the agent also observes the share of renewable energy carriers in the primary mix and the efficiency of the system. The share of renewable energy carriers in the primary mix allows identifying intermediate milestones along successful transitions (see Figure 4.6). From the initial state of 10% in 2020, a boost of integration of renewables in the near-term is needed to hope for a successful transition. For the successful occurrences to exceed failures, this share increases to 54% in 2025. Along the transitions, this increase goes with the import of electrofuels and the full deployment of local VRES. In 2050, the threshold where successes occur more often than failures was at 82% of renewable share. In the REF case of Chapter 3, this share reached 86% by 2050. However, by 2050, Figure 4.6 shows another “bump” at lower share of renewables in the mix. This area corresponds to the possibility to install SMR. As uranium is considered as a non-renewable resource [132], installing SMR allows lowering the threshold as in the SMR case of Chapter 3. Besides these milestones to respect the CO₂ budget of the transition, one can also look at the other side of the thresholds. Below the near-term threshold of ~60%, this is the

“no-go zone” where succeeding the transition becomes unlikely, except if betting on the future installation of SMR.

The efficiency, as defined in Section 4.1, gives less valuable information towards successful transitions. Through the transition, besides the share of success increasing over the failures, the distributions of success and failure indistinguishably spread over the whole range. Similarly than the emissions, we observe a bump at lower efficiencies by 2050 due to the installation of SMR.

4.2.3 Actions

After investigating the intermediate milestones to meet the CO₂ budget by 2050, this section details the actions the agent has taken during the learning process (see Figure 4.7). Rows represent the beginning of the time window at which the set of actions is taken. Similarly to the state space, we observe a wide exploration of the action space. The more the agent was able to progress through transition, without exceeding the CO₂ budget, the bigger is the share of successes compared to failures. Besides this observation, no specific range of values for the different actions at the different timing seems to lead to more successes. Looking at action individually, there does not seem to be any that supports more effectively the transition. The success comes from the combination of these actions.

To identify the actions that have an actual impact on the environment, we can check if they are binding or not. In a LP problem, constraints represent hyperplanes in the domain of variables. In a two-dimension space, these are straight lines (see Figure 4.8). When the problem is bounded and feasible, these lines are the edges of a convex polygon: the domain of feasibility. The optimal solution, \mathbf{x}^* , is the combination of variables leading to the optimal value of the objective function. Besides being within the domain of feasibility, it is proven that this optimal solution, when unique¹, locates on a vertex of the domain [171]. The constraints intersecting at this vertex are considered as binding, actually limiting the objective function to be more optimal. In other words, binding constraints, when tightened, aggravate the objective value function. If these are inequality constraints, as represented in Figure 4.8, it means that their left and right sides of the equation are equal.

After filtering out failures of the learning episodes and keeping only the successful transitions, only a limited set of the actions are binding and have an actual impact on the result of the optimisation in EnergyScope Pathway (see Figure 4.9). This allows

¹There are cases where the objective function has the same optimal value along an entire edge. In this case, there is an infinity of solutions and the problem is indeterminate.

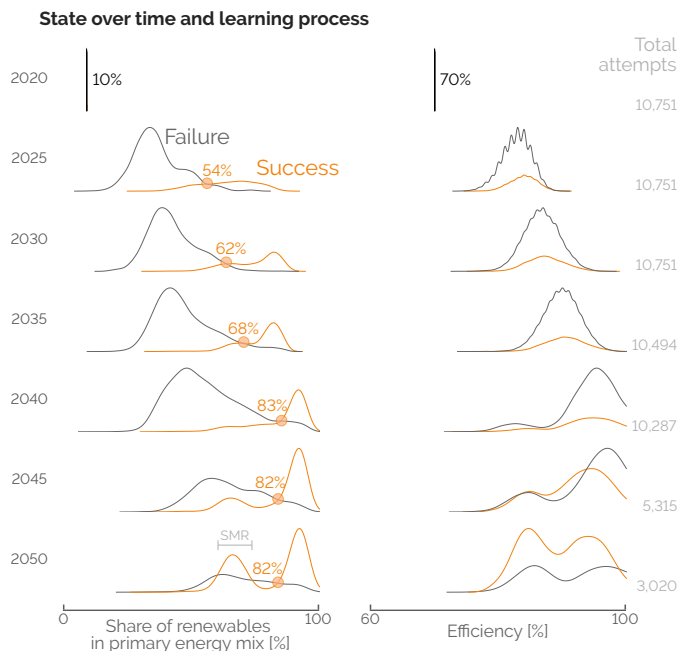


Figure 4.6. Exploration of the state space over the learning process: distribution of occurrence of share of renewable energy carriers in the primary energy mix (left) and efficiency (right). Number of remaining attempts decrease with time since infeasible problem and solutions overshooting the CO₂ budget are discarded prematurely, i.e., before reaching 2050. Besides infeasible problems, distributions labelled as “Failure” represent the attempts that overshot the CO₂ budget by 2050 at the latest. Integration of local VRES at early stages then massive import of electrofuels later are needed to secure successful transitions. Below a near-term threshold (~60%), the chances of success are limited, i.e., no-go zones. Efficiency is a less valuable information for the agent to succeed transitions as failures and successes indistinguishably spread over the whole range.

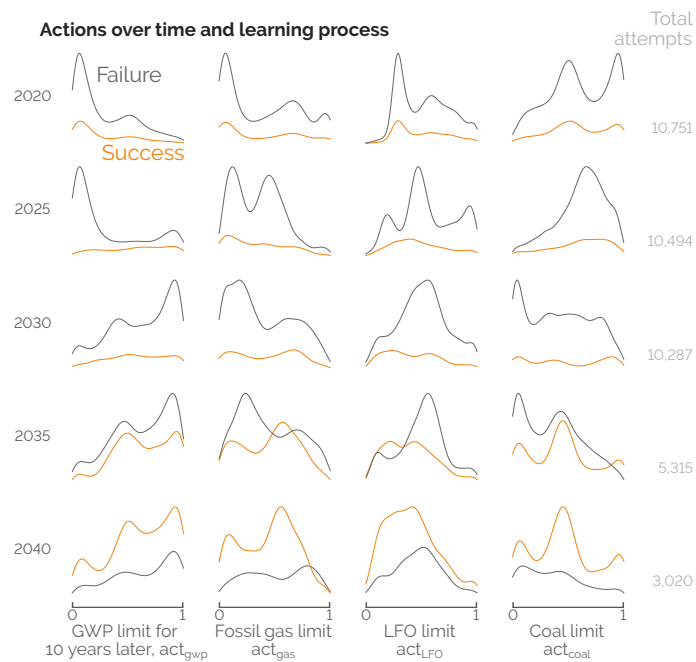


Figure 4.7. Exploration of the action space over the learning process: distribution of occurrence of the different actions at the time they are taken by the agent. Number of remaining attempts decrease with time since infeasible problem and solutions overshooting the CO₂ budget are discarded prematurely, i.e., before reaching 2050. Besides infeasible problems, distributions labelled as “Failure” represent the attempts that overshot the CO₂ budget by 2050 at the latest. Besides this wide exploration, successes and failures indistinguishably spread over the whole ranges of actions. In other words, it does not seem to be any clear set of actions to support successful transitions.

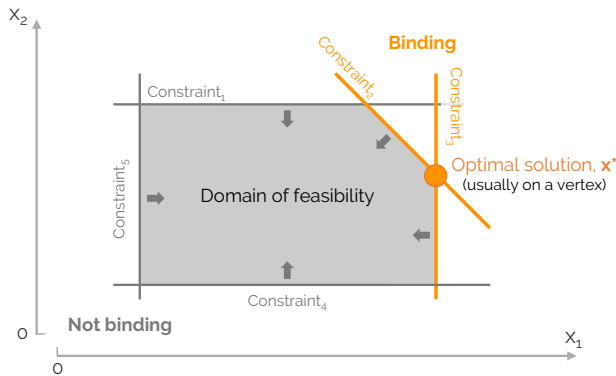


Figure 4.8. Binding versus non-binding constraints. In LP where the feasibility domain is non-empty and bounded, the constraints defined a convex feasibility domain in the space of variables (here, x_1 and x_2). The optimal solution usually locates on a vertex of this domain, i.e., the intersection of several constraints (here, constraints 2 and 3) limiting the solution. These constraints are considered as binding, i.e., having a limiting impact on the optimal solution.

identifying key actions to support the myopic transition. Limiting the GWP in the near-term is a key-factor for success. However, this action has a binding effect on the environment only at the end of the transition. The range over which limiting the use of fossil gas binds the optimisation is wider. Compared to other non-renewable fuels, this is due to the longer use of this energy carrier favoured by its low GWP (the second after uranium) and its versatility (applications in the electricity, heat and mobility sectors). In line with Vogt-Schilb et al. [141], the early constraints on generation and the sharper decrease of the emissions avoid lock-in situations.

When it comes to limiting the use of LFO and coal, the conclusions are more straightforward. At the beginning of the transition, most of the 159 TWh of LFO are consumed by naphtha-cracker (46%) and decentralised boilers (45%). The remaining 10% are consumed by industrial boilers. Even though LFO represents 30% of the primary energy mix in 2020, the cost-based model removes it from the mix without requiring the action of the agent. Naphtha-crackers, decentralised and industrial boilers get substituted by MTO, decentralised HP and industrial resistors and CHP, respectively. This “non-bindness” of limiting LFO is an indication that this action could be removed from the agent’s levers of action without impacting the optimisation of its policy.

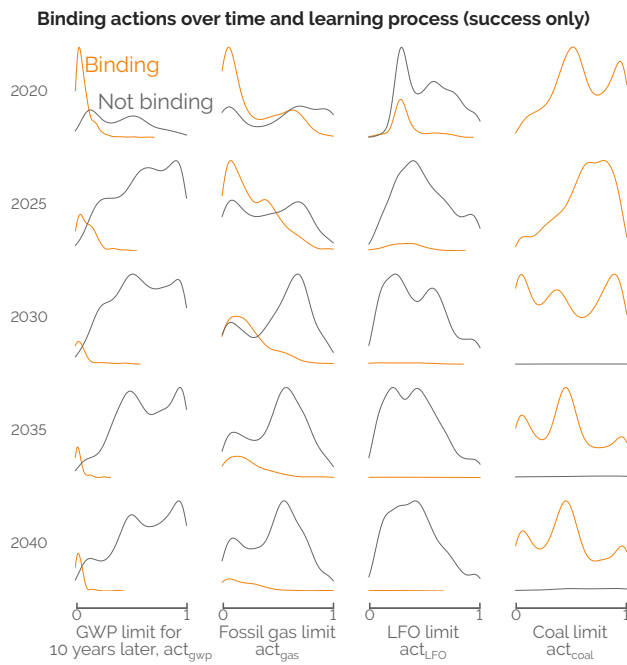


Figure 4.9. Keeping only the successful transitions, distribution of occurrence of binding and not binding actions. Depending on the action and its timing, it is actually constraining the optimisation through EnergyScope Pathway or not. Sweet spots can be identified when considering the limits of GWP and fossil gas consumption. Limiting coal consumption is always constraining, unlike LFO that is “naturally” substituted by EnergyScope Pathway in the near-term.

On the contrary, limiting coal is always binding. Before all, this is due because coal is a cheap resource (17 €/MWh). In other words, the cost-driven environment will favour it. Then, as the maximum amount of coal (28 TWh) is much smaller than fossil gas and LFO, high value of act_{coal} still represents small consumption of coal. Whatever the stage in the transition, a policy limiting the use of coal will always be effective, whereas one could think that coal should be limited only at early stages to get rid of coal-driven technologies once and for all for the rest of the transition. Consistency towards banning coal is needed.

4.2.4 Discussion and guidelines for future researchers

As introduced in Chapter 1, most of the work in applying RL is the definition of the interactions between the agent and its environment (i.e., actions, reward and states) that are very dependent on the case study and the research questions to answer. The elements presented in this work result from several trial and errors to end up with meaningful results according to our research questions.

Besides mimicking potential actual policies, the actions chosen in this work have a direct translation into constraints and we can therefore assess their effectiveness through the fact they are binding or not. In this work, we have investigated other actions like incentivising solar PV panels and wind turbines by “artificially” reducing their CAPEX. The result was not conclusive as these technologies need to take part to the Belgian energy transition and because it was harder to assess the impact of this action.

The reward function was designed to first aiming at respecting the CO₂ budget then minimising the total transition cost. The -300 penalty given in case of an infeasible optimisation problem was arbitrarily set. *A posteriori*, it seems to be a well-defined penalty given its significant relative difference with the values taken by the reward otherwise, between -120 and 44 (see Figure 4.4). Besides this penalty and given the observed results, we recommend to start with the same reward function if the objective is similar, first target cumulative emissions then cumulative costs. This requires to define the CO₂ budget according to a certain sharing principle (see Section 2.5) and to compute reference total transition cost. However, other researches focusing on reaching carbon neutrality by 2050 could define a binary reward function as +1 for reaching the objective and -1 otherwise.

Finally, states aim at representing the information relevant to the agent to efficiently learn and progress through the transitions. For this reason, on top reward-related features (cumulative emissions and costs), we added other indicators that are actually monitored to help decision-makers assessing their policies to reach their targets (share of renewables in the mix and the system overall efficiency). For other studies, one might consider other information like the metrics considered by Pickering et al. [163] (e.g., heat electrification, average national import or level of curtailment).

In conclusion, future studies might start from the actions-reward-states defined in this work and adapt these rules depending on the research questions to answer, the case study and the energy system optimisation model.

4.3 Comparison with references

After investigating the exploration of myopic transitions, this section compares these results with the perfect foresight under uncertainties from the GSA presented in Chapter 3. To reduce the computational time, the monthly model could also be used to carry out RL-based exploration of myopic pathways. Appendix E presents the comparison between the results obtained from the learning process on the hourly and monthly models.

RL-based myopic optimisation provides CO₂-emissions pathways different from the perfect foresight approach to respect the same CO₂ budget (see left side of Figure 4.10). However, driven first by this CO₂ budget, the agent often reaches much lower cumulative emissions when succeeding the transition (see Figure 4.5). This comes from the agent's actions that limit the emissions and/or the consumption of fossil resources at the early stages. Thanks to the bigger reduction of emissions at these early stages, the RL-based optimisation can benefit from a “CO₂-buffer” at the end of the transition. This buffer is compensated by the end of the transition where 50% of the myopic transitions reach 2050 with 10 or more remaining Mt_{CO₂,eq} compared to 4 for the perfect foresight approach. These remaining emissions by 2050 come from the consumption in industrial boilers of waste and coal that account for 3.5% and 2.4% of the primary mix on average by 2050. Finally, the long-term vision of the perfect foresight approach results in smoother reduction of the emissions to end up with less emissions by 2050.

The comparison between the failures and the successes demonstrates the added-value brought by myopic pathway optimisation. In the near-term (2025-2030), levels of emission are similar between perfect foresight and myopic cases that have failed. This shows that limited foresight encourages to strongly act at the early stages. On top of this, following the initial steps of CO₂-emissions pathways resulting from PF approach would likely (~80%) lead to fail the transition.

Looking at the total transition cost, the combination of the agent's actions and favourable economic conditions (see Section 4.2.2) make the myopic transitions cheaper, on average, than the PF cases (see right side of Figure 4.10). This is also due to the fact that the perfect foresight approach always finds a solution even in worst conditions such as high cost of purchasing resources and high EUD. This explains the wider variability of the PF results too. However, with the same sample of uncertain parameters, given the assumed full knowledge over the whole time horizon, PF naturally results in a cheaper transition than its myopic equivalent.

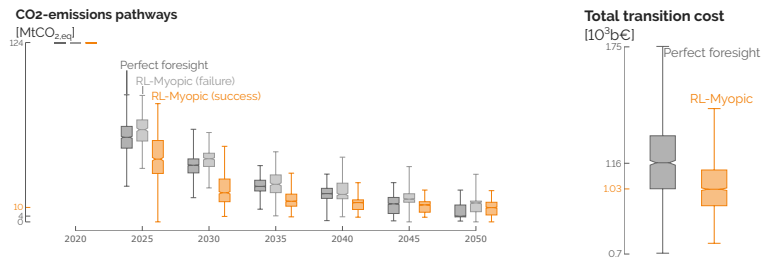


Figure 4.10. Comparison of CO₂-emissions pathways (left) and total transition cost (right) from the perfect foresight optimisation under uncertainties and the RL-based myopic optimisation. Myopic transitions succeed with a more drastic reduction of emissions in the short-term and, on average, more favourable economic conditions.

The analysis of the cumulative costs shows that the OPEX is the main difference between myopic and perfect foresight transitions (see Figure 4.11). Supported by the agent's actions, successful myopic transitions have a lower OPEX than the perfect foresight ones.

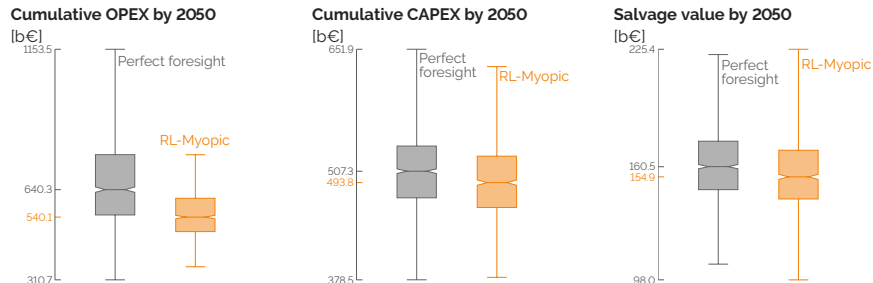


Figure 4.11. Comparison of cumulative OPEX (left), CAPEX (center) and salvage value (right) in 2050 from the perfect foresight optimisation under uncertainties and the RL-based myopic optimisation.

The cost of purchasing the energy carriers represents about 70% of the total cumulative OPEX. The assessment of the primary energy mix by 2050 highlights that the difference of OPEX between the perfect foresight and the myopic pathways come from the import of electrofuels, and especially of e-ammonia (see Figure 4.12). In the majority of the cases, e-ammonia is more than two times more imported in the myopic transitions. Being cheaper than e-methane (see Chapter 2), e-ammonia brings flexibility in the production of electricity via CCGT (see Chapter 3). Besides the slightly

favourable economical conditions (see Table 4.2), the myopic optimisations opt to invest massively into importing renewable molecules because of the limited knowledge in the future, and, among others, the availability of SMR. This explains why 50% of the successful transitions reached cumulative emissions below 900 Mt_{CO₂,eq} (see Figure 4.5).

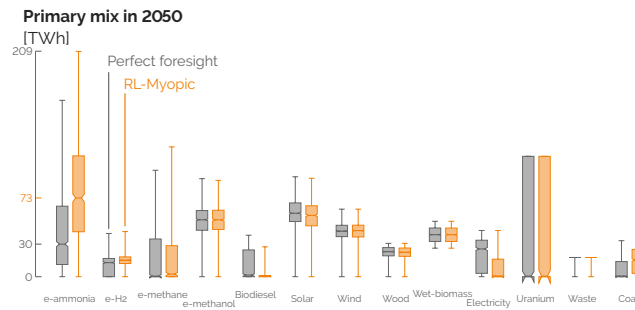


Figure 4.12. Comparison of the primary energy mix in 2050 from the perfect foresight optimisation under uncertainties and the RL-based myopic optimisation. The biggest difference is about e-ammonia to supply CCGT.

4.4 Conclusions

In the literature, two options are investigated to explore transition pathways of a whole-energy system: perfect foresight and myopic. In perfect foresight optimisation, a full knowledge of the parameters is assumed over the entire time horizon. To add more realism, myopic optimisation considers a sequence of more limited time windows leading to the end of the time horizon [38]. To respect a CO₂ budget over the transition, this case requires a prescribed CO₂-trajectory [172]. However, since the effect of CO₂-emissions in climate change is cumulative, the total amount of these emissions matters more than the trajectory itself. Consequently, we have applied the Reinforcement Learning (RL) approach on the environment of the Belgian myopic pathway optimisation under uncertainties.

This RL-based exploration pointed out that short-term actions were needed to hope succeeding such a transition, as also demonstrated by Luderer et al. [13]. Where LFO becomes less cost-competitive in the near-future, limiting the use of coal should be done at any cost. Then, fossil gas should be replaced by e-methane in the mid-term while putting a strict limit on the overall emissions becomes the most effective action

by the end of the transition. The analysis of the share of renewables in the primary energy mix highlighted intermediate milestones to have higher chances to succeed the transition. Below 54% of renewables in the mix in the near-future, these chances become much more limited, i.e., the no-go zone.

We have compared the results coming from this RL-based myopic optimisation with the hourly perfect foresight approach. These myopic optimisations provided pathways respecting the CO₂ budget that were more drastic in cutting emissions in the short-term than the perfect. Supported by the agent's actions, we could reach cheaper energy system than what the perfect foresight could give. This comparative analysis also pointed out that investing more into renewable electrofuels was the option when knowledge about the future is limited. To do so, it requires reducing the uncertainties of their cost of purchasing.

Further analyses should assess more accurately the impact of uncertainties on the agent's capacity to succeed the myopic transition. These analyses would aim at identifying the parameters that should necessarily be in specific ranges to allow the agent to succeed. On the contrary, there could be ranges of values for which the chances of success would be much more limited.

In conclusion, via the application of the RL approach, we have widely explored the different myopic transition pathways and identified sweet-spots (and no-go zones) to succeed a transition with an ambitious CO₂ budget target. It also highlighted the actions to take to effectively support a whole-energy system transition. This framework allows future research to test other policies on other case studies and identify the key actions and the timing to take them through the transition.

Chapter 5

Robustness assessment of pathway roadmaps

“The more data we have, the more likely we are to drown in it.”

Nassim Nicholas Taleb, in *Fooled by Randomness: The Hidden Role of Chance in Life and in the Markets*, 2008

Assessing the robustness of a roadmap driving the transition pathway of a whole-energy system is complex, especially due to the curse of dimensionality. This curse comes from the number of variables of the system (e.g., the installed capacity of technologies), the multiple-year approach specific to the pathway optimisation (i.e., versus the snapshot approach) or the number of uncertain parameters. On top of this, the sector coupling interconnecting the installed capacities and the used resources among the different (non-)energy sectors can make harder the understanding of big trends of such a system. To navigate through this load of uncertain and interconnected data, it is necessary to assess the robustness of pathway roadmaps.

To deal with such uncertainties, decision-makers have several options: (i) resistance; (ii) resilience; (iii) static robustness; and (iv) adaptive robustness [173]. Where resistance consists in planning for the worst-case scenario, resilience aims at a fast recovery whatever the conditions in the future. In static robustness, one seeks for a roadmap that would perform “satisfactorily” in a wide range of plausible futures, whereas, a roadmap would be dynamically robust if it is prepared to adapt in case of a change in conditions. Where Chapter 4 addressed the static robustness of a policy as its ability to maximise the chances to succeed a myopic transition, the objective of this chapter is to apply the method described in Section 1.4 to deal with the static ro-

bustness of pathway technological roadmaps, defined as their ability to limit the need to invest into additional capacities.

Castrejon-Campos et al. [167] assessed policy mix following the same philosophy of “satisfactory level of performance” as [173]. In their work, they mostly focused on the electricity sector, accounting for a variety of stakeholders and related interests using STET (Socio-Technical Energy Transition) models to capture more properly societal and behavioral aspects in relation with policy implementation, enriching purely techno-economic model, like EnergyScope, that usually assume rational choice within an overall cost minimization. However, in the case of the transition pathway of a whole-energy system, the challenges stand here in the definition of the “performance metric” as well as the “satisfactory level of performance”. Between the total transition cost giving too few information and the entire set of installed technologies giving too much, the performance metric here is defined through the PCA approach. Then, when comes the “satisfactory level of performance”, we propose a relative level of performance through a comparative analysis of different roadmaps. Each roadmap will be ranked in terms of robustness.

Contributions

The main contributions of this chapter is the application of the methodology proposed in Section 1.4 to the case study of the Belgian energy transition. First, we apply the different steps that lead to the principal components of the transition. We analyse these big trends of variation and highlight the fact that these variations stand for the entire pathway, a group of consecutive representative years or rather on a tipping-year. Then, and most importantly, we assess the robustness of different technological roadmaps by projecting their resulting myopic pathway against these directions of variation. The application of PCA to provide a new metric for robustness applied to the case of Belgium is the added-value of this chapter.

5.1 Definition of the principal components of the transition

The directions of variation, i.e., the robustness metrics, are based on the installed capacities through the transition in the different end-use sectors, i.e., electricity, HT heat, LT heat, passenger mobility, freight mobility, HVC, ammonia and methanol (see Section 1.4.2). These capacities represent the technological roadmaps to supply these EUD while respecting the CO₂ budget. Data considered in this method come from the GSA carried out on the perfect foresight optimisation of the Belgian transition pathway (see

Chapter 3). This gave 1260 different transitions resulting, for each of them, from the pathway optimisation subject to a sample of uncertain parameters (see Section 1.2.1). Appendix D.3 gives the exhaustive distributions of the installed capacities among the different end-use sectors from the GSA.

5.1.1 Principal components of each representative year

Before computing the Principal Components (PCs) of each representative year, we pre-preprocessed the raw data through scaling and managing the outliers (see Section 1.4.2). Managing the outliers is needed when assessing the main directions of variation of the transition. For example, decentralised HP running on methane is discarded. This technology would have a contribution in the PCs of transition for several reasons. First of all, the LT heating sector represents between 22% and 27% of the EUD in the case of Belgium. Being part of this major sector, the scaling of decentralised gas HP is higher than technologies in other sectors. Then, given the LP implementation of EnergyScope Pathway, the gas heat pumps completely substitute electric heat pumps in specific conditions (less electricity and cheaper methane). However, these cases represent less than 10% of the 1260 runs. For these reasons, we have decided that managing the outliers was needed to assess the main directions of variation of the transition.

The total variance decreases by more than 50% between the earlier stages and the final ones (see Table 5.1). Even though the absolute value of these variances has no physical meaning, we observe that the variations are more important at earlier stages of the transition. In other words, the further the transition goes, the more limited the degrees of freedom are to respect the CO₂ budget.

Table 5.1. Whole-system design variance of the different representative years and their comparison with 2025.

| Year | Design variance [10 ⁻³] | vs. 2025 |
|------|-------------------------------------|----------|
| 2025 | 10.4 | - |
| 2030 | 12.1 | +15% |
| 2035 | 9.7 | -7% |
| 2040 | 6.1 | -42% |
| 2045 | 5.1 | -51% |
| 2050 | 4.8 | -54% |

Then, keeping the PCs capturing at least 90% of the total variance of each representative year, this gives between four, in 2035, and seven, in 2050, PCs depending

on the year (see Figure 5.1), and a total of 34 PCs. At later stages of the transition, the increasing number of required PCs, in line with their smaller share of explained variance, is another indication that the variance of the system design is more spread over a wider range of technologies and with a more limited amplitude.

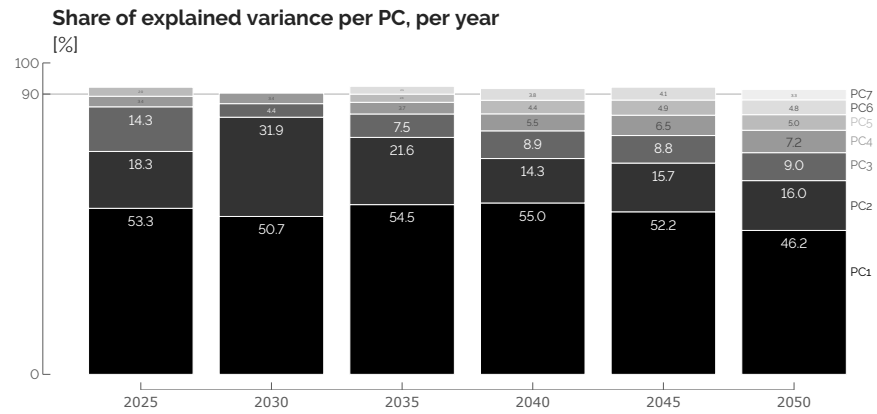


Figure 5.1. PCs capturing at least 90% of the total variance of their respective representative year of the transition.

Finally, we consider the respective contribution of the different technologies in the different PC_y , i.e., their corresponding component in the different eigenvectors. Highlighting the top-5 technologies for $\text{PC}_{y,1}$, $\text{PC}_{y,2}$ and $\text{PC}_{y,3}$, we observe general trends over the whole transition as well as tipping year where there is a clear trade-off between several technologies (see Figure 5.2). The top-5 technologies of $\text{PC}_{y,1}$ represent on average 99.4% of the norm of their respective PC. For $\text{PC}_{y,2}$ and $\text{PC}_{y,3}$, this share decreases to 97.6% and 90.9%, respectively. As pointed out in Section 1.4.2, PCA does not make any distinction between a vector of variation and its opposite. This is why $\text{PC}_{2025,1}$ and $\text{PC}_{2035,1}$ are actually very similar even though there are mostly on the opposite sides of the 0-axis.

Even though the following observations could be made by analysing the distribution of installed capacities (see Appendix D.3) or the covariance matrices, the PCA decomposition offers a more visual and summarising representation of the main trends of variation. Due to their intermittency, increasing the integration of PV panels requires the installation of other technologies to benefit from free and renewable electricity when it exceeds the electrical EUD. Therefore, we observe that the variation of installed PV is directly linked with the variation of installed industrial electrical resistors and, to a smaller extent, of decentralised and DHN electrical HP. These vari-

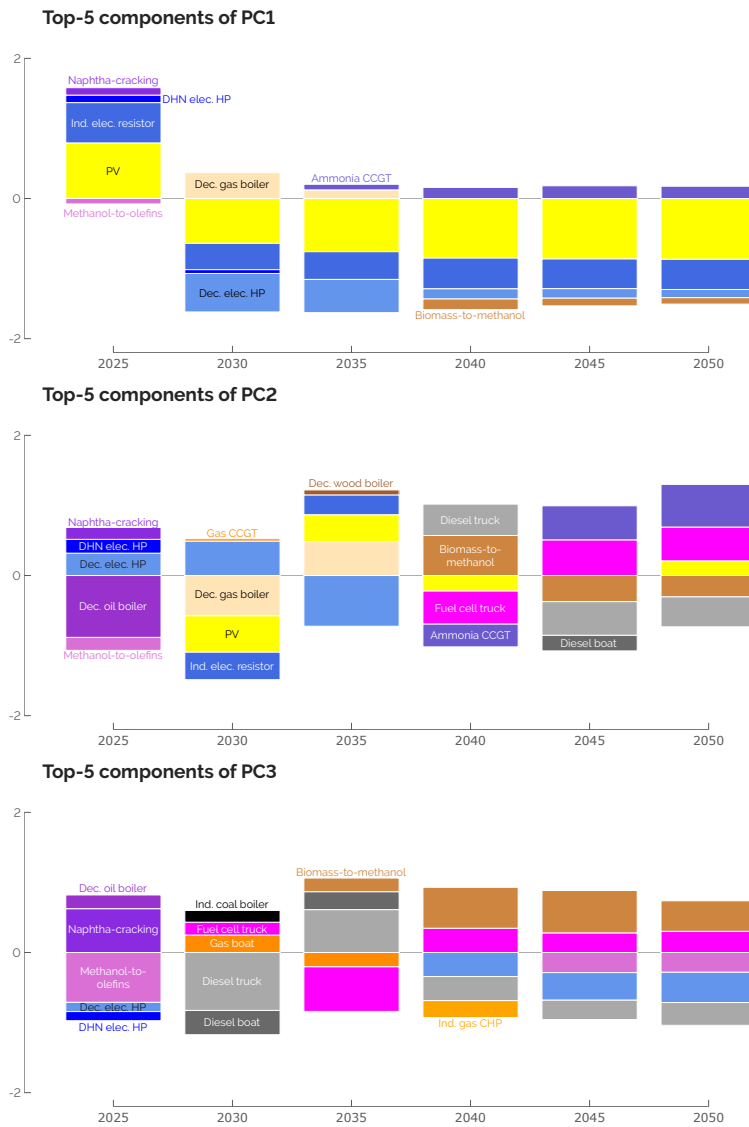


Figure 5.2. Contribution of the top-5 technologies to the first three PCs over the different representative years. Where the variation of PV panels supported by the electrification of the HT heat via industrial electric resistors are the main varying drivers over the whole transition, there are tipping years like 2025 for the production of HVC (i.e., naphtha-cracker to MTO) or 2025-2030 for the production of LT heat (i.e., from oil and gas boilers to electric HP).

ations spread over the whole transition and they are the main varying factors to the first $\text{PC}_{\text{transition}}$. Where this was an example for correlated technologies, we can also identify some key modal shifts where one technology is either substituted or in balance with others. First, about the LT heat sector, the early stages of the transition, i.e., 2025-2030, sees the shift from mainly decentralised oil and gas boilers towards decentralised and DHN electrical HP. Later in the transition, there seems to be a tight competition between (bio)diesel and FC trucks that drive the design variance to a smaller extent as they mostly appear in the second and third PCs of the representative years. Representing a smaller share of the total variance, there are other modal shifts (e.g., BEV substituting diesel and gasoline cars) that are not visible through the PCs. Besides these modal shifts spread over several representative years, 2025 is the tipping year concerning the shift from naphtha-cracker to methanol-to-olefins to supply HVC. Finally, there are also technologies contributing to PCs because they are the main producing assets of their respective end-use sector and the demand varies significantly, e.g., biomass-to-methanol.

5.1.2 Principal components of the perfect foresight REF transitions

Based on the PCs of each representative year (34 in total), this section identifies a sufficient subset to characterise the roadmaps (and assess their robustness in Section 5.2.2).

Before aggregating and averaging similar PC_y , it is necessary to rank them to ensure capturing most of the transition variance in the subsequent $\text{PC}_{\text{transition}}$. This ranking is based on the design variance captured by each PC_y in their respective representative year (see Table 5.2). Summing all of these variances over the different years results in a “pseudo” total variance of the transition. To construct the PCs of the transition, $\text{PC}_{\text{transition}}$, we keep the PC_y that captures at least 85% of this total variance of the transition (see Section 1.4.2). This results in keeping 14 PC_y : the first and second PCs of each representative year and the third PC of 2025 and 2035.

Given the similarity between PC_y (see Figure 5.2), some $\text{PC}_{\text{transition}}$ result from the aggregation and averaging of the components of several PC_y (see Table 5.3). This aggregation step has a double objective: limiting the dimension of the robustness metrics and avoiding ineffective redundancy in terms of $\text{PC}_{\text{transition}}$ where several of them would otherwise point towards similar directions of variation.

Table 5.2. Ranking of PCs per design variance captured in their respective representative year and cumulative share of the captured total variance of the transition

| Ranking | Year | PC | Design variance [10^{-4}] | Cumulative share of total variance [%] |
|---------|------|-----------------|-------------------------------|--|
| 1 | 2030 | PC ₁ | 61.1 | 13.9 |
| 2 | 2025 | PC ₁ | 55.7 | 26.5 |
| 3 | 2035 | PC ₁ | 52.7 | 38.4 |
| 4 | 2030 | PC ₂ | 38.4 | 47.2 |
| 5 | 2040 | PC ₁ | 33.4 | 54.7 |
| 6 | 2045 | PC ₁ | 26.5 | 60.7 |
| 7 | 2050 | PC ₁ | 22.2 | 65.8 |
| 8 | 2035 | PC ₂ | 20.9 | 70.5 |
| 9 | 2025 | PC ₂ | 19.1 | 74.8 |
| 10 | 2025 | PC ₃ | 15.0 | 78.2 |
| 11 | 2040 | PC ₂ | 8.7 | 80.2 |
| 12 | 2045 | PC ₂ | 7.9 | 82.0 |
| 13 | 2050 | PC ₂ | 7.7 | 83.7 |
| 14 | 2035 | PC ₃ | 7.3 | 85.4 |
| ⋮ | ⋮ | ⋮ | ⋮ | ⋮ |
| 34 | 2050 | PC ₇ | 1.6 | 100 |

Averaging the components of similar PC_y allows constructing the PC_{transition} (see Figure 5.3). These directions of variation form the robustness matrix on which it is possible to project the results of transition roadmaps tested under uncertainties and myopic pathway optimisation.

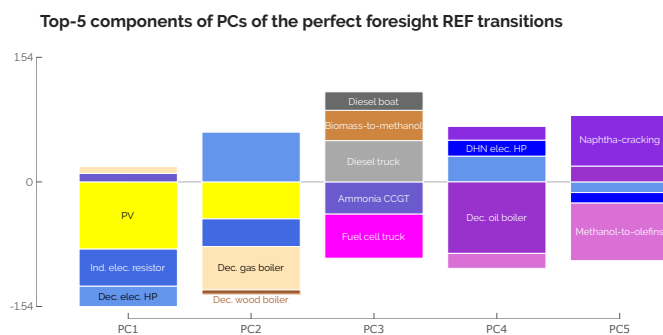


Figure 5.3. Contribution of the top-5 technologies to the different PC_{transition}.

Table 5.3. Aggregation of PC_y to construct the $\text{PC}_{\text{transition}}$ and share of the captured total variance of the transition by each $\text{PC}_{\text{transition}}$.

| $\text{PC}_{\text{transition}}$ | PC_y | Share of total variance [%] |
|-----------------------------------|----------------------|-----------------------------|
| $\text{PC}_{\text{transition},1}$ | $\text{PC}_{2025,1}$ | |
| | $\text{PC}_{2030,1}$ | |
| | $\text{PC}_{2035,1}$ | |
| | $\text{PC}_{2040,1}$ | 57.0 |
| | $\text{PC}_{2045,1}$ | |
| | $\text{PC}_{2050,1}$ | |
| $\text{PC}_{\text{transition},2}$ | $\text{PC}_{2030,2}$ | |
| | $\text{PC}_{2035,2}$ | 13.4 |
| $\text{PC}_{\text{transition},3}$ | $\text{PC}_{2040,2}$ | |
| | $\text{PC}_{2045,2}$ | |
| | $\text{PC}_{2050,2}$ | 7.2 |
| | $\text{PC}_{2035,3}$ | |
| $\text{PC}_{\text{transition},4}$ | $\text{PC}_{2025,2}$ | 4.3 |
| $\text{PC}_{\text{transition},5}$ | $\text{PC}_{2025,3}$ | 3.4 |

5.2 Robustness assessment of pathway roadmaps

Now that the performance metric is defined, we can assess the robustness of different roadmaps. These roadmaps are defined as the technological mix given by the deterministic optimisation of the perfect foresight pathway under certain conditions. The two first roadmaps are the **REF** and **SMR** cases (see Chapter 3). All the uncertain parameters are considered at their nominal value in these two cases. The only difference consists in allowing SMR from 2040 onward in the **SMR** case. On top of these two cases, we add a so-called “robust” case, **ROB**, in the same sense as in the works of Bertsimas and Sim [87] or Moret [42] accounting for a “protection parameter”. Then, we assess the robustness of these three roadmaps via a “three-step rolling horizon approach” extended from the work of Moret et al. [39]: (i) setting the initial investment strategies provided by the roadmaps and, (ii) assessing the variation of additional investments needed through myopic pathway optimisation under uncertainties and, (iii) projecting the strategies from the myopic optimisations on the robustness metrics defined via PCA. Finally, we assess the variation of the transition costs resulting from these myopic transitions under uncertainties.

5.2.1 A robust roadmap?

Rather than considering all the uncertain parameters at their worst values as in the work of Soyster [174], we follow a method inspired by the robust approach of Bertsimas and Sim [87] and Moret [42]. In their works, the authors consider a factor $\Gamma_{\text{obj}} \in [0, d]$ that represents a “protection parameter” of the objective function where d is the total number of uncertain parameters (see Section 1.2.2). If $\Gamma_{\text{obj}} = 0$, where all the uncertain parameters are at their nominal value, we obtain the deterministic solution of the **REF** case. If $\Gamma_{\text{obj}} = d$, this means considering the “fully robust” solution where all the uncertain parameters are their worst value, as in Soyster [174]. Between these two extreme cases, the uncertain parameters to account for at their worst values follow the ranking given by the GSA (see Chapter 3). In practice, $\Gamma_{\text{obj}} = 1$ means considering the cost of purchasing electrofuels at its worst value. $\Gamma_{\text{obj}} = 2$ adds the industry EUD at its worst value, and so on. In the present analysis, we label the roadmap as “robust” (**ROB**) by arbitrarily setting $\Gamma_{\text{obj}} = 6$. The ROB roadmap results from the deterministic optimisation of the perfect foresight pathway where the following six parameters are set at their worst-case value (upper bound of their range): costs of purchasing electrofuels, fossil fuels and biofuels as well as the industry EUD, the discount rate and the variable OPEX of technologies. In practice, this means that, in the ROB case, imported energy carriers, except electricity, are 179.8% more expensive, the industrial demand is, by 2050, 23.9% higher¹, the discount rate is increased by 46.2% (i.e., 2.2% versus 1.5% in the REF case) and the variable OPEX of technologies, c_{main_t} , is 35.7% higher.

Besides the additional operational costs due to more expensive energy carriers, this case presents cumulative investments over the transition that are 2.6% (17 b€) higher than the REF case. The following paragraphs investigate the differences in the different sectors between the ROB and the REF cases, similarly to the comparison carried out with the SMR case in Chapter 3.

Power sector

Given the more expensive imported energy carriers, the model opts for an earlier electrification of the system and more efficiency. Consequently, the power sector is one of the most impacted ones (see Figure 5.4). At the earlier stages of the transition, the model opts for the full deployment of local VRES as soon as possible and importing more electricity (i.e., +8.7 TWh, +52%) from abroad in 2025. This earlier and bigger integration of VRES is supported by the higher electrification of HT and, to a smaller

¹As detailed in Chapter 2, the industrial demand encompasses the whole NED and HT heat demand, as well as the industrial share of electricity and LT heat demands.

extent the LT, heating sector as well as in the mobility sectors. It is mostly the industrial electric heaters that absorb the abundant and intermittent electricity produced by PV panels and wind turbines. In the mobility sectors, BEV substitutes gasoline cars from 2025 onward and electric trucks substitute diesel trucks in the near-term before being substituted by FC trucks at the end of the transition. On the supply side, besides the local VRES and the direct import of electricity from abroad, CHP units, mostly industrial, are favoured given their higher efficiency at the expense of ammonia-CCGT. In the ROB case, by 2050, these CHP units produce 43.3 TWh, i.e., 23% of the total electricity production, versus 21.9 TWh in the REF case. These observations are in line with the work of Moret et al. [39] focusing on the problem of overcapacity in the European power sector. The authors highlighted that the robust strategy diversified the supply sources of electricity between VRES, import of electricity and more efficient technologies like CHP and HP.

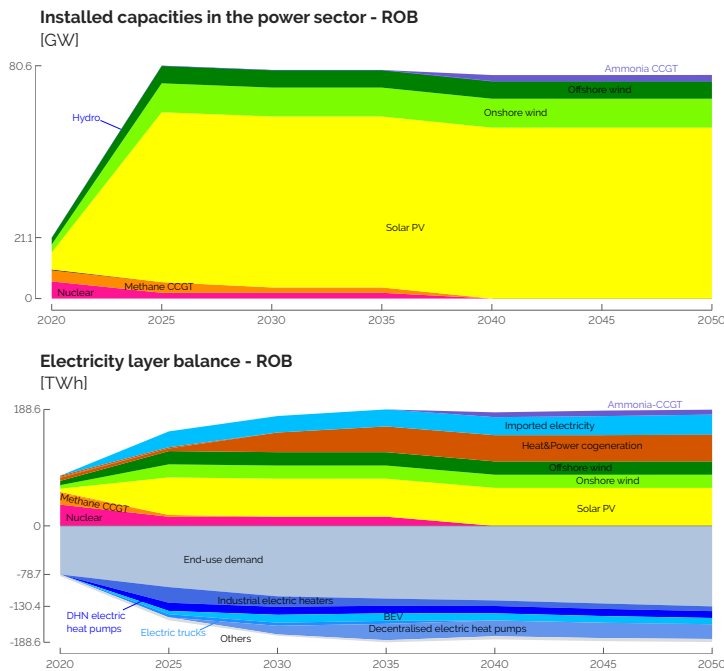


Figure 5.4. Installed capacities and layer balance of the power sector in the ROB case. Compared to the REF case, local VRES are deployed as soon as possible supported by an earlier electrification of the heat and transport sectors. CHP units also represents a higher share of the electricity supply given their higher efficiency at the expense of other flexible production units like ammonia-CCGT.

Heating sectors

By 2050, the additional 23.9% of industrial EUD directly impacts the technological mix to supply the HT heat, i.e., +13.6 TWh as direct HT heat EUD on top of the extra 3.4 TWh consumed by the MTO process. As aforementioned, at earlier stages of the transition, up to 20.9 GW of industrial electric heaters supply the additional demand and support the integration of solar PV. However, in the mid-term, 27% of these heaters are prematurely decommissioned where 24% are not renewed after reaching the end of their lifetime. Instead, up to +3.5 GW of industrial CHP units are installed to efficiently use e-methane that is considered more expensive in the ROB case to supply electricity and 52% of the HT heat demand. About the LT heat sector, the principal impact is the bigger installation of DHN and decentralised electric HP, up to +2.1 GW and +0.8 GW respectively.

Mobility sectors

In the ROB roadmap, the transport of freight by trucks first transitions from diesel to electric trucks and then, after 2035, to FC trucks. Used as a way to support the early installation of solar PV, electric trucks are then replaced by FC ones given the limited availability of renewable electricity and its more cost-effective use in other sectors such as private mobility. Freight transport via trains and boats are not different from the REF roadmap. About the passenger mobility, compared to the REF case, the shift from ICE cars to BEV occurs earlier in the transition, in line with the increased production of intermittent electricity from VRES.

Non-energy

Technologically speaking, by 2050, the ROB case accounts for an additional 1.2 GW of MTO to supply the extra 10.3 TWh of HVC. Besides this, the extra 2.5 TWh and 0.4 TWh of e-ammonia and e-methanol are supplied by the import of their respective energy carrier.

In conclusion, the two main assumptions impacting the ROB roadmap strategy compared to the REF one were the higher cost of purchasing imported energy carriers (except electricity) and higher industrial EUD. More expensive imported energy carriers lead to an earlier full deployment of local VRES (i.e., PV, wind onshore and offshore) and an increase of the share of the total OPEX due to the consumption of resources (i.e., excluding the OPEX of the technologies) in the total transition cost: i.e., 56% versus 38% in the REF case. This, combined with the increase of industrial EUD,

encourages a more efficient use of the resources, i.e., CHP and HP. The increased discount rate and variable OPEX of technologies have a more negligible impact on the roadmap strategy as they identically affect the entire set of technologies.

5.2.2 Projection on robustness metric

After defining the robustness metric and describing the roadmaps to assess (i.e., REF, SMR and ROB), the final step consists in testing these roadmaps under uncertainties in myopic pathway optimisations. This aims at assessing the adaptation of the roadmaps as uncertainty gradually unfolds over time [39], which brings more realism than perfect foresight [38]. The three roadmaps are tested 500 times fixing the installed capacities $f_{\max} \geq F \geq F^*$ for all the end-use technologies, and taking values of the 34 uncertain parameters (see Section 2.4) following the Sobol' sequence. However, some uncertain parameters limit the potential installed capacity, f_{\max} , of PV panels, onshore and offshore wind turbines and SMR. For these, in case the installed capacity prescribed by the roadmap is higher than the maximum potential affected by the value of the uncertain parameter, the actual installed capacity is set to this new limit. In reality, this would be similar to revise to a smaller extent the expected roadmap due to external events (e.g., smaller public acceptance [175, 176], lower Technology Readiness Level (TRL) or longer installation time than expected).

The SMR roadmap spans over similar ranges as the REF case (see Table 5.4). The most significant difference concerns PC 5. This PC is driven by the variations in the HVC sector. As detailed in Chapter 3, one of the impacts of the installation of SMR from 2040 onward is the delayed substitution of naphtha-crackers by MTO. As naphtha-cracker is the more economical option in the near-term of a myopic transition, this smoother modal shift leads to less variations of installed capacities. This makes the SMR roadmap more robust than the REF case.

The ROB roadmap is more robust than the REF case for the first three PCs. About PC 1, it is driven by the variation of installed capacities of PV supported by the electrification of HT and LT heating sectors. In the ROB case, the earlier full deployment of solar PV makes this roadmap 49% more robust towards these variations. For the same reasons, the ROB roadmap is 37% more robust for PC 2. The level of robustness is smaller than for PC 1 as the ROB roadmap substitutes sooner its decentralised gas boilers. In myopic transitions though, this technology keeps on being installed in the mid-term. Concerning PC 3, this higher robustness is explained by variations in the installed capacities of diesel trucks, biomass-to-methanol and ammonia-CCGT that are 32%, 30% and 15% smaller than in the REF case, respectively. Finally, the ROB

roadmap is 21% less robust for PC 5. Even though this roadmap accounts for the additional capacities of MTO in the long-term to supply the potential additional demand of HVC, the near-term capacities of naphtha-crackers are smaller. As aforementioned, this solution is favoured in the myopic optimisation which makes the ROB roadmap less robust to these variations.

Table 5.4. Comparison of the robustness with the REF case where robustness is defined by the width of the 95% confidence range of the additional installed capacities projected on the PC. Differences below 5% are not shown (\simeq).

| PC | Main contributors | Robustness comparison versus REF | |
|----|--------------------------|----------------------------------|----------|
| | | SMR | ROB |
| 1 | PV and electrification | \simeq | +49% |
| 2 | PV and dec. heating | \simeq | +37% |
| 3 | Freight transport | \simeq | +33% |
| 4 | Dec. oil boilers | \simeq | \simeq |
| 5 | Naphtha-crackers and MTO | +34% | -21% |

5.2.3 Principal components of myopic transitions

When computing the PCs of the different myopic transitions, the ROB case has a variance that is 10% smaller than the one of the REF case. Moreover, we observe that the variations of PV, industrial resistors and LT-heat technologies still have a major contribution on the variation of the system roadmaps (see Figure 5.5). More surprising is the contribution of the variation of the technology to produce methanol from methane. Where methanol is preferably imported from abroad (or produced from biomass) in the perfect foresight approach, the myopic optimisation opts for this technology in the near-term (2025) to compete with the imports as the main supplier of this energy carrier.

5.2.4 What about the costs over the transition?

Besides the additional capacities needed through the myopic transitions, this section takes a step back to assess the variations of costs over the transition: the total transition cost, the cumulative OPEX by 2050 and the cumulative CAPEX by 2050 (see Figure 5.6). We observe that the differences are marginal. This validates the initial rationale to go beyond these costs to assess the robustness of roadmaps.

Considering the median values, the ROB roadmap leads to a 1.6% more expensive total transition. This comes from the earlier investments in PV panels together with

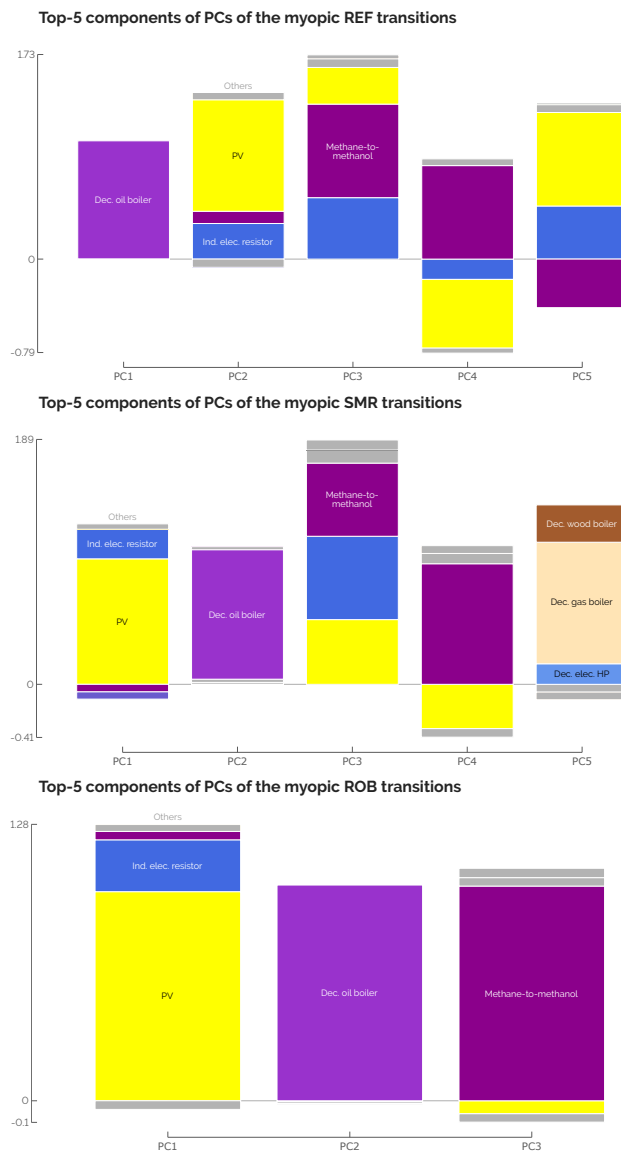


Figure 5.5. Contribution of the top-5 technologies to the PCs of myopic transitions for the REF, SMR and ROB cases. The variation of PV, industrial electric resistors and LT-heat technologies still have a major contribution of the variation in the system roadmaps. At the early stages of the myopic transitions, the installation methane-to-methanol is also subject to significant variations.

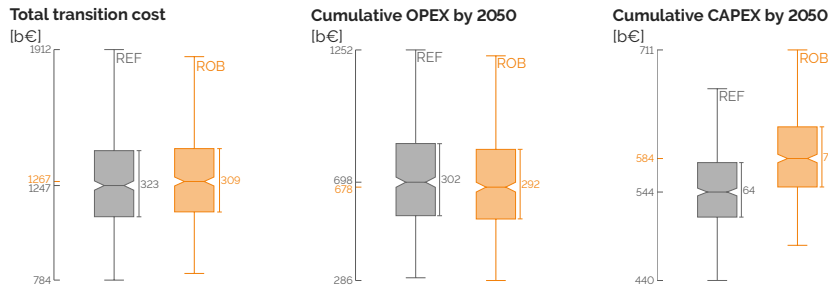


Figure 5.6. Comparison of total transition cost (left), cumulative OPEX (center) and CAPEX (right) by 2050 from the REF and ROB myopic transitions. The differences are marginal. However, the ROB roadmap lead to cheaper and less varying total transition cost. Requiring more investments at earlier stages, this roadmap is less affected by the variation of the operational costs.

electrified solutions in the heating sector that need to be renewed before the end of the transition. The extra-CAPEX also comes from more efficient (and more expensive) technologies such as CHP. These decisions allow being less affected by the variation of the cumulative operational costs that are dominated ($\sim 70\%$) by the cost of purchasing energy carriers. This makes the investment-to-operation ratio slightly higher for the ROB case (46%) than for the REF case (44%).

We can assess the variation of these costs with the quartile coefficient of dispersion. This coefficient of dispersion is defined as $(Q_3 - Q_1) / (Q_3 + Q_1)$ where $Q_1 = P_{25}$ and $Q_3 = P_{75}$ are the first and third quartiles of the data, respectively. We observe that the ROB case has a smaller quartile coefficient of dispersion for the total transition cost and cumulative OPEX but higher for the cumulative CAPEX (see Table 5.5). The biggest decrease of these coefficients of dispersion between the REF and the ROB cases concerns the total transition cost. This means that the ROB case ensures to decrease more the uncertainty on this cost.

All these conclusions are similar to the ones observed on the study of overcapacity of Moret et al. [39]). Working on the snapshot model and fixing the installed capacities only in the power sector, they although observed bigger gain to opt for a robust strategy rather than the deterministic solution.

Table 5.5. Quartile coefficient of dispersion for the total transition cost, cumulative OPEX and CAPEX by 2050 from the REF and ROB myopic transitions. The ROB case leads to more certain total transition cost and cumulative OPEX than the REF case.

| Quartile coefficient of dispersion | REF | ROB |
|------------------------------------|-------|-------|
| Total transition cost | 12.9% | 12.2% |
| Cumulative OPEX by 2050 | 21.3% | 21.1% |
| Cumulative CAPEX by 2050 | 5.9% | 6.0% |

5.3 Conclusions

In this chapter, we applied the PCA-based approach detailed in Chapter 1 to assess the robustness of different transition roadmaps for the case of Belgium. First, starting from the principal components of each representative year, we have computed the PCs of the transition to serve as robustness metric. This showed that the variation of installed capacities of PV, industrial electric resistors and LT-heat technologies drove the major share (75%) of the variation of the transition design strategy.

Then, we have tested three roadmaps resulting from different perfect foresight optimisations: REF, SMR and ROB. Where the first two have been broadly discussed in Chapter 3, the “robust” (ROB) case was considering the worst value of the uncertain parameters impacting the most the total transition cost following the same approach as Moret [42]. From these roadmaps setting the minimal installed capacities over the transition, we have assessed the variation of the additional capacities needed in myopic optimisations subject to uncertainties. This showed that counting on the installation of SMR by 2040 was providing the same level of robustness as the reference case in the key directions of variation. However, the robust (ROB) investment roadmap — which, in our case, anticipates the full deployment of local VRES and the integration of efficient technologies — is more robust than the reference scenario. Even though this roadmap represents 7.4% more cumulative CAPEX over the transition than the REF case, it provides more robustness towards the variations of PV supported by the electrification of HT and LT heating sectors (49%) and technologies in the transport of freight (33%). On top of decreasing the risk to invest into additional capacities, the ROB is also less sensitive to the variation of the costs of purchasing the energy carriers that are the main contributors of uncertainty.

Overall, this PCA-based approach allows evaluating the variation of multiple-year transition pathway of a whole-energy system and assessing its robustness. Doing so,

it brings more information than when considering only the variation of the objective function.

Conclusions and perspectives

The general objective of this thesis has been to investigate the impact of uncertainties and limited foresight on the transition pathway of a whole-energy system, accounting for multi-energy carriers and multi-sectors, subject to CO₂ budget without prescribed trajectory for the reduction of the emissions. We have studied the case study of Belgium with a focus on the role that renewable electrofuels (e-ammonia, e-methane, e-methanol and e-hydrogen) could play in this densely-populated and highly industrialised country with limited local renewable potentials. To have 66% chance of limiting warming to 1.5°C and using the “grandfathering” sharing principle of the global budget, the CO₂ budget of the 2020-2050 transition of Belgium has been set to 1.2 Gt_{CO₂,eq}.

To optimise such a system, we have developed EnergyScope Pathway: a whole-energy system that minimises the total transition cost of the system from 2020 to 2050. A myopic approach has been implemented, considering a sequence of 10-year time windows with an overlap of 5 years rather than one global optimisation over the 30 years of the transition. It allows assessing the realism of the decision making process where knowledge about the future is progressively unfold, rather than assumed to be fully known from the beginning of the transition as in the perfect foresight (PF) approach.

The future of a national whole-energy system is subject to a plethora of uncertainties. Main examples fo uncertainties are the cost of purchasing resources, their availabilities, the Capital Expenditure (CAPEX) of technologies and the level of demands. In this thesis, we have used the uncertainty characterisation approach developed by Moret et al. [51] to provide the range of variation of the uncertain parameters. To propagate uncertainties in the model and quantify their impact on the outputs of interest, we have used the Polynomial Chaos Expansion (PCE) method as implemented in the Coppitters' RHEIA framework [43].

The Reinforcement Learning (RL) approach was adopted to explore the myopic pathways respecting a CO₂ budget equivalent to 10 years of current emissions, without CO₂-trajectory. In this framework, an agent takes actions at the beginning of each time window to limit the emissions of the system, the *environment*, and the consumption of fossil fuels. Starting from the initial state of the energy system in 2020, the agent takes every five years a set of actions until reaching 2050 where a transition was considered as successful when respecting the CO₂ budget. Repeating the whole transition with different sequences of actions-states allowed the agent coming up with an effective policy towards sustainability, considering the variation of the parameters of its environment.

Finally, we have assessed the robustness of technological roadmaps tested in myopic transitions. To do so, the approach of Principal Component Analysis (PCA) was mobilised to identify the technologies that are more sensitive to uncertainties and that are more likely to impact the overall variance of the transition design. Projecting the results of myopic transitions on these principal components of the transition pointed out which roadmap is more robust and less likely to require additional investments along the transition.

Given the CO₂ budget to stick to a +1.5°C increase of global temperature and the presumably high levels of demands, aiming at a cost-optimum transition, Belgium should first opt for more efficiency to reduce by one third the primary energy consumption. Then comes the full deployment of local solar and wind energies that would represent about 30% of the mix by 2050. Due to the limited potential of local renewables, electrofuels are found to be the third pillar of the Belgian transition. The uncertainty on the total cost of the transition is mainly due to the uncertainty on the cost of purchasing electrofuels (47%), on the industrial end-use demand (23%), on the discount rate (12%) and on the price of fossil fuels (6%).

E-methanol is the key molecule to import in the mid-term to defossilise the non-energy demand of High-Value Chemicals (HVC), about 43 TWh/year, by substituting naphtha-crackers by Methanol-to-olefins (MTO). The uncertainty on this demand is the most impacting parameter (80%) on the variation of the quantity of imported e-methanol.

In the longer-term, on top of the non-energy demand to further produce fertilizers (about 10 TWh), importing e-ammonia becomes crucial to supply Combined Cycle Gas Turbine (CCGT) and to provide flexibility in the production of electricity in competition with nuclear Small Modular Reactor (SMR). For this reason, where the variation of the quantity of imported e-ammonia is mostly driven by the uncertainty on its

cost of purchasing (50%), the uncertainty on the availability of nuclear SMR by 2040 is the second most impacting parameter (20%). To a smaller extent, e-methane helps defossilising the industrial boilers and Combined Heat and Power (CHP). E-methane imports is mostly impacted by industrial demands (45%).

By 2050, in 88% of the transitions, e-hydrogen is only imported from abroad rather than locally produced. This molecule supports the defossilisation of the freight-transport by trucks. The variation of the imported quantity of e-hydrogen is mainly caused by the uncertainty on the CAPEX of fuel cell vehicles (25%) and its cost of purchasing (20%). In 12% of the transition pathways, up to 10.5 GW of electrolyzers are installed when local renewable electricity is abundant, SMR is available and imported e-hydrogen is expensive. These electrolyzers would locally produce up to 27 TWh of e-hydrogen.

The Reinforcement Learning-based exploration of myopic transitions points out that near-term actions are mandatory to hope succeeding this ambitious transition. Beyond 2030, if the right actions are not taken, the cumulative emissions are likely to overshoot the CO₂ budget. On top of strongly reducing the use of coal, fossil gas consumption should also be limited within 5 to 10 years. Once the fuel switch is operated from fossil gas to e-methane, putting a strong limit on the overall emissions is the most effective action to stick to the direction towards sustainability and encourage the import of renewable energy carriers. In the RL framework, the agent's actions are mainly driven by the share of renewable energy carriers in the primary energy mix rather than the overall system efficiency. This share of renewable energy carriers shows intermediate milestones to reach, 62%-share by 2030, to have higher chance to succeed the transition by 2050. Below this threshold, we find the so-called “no-go zone” where the chances of success are much lower. Due to limited foresight into the future and uncertainties like the possibility to install SMR by 2040, successful myopic transitions rely more on importing renewable electrofuels than the perfect foresight approach. An illustrative example is the case of e-ammonia, for which imports by 2050 are in general twice larger in the myopic transition. This work also highlighted a major difference between the perfect foresight (PF) approach and the agent-based myopic transitions. Given the assumed full knowledge on the future, the trajectories to decrease the CO₂ emissions resulting from perfect foresight are more progressive, and foreseen to be more applicable, compared to a sharper drop at the early stages of the transition, like in the myopic approach.

The uncertainty on the maximum installed capacity of solar PV, which is supported by the electrification of the industrial and decentralised heating sectors, drives 57% of the variance of the entire technological mix through the whole transition. On the

contrary, other key contributions to this variance are more focused on tipping years such as the low-temperature heating sectors shift from oil and gas decentralised boilers to electric Heat Pumps (HP) and Decentralised Heating Networks (DHN) from 2025 to 2035. In the non-energy sector, the shift from naphtha-crackers to Methanol-to-olefins (MTO) takes place in 2025.

Finally, testing technological roadmaps in myopic conditions has shown that cases relying or not on 6 GW of SMR by 2040 onward provide the same level of robustness in terms of additional capacities to install. Despite representing an additional 2.6% cumulative CAPEX over the transition, investing as soon as possible in local PV, the electrification of heating sectors and more efficient technologies such as CHP provides significantly better level of robustness (between 33% and 49%).

In the context of the energy transition, this thesis aimed at providing decision-makers with information and new methods considering the intrinsic uncertainties of the future. Even though the following messages result from studies on Belgium, the trends can be transposed to other countries with a high demand and low renewable potentials such as the Netherlands or Germany.

Besides a wider electrification of the system and the integration of more efficient technologies, Belgium needs to go for radical changes, “unicorn” solutions. One robust policy would consist in massively investing in electrofuels. Chemically similar to their fossil-based equivalents, they can benefit from the current infrastructures and provide seasonal storage and flexibility against the intrinsic intermittency of solar and wind electricity. Electrofuels should be imported from countries where the potential wind and solar electricity production largely exceeds the local consumption (Australia [177], Chile [178] or Spain [179]). The optimisation of the whole transition pathway indicates that we should aim at reducing the uncertainty on the cost of purchasing these energy carriers. On the road to a robust whole-energy system in Belgium, the policy makers, the industries and academia should invest in projects to produce and use these fuels or developing the exchange networks with foreign countries. This would provide significant reduction in the variation of the total transition cost and robustness towards uncertainties progressively unfolding with the future.

About the use of the electrofuels, there are two molecules imported in larger quantities: e-methanol and e-ammonia. E-methanol would aim at defossilising the production of High-Value Chemicals (HVC) in the non-energy sector and e-ammonia would dominantly provide flexibility in the production of electricity, respectively. The main use of e-hydrogen is in the freight transport via trucks and e-methane would supply the industrial sectors through CHP and boilers.

Often brought up as a “unicorn” solution to the energy transition, nuclear SMR would be a cost-competitive option against the import of electrofuels, especially e-ammonia and e-methane, but not against the deployment of local Variable Renewable Energy Sources (VRES) such as solar and wind. This confirmed that investing as soon as possible in local renewables is one pillar of the energy transition, especially when accounting for uncertainties and with the goal to respect an ambitious CO₂ budget of the transition.

Regarding methodologies, this thesis developed novel approaches to explore myopic pathway transitions, highlight intermediate milestones and no-go zones towards sustainability and assess the robustness of transition technological roadmaps. Keeping this work open-source allows the scientific community and the decision-makers to use these methods and adapt them on their specific case study and energy system optimisation model. Besides the formulated recommendations, the assumptions and the formulation choices made in this work can serve as a basis for further researches but will need to be adapted according to model that is used or the case study that is studied.

We conclude with perspectives that could benefit from the methods and the results developed in this thesis. Future studies could focus on different scenario analyses, the development of EnergyScope Pathway or the approaches applied to it such as RL.

The Belgian transition pathways explored in this thesis massively relied on the early deployment of local VRES and import of electrofuels. In some pathways, the current capacities of PV and wind turbines are multiplied by 10 and 6 over a 5 to 10 year time window. This is much faster than the multiplication by 2 and 2.5 of PV and wind capacities from 2024 and 2034 projected by Elia, Belgium Transmission System Operator (TSO), in their adequacy analysis [180]. The necessary amount of imported electrofuels could be 10 to 20 times higher than the potential that Belgium could benefit from considering the existing agreements with exporting countries [158]. A future work would be to constrain the deployment of local renewables or the availability of electrofuels. This could provide different pathways where electrofuels would be produced more locally using carbon capture technologies. This could also show the limits of the Belgian energy system to meet such an ambitious CO₂ budget in its energy transition when solely relying on technological progress, highlighting the need for demand reduction. One could then question the level of demands and address the question of the sufficiency. For a growing part of the scientific community, sufficiency is seen as a no-regret lever of action to reduce the anthropogenic GHG. A study could consist in analysing the level of demands, within their respective sector, we should reach to stay

within the CO₂ budget and limit the installation of solar PV, wind turbines, nuclear energy or the import of electrofuels.

To assess more accurately the boundary conditions of the Belgium in its transition pathway, a future work could be to merge the EnergyScope Pathway with EnergyScope Multi-Cells [181]. Rather than model a single country and the rest of the world as the exterior, the Multi-Cells optimises multiple interconnected regions. At a European scale, Belgium could benefit from energy exchanges with countries where the renewable potential is more important such as France or Spain.

On the methodological side, several perspectives could be considered about the whole-energy system model or the implementation of RL. The cumulative Greenhouse Gases (GHG) emissions of the transition has been constrained based on the use of the resources. However, in a system reducing drastically its emissions, indirect emissions such as the ones related to the construction and dismantling of assets would have a much higher share of the total emissions. Depending on the level of emission reduction, these indirect emissions could be one to three times higher than the direct emissions. To accurately integrate these emissions in the model and account for them in the CO₂ budget, LCA can compute these indirect emissions. On top of this, LCA could provide data to assess other impact indicators besides climate change [182]. Based on this multi-criteria approach, another thread of future work would be to implement multi-objective optimisation [183]. In this method, objectives other than the sole total transition cost such as the ones identified as planetary boundaries [142] would be minimised.

Regarding the RL approach, two threads of future development have been identified: reward shaping and multi-fidelity. First, the reward function could be adapted to incentivise more the successful transitions. Then, rather than giving a sparse reward at the end of the episode, reward shaping provides additional, intermediate rewards during the learning process based on various heuristics, domain knowledge, or problem-specific insights [184]. Reward shaping aims at accelerating the learning or guiding the agent towards achieving the desired behaviour more efficiently. In our case, the agent receives a sparse reward signal, indicating success or failure at the end of an episode. However, this sparse reward signal may not provide enough information for the agent to learn effectively, leading to slow convergence or difficulty in learning the optimal policy. Reward shaping addresses this issue. These intermediate rewards can help guide the agent towards desirable states or actions, making the learning process more efficient and effective. However, reward shaping should be applied with caution, as poorly designed reward functions can lead to unintended consequences such as

suboptimal policies, reward hacking, or overfitting to the shaped rewards rather than learning the underlying task.

Given the similarities between the policy learned on the monthly (coarse) and the hourly (fine) model, another way to improve the efficiency of the RL process would be to implement transfer knowledge [185], or even multi-fidelity [186]. The first step, transfer learning, would consist in starting the learning process on the monthly and faster model, refine the action space, and continue learning on the more accurate hourly model. More than this unidirectional transfer of information, Cutler et al. [186] developed the Multi-Fidelity Reinforcement Learning (MFRL) framework that defines rules for when the agent should move up to a higher fidelity environment, as well as moving down in fidelity before over-exploring in a more expensive optimisation. This would result in an agent that can, on the one hand, use information from the monthly model to limit the exploration in the hourly model, and, on the other hand, exploit the data of the hourly model to update the policy learned on the monthly one.

Nowadays, the development on solar and wind energies supported by other technical solutions such as electrofuels exchange market or nuclear energy, is not fast enough to stick to the +1.5° C of global warming. Even though it represents a growing part of the literature, sufficiency is rarely brought up by decision-makers as a solution. Whole-energy system models and related methodologies do not claim to predict the future but rather aims at quantifying options under several assumptions. In this sense, this work provided insight about possible transition pathways for Belgium to bring the technical dimension into the intrinsically political and interdisciplinary discussions and decisions that must be made in the coming years.

Bibliography

- [1] Intergovernmental Panel on Climate Change (IPCC), Global Warming of 1.5°C. An IPCC Special Report on the impacts of global warming of 1.5°C above pre-industrial levels and related global greenhouse gas emission pathways, in the context of strengthening the global response to the threat of climate change, sustainable development, and efforts to eradicate poverty, Technical Report, IPCC, 2018.
- [2] Our World in Data, Global co2 emissions from fossil fuels, <https://ourworldindata.org/co2-emissions>, (Accessed July 2023).
- [3] Y. Kaya, K. Yokobori, et al., Environment, energy, and economy: strategies for sustainability, volume 4, United Nations University Press Tokyo, 1997.
- [4] IPCC, Emissions Scenarios, Technical Report, Intergovernmental Panel on Climate Change, 2000.
- [5] J. C. Dodson, P. Dérrer, P. Cafaro, F. Götmark, Population growth and climate change: Addressing the overlooked threat multiplier, *Science of the Total Environment* 748 (2020) 141346.
- [6] N. Scovronick, M. B. Budolfson, F. Dennig, M. Fleurbaej, A. Siebert, R. H. Socolow, D. Spears, F. Wagner, Impact of population growth and population ethics on climate change mitigation policy, *Proceedings of the National Academy of Sciences* 114 (2017) 12338–12343.
- [7] European Parliament, Directive (EU) 2023/2413 of the European Parliament and of the Council of 18 October 2023 amending Directive (EU) 2018/2001, Regulation (EU) 2018/1999 and Directive 98/70/EC as regards the promotion of energy from renewable sources, and repealing Council Directive (EU) 2015/652, Technical Report, European Parliament, 2023. Official Journal of the European Union 2413, 1-77.
- [8] D. W. O'Neill, A. L. Fanning, W. F. Lamb, J. K. Steinberger, A good life for all within planetary boundaries, *Nature sustainability* 1 (2018) 88–95.
- [9] IPCC, Climate Change 2022: Mitigation of Climate Change - Summary for Policymakers, Technical Report, Intergovernmental Panel on Climate Change, 2022.
- [10] J. Lage, J. Thema, C. Zell-Ziegler, B. Best, L. Cordroch, F. Wiese, Citizens call for sufficiency and regulation—a comparison of european citizen assemblies and national energy and climate plans, *Energy Research & Social Science* 104 (2023) 103254.

- [11] S. Schmidt, H. Weigt, Interdisciplinary energy research and energy consumption: what, why, and how?, *Energy Research & Social Science* 10 (2015) 206–219.
- [12] International Energy Agency, World energy outlook 2019, <https://www.iea.org/reports/world-energy-outlook-2019>, 2020.
- [13] G. Luderer, Z. Vrontisi, C. Bertram, O. Y. Edelenbosch, R. C. Pietzcker, J. Rogelj, H. S. De Boer, L. Drouet, J. Emmerling, O. Fricko, et al., Residual fossil CO₂ emissions in 1.5–2 C pathways, *Nature Climate Change* 8 (2018) 626–633.
- [14] M. Robinius, A. Otto, P. Heuser, L. Welder, K. Syranidis, D. S. Ryberg, T. Grube, P. Markewitz, R. Peters, D. Stolten, Linking the power and transport sectors—part 1: The principle of sector coupling, *Energies* 10 (2017) 956.
- [15] T. W. Brown, T. Bischof-Niemz, K. Blok, C. Breyer, H. Lund, B. V. Mathiesen, Response to ‘burden of proof: A comprehensive review of the feasibility of 100% renewable-electricity systems’, *Renewable and sustainable energy reviews* 92 (2018) 834–847.
- [16] G. Limpens, H. Jeanmart, System lcoe: applying a whole-energy system model to estimate the integration costs of photovoltaic, in: 34th International Conference on Efficiency, Cost, Optimization, Simulation and Environmental Impact of Energy Systems (ECOS 2021). Taormina, Italy, 2021.
- [17] S. Horvath, M. Fasihi, C. Breyer, Techno-economic analysis of a decarbonized shipping sector: Technology suggestions for a fleet in 2030 and 2040, *Energy Conversion and Management* 164 (2018) 230–241.
- [18] S. Brynolf, M. Taljegard, M. Grahn, J. Hansson, Electrofuels for the transport sector: A review of production costs, *Renewable and Sustainable Energy Reviews* 81 (2018) 1887–1905.
- [19] IEA, Net Zero by 2050, Technical Report, IEA, 2021. URL: <https://www.iea.org/reports/net-zero-by-2050>.
- [20] E. Rozzi, F. D. Minuto, A. Lanzini, P. Leone, Green synthetic fuels: Renewable routes for the conversion of non-fossil feedstocks into gaseous fuels and their end uses, *Energies* 13 (2020) 420.
- [21] C. Lhuillier, P. Brequigny, F. Contino, C. Mounaïm-Rousselle, Experimental study on ammonia/hydrogen/air combustion in spark ignition engine conditions, *Fuel* 269 (2020) 117448.
- [22] M. Pochet, H. Jeanmart, F. Contino, A 22: 1 compression ratio ammonia-hydrogen hcci engine: Combustion, load, and emission performances, *Frontiers in Mechanical Engineering* 6 (2020) 43.
- [23] H. Stančin, H. Mikulčić, X. Wang, N. Duić, A review on alternative fuels in future energy system, *Renewable and Sustainable Energy Reviews* 128 (2020). doi:10.1016/j.rser.2020.109927.
- [24] K. Verleysen, D. Coppitters, A. Parente, W. De Paepe, F. Contino, How can power-to-ammonia be robust? Optimization of an ammonia synthesis plant powered by a wind turbine considering operational uncertainties, *Fuel* 266 (2020) 117049.
- [25] M. Child, D. Bogdanov, C. Breyer, The role of storage technologies for the transition to a 100% renewable energy system in europe, *Energy Procedia* 155 (2018) 44–60.

- [26] V. Dias, M. Pochet, F. Contino, H. Jeanmart, Energy and economic costs of chemical storage, *Frontiers in Mechanical Engineering* 6 (2020) 21.
- [27] M. Millinger, P. Tafarte, M. Jordan, A. Hahn, K. Meisel, D. Thrän, Electrofuels from excess renewable electricity at high variable renewable shares: cost, greenhouse gas abatement, carbon use and competition, *Sustainable Energy & Fuels* 5 (2021) 828–843.
- [28] R. Rosa, The Role of Synthetic Fuels for a Carbon Neutral Economy, *C* 3 (2017) 11. doi:10.3390/c3020011.
- [29] Institute for Sustainable Process Technology, Power to Ammonia (2017). URL: <http://www.ispt.eu/media/ISPT-P2A-Final-Report.pdf>.
- [30] W. L. Ahlgren, The dual-fuel strategy: An energy transition plan, *Proceedings of the IEEE* 100 (2012) 3001–3052. doi:10.1109/JPROC.2012.2192469.
- [31] J. Mertens, R. Belmans, M. Webber, Why the carbon-neutral energy transition will imply the use of lots of carbon, *C—Journal of Carbon Research* 6 (2020) 39.
- [32] B. V. Mathiesen, H. Lund, D. Connolly, H. Wenzel, P. A. Østergaard, B. Möller, S. Nielsen, I. Ridjan, P. Karnøe, K. Sperling, et al., Smart energy systems for coherent 100% renewable energy and transport solutions, *Applied Energy* 145 (2015) 139–154.
- [33] F. Contino, S. Moret, G. Limpens, H. Jeanmart, Whole-energy system models: The advisors for the energy transition, *Progress in Energy and Combustion Science* 81 (2020) 100872. URL: <https://doi.org/10.1016/j.pecs.2020.100872>.
- [34] Y. Zeng, Y. Cai, G. Huang, J. Dai, A review on optimization modeling of energy systems planning and ghg emission mitigation under uncertainty, *Energies* 4 (2011) 1624–1656.
- [35] X. Yue, S. Pye, J. DeCarolis, F. G. Li, F. Rogan, B. Ó. Gallachóir, A review of approaches to uncertainty assessment in energy system optimization models, *Energy strategy reviews* 21 (2018) 204–217.
- [36] S. Moret, V. Codina Gironès, M. Bierlaire, F. Maréchal, Characterization of input uncertainties in strategic energy planning models, *Applied Energy* 202 (2017) 597–617.
- [37] S. Pfenninger, A. Hawkes, J. Keirstead, Energy systems modeling for twenty-first century energy challenges, *Renewable and Sustainable Energy Reviews* 33 (2014) 74–86.
- [38] K. Poncelet, E. Delarue, D. Six, W. D'haeseleer, Myopic optimization models for simulation of investment decisions in the electric power sector, in: 2016 13th International Conference on the European Energy Market (EEM), IEEE, 2016, pp. 1–9.
- [39] S. Moret, F. Babonneau, M. Bierlaire, F. Maréchal, Overcapacity in european power systems: Analysis and robust optimization approach, *Applied Energy* 259 (2020) 113970.
- [40] G. Limpens, X. Rixhon, F. Contino, H. Jeanmart, Energyscope pathway: an open-source model to optimise the energy transition pathways of a regional whole-energy system, Elsevier in *Applied Energy* 358 (2024). doi:<https://doi.org/10.1016/j.apenergy.2023.122501>.

- [41] G. Limpens, Generating energy transition pathways: application to Belgium, Ph.D. thesis, Université Catholique de Louvain, 2021.
- [42] S. Moret, Strategic energy planning under uncertainty, Ph.D. thesis, EPFL, 2017.
- [43] D. Coppitters, Robust design optimization of hybrid renewable energy systems, Vrije Universiteit Brussel (VUB), University of Mons (UMONS), Mons (2021).
- [44] G. Limpens, H. Jeanmart, F. Maréchal, Belgian Energy Transition: What Are the Options?, *Energies* 13 (2020) 261.
- [45] SPF Economie, Energy - key data - edition february 2022, Brussels, February 2022.
- [46] S. Babrowski, T. Heffels, P. Jochem, W. Fichtner, Reducing computing time of energy system models by a myopic approach: A case study based on the perseus-net model, *Energy systems* 5 (2014) 65–83.
- [47] E. Guevara, F. Babonneau, T. Homem-de Mello, Modeling uncertainty processes for multi-stage optimization of strategic energy planning: An auto-regressive and markov chain formulation (2022).
- [48] G. Limpens, D. Coppitters, X. Rixhon, F. Contino, H. Jeanmart, The impact of uncertainties on the Belgian energy system: Application of the Polynomial Chaos Expansion to the EnergyScope model, *Proceedings of the ECOS* (2020).
- [49] X. Rixhon, G. Limpens, D. Coppitters, H. Jeanmart, F. Contino, The role of electrofuels under uncertainties for the Belgian energy transition, *Energies* 14 (2021) 4027.
- [50] B. Goffaux, Pathway towards energy sustainability in Belgium under uncertainties, 2021. URL: <https://dial.uclouvain.be/memoire/ucl/object/thesis:30574>.
- [51] S. Moret, M. Bierlaire, F. Maréchal, Strategic energy planning under uncertainty: a mixed-integer linear programming modeling framework for large-scale energy systems, in: *Computer Aided Chemical Engineering*, volume 38, Elsevier, 2016, pp. 1899–1904.
- [52] G. Limpens, S. Moret, H. Jeanmart, F. Maréchal, EnergyScope TD: A novel open-source model for regional energy systems, *Applied Energy* 255 (2019) 113729.
- [53] M. Geidl, P. Favre-Perrod, B. Klöckl, G. Koeppel, A greenfield approach for future power systems, *Proc. of Cigre General Session* 41 (2006) 136.
- [54] G. Limpens, EnergyScope Pathway documentation, Accessed 2022. URL: <https://energyscope.readthedocs.io/en/v2.2/index.html>.
- [55] F. Meinke-Hubeny, L. P. de Oliveira, J. Duerinck, P. Lodewijks, R. Belmans, Energy transition in belgium–choices and costs, *EnergyVille in Opdracht van Febeliec: Genk, Belgium* (2017).
- [56] S. Simoes, W. Nijs, P. Ruiz, A. Sgobbi, D. Radu, P. Bolat, C. Thiel, S. Peteves, The jrc-eu-times model, Assessing the long-term role of the SET Plan Energy technologies (2013).
- [57] P. Capros, A. De Vita, N. Tasios, P. Siskos, M. Kannavou, A. Petropoulos, S. Evangelopoulou, M. Zampara, D. Papadopoulos, C. Nakos, et al., Eu reference scenario 2016-energy, transport and ghg emissions trends to 2050., European Commission Directorate-General for Energy (2016). doi:10.2833/9127.

- [58] M. G. Prina, M. Lionetti, G. Manzolini, W. Sparber, D. Moser, Transition pathways optimization methodology through EnergyPLAN software for long-term energy planning, *Applied Energy* 235 (2019) 356–368. doi:10.1016/j.apenergy.2018.10.099.
- [59] T. Stocker, Climate change 2013: the physical science basis: Working Group I contribution to the Fifth assessment report of the Intergovernmental Panel on Climate Change, Cambridge university press, 2014.
- [60] J. Schnidrig, J. Brun, F. Maréchal, M. Margni, Integration of life cycle impact assessment in energy system modelling, *Proceedings of ECOS 2023* (2023).
- [61] H. Blanco, V. Codina, A. Laurent, W. Nijs, F. Maréchal, A. Faaij, Life cycle assessment integration into energy system models: An application for power-to-methane in the eu, *Applied Energy* 259 (2020) 114160.
- [62] D. L. McCollum, A. Gambhir, J. Rogelj, C. Wilson, Energy modellers should explore extremes more systematically in scenarios, *Nature Energy* 5 (2020) 104–107.
- [63] F. F. Nerini, I. Keppo, N. Strachan, Myopic decision making in energy system decarbonisation pathways. a uk case study, *Energy strategy reviews* 17 (2017) 19–26.
- [64] C. F. Heuberger, I. Staffell, N. Shah, N. Mac Dowell, Impact of myopic decision-making and disruptive events in power systems planning, *Nature Energy* 3 (2018) 634–640.
- [65] AMPL Optimization Inc., AMPL Python API, <https://amplpyAMPL.com/en/latest/>, 2024.
- [66] V. Krey, Vergleich kurz-und langfristig ausgerichteter optimierungsansätze mit einem multi-regionalen energiesystemmodell unter berücksichtigung stochastischer parameter (2006).
- [67] G. Mavromatidis, K. Orehonig, J. Carmeliet, Uncertainty and global sensitivity analysis for the optimal design of distributed energy systems, *Applied Energy* 214 (2018) 219–238.
- [68] J. Peace, J. Weyant, Insights not numbers: the appropriate use of economic models, White paper of Pew Center on Global Climate Change (2008).
- [69] C. Marnay, A. S. Siddiqui, Addressing an uncertain future using scenario analysis, Lawrence Berkeley National Laboratory, 2006.
- [70] X. Li, S. Moret, F. Baldi, F. Maréchal, Are renewables really that expensive? the impact of uncertainty on the cost of the energy transition, in: Computer Aided Chemical Engineering, volume 46, Elsevier, 2019, pp. 1753–1758.
- [71] D. Coppitters, W. De Paepe, F. Contino, Robust design optimization of a photovoltaic-battery-heat pump system with thermal storage under aleatory and epistemic uncertainty, *Energy* 229 (2021) 120692.
- [72] Climact, VITO, New scenarios for a climate neutral Belgium by 2050, Technical Report, 2021. URL: <https://klimaat.be/doc/climate-neutral-belgium-by-2050-report.pdf>.
- [73] Hydrogen Import Coalition, Shipping sun and wind to Belgium is key in climate neutral economy, <https://www.portofantwerp.com/sites/default/files/Hydrogen%20Import%20Coalition.pdf>, 2021.

- [74] D. Coppitters, W. De Paepe, F. Contino, Robust design optimization and stochastic performance analysis of a grid-connected photovoltaic system with battery storage and hydrogen storage, *Energy* 213 (2020) 118798.
- [75] D. Coppitters, P. Tsirikoglou, W. D. Paepe, K. Kyriandis, A. Kalfas, F. Contino, RHEIA: Robust design optimization of renewable Hydrogen and dErvived energy cArrier systems, *Journal of Open Source Software* 7 (2022) 4370. doi:10.21105/joss.04370.
- [76] D. Coppitters, RHEIA documentation, Accessed 2022. URL: <https://rheia.readthedocs.io/en/latest/index.html>.
- [77] B. Sudret, Polynomial chaos expansions and stochastic finite element methods, *Risk and reliability in geotechnical engineering* (2014) 265–300.
- [78] P. Bratley, B. Fox, Implementing sobols quasirandom sequence generator (algorithm 659), *ACM Transactions on Mathematical Software* 29 (2003) 49–57.
- [79] M. D. Morris, Factorial Sampling Plans for Preliminary Computational Experiments, *Technometrics* 33 (1991) 161–174.
- [80] G. Sin, K. V. Gernaey, Improving the morris method for sensitivity analysis by scaling the elementary effects, in: *Computer Aided Chemical Engineering*, volume 26, Elsevier, 2009, pp. 925–930.
- [81] G. Sin, K. V. Gernaey, A. E. Lantz, Good modeling practice for pat applications: propagation of input uncertainty and sensitivity analysis, *Biotechnology progress* 25 (2009) 1043–1053.
- [82] P. Turati, N. Pedroni, E. Zio, Simulation-based exploration of high-dimensional system models for identifying unexpected events, *Reliability Engineering and System Safety* 165 (2017) 317–330.
- [83] I. E. Grossmann, R. M. Apap, B. A. Calfa, P. García-Herreros, Q. Zhang, Recent advances in mathematical programming techniques for the optimization of process systems under uncertainty, *Computers & Chemical Engineering* 91 (2016) 3–14.
- [84] L. G. Fishbone, H. Abilock, Markal, a linear-programming model for energy systems analysis: Technical description of the bnl version, *International journal of Energy research* 5 (1981) 353–375.
- [85] A. Kanudia, R. Loulou, Robust responses to climate change via stochastic MARKAL: The case of Québec, *European Journal of Operational Research* 106 (1998) 15–30.
- [86] C. Nicolas, S. Tchung-Ming, O. Bahn, E. Delage, Robust Enough? Exploring Temperature-Constrained Energy Transition Pathways under Climate Uncertainty, *Energies* 14 (2021) 8595.
- [87] D. Bertsimas, M. Sim, The price of robustness, *Operations research* 52 (2004) 35–53.
- [88] R. Loulou, U. Remme, A. Kanudia, A. Lehtila, G. Goldstein, Documentation for the times model part ii, *Energy technology systems analysis programme* (2005).
- [89] M. Howlett, M. Ramesh, A. Perl, et al., *Studying public policy: Policy cycles and policy subsystems*, volume 3, Oxford university press Toronto, 1995.
- [90] A. Perera, P. Kamalaruban, Applications of reinforcement learning in energy systems, *Renewable and Sustainable Energy Reviews* 137 (2021) 110618.

- [91] D. Cao, W. Hu, J. Zhao, G. Zhang, B. Zhang, Z. Liu, Z. Chen, F. Blaabjerg, Reinforcement learning and its applications in modern power and energy systems: A review, *Journal of modern power systems and clean energy* 8 (2020) 1029–1042.
- [92] R. S. Sutton, A. G. Barto, *Reinforcement learning: An introduction*, MIT press, 2018.
- [93] David Silver, RL Course by David Silver, <https://www.youtube.com/watch?v=2pWv7G0vuf0&list=PLzvuuYNsE1EZAXYR4FJ75jcJseBmo4KQ9->, 2016.
- [94] T. Haarnoja, A. Zhou, P. Abbeel, S. Levine, Soft actor-critic: Off-policy maximum entropy deep reinforcement learning with a stochastic actor, in: International conference on machine learning, PMLR, 2018, pp. 1861–1870.
- [95] T. Haarnoja, H. Tang, P. Abbeel, S. Levine, Reinforcement learning with deep energy-based policies, in: International conference on machine learning, PMLR, 2017, pp. 1352–1361.
- [96] B. D. Ziebart, Modeling purposeful adaptive behavior with the principle of maximum causal entropy, Carnegie Mellon University, 2010.
- [97] A. Raffin, A. Hill, A. Gleave, A. Kanervisto, M. Ernestus, N. Dormann, Stable-baselines3: Reliable reinforcement learning implementations, *The Journal of Machine Learning Research* 22 (2021) 12348–12355.
- [98] M. Abadi, A. Agarwal, P. Barham, E. Brevdo, Z. Chen, C. Citro, G. S. Corrado, A. Davis, J. Dean, M. Devin, et al., Tensorflow: Large-scale machine learning on heterogeneous distributed systems, arXiv preprint arXiv:1603.04467 (2016).
- [99] K. Pearson, On lines and planes of closest fit to systems of points in space., *The London, Edinburgh, and Dublin philosophical magazine and journal of science* 2 (1901) 559–572.
- [100] H. Hotelling, Analysis of a complex of statistical variables into principal components., *Journal of educational psychology* 24 (1933) 417.
- [101] I. T. Jolliffe, *Principal component analysis for special types of data*, Springer, 2002.
- [102] K. Zdybal, G. D'Alessio, G. Aversano, M. R. Malik, A. Coussement, J. C. Sutherland, A. Parente, Advancing reacting flow simulations with data-driven models, arXiv preprint arXiv:2209.02051 (2022).
- [103] A. Parente, J. C. Sutherland, Principal component analysis of turbulent combustion data: Data preprocessing and manifold sensitivity, *Combustion and flame* 160 (2013) 340–350.
- [104] K. Peerenboom, A. Parente, T. Kozák, A. Bogaerts, G. Degrez, Dimension reduction of non-equilibrium plasma kinetic models using principal component analysis, *Plasma Sources Science and Technology* 24 (2015) 025004.
- [105] H. Aguinis, R. K. Gottfredson, H. Joo, Best-practice recommendations for defining, identifying, and handling outliers, *Organizational research methods* 16 (2013) 270–301.
- [106] I. Stanimirova, M. Daszykowski, B. Walczak, Dealing with missing values and outliers in principal component analysis, *Talanta* 72 (2007) 172–178.

- [107] P. Xia, L. Zhang, F. Li, Learning similarity with cosine similarity ensemble, *Information sciences* 307 (2015) 39–52.
- [108] J. Dommisce, J.-L. Tychon, Modelling of Low Carbon Energy Systems for 26 European Countries with EnergyScopeTD : Can European Energy Systems Reach Carbon Neutrality Independently?, Master's thesis, UCLouvain, 2020. URL: <http://hdl.handle.net/2078.1/thesis:25202>.
- [109] X. Rixhon, D. Tonelli, M. Colla, K. Verleysen, G. Limpens, H. Jeanmart, F. Contino, Integration of non-energy among the end-use demands of bottom-up whole-energy system models, *Frontiers in Energy Research-Process and Energy Systems Engineering* 10 (2022).
- [110] Eurostat, *Energy, Transport and environment statistics, 2019 edition*, 2019.
- [111] E. Commission, D.-G. for Climate Action, D.-G. for Energy, D.-G. for Mobility, Transport, A. De Vita, P. Capros, L. Paroussos, K. Fragkiadakis, P. Karkatsoulis, L. Höglund-Isaksson, W. Winiwarter, P. Purohit, A. Gómez-Sanabria, P. Rafaj, L. Warnecke, A. Deppermann, M. Gusti, S. Frank, P. Lauri, F. Fulvio, A. Florou, M. Kannavou, N. Forsell, T. Fotiou, P. Siskos, P. Havlík, I. Tsiropoulos, S. Evangelopoulou, P. Witzke, M. Kesting, N. Katoufa, I. Mitsios, G. Asimakopoulou, T. Kalokyris, EU reference scenario 2020 : energy, transport and GHG emissions : trends to 2050, Publications Office, 2021. doi:[doi:10.2833/35750](https://doi.org/10.2833/35750).
- [112] IEA, Nuclear Power and Secure Energy Transitions, Technical Report, IEA, Paris, 2022. <https://www.iea.org/reports/nuclear-power-and-secure-energy-transitions>, License: CC BY 4.0.
- [113] M. E. Biresselioglu, M. D. Kaplan, B. K. Yilmaz, Electric mobility in europe: A comprehensive review of motivators and barriers in decision making processes, *Transportation Research Part A: Policy and Practice* 109 (2018) 1–13.
- [114] Bureau Fédéral du Plan, Perspectives de l'évolution de la demande de transport en Belgique à l'horizon 2030, 2015.
- [115] National Research Council, *Transitions to alternative vehicles and fuels*, National Academies Press (2013).
- [116] J. Schnidrig, T.-V. Nguyen, X. Li, F. Maréchal, A modelling framework for assessing the impact of green mobility technologies on energy systems, Technical Report, EPFL, 2021.
- [117] FPS Economy, ENERGY Key Data, 2021.
- [118] IEA, The Future of Petrochemicals – Analysis, <https://www.iea.org/reports/the-future-of-petrochemicals>, 2018.
- [119] V. Daioglou, A. P. Faaij, D. Saygin, M. K. Patel, B. Wicke, D. P. van Vuuren, Energy demand and emissions of the non-energy sector, *Energy & Environmental Science* 7 (2014) 482–498.
- [120] Statbel, Energy statistics by economic sector and by energy source, <https://statbel.fgov.be/en/themes/energy/energy-statistics-economic-sector-and-energy-source>, (Accessed February 11, 2021).

- [121] X. Rixhon, M. Colla, D. Tonelli, K. Verleysen, G. Limpens, H. Jeanmart, F. Contino, Comprehensive integration of the non-energy demand within a whole-energy system: towards a defossilisation of the chemical industry in Belgium, in: 34th International Conference on Efficiency, Cost, Optimization, Simulation and Environmental Impact of Energy Systems (ECOS 2021). Taormina, Italy, 2021, pp. 152–163.
- [122] European Commission, European strategy for plastics, https://ec.europa.eu/environment/waste/plastic_waste.htm, (Accessed February 16, 2021).
- [123] Agoria & essenscia, The Belgian plastics industry and the circular economy, https://www.essenscia.be/wp-content/uploads/2019/11/Plast_BROCH_A5_HR.pdf, (Accessed February 16, 2021).
- [124] United Nations - Climate change, National inventory submissions 2020, <https://unfccc.int/ghg-inventories-annex-i-parties/2020>, (Accessed February 16, 2021).
- [125] M. M. S. Asia), Mmsa supply and demand forecast, <https://www.methanolmsa.com/additional-mmsa-services/temp-price-forecasts/>, (Accessed February 16, 2021).
- [126] L. Genge, F. Scheller, F. Müsgens, Supply costs of green chemical energy carriers at the european border: A meta-analysis, *International Journal of Hydrogen Energy* (2023).
- [127] M. J. Grant, A. Booth, A typology of reviews: an analysis of 14 review types and associated methodologies, *Health information & libraries journal* 26 (2009) 91–108.
- [128] M. J. Page, J. E. McKenzie, P. M. Bossuyt, I. Boutron, T. C. Hoffmann, C. D. Mulrow, L. Shamseer, J. M. Tetzlaff, E. A. Akl, S. E. Brennan, et al., The prisma 2020 statement: an updated guideline for reporting systematic reviews, *International journal of surgery* 88 (2021) 105906.
- [129] M. Colla, K. Verleysen, J. Blondeau, H. Jeanmart, Navigating Bioenergy Horizons: A Critical Examination of Europe's Potential, with Belgium as a Case, Under review (2024) 1–21.
- [130] EnergyVille, PATHS2050 - The Power of Perspective, <https://perspective2050.energyville.be/>, 2022 (accessed December 2022).
- [131] ELIA, Electricity scenarios for Belgium towards 2050, Technical Report, ELIA, 2017.
- [132] X. Rixhon, G. Limpens, F. Contino, H. Jeanmart, Taxonomy of the fuels in a whole-energy system, *Frontiers in Energy Research - Sustainable Energy Systems and Policies* (2021). doi:10.3389/fenrg.2021.660073.
- [133] D. Coppitters, N. Ghuys, K. Verleysen, G. Limpens, H. Jeanmart, F. Contino, Towards importing renewable hydrogen within planetary boundaries, Under review (2024). doi:10.21203/rs.3.rs-3920745/v1.
- [134] SCK-CEN, Small modular reactor (smr), <https://www.sckcen.be/en/expertises/nuclear-systems/small-modular-reactor-smr>, (Accessed July 2023).
- [135] F. Caron, M. Moore, D. Zekveld, Small Modular Reactor (SMR) Economic Feasibility and Cost-Benefit Study for Remote Mining in the Canadian North: A Case Study, 2021.

- [136] I. Tsiropoulos, R. Hoefnagels, S. de Jong, M. van den Broek, M. Patel, A. Faaij, Emerging bioeconomy sectors in energy systems modeling—integrated systems analysis of electricity, heat, road transport, aviation, and chemicals: a case study for the netherlands, *Biofuels, Bioproducts and Biorefining* 12 (2018) 665–693.
- [137] X. Rixhon, https://github.com/xrixhon/Non_energy_demand/tree/NED, March 2021.
- [138] F. Licandeo, F. Flores, F. Feijoo, Assessing the impacts of economy-wide emissions policies in the water, energy, and land systems considering water scarcity scenarios, *Applied Energy* 342 (2023) 121115.
- [139] N. Kaufman, A. R. Barron, W. Krawczyk, P. Marsters, H. McJeon, A near-term to net zero alternative to the social cost of carbon for setting carbon prices, *Nature Climate Change* 10 (2020) 1010–1014.
- [140] T. M. Wigley, R. Richels, J. A. Edmonds, Economic and environmental choices in the stabilization of atmospheric co₂ concentrations, *Nature* 379 (1996) 240–243.
- [141] A. Vogt-Schilb, G. Meunier, S. Hallegatte, When starting with the most expensive option makes sense: Optimal timing, cost and sectoral allocation of abatement investment, *Journal of Environmental Economics and Management* 88 (2018) 210–233.
- [142] K. Richardson, W. Steffen, W. Lucht, J. Bendtsen, S. E. Cornell, J. F. Donges, M. Drücke, I. Fetzer, G. Bala, W. von Bloh, et al., Earth beyond six of nine planetary boundaries, *Science advances* 9 (2023) eadh2458.
- [143] W. Steffen, K. Richardson, J. Rockström, S. E. Cornell, I. Fetzer, E. M. Bennett, R. Biggs, S. R. Carpenter, W. De Vries, C. A. De Wit, et al., Planetary boundaries: Guiding human development on a changing planet, *Science* 347 (2015) 1259855.
- [144] J. Rockström, W. Steffen, K. Noone, Å. Persson, F. S. Chapin, E. F. Lambin, T. M. Lenton, M. Schefter, C. Folke, H. J. Schellnhuber, et al., A safe operating space for humanity, *nature* 461 (2009) 472–475.
- [145] M. W. Ryberg, M. M. Andersen, M. Owsiania, M. Z. Hauschild, Downscaling the planetary boundaries in absolute environmental sustainability assessments—a review, *Journal of cleaner production* 276 (2020) 123287.
- [146] M. W. Ryberg, M. Owsiania, J. Clavreul, C. Mueller, S. Sim, H. King, M. Z. Hauschild, How to bring absolute sustainability into decision-making: an industry case study using a planetary boundary-based methodology, *Science of the Total Environment* 634 (2018) 1406–1416.
- [147] K. N. Brejnrod, P. Kalbar, S. Petersen, M. Birkved, The absolute environmental performance of buildings, *Building and environment* 119 (2017) 87–98.
- [148] H. Hoff, H. Tiina, C. Sarah, L. Paul, Bringing EU policy into line with the Planetary Boundaries (2017).
- [149] C. Knight, What is grandfathering?, *Environmental Politics* 22 (2013) 410–427.
- [150] IEA, Nuclear power and secure energy transitions, 2022. URL: <https://www.iea.org/reports/nuclear-power-and-secure-energy-transitions>, license: CC BY 4.0.

- [151] B. Padoan, Nucléaire du futur : la Belgique va coopérer avec la Roumanie et l'Italie sur le développement de SMR, *Le Soir* (2023, 8th of November).
- [152] IEA, Tracking Clean Energy Progress 2023, Technical Report, IEA, Paris, 2023. <https://www.iea.org/reports/tracking-clean-energy-progress-2023>, License: CC BY 4.0.
- [153] IAEA, Competitiveness of Nuclear Energy: IAEA's Perspective and Study Results for Europe, <https://sdgs.un.org/goals>, February 2018 (accessed February 16, 2024).
- [154] European Commission, REPowerEU Plan, Technical Report, European Commission, 2022.
- [155] D. Suna, G. Resch, Is nuclear economical in comparison to renewables?, *Energy Policy* 98 (2016) 199–209.
- [156] H. Khatib, C. Difiglio, Economics of nuclear and renewables, *Energy Policy* 96 (2016) 740–750.
- [157] H. Kempf, *Le Nucléaire n'est pas bon pour le climat*, Seuil, 2022.
- [158] C. Lefebvre, S. Van Brussel, Electrofuel supply in Belgium towards carbon neutrality, using EnergyScope TD to study its impact in 2030 and 2050, Master's thesis, UCLouvain, 2022. URL: <https://dial.uclouvain.be/memoire/ucl/en/object/thesis%3A35660>.
- [159] Eurostat, Share of energy from renewable sources, https://ec.europa.eu/eurostat/databrowser/view/NRG_IND_REN__custom_4442440/default/table?lang=en, (Accessed April 2023).
- [160] E. Guevara, F. Babonneau, T. Homem-de Mello, S. Moret, A machine learning and distributionally robust optimization framework for strategic energy planning under uncertainty, *Applied energy* 271 (2020) 115005.
- [161] World Nuclear Association, Economics of nuclear power, August 2022. URL: <https://world-nuclear.org/information-library/economic-aspects/economics-of-nuclear-power.aspx>.
- [162] D. Coppitters, F. Contino, Optimizing upside variability and antifragility in renewable energy system design, *Scientific Reports* 13 (2023) 9138.
- [163] B. Pickering, F. Lombardi, S. Pfenninger, Diversity of options to eliminate fossil fuels and reach carbon neutrality across the entire european energy system, *Joule* 6 (2022) 1253–1276.
- [164] Fluxys, Programme indicatif d'investissements Fluxys Belgium & Fluxys LNG 2023-2032, Technical Report, Fluxys, 2023.
- [165] W. Steffen, J. Rockström, K. Richardson, T. M. Lenton, C. Folke, D. Liverman, C. P. Summerhayes, A. D. Barnosky, S. E. Cornell, M. Crucifix, et al., Trajectories of the earth system in the anthropocene, *Proceedings of the National Academy of Sciences* 115 (2018) 8252–8259.
- [166] W. Nordhaus, *A question of balance: Weighing the options on global warming policies*, Yale University Press, 2014.

- [167] O. Castrejon-Campos, L. Aye, F. K. P. Hui, Making policy mixes more robust: An integrative and interdisciplinary approach for clean energy transitions, *Energy Research & Social Science* 64 (2020) 101425.
- [168] P. F. Christiano, J. Leike, T. Brown, M. Martic, S. Legg, D. Amodei, Deep reinforcement learning from human preferences, *Advances in neural information processing systems* 30 (2017).
- [169] D. Amodei, C. Olah, J. Steinhardt, P. Christiano, J. Schulman, D. Mané, Concrete problems in ai safety, arXiv preprint arXiv:1606.06565 (2016).
- [170] P. Henderson, R. Islam, P. Bachman, J. Pineau, D. Precup, D. Meger, Deep reinforcement learning that matters, in: *Proceedings of the AAAI conference on artificial intelligence*, volume 32, 2018.
- [171] D. Bertsimas, J. N. Tsitsiklis, *Introduction to linear optimization*, volume 6, Athena Scientific Belmont, MA, 1997.
- [172] B. Fais, I. Keppo, M. Zeyringer, W. Usher, H. Daly, Impact of technology uncertainty on future low-carbon pathways in the UK, *Energy Strategy Reviews* 13 (2016) 154–168.
- [173] W. E. Walker, R. J. Lempert, J. H. Kwakkel, Deep uncertainty, *Delft University of Technology* 1 (2012).
- [174] A. L. Soyster, Convex programming with set-inclusive constraints and applications to inexact linear programming, *Operations research* 21 (1973) 1154–1157.
- [175] J. Zoellner, P. Schweizer-Ries, C. Wemheuer, Public acceptance of renewable energies: Results from case studies in germany, *Energy policy* 36 (2008) 4136–4141.
- [176] H. Sam-Aggrey, Small Modulator Reactors (SMRs)-the key to increased social acceptance of nuclear power?, Technical Report, Atomic Energy of Canada Limited, 2014.
- [177] Acil Allen Consulting for ARENA, Opportunities for Australia from Hydrogen Exports, Technical Report, Australian Renewable Energy Agency, 2018.
- [178] Miniserio de Energía, National Green Hydrogen Strategy, Technical Report, Gobierno de Chile, 2020.
- [179] Euractiv, Spain approves hydrogen strategy to spur low-carbon economy, <https://www.euractiv.com/section/energy/news/spain-approves-hydrogen-strategy-to-spur-low-carbon-economy/>, October 2020.
- [180] Elia, Adequacy & flexibility study for Belgium (2024-2034), <https://www.elia.be/en/electricity-market-and-system/adequacy/adequacy-studies>, 2024.
- [181] P. Thiran, H. Jeanmart, F. Contino, Validation of a method to select a priori the number of typical days for energy system optimisation models, *Energies* 16 (2023) 2772.
- [182] M. F. Astudillo, K. Vaillancourt, P.-O. Pineau, B. Amor, Integrating energy system models in life cycle management, *Designing sustainable technologies, products and policies: from science to innovation* (2018) 249–259.

- [183] A. Dubois, J. Dumas, P. Thiran, G. Limpens, D. Ernst, Multi-objective near-optimal necessary conditions for multi-sectoral planning, arXiv preprint arXiv:2302.12654 (2023).
- [184] Y. Hu, W. Wang, H. Jia, Y. Wang, Y. Chen, J. Hao, F. Wu, C. Fan, Learning to utilize shaping rewards: A new approach of reward shaping, Advances in Neural Information Processing Systems 33 (2020) 15931–15941.
- [185] T. A. Mann, Y. Choe, Directed exploration in reinforcement learning with transferred knowledge, in: European Workshop on Reinforcement Learning, PMLR, 2013, pp. 59–76.
- [186] M. Cutler, T. J. Walsh, J. P. How, Reinforcement learning with multi-fidelity simulators, in: 2014 IEEE International Conference on Robotics and Automation (ICRA), IEEE, 2014, pp. 3888–3895.
- [187] Food and Agriculture Organization of the United Nations, Unified Bioenergy Terminology - UBET, Technical Report, Food and Agriculture Organization of the United Nations, 2004.
- [188] International Organization for Standardization, ISO 16559:2014 - Solid biofuels — Terminology, definitions and descriptions, Standard, International Organization for Standardization, Geneva, CH, 2014.
- [189] N. Alperson-Afil, N. Goren-Inbar, The Acheulian site of Gesher Benot Ya'aqov volume II: Ancient flames and controlled use of fire, Springer Science & Business Media, 2010.
- [190] Our World in Data, Global energy consumption is still rising, <https://ourworldindata.org/energy>, Accessed January 28, 2021.
- [191] A. S. Brouwer, M. van den Broek, W. Zappa, W. C. Turkenburg, A. Faaij, Least-cost options for integrating intermittent renewables in low-carbon power systems, Applied Energy 161 (2016) 48–74. URL: <http://dx.doi.org/10.1016/j.apenergy.2015.09.090>. doi:10.1016/j.apenergy.2015.09.090.
- [192] A. Evans, V. Strezov, T. J. Evans, Assessment of utility energy storage options for increased renewable energy penetration, Renewable and Sustainable Energy Reviews 16 (2012) 4141–4147. URL: <http://dx.doi.org/10.1016/j.rser.2012.03.048>. doi:10.1016/j.rser.2012.03.048.
- [193] A. B. Gallo, J. R. Simões-Moreira, H. K. Costa, M. M. Santos, E. Moutinho dos Santos, Energy storage in the energy transition context: A technology review, 2016. doi:10.1016/j.rser.2016.07.028.
- [194] P. J. Hall, E. J. Bain, Energy-storage technologies and electricity generation, Energy policy 36 (2008) 4352–4355.
- [195] F. G. Albrecht, T. V. Nguyen, Prospects of electrofuels to defossilize transportation in Denmark – A techno-economic and ecological analysis, Energy 192 (2020) 116511. URL: <https://doi.org/10.1016/j.energy.2019.116511>. doi:10.1016/j.energy.2019.116511.
- [196] M. Decker, F. Schorn, R. C. Samsun, R. Peters, D. Stolten, Off-grid power-to-fuel systems for a market launch scenario—a techno-economic assessment, Applied energy 250 (2019) 1099–1109.
- [197] A. P. Goede, CO₂ neutral fuels, EPJ Web of Conferences 189 (2018). doi:10.1051/epjconf/201818900010.

- [198] B. R. J. Pearson, M. D. Eisaman, J. W. G. Turner, P. P. Edwards, Z. Jiang, V. L. Kuznetsov, K. A. Littau, L. Marco, S. R. G. Taylor, Energy storage via carbon-neutral fuels made from co₂, water , and renewable energy 100 (2012).
- [199] F. Trieb, M. Moser, J. Kern, Liquid solar fuel–liquid hydrocarbons from solar energy and biomass, Energy 153 (2018) 1–11.
- [200] F. S. Zeman, D. W. Keith, Carbon neutral hydrocarbons, Philosophical Transactions of the Royal Society A: Mathematical, Physical and Engineering Sciences 366 (2008) 3901–3918. doi:10.1098/rsta.2008.0143.
- [201] IEA, Renewables, <https://www.iea.org/fuels-and-technologies/renewables>, June 16 2020 (accessed July 9, 2020).
- [202] M. Bailera, P. Lisboa, L. M. Romeo, S. Espatolero, Power to gas projects review: Lab, pilot and demo plants for storing renewable energy and co₂, Renewable and Sustainable Energy Reviews 69 (2017) 292–312.
- [203] I. Ridjan, B. V. Mathiesen, D. Connolly, Terminology used for renewable liquid and gaseous fuels based on the conversion of electricity: a review, Journal of Cleaner Production 112 (2016) 3709–3720.
- [204] E. I. A. (EIA), Annual Energy Outlook 2006 With Projections to 2030, 2006. doi:DOE/EIA-0383(2006).
- [205] International Energy Agency, Tracking industrial energy efficiency and CO₂ emissions, Organisation for Economic Co-operation and Development, 2007.
- [206] E. Commission, Proposal for a directive of the european parliament and of the council on the deployment of alternative fuels infrastructure (2013).
- [207] G. Haarlemmer, G. Boissonnet, E. Peduzzi, P.-A. Setier, Investment and production costs of synthetic fuels—a literature survey, Energy 66 (2014) 667–676.
- [208] E. Bargiacchi, M. Antonelli, U. Desideri, A comparative assessment of power-to-fuel production pathways, Energy 183 (2019) 1253–1265.
- [209] F. Monaco, A. Lanzini, M. Santarelli, Making synthetic fuels for the road transportation sector via solid oxide electrolysis and catalytic upgrade using recovered carbon dioxide and residual biomass, Journal of Cleaner Production 170 (2018) 160–173.
- [210] A. Rao, Sustainable energy conversion for electricity and coproducts: principles, technologies, and equipment, John Wiley & Sons, 2015.
- [211] S. Hänggi, P. Elbert, T. Büttler, U. Cabalzar, S. Teske, C. Bach, C. Onder, A review of synthetic fuels for passenger vehicles, Energy Reports 5 (2019) 555–569.
- [212] M. Larsson, S. Grönkvist, P. Alvfors, Synthetic fuels from electricity for the swedish transport sector: comparison of well to wheel energy efficiencies and costs, in: Energy Procedia, volume 75, 2015, pp. 1875–1880.

- [213] National Center for Biotechnology Information, Fossil fuels, <https://www.ncbi.nlm.nih.gov/mesh/?term=fossil+fuel>, Accessed April 27, 2021.
- [214] EU-Commission, et al., Directive 2003/30/ec of the european parliament and of the council of 8 may 2003 on the promotion of the use of biofuels or other renewable fuels for transport, Official Journal of the European Union 5 (2003).
- [215] O. Ellabban, H. Abu-Rub, F. Blaabjerg, Renewable energy resources: Current status, future prospects and their enabling technology, *Renewable and Sustainable Energy Reviews* 39 (2014) 748–764.
- [216] I. Dincer, Y. Bicer, Enhanced dimensions of integrated energy systems for environment and sustainability, 2020. doi:10.1016/b978-0-12-809943-8.00007-8.
- [217] European Commission, A sustainable europe by 2030, https://commission.europa.eu/publications/sustainable-europe-2030_en, January 30 2019 (accessed January 20, 2021).
- [218] International Energy Agency, The future of hydrogen, <https://www.iea.org/reports/the-future-of-hydrogen>, 2019.
- [219] C. Acar, I. Dincer, Comparative assessment of hydrogen production methods from renewable and non-renewable sources, *International journal of hydrogen energy* 39 (2014) 1–12.
- [220] Office of Energy Efficiency & Renewable Energy, Full text glossary, <https://www.energy.gov/eere/bioenergy/full-text-glossary>, Accessed April 14, 2021.
- [221] H. Pöttering, P. Necas, Directive 2009/30/ec of the european parliament and of the council of 23 april 2009 amending directive 98/70/ec as regards the specification of petrol, diesel and gas-oil introducing a mechanism to monitor and reduce greenhouse gas emissions and amending council directive 1999/32/ec as regards the specification of fuel used by inland waterway vessels and repealing directive 93/12/ec, Off. J. Eur. Union 140 (2009) 88–112.
- [222] European Commission, Glossary: Biofuels, <https://ec.europa.eu/eurostat/statistics-explained/index.php?title=Glossary:Biofuels>, 2019.
- [223] A. O'Connell, M. Prussi, M. Padella, A. Konti, L. Lonza, Advanced Alternative Fuels Technology Development Report 2020, Technical Report JRC123166, Publications Office of the European Union, Luxembourg, 2020. doi:10.2760/412802.
- [224] A. Goldmann, W. Sauter, M. Oettinger, T. Kluge, U. Schröder, J. R. Seume, J. Friedrichs, F. Dinkelacker, A study on electrofuels in aviation, *Energies* 11 (2018) 392.
- [225] R. Bhandari, C. A. Trudewind, P. Zapp, Life cycle assessment of hydrogen production via electrolysis—a review, *Journal of cleaner production* 85 (2014) 151–163.
- [226] European Commission, Synthetic fuels, https://ec.europa.eu/knowledge4policy/glossary/synthetic-fuels_en, 2018 (accessed July 7, 2020).
- [227] J. G. Speight, Synthetic fuels handbook: properties, process, and performance, McGraw-Hill Education, 2020.

- [228] D. Mignard, C. Pritchard, On the use of electrolytic hydrogen from variable renewable energies for the enhanced conversion of biomass to fuels, *Chemical engineering research and design* 86 (2008) 473–487.
- [229] A. O'Connell, M. Kousoulidou, L. Lonza, W. Weindorf, Considerations on GHG emissions and energy balances of promising aviation biofuel pathways, *Renewable and Sustainable Energy Reviews* 101 (2019) 504–515. URL: <https://doi.org/10.1016/j.rser.2018.11.033>. doi:10.1016/j.rser.2018.11.033.
- [230] R. Slade, A. Bauen, Micro-algae cultivation for biofuels: cost, energy balance, environmental impacts and future prospects, *Biomass and bioenergy* 53 (2013) 29–38.
- [231] M. M. Dekker, V. Daioglou, R. Pietzcker, R. Rodrigues, H.-S. de Boer, F. Dalla Longa, L. Drouet, J. Emmerling, A. Fattah, T. Fotiou, et al., Identifying energy model fingerprints in mitigation scenarios, *Nature Energy* 8 (2023) 1395–1404.
- [232] B. S. Palmintier, Incorporating operational flexibility into electric generation planning: Impacts and methods for system design and policy analysis, Ph.D. thesis, Massachusetts Institute of Technology, 2013.
- [233] D. Connolly, H. Lund, B. V. Mathiesen, M. Leahy, A review of computer tools for analysing the integration of renewable energy into various energy systems, *Applied Energy* 87 (2010) 1059–1082. doi:10.1016/j.apenergy.2009.09.026.
- [234] P. Lopion, P. Markewitz, M. Robinius, D. Stolten, A review of current challenges and trends in energy systems modeling, *Renewable and sustainable energy reviews* 96 (2018) 156–166.
- [235] M. G. Prina, G. Manzolini, D. Moser, B. Nastasi, W. Sparber, Classification and challenges of bottom-up energy system models - a review, *Renewable and Sustainable Energy Reviews* 129 (2020) 109917.
- [236] M. Chang, J. Z. Thellufsen, B. Zakeri, B. Pickering, S. Pfenninger, H. Lund, P. A. Østergaard, Trends in tools and approaches for modelling the energy transition, *Applied Energy* 290 (2021) 116731.
- [237] R. Atlason, R. Unnithorsson, Ideal EROI (energy return on investment) deepens the understanding of energy systems, *Energy* 67 (2014) 241–245. doi:10.1016/j.energy.2014.01.096.
- [238] Pfenninger and Pickering, Calliope - a multi-scale energy systems modelling framework, Accessed 2023. URL: <https://www.calliope.pe/>.
- [239] A. University, EnergyInteractive.NET, Accessed July 17th, 2018. URL: <http://energyinteractive.net/>.
- [240] Ž. Popović, B. Brbaklić, S. Knežević, A mixed integer linear programming based approach for optimal placement of different types of automation devices in distribution networks, *Electric Power Systems Research* 148 (2017) 136–146.
- [241] Berkeley Lab, Der-cam, Accessed June 12th, 2023. URL: <https://gridintegration.lbl.gov/der-cam>.
- [242] A. Zerrahn, W.-P. Schill, Long-run power storage requirements for high shares of renewables: review and a new model, *Renewable and Sustainable Energy Reviews* 79 (2017) 1518–1534.

- [243] University of Stuttgart, European Electricity Market Model, Accessed June 12th, 2023. URL: <https://www.ier.uni-stuttgart.de/forschung/modelle/E2M2/>.
- [244] S. Backe, C. Skar, P. C. del Granado, O. Turgut, A. Tomasdard, Empire: An open-source model based on multi-horizon programming for energy transition analyses, SoftwareX 17 (2022) 100877.
- [245] Quintel Intelligence, Energy Transition Model, Accessed September 17th, 2023. URL: <https://docs.energytransitionmodel.com/main/intro/>.
- [246] H. Lund, J. Z. Thellufsen, Energyplan - advanced energy systems analysis computer model (version 15.1), <https://doi.org/10.5281/zenodo.4001540>, 2020. [Accessed September 17, 2020].
- [247] O. Lugovoy, V. Potashnikov, energyRt: Energy systems modeling toolbox in R, development version, 2022. URL: <https://github.com/energyRt/energyRt>, r package version 0.01.21.9003.
- [248] Fraunhofer ISI, Enertile, Accessed June 12th, 2023. URL: <https://www.enertile.eu/enertile-en>.
- [249] C. F. Heuberger, Electricity systems optimisation with capacity expansion and endogenous technology learning (eso-xel), Zenodo (2017).
- [250] K. Löffler, K. Hainsch, T. Burandt, P.-Y. Oei, C. Kemfert, C. Von Hirschhausen, Designing a model for the global energy system—genesys-mod: an application of the open-source energy modeling system (osemosys), Energies 10 (2017) 1468.
- [251] L. Herc, A. Pfeifer, F. Feijoo, N. Duić, Energy system transitions pathways with the new h2res model: a comparison with existing planning tool, e-Prime-Advances in Electrical Engineering, Electronics and Energy 1 (2021) 100024.
- [252] R. Dufo López, ihoga, Accessed June 12th, 2023. URL: <https://ihoga.unizar.es/en/>.
- [253] P. Kuhn, Iteratives Modell zur Optimierung von Speicherausbau und-Betrieb in einem Stromsystem mit zunehmend fluktuierender Erzeugung, Ph.D. thesis, Technische Universität München, 2012.
- [254] Electric Power Research Institute, Open distribution system simulator (opendss), Accessed June 12th, 2023. URL: <https://sourceforge.net/projects/electricdss/>.
- [255] Energy Exemplar, Plexos (version 9.0), 2023. URL: <https://plexos9.com/>.
- [256] V. Waucquez, Validation of the cost optimization model, pathway energyscope, for scenario analysis, 2023. URL: <http://hdl.handle.net/2078.1/thesis:40534>.
- [257] T. Brown, J. Hörsch, D. Schlachtberger, Pypsa: Python for power system analysis, arXiv preprint arXiv:1707.09913 (2017).
- [258] T. Brown, J. Hörsch, D. Schlachtberger, PyPSA: Python for Power System Analysis, 2018. URL: <https://pypsa.org/>.
- [259] T. T. Pedersen, E. K. Gøtske, A. Dvorak, G. B. Andresen, M. Victoria, Long-term implications of reduced gas imports on the decarbonization of the european energy system, Joule 6 (2022) 1566–1580.

- [260] Energistyrelsen, Modelldokumentation – Ramses energisystemmodel , Technical Report, 2023. URL: https://ens.dk/sites/ens.dk/files/Analyser/ramses_energisystemmodel.pdf.
- [261] W. Short, P. Sullivan, T. Mai, M. Mowers, C. Uriarte, N. Blair, D. Heimiller, A. Martinez, Regional energy deployment system (ReEDS), Technical Report, National Renewable Energy Lab.(NREL), Golden, CO (United States), 2011.
- [262] IEA-ET SAP, Times model description, 2021. URL: <https://wiki.openmod-initiative.org/wiki/TIMES>.
- [263] S. Pfenniger, J. Keirstead, Renewables, nuclear, or fossil fuels? Scenarios for Great Britain's power system considering costs, emissions and energy security, *Applied Energy* 152 (2015) 83–93. doi:10.1016/j.apenergy.2015.04.102.
- [264] B. Pickering, R. Choudhary, Quantifying resilience in energy systems with out-of-sample testing, *Applied Energy* 285 (2021) 116465.
- [265] S. Pfenniger, Dealing with multiple decades of hourly wind and pv time series in energy models: A comparison of methods to reduce time resolution and the planning implications of inter-annual variability, *Applied energy* 197 (2017) 1–13.
- [266] H.-K. Bartholdsen, A. Eidens, K. Löffler, F. Seehaus, F. Wejda, T. Burandt, P.-Y. Oei, C. Kemfert, C. v. Hirschhausen, Pathways for Germany's low-carbon energy transformation towards 2050, *Energies* 12 (2019) 2988.
- [267] M. Welsch, P. Deane, M. Howells, B. Ó. Gallachóir, F. Rogan, M. Bazilian, H.-H. Rogner, Incorporating flexibility requirements into long-term energy system models—A case study on high levels of renewable electricity penetration in Ireland, *Applied Energy* 135 (2014) 600–615.
- [268] G. Haydt, V. Leal, A. Pina, C. A. Silva, The relevance of the energy resource dynamics in the mid/long-term energy planning models, *Renewable energy* 36 (2011) 3068–3074.
- [269] G. Limpens, Pathway extension of model EnergyScope TD, Accessed 2023. URL: https://github.com/energyscope/EnergyScope_pathway/tree/v1.1.
- [270] V. Codina Gironès, S. Moret, F. Maréchal, D. Favrat, Strategic energy planning for large-scale energy systems: A modelling framework to aid decision-making, *Energy* 90, Part 1 (2015) 173–186. doi:10.1016/j.energy.2015.06.008.
- [271] F. Y. Kuo, I. H. Sloan, Lifting the curse of dimensionality, *Notices of the AMS* 52 (2005) 1320–1328.
- [272] P. Gabrielli, M. Gazzani, E. Martelli, M. Mazzotti, Corrigendum to “Optimal design of multi-energy systems with seasonal storage” [Appl. Energy (2017)], *Applied Energy* 212 (2018) 720. doi:10.1016/j.apenergy.2017.12.070.
- [273] J. Després, S. Mima, A. Kitous, P. Criqui, N. Hadjsaid, I. Noirot, Storage as a flexibility option in power systems with high shares of variable renewable energy sources: a POLES-based analysis, *Energy Economics* 64 (2017) 638–650. doi:10.1016/j.eneco.2016.03.006.
- [274] P. Nahmmacher, E. Schmid, L. Hirth, B. Knopf, Carpe diem: A novel approach to select representative days for long-term power system modeling, *Energy* 112 (2016) 430–442.

- [275] J. E. Gentle, L. Kaufman, P. J. Rousseeuw, Finding Groups in Data: An Introduction to Cluster Analysis., John Wiley & Sons 47 (2006) 788. doi:10.2307/2532178.
- [276] H. S. Park, C. H. Jun, A simple and fast algorithm for K-medoids clustering, Expert Systems with Applications 36 (2009) 3336–3341. doi:10.1016/j.eswa.2008.01.039.
- [277] G. Limpens, S. Moret, G. Guidati, X. Li, F. Maréchal, H. Jeanmart, The role of storage in the Swiss energy transition, in: proceedings of ECOS 2019 conference, 2019, pp. 761–774.
- [278] M. Borasio, S. Moret, Deep decarbonisation of regional energy systems: A novel modelling approach and its application to the italian energy transition, Renewable and Sustainable Energy Reviews 153 (2022) 111730.
- [279] M. Pavičević, P. Thiran, G. Limpens, F. Contino, H. Jeanmart, S. Quoilin, Bi-directional soft-linking between a whole energy system model and a power systems model, in: 2022 IEEE PES/IAS Power-Africa, IEEE, 2022, pp. 1–5.
- [280] J. Schnidrig, R. Cherkaoui, Y. Calisesi, M. Margni, F. Maréchal, On the role of energy infrastructure in the energy transition. case study of an energy independent and co2 neutral energy system for switzerland, Frontiers in Energy Research 11 (2023) 1164813. URL: <https://doi.org/10.3389/fenrg.2023.1164813>. doi:10.3389/fenrg.2023.1164813.
- [281] G. Limpens, EnergyScope TD documentation, Accessed 2023. URL: <https://energyscope.readthedocs.io/en/v2.2/>.
- [282] IPCC, Climate Change 2013 - The Physical Science Basis, 2014. URL: <https://www.ipcc.ch/report/ar5/wg1/>.
- [283] D. Devogelaer, J. Duerinck, D. Gusbin, Y. Marenne, W. Nijs, M. Orsini, M. Pairon, Towards 100% renewable energy in Belgium by 2050, Technical Report, 2013.
- [284] M. Cornet, J. Duerinck, E. Laes, P. Lodewijks, E. Meynaerts, J. Pestiaux, N. Renders, P. Vermeulen, Scenarios for a Low Carbon Belgium by 2050, Technical Report November, Climact, VITO, 2013.
- [285] Société Française d'énergie nucléaire, La Belgique repousse de 10 ans sa sortie du nucléaire, <https://www.sfen.org/rgn/la-belgique-repousse-de-10-ans-sa-sortie-du-nucleaire/>, January 2023 (accessed April 17, 2023).
- [286] D. Devogelaer, Fuel for the future - More molecules or deep electrification of Belgium's energy system by 2050, Technical Report, Federal Planning Bureau, 2013.
- [287] IRENA, World Energy Transitions Outlook: 1.5°C Pathway, Technical Report, Internation Renewable Energy Agency, 2021. URL: <https://www.irena.org/publications/2021/Jun/World-Energy-Transitions-Outlook>.
- [288] A. Widuto, Energy transition in the EU, Technical Report, European Parliamentary Research Service, 2023. URL: [https://www.europarl.europa.eu/RegData/etudes/BRIE/2023/754623/EPRS_BRI\(2023\)754623_EN.pdf](https://www.europarl.europa.eu/RegData/etudes/BRIE/2023/754623/EPRS_BRI(2023)754623_EN.pdf).
- [289] Fédération Belge et Luxembourgeoise de l'automobile et du cycle, Automotive Pocket Guide Belgium - Chiffres clefs, Technical Report, 2021. URL: <https://www.febiac.be/public/statistics.aspx?FID=23>.

- [290] I. Keppo, M. Strubegger, Short term decisions for long term problems—the effect of foresight on model based energy systems analysis, *Energy* 35 (2010) 2033–2042.
- [291] B. Nyqvist, Limited foresight in a linear cost minimisation model of the global energy system, Gothenburg: Master's Thesis in Complex Adaptive Systems, Physical Resource Theory, Chalmers University of Technology (2005).
- [292] F. Hedenus, C. Azar, K. Lindgren, Induced technological change in a limited foresight optimization model, *The Energy Journal* (2006).
- [293] K. Poncelet, E. Delarue, D. Six, J. Duerinck, W. D'haeseleer, Impact of the level of temporal and operational detail in energy-system planning models, *Applied Energy* 162 (2016) 631–643. doi:10.1016/j.apenergy.2015.10.100.
- [294] SPF Economie, Vision and strategy hydrogen, October 2022. URL: <https://economie.fgov.be/sites/default/files/Files/Energy/View-strategy-hydrogen.pdf>.

Appendix A

Taxonomy of the fuels in a whole-energy system

Since stone age, humans use fuels, defined as any energy carriers intended for energy conversion [187, 188]. First evidence of the use of domesticated fire was established in 790 000 B.C. [189]. Thus, biomass has been the first fuel used by the human kind for security, cooking and heating. Nowadays, most of the used energy sources are fossil fuels. In 2019, oil, coal and gas represented respectively 31%, 25% and 23% of the global primary energy consumption [190]. Despite their great advantage, high energy density, these fuels have a major drawback: their combustion releases huge quantities of carbon dioxide (35 Gt of CO₂ in 2019) mainly responsible for climate change [12]. The biggest challenge of the energy transition is to secure the energy supply while reducing the greenhouse gas emissions. In practice, this means finding alternatives to fossil fuels.

First and foremost, in the context of the energy transition, fuels will keep playing a major role in the global energy system [30]. Even if electricity gains shares through the electrification of the energy demand, it will not entirely displace fuels for three main reasons: storage, infrastructure compatibility and cross-sectorial links. Because of their intermittency and space disparity, a deeper integration of VRES requires storage and transport in order to supply the energy demand at the right time and in the right place [28, 191–194]. Where typical container of batteries are limited in terms of storage capacity (up to 10 MWh) and present significant costs and self-discharge losses, the energy conversion into fuels provides a more affordable solution for higher storage capacity (from 100 GWh) and longer storage time scales (months to year) [28]. Due to the economic inertia and their infrastructure legacy [30], fuels remain the most

appropriate solution for sectors requiring high energy density (e.g., heavy-duty transport, shipping, aviation or chemical industry) [23, 28, 195–200]. Contino et al. [33] point out that the energy transition is an interdisciplinary effort and not solely about the power sector. The latter represents only a fifth of the global energy consumption [201]. Also, Goede [197] has shown in 2018 that CO₂ emissions of the Netherlands are equally apportioned between the different types of end-use-demands (i.e., power, heat, mobility and non-energy). This highlights the necessity to consider every energy sector rather than focusing all efforts on the power system and even more, to shift towards a multi-vector interconnected energy system. In this cross-sectorial approach and with the perspective of increasing shares of VRES, fuels are promising energy carriers in order to maximise the overall system efficiency [23, 32].

Given the growing diversity of pathways for transforming the renewable energy sources into fuels, clear classification and terminology are necessary [202]. As predicted by Ridjan et al. [203], there is now a need to support the right fuel technology development, via the use of a more comprehensive and quantitative terminology (e.g., specifying the share of biomass in the energy balance of the production of a biofuel). The objective of this terminology is to avoid the confusion between these fuels and thereby reduce misunderstanding in political or academic discussions. To a further extent, such an harmonisation may help “to facilitate comparison between national fuel market and enhance trading” [187]. It also aims at promoting and increasing the use of biomass as energy carriers and electricity transformed into fuel. On a general public perspective, this terminology aims at simplifying and clarifying the addressed terms and allows to have a more critical mind. In Section A.1, we present the terminology currently used in the literature. On top of this review of the scientific literature, this work also includes review of terminology defined by the International Organization for Standardization (ISO) and other official institutions (e.g., the Food and Agriculture Organisation of the United Nations (FAO) or the International Energy Agency (IEA)) and presents the motivation for a new one, more quantitative and measurable. The latter is introduced in Section A.2. Finally, Section A.3 gives the room for a discussion and the actual recommendations.

A.1 Terminology used in the literature

Ridjan et al. [203] performed a first literature review between 2006 and 2014, looking in Scopus for the three keywords: (i) “synthetic fuels”, (ii) “electrofuels” and (iii)“alternative fuels”. Based on this extensive review work, they proposed the following definitions: (i) *Synthetic fuels* were defined as x-To-Liquid (xTL) processed fuels,

within the scope of “Fischer-Tropsch fuels that are produced by gasification of either coal, natural gas or biomass”. Comparatively, similar definitions are given in [204] and [205], except that the latter excludes biomass from the potential feedstocks. (ii) *Electrofuels* were considered as a storage capacity of electricity into chemical bonds through so called coal-, biomass- and emission(CO_2)-to-electrofuel (xTE) processes. (iii) In accordance with [206], they presented *alternative fuels* as any fuel used as a substitution for fossil oil sources in the energy supply with no specific restrictions regarding the feedstock.

More recently, Stančin et al. [23] has shown that scientific research about “*alternative fuels*” has experienced a significant impulse since the 2000s. Therefore, in the continuity of [203], we performed a similar literature review in order to update the terminology used by the scientific community. Hence, the current work extends the previous review to cover publications from 2015 to 2020. The same methodology was followed, through a manual identification, and the same search terms were looked for in Scopus: the first search screened the terms of interest (i.e., synthetic fuels or electrofuels) complemented by narrowing-down terms (e.g., “*alternative fuels*”, “hydrocarbon”, “biomass”, or “ammonia”). This initial search resulted in 251 documents. Then, after screening the abstract (and, if necessary, the articles themselves), 75 relevant documents were selected as they used the searched terminology and gave an actual definition as well as identified the production process. The non-relevant documents usually contained information that fall out of the scope of the current work, e.g., information on specific catalysts. Out of the relevant documents, the main outcomes concern the relative majority of “synthetic fuels”, the emergence of “electrofuels” and the scattered diversity of other terms.

Where terms like “synthetic gas”, “electrofuels” or “synthetic natural gas” account for 19%, 13% and 8% of the additional relevant literature, respectively, “synthetic fuels” is used in 35% of the case to cover fuels produced from a wide variety of primary resources (renewable or not) and through various conversion processes. To pick only a few examples, its usage ranged from liquid hydrocarbons produced from synthesis gas through the Fischer-Tropsch process [199, 207] to ammonia from the Haber-Bosch process [208] or biomass gasification or pyrolysis [209, 210]. As a consequence of an increasing share of VRES in the energy system, “electrofuels” are gaining more popularity: where this term was used in 4% of the relevant literature between 2006 and 2014 [203], it is now present in 13% of the additional relevant literature reviewed for this work. These fuels are considered as being produced mainly based on the electricity provided by VRES [18]. Besides water electrolysis, this electricity also supplies processes like CO_2 hydrogenation [18, 196, 198] or co-electrolysis of CO_2 and H_2O .

[211, 212]. Aside the two aforementioned keywords, the literature makes use of a scattered diversity of terms that aim at precising the features of the considered fuel: for instance, “solar fuel”, “power gas” or “green synthetic fuel”. However, out of context, words like “green fuel”, “advanced fuel” or “solar fuel” may be misunderstood because of their multiple interpretations [203].

Consequently, in the context of the energy transition where new use of primary resources and conversion technologies are booming, we encompass in this work all the resources and conversion processes one might consider in the production of fuels. The objective of this taxonomy is to fit with the long-term perspective of this transition (e.g., carbon neutrality, defossilisation) while being adapted for the current context. We do not only focus on carbon-based fuels nor on specific end-use sectors (e.g., transport), contrary to what is mostly seen in the literature. We propose a comprehensive and harmonised taxonomy, without having the ambition to apply strict classification methodologies (e.g., questionnaires, text-mining of corpora of the domain) [213].

A.2 Classification and definition of the fuels

Given the difficulty to quantify and circumscribe the sustainability of a fuel, we decided here to suggest classification and definition of the fuels regardless of this feature. As described below, we opted for a focus on the energy balance of a fuel with regard to its chemical building blocks and the origin of the energy to supply the conversion and production process, without having the ambition to quantify the sustainability of the different fuels.

An essential distinction has to be pointed out between renewable and non-renewable fuels. In accordance with [214], *renewable fuels are fuels produced from renewable energy sources*. Renewable energy sources are non-fossil sources that are naturally replenished on a human timescale (wind, solar, geothermal, wave, tidal, hydro-power, biomass) [215]. A fuel can be defined as “renewable” only when it is based on renewable sources. To be “sustainable”, a “renewable fuel” should not increase the concentration of CO₂ in the atmosphere [216], among other things [217]. On the contrary, non-renewable fuels are those that are not based on renewable sources. In practice, these cluster fuels produced from fossil sources (e.g., coal, natural gas, oil). Finally, the nuclear-based fuels are considered separately. Even though nuclear power plants do not emit CO₂ to produce electricity or heat, uranium is not a renewable resource.

Given these definitions and looking at the primary resources, the distinction is clear between renewable and non-renewable sources. However, the production and end-use

fuels are harder to group as they can use both renewable and non-renewable resources. In other words, the same end-use fuel can be produced from different resources by different processes, which explains the ambiguity in the definition of these fuels. As illustrated on Figure A.1, hydrogen is a good example as it can be produced from fossil or renewable resources and by different processes: for instance, (i) steam reforming of fossil natural gas (75% of the current global production of hydrogen today [218]); (ii) partial oxidation of heavy hydrocarbons; (iii) coal gasification; (iv) electrolysis with electricity generated from fossil fuels; (v) electrolysis with electricity generated from renewable sources; (vi) thermochemical conversion of ligno-cellulosic biomass; (vii) steam reforming of biogas or even (viii) thermochemical water splitting using heat from concentrated solar power or nuclear wastes [219].

Therefore, besides the aforementioned renewable/non-renewable distinction, we propose to categorise fuels in three groups whose definitions are broad enough to capture the diversity of the fuels while maintaining a simplified representation: (i) *Biofuels* as the absolute majority of the energy balance of their production consists of biomass; (ii) *Electrofuels*, similarly to biofuels, but with electricity instead of biomass. *A priori*, it is complicated to give an exact number to quantify this “majority” of the energy balance but we propose a solution in Section A.3 to remove this ambiguity. (iii) *Synthetic fuels* when the end-use fuel results from the upgrade of another fuel to improve physical and/or chemical characteristics (e.g., to increase the volumetric energy density). Figure A.1 illustrates this taxonomy by representing the physical, not lexical, link between different kinds of concepts (e.g., resource, conversion and fuel).

Biofuels are those based on biomass as their chemical building blocks and energy supply for their own conversion process (Figure A.1). Biomass is mainly harvested in a solid form and has a lower energy density than fossil hydrocarbons. Thus, the “bio” processes aim at concentrating the energy and converting it into a fuel more convenient to use (e.g., pellet from woody wastes). Similarly to the Office of Energy Efficiency & Renewable Energy [220], in the literature, biofuels mainly target liquid or gaseous transport fuels (e.g., biodiesel and bioethanol) and imply a sustainable production [221?]. The definition given by official institutions (e.g., the FAO or the European Commission) is aligned with the ISO 16559:2014: “biofuel is a solid, liquid or gaseous fuel produced directly or indirectly from biomass” [187, 188, 222]. To add a quantitative and measurable aspect in the terminology, we propose the following definition: *biofuels are fuels produced from biomass as the major component of their energy balance*. Even if our terminology lacks the subtlety brought by terms like “woodfuels”, “agrofuels”, or “municipal by-products”, that allow to highlight the

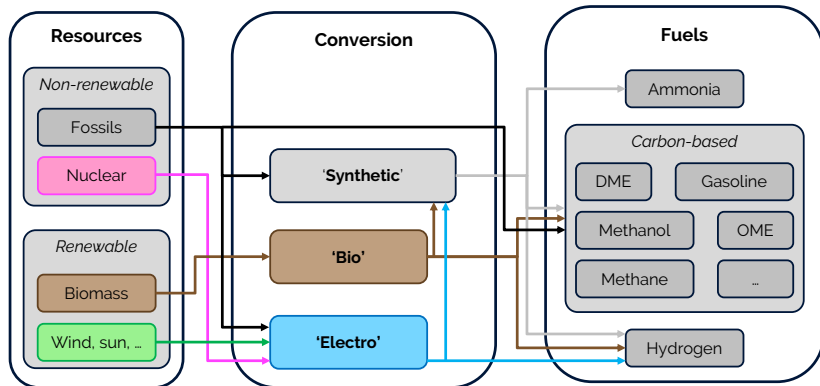


Figure A.1. Overview of the main pathways to produce fuels. The boxes in the “conversion” category illustrates the terminology to use in the different cases: first, a fuel can be defined as *bio* or *electro* if the absolute majority of the energy balance of its production consists of biomass or electricity, respectively. Then, a fuel can be defined as *synthetic* if it has been obtained through a synthesis process from another fuel, regardless of the feedstock. The box “Fuels” gives some examples to illustrate the terminology used and applied to very common fuels.

source of biomass at stake, provided by the FAO [187], this terminology aims at harmonising and desambiguating the meaning of the general term “biofuel”.

Electrofuels are, according to O’Connell et al. [223], fuels whose energy content comes from renewable electricity. On top of that, Goldmann et al. [224] even add that they should be carbon-neutral and serve as a storage capacity of electricity. To be more comprehensive, we define *electrofuels as fuels produced from electricity*, as the resource used to produce this electricity may vary. This electricity is transformed into hydrogen through electrolysis. This hydrogen can be upgraded in more complex fuels when combined with other molecules (e.g., carbon mono/dioxide or nitrogen). Electrofuels group all the fuels where the absolute majority of the energy contained into the fuel comes from electricity. In this sense, it is important to point out that “electrofuels” do not especially imply “renewable fuels” (Figure A.1). For instance, the electricity needed to produce H₂ through an electrolyser can be generated from renewable or non-renewable sources [225], even if the most sustainable way to produce electrofuels remains through the electricity produced in excess from VRES.

Synthetic fuels are fuels which have been obtained through a synthesis process from another fuel. It encompasses upgrading processes, such as methane produced through the Sabatier process or longer hydrocarbons based on syngas through the Fischer-Tropsch process. We extend the definition of the European Commission and Energy

Information Agency who consider synthetic fuels as “any liquid fuel obtained from coal, natural gas or biomass” [204, 226]. By extending this definition and focusing on the synthesis operation, similarly to Speight [227], we are able to include emerging fuels like ammonia from the Haber-Bosch process. Contrary to biofuels and electrofuels, the resources used for producing synthetic fuels are not strictly identified. For instance, electrolysis-produced H₂ can be upgraded with synthesis gas from the gasification of biomass to form methanol [228]. Another example could be the production of ammonia via the synthesis of H₂ from methane-reforming. Consequently, defining a fuel only as “synthetic” gives a reduced insight about the fuel, especially about its “renewability”. Therefore, we recommend to avoid using “synthetic fuel”. In the former example, one would then rather define the produced methanol as a “bio-electrofuel” given that its main sources are electricity and biomass.

Finally, besides these recommended terms in the context of the energy transition, others are mainly misleading: “alternative” or “non-conventional” fuels. These terms are defined in opposition to another kind of fuels, mostly fossil. However, alternatives of today will be conventions of tomorrow. This means that depending on the “conventional” of the context, these terms will represent different fuels. Because of this implied ambiguity, we recommend not to use these words as their interpretation is case and time sensitive.

A.3 Discussion

In the urging necessity for an energy transition and the persisting need for fuels, technologies to convert primary resources into end-use fuels are rapidly multiplying. In this context, we suggest comprehensive terminology and classification to characterise the fuels. Given the limited insight provided by the widely-used term “synthetic fuels”, we recommend to use more specific terms like “biofuels”, “electrofuels”, or even hybridised terms (e.g., “bio-electrofuels”). These allow to highlight the contribution of biomass and electricity in the energy balance of the fuel.

Giving an exact share of biomass (or electricity) above which a fuel can be defined as biofuel (or electrofuel) would open an endless debate. Therefore, to emphasise the effort to step away from fossil fuels, we suggest to specify the contribution of biomass (or electricity) within the energy balance of the production of the fuel looking at both the feedstock and the energy to supply the conversion or production process. This would give, for instance, “bio(25) methanol” if 25% of the energy balance to produce the methanol comes from biomass (e.g., biomass gasification). Another example could be “electro(40) ammonia” if 40% of the energy balance comes from electricity (e.g.,

water electrolysis, air-captured nitrogen and power supply of the Haber-Bosch process). As electricity can be produced from a wide variety of sources (Figure A.1), we recommend to give insights on the composition of this electricity (e.g., from wind, solar or the grid mix).

To fully embrace these new terminology and classification, industries and academics will have to switch of perspective as studies on energy balance of biofuels or electrofuels too often consider the energy distribution over the different production steps or the feedstock only rather than over all the resources at stake [229, 230].

Appendix B

EnergyScope Pathway: Its choice and its formulation

B.1 EnergyScope Pathway: The right model

“Only when single-model results are contextualised by the model’s position in the larger ensemble, the reader would be able to have a complete and correct interpretation of the output” [231]. Energy system models of varying complexity are valuable tools for guiding policymakers and projecting future trends. These models enable the exploration of different energy scenarios and the assessment of their consequences. Specifically, techno-economic models play a crucial role in identifying technically feasible pathways for the energy transition while considering the associated economic costs. These models can be classified based on two key factors: technical resolution and simulation horizon, as illustrated in Figure B.1.

Increasing the technical resolution of energy system models often comes at the expense of a shorter simulation horizon, and vice versa. For instance, day-ahead grid operation models prioritise accurate grid resolution and capacity reserves in case of foreseeable deviations, but they may not incorporate long-term market trends. Different model classes cater to various needs, with decreasing technical resolution. These include machine-level control, network dispatch, unit commitment, maintenance, power plant expansion, planning for new infrastructure, and scenario analysis. Each class serves a specific purpose, from fine-grained control within a machine to the exploration of multiple assumptions across different scenarios.

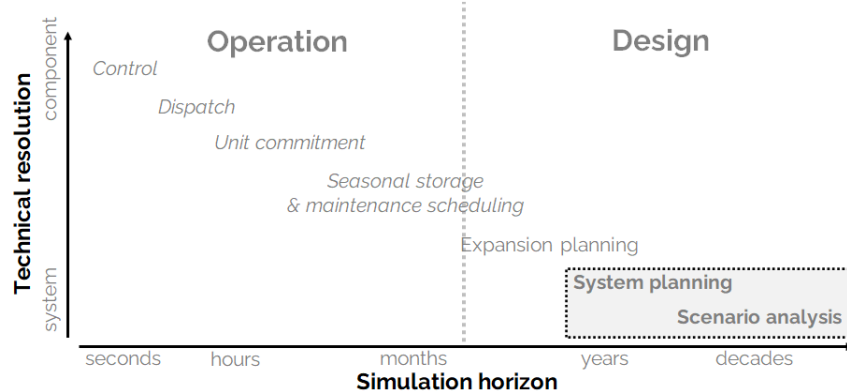


Figure B.1. Models can be classified by their core focus: **Operation** or **Design**. These categories can be broken down into subcategories. This work focuses on the system planning and scenario analysis models. Inspired from [232].

In accordance with the previous classification, models aimed at aiding decision-makers in the energy transition primarily fall under the categories of planning and scenario analysis, with a lower technical resolution than the other classes of model (see Figure B.1). Nonetheless, ensuring technical accuracy is of paramount importance to ensure the effective performance of future energy systems. Hence, these models should meet the following requirements as a minimum: (i) assessment of intermittent renewable energy integration thanks to an **hourly resolution** spanning a one-year time horizon; (ii) accounting for the **whole-energy system** by including all energy (i.e., heat, electricity and mobility) and non-energy flows in different sectors, accounting for their respective greenhouse gas emissions, as well as all resources, conversion processes, and storage technologies; (iii) exploration of all available options through the **optimisation of investments and operations**; (iv) consideration of long-term investments throughout the **transition pathway** process (i.e., 30 years up to 2050, in our case); and (v) ensuring a reasonable **computational time** (i.e., less than one hour on a personal laptop) for analysing different trajectories. Additionally, to enhance result reproducibility and user understanding, it is advantageous for such models to: (vi) maintain transparency and preferably be **open-source**, with accessible data and accompanied by collaborative documentation.

These requirements are commonly found in reviews on energy system models. In 2010, Connolly et al. [233] reviewed 68 tools, considering similar criteria (i.e., (i-iv) and (vi)), along with others such as the “popularity” of the models via the number

of downloads/sales or the integration of economic market equilibrium. Eight years later, Lopian et al. [234] enriched the review of Connolly et al. [233] using similar critieria and including models developed in the 2010s. In 2014, Pfenninger et al. [37] pointed out the current paradigms and challenges to face as well as the emerging approaches to address them in the 21st century energy systems modeling community. Besides the behavioral and social factors, they also highlighted the challenges related to mutli-sectorial systems, time and space resolution or the open-accessibility of data and models and their ability to account for uncertainties. In 2019, Prina et al. [58] reviewed 12 “*most established*” models, focusing on criteria (i-ii) and (iv). This review was followed by a classification where criteria (i-iv) were taken into account [235]. In 2021, Chang et al. [236] conducted a survey-based review of 42 models for energy transition modelling, covering all criteria except computational time. Based on these reviews, models are compared based on all the previous criteria except the computational time (v) (see Table B.1). Indeed, the latter is hard to compare as models are not applied to the same case study and the information is rarely given. The table includes only the models that achieved partially at least four out of the five criteria. We endeavored to update the model’s information by consulting the model’s website and repository, yet there is a possibility that some information might have been overlooked or omitted inadvertently.

From Table B.1, four models almost check all the boxes (partially the pathway one): Calliope, GENeSYS-MOD, PyPSA and TIMES.

Calliope

Calliope is a “*tool that makes it easy to build energy system models*” at different geographical scale. Even if the framework offers the possibility of modelling multi-year systems, we did not find a relevant publication on this topic. In fact, the model is typically employed for snapshot analysis, i.e., optimisation of a target future year. Previous studies have used the model to investigate the phasing out of fossil and nuclear energies in a multi-regional UK power system [263]. More recently, the model has been applied to analyse a scenario of a multi-energy district in Switzerland [264]. Moreover, the model has been used with decades of weather data. However, its application has been limited to assessing the impact of inter-year variability in wind and PV on the results, rather than evaluating a transition pathway [265].

GENeSYS-MOD

Table B.1. Comparison of existing models that partially satisfy at least four of the five criteria (in alphabetical order). Legend: ✓ criterion satisfied; \checkmark criterion partially satisfied; ✗ criterion not satisfied. Data from [58, 233, 235, 236]

| Model | Ref. | Hourly | Whole-energy | Optimis. invest. & operation | Pathway | Open-source |
|--------------------|------------|----------------|----------------------|------------------------------------|----------------|----------------|
| Calliope | [237, 238] | ✓ | ✓ | ✓ | ✗ ^a | ✓ |
| COMPOSE | [239] | ✓ | ✓ | ✓ | ✓ | ✓ ^b |
| DER-CAM | [240, 241] | ✓ | ✓ ^{c,d} | ✓ | ✗ ^e | ✓ ^f |
| DIETER | [242] | ✓ | ✓ ^{d,g} | ✓ | ✗ ^e | ✓ |
| E2M2 | [243] | ✓ | ✓ ^{c,d,h} | ✓ | ✓ | ✗ ⁱ |
| EMPIRE | [244] | ✓ | ✗ ^{c,d,g,h} | ✓ | ✓ | ✓ ^b |
| Ener. Trans. Model | [245] | ✓ | ✓ | ✗ ^j | ✓ | ✓ |
| EnergyPLAN | [246] | ✓ | ✓ | ✗ ^k | ✗ ^l | ✓ ^f |
| energyRt | [247] | ✓ | ✓ | ✓ ^m | ✓ | ✓ |
| EnergyScope TD | [52] | ✓ | ✓ | ✓ | ✗ ^l | ✓ |
| Enertile | [248] | ✓ | ✓ ^d | ✓ | ✓ | ✗ ⁿ |
| ESO-XEL | [249] | ✓ | ✗ ^{c,d,g,h} | ✓ | ✓ | ✓ |
| GENeSYS-MOD | [250] | ✓ | ✓ | ✓ | ✓ | ✓ |
| H2RES | [251] | ✓ | ✗ | ✓ | ✓ | ✓ |
| iHOGA | [252] | ✓ | ✗ ^{c,d,g,h} | ✓ ^m | ✓ | ✓ ^b |
| IMAKUS | [253] | ✓ | ✓ ^{c,d} | ✓ | ✓ | ✗ ⁱ |
| OpenDSS | [254] | ✓ | ✓ | ✗ ^k | ✓ | ✓ |
| Plexos | [255] | ✓ | ✓ ^o | ✓ | ✓ | ✗ ⁱ |
| PyPSA | [257, 258] | ✓ | ✓ | ✓ | ✓ ^p | ✓ |
| RamsesR | [260] | ✓ | ✓ ^{c,d,h} | ✓ | ✓ | ✓ |
| ReEDS | [261] | ✗ ^q | ✓ ^{d,g,h} | ✓ | ✓ | ✓ ^b |
| TIMES | [88] | ✓ | ✓ | ✓ | ✓ | ✓ ^r |

^aTopic is being discussed in the chat of their repository but not yet included in their documentation.

^b‘Free under some special conditions’.

^c Transport not accounted for.

^d Industry not accounted for.

^e Not specified but time horizon is 1 year.

^f Freeware.

^g DHN not accounted for.

^h Individual heating not accounted for.

ⁱ Commercially (paid) licensed.

^jThe ETM is a simulation model with a simple merit order ‘optimisation’ for electricity, flexibility and heat.

^k Simulation model.

^l Yearly horizon without pathway.

^m EnergyRT optimises investments only.

ⁿOnly for internal use.

^oDoes not account for all sectors but allow to implement them according to Waucquez [256].

^pPedersen et al. [259] applied PyPSA to a whole energy system split in 37 nodes. Using a myopic approach, the model optimises the energy transition with a 3-hours resolution).

^qSeasonal time slice.

^rModel is now open-source with limited access to data [262].

Similarly GENeSYS-MOD presents some limitations. This model is an application of the open-source energy modelling system (OSeMOSYS), itself represented as a model with a poor time discretisation and a heavy computational burden according to [58]. Löffler et al. [250] applied the model to the world by splitting it into 10 regions and most of the energy demand sectors, leaving to the user the choice of the time resolution. For their application they used representative years with three days and two time slice per day.

PyPSA

Among the open-source models with an active community, PyPSA is one of the best-performing, with a large and active community, development at the state of the art, worldwide applications, and usage not only limited to academia. A study conducted by Bartholdsen et al. [266] centered on Germany employed a representation comprising 16 time slices per representative year. This choice was substantiated by the work of Welsch et al. [267], which demonstrated that this level of temporal granularity yields consistent results in comparison to hourly time resolution over a year. However, it is noteworthy that the utilisation of a limited number of time slices may oversimplify the optimisation of storage technologies, especially those designed for inter-month energy storage. This simplification can be viewed as a pragmatic approach to reduce the computational burden while over-simplifying the challenge of accurately integrating intermittent renewable energy sources. Furthermore, PyPSA, a modeling framework recognised for its robustness and active user community, has also been employed to investigate scenarios related to myopic transitions [259].

TIMES

The TIMES model, short for The Integrated MARKAL-EFOM System, is a well-established framework renowned for its capacity to generate comprehensive energy models. It encompasses a rich array of features, including support for multi-cell modeling, pathway analysis, full-scale representation of energy systems, and the consideration of market equilibrium dynamics, all of which facilitate thorough scenario exploration. This model has a widespread adoption and has been utilised by worldwide institutions such as the International Energy Agency (IEA) or technical ones such as VITO (Vlaamse Instelling voor Technologisch Onderzoek) research institute. Notably, TIMES was reported as commercial (i.e., not free to download) in 2010 [233]. A more recent survey conducted in 2020-2021 confirmed that the model was using a commercial interface [236]. Recent developments by the IEA-ETSAP

have resulted in a version that is compatible with the open-source solver CBC. In various studies conducted in different regions, including Canada, Sweden, the EU, and Denmark, TIMES has been shown to utilise 12 to 32 time-slices annually [235]. To highlight the sensitivity of results to time resolution, Haydt et al. [268] conducted a study focusing on the electrical sector, using up to 12 typical days with an hourly resolution. Regarding data accessibility, while some publications partially present the used dataset, the overall accessibility of TIMES data is not ensured [262].

While Calliope, OSeMOSYS, PyPSA and TIMES frameworks have the potential to be used for evaluating a transition pathway, we have not come across any publication that explicitly demonstrates their application to such cases with an hourly time resolution over significant time slices to accurately capture the seasonality within each representative year. Hence, it appears that none of the models of Table B.1 fully meets the five criteria outlined in the table, topped with the additional consideration of acceptable computational time. This observation is consistent with the findings presented by Prina et al. [58] who identified two approaches for optimising the energy transition pathway based on the six criteria. The first approach involves running a snapshot model multiple times using an algorithm that optimises the transition path and validates the operability of the system. The second approach aims to extend a snapshot model to represent the entire transition pathway. However, they excluded this option due to the lack of models that met the requirements of being fast enough and easily adaptable. Therefore, they developed a new model based on the first methodology, named EPLANoptTP. It uses a multi-objective evolutionary algorithm to optimise the EnergyPLAN model [246]. To manage computational time, the number of decision variables is limited to three: PV, wind turbine and battery capacities. Thus, the model does not investigate all the options (i.e., criteria (iii)).

For the aforementioned reasons, the current work opted for EnergyScope Pathway, an extension of the open-source and documented EnergyScope TD model [52] listed in Table B.1. The latter has a time horizon of one year and does not account for the pathway from an existing energy system to a long-term target. The pathway version extends the time horizon to decades and accounts for the pathway transition from an existing energy system to a long term target. The computational time is kept low (i.e., around 15 minutes on a personal laptop), mostly due to keeping the linear formulation after extending the snapshot model. Limpens et al. [40] provides more detailed insights into the modeling choices made during methodological development. In the spirit of the EnergyScope project, the code is fully open-source (under the License Apache 2.0, see repo [269]) with a collaborative documentation [54]. Compared to existing models,

EnergyScope Pathway introduces a rapid computational optimisation tool for exploring diverse transition pathways within an entire energy system while maintaining high temporal precision to accurately capture the integration of intermittent renewables. To the best of our knowledge, there are potentially other frameworks that could be extended to similar capabilities, but their computational times for similar case studies have not been found.

B.2 EnergyScope Pathway and its linear formulation

EnergyScope Pathway is the extension of EnergyScope TD [52] that follows the snapshot approach [270]. The objective of this section is to present the fundamental variables and constraints of the latter based on which the former was developed. Formulation choices have been made but they are not discussed here. The interested reader is invited to refer to Appendix B of [40] for further information in this regard.

B.2.1 The starting point: a scenario analysis model

Typical days to break the curse of dimensionality

In the field of bottom-up energy system modelling¹, one of the biggest challenges is the time resolution [235]. With the rise of VRES, being able to integrate them and capture their interactions with the rest of the energy system requires an hourly time resolution while optimising a whole year (i.e., 8760 hours), if not a whole transition (i.e., several decades). This long-term target combined with a fine time resolution usually leads to the so-called “curse of dimensionality” [271]. As an example, running EnergyScope TD over each of the 8760 hours to optimise a single target year takes more than 19h [52].

To break this curse, EnergyScope TD, like other models [272–274], relies on a subset of representative days called typical days (TDs). This more limited number of days, i.e., 12 in the rest of this thesis, clusters the days of the year that have similar time series of demands (i.e., varying electricity and heat demands) and weather data (i.e., sun, onshore and offshore wind). This way, each day of the year is associated to one of these typical days (see Figure B.2).

¹As detailed by Prina et al. [235], bottom-up models offer a detailed analysis of components and interconnections within different energy sectors, allowing for a techno-economic comparison of technologies and assessment of alternatives for achieving energy targets and reducing greenhouse gas emissions. On the contrary, top-down modes, mostly used by economists and administrations, integrate a simplified representation of the energy system as interacting with the other macro-economic sectors.

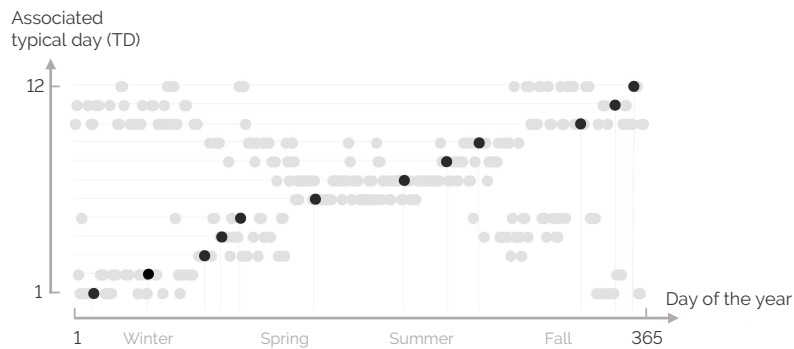


Figure B.2. Association of each day of the year (gray dots) to one of the 12 typical days (TDs) (black dots). Graph adapted from Limpens et al. [52].

Finally, to properly capture the inter days dynamics, EnergyScope TD uses the “Coupling typical days” method from Gabrielli et al. [272]. Among others, this allows representing the dynamics and the seasonality of storage capacities. This method as well as the clustering approach selected in our case, i.e., k-medoids [275, 276], are extensively detailed and compared to other methods, in the work of Limpens et al. [52].

Overview of the snapshot model

EnergyScope TD [52] is a model that optimises both the investment and operating strategy of a ‘whole’-energy system, encompassing electricity, heating, mobility, and non-energy sectors. According to Contino et al. [33], a model qualifies as a ‘whole-energy’ system when it considers all energy sectors, including the non-energy demand such as the production of plastics and other materials using feedstocks that are also considered as energy carriers, with the same level of detail.

The model’s hourly resolution over a year makes it well-suited for integrating intermittent renewables. Its formulation incorporates a reconstruction method that captures different time scales from the hour to the season while accounting for the inter-weeks patterns of wind. The model optimises the investment decisions and hourly operations over a year, with a computational time of less than a minute on a personal laptop. This characteristic was intentionally incorporated into the model design to facilitate uncertainty quantification and other studies that require numerous iterations [49].

EnergyScope TD has been successfully applied to various national energy systems, including Switzerland [52, 277], Belgium [44], Italy [278], and other European countries [108]. Furthermore, it has been extended to a multi-region

energy system model [181], coupled with other energy models [279], or employed to focus on specific sectors such as the networks of electricity, gas, and hydrogen [280].

Formulation of the snapshot model

The conceptual structure of the model is illustrated in Figure B.3: given the end-use energy demand, the efficiency and cost of energy conversion technologies, the availability and cost of energy resources, the model identifies the optimal investment and hourly operation strategies to meet the demand and minimise the total annual cost and greenhouse gas emissions of the energy system. Typically, the two objectives are integrated by placing a limit on emissions while simultaneously minimising the costs.

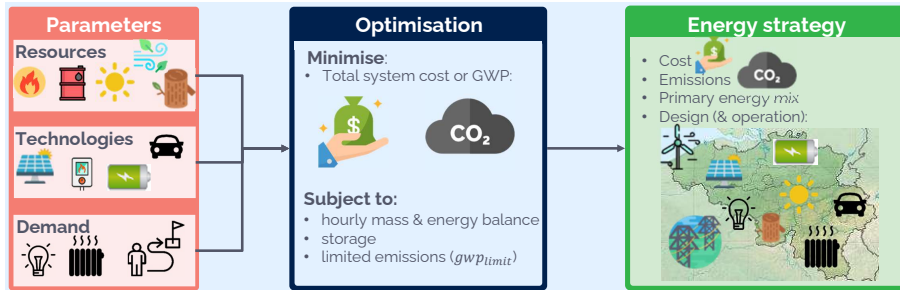


Figure B.3. EnergyScope TD model is a flow model with inputs (Parameters), an optimising model (Optimisation) and results (Energy strategy).

Linear formulation

The following section illustrates the formulation of the original EnergyScope TD model. The objective function, cost and GHG formulation are detailed. The rest of the formulation is detailed and available in a previous work [41]. This work uses the following nomenclature: SETs are in capital letters, **Variables** are in bold and with the first letter in upper case, and *parameters* are in italic.

$$\min \mathbf{C}_{\text{tot}} = \sum_{j \in TECH} (\tau(j) \mathbf{C}_{\text{inv}}(j) + \mathbf{C}_{\text{maint}}(j)) + \sum_{i \in RES} \mathbf{C}_{\text{op}}(i) \quad (\text{B.1})$$

$$\text{s.t. } \tau(j) = \frac{i_{rate}(i_{rate} + 1)^{lifetime(j)}}{\left((i_{rate} + 1)^{lifetime(j)}\right) - 1} \quad \forall j \in TECH \quad (\text{B.2})$$

The objective, Equation (B.1), is the minimisation of the total annual cost of the energy system (\mathbf{C}_{tot}), defined as the sum of the annualised investment cost of the technologies ($\tau \cdot \mathbf{C}_{\text{inv}}$), the operating and maintenance costs of the technologies ($\mathbf{C}_{\text{maint}}$)

and the operating cost of the resources (\mathbf{C}_{op}). The annualised factor τ is computed *a priori* based on the discount rate (i_{rate}) and the technology lifetime, (*lifetime*), Equation (B.2).

$$\mathbf{C}_{\text{inv}}(j) = c_{\text{inv}}(j)\mathbf{F}(j) \quad \forall j \in \text{TECH} \quad (\text{B.3})$$

$$\mathbf{C}_{\text{maint}}(j) = c_{\text{maint}}(j)\mathbf{F}(j) \quad \forall j \in \text{TECH} \quad (\text{B.4})$$

The total investment cost (\mathbf{C}_{inv}) of each technology results from the multiplication of its specific investment cost (c_{inv}) and its installed capacity (\mathbf{F}), see Equation (B.3). The installed capacity is defined with respect to the main end-uses output type, such as electricity for PV or heat for a boiler. The total operation and maintenance costs ($\mathbf{C}_{\text{maint}}$) are calculated in the same way, Equation (B.4).

$$\mathbf{C}_{\text{op}}(i) = \sum_{t \in T} c_{\text{op}}(i)\mathbf{F}_t(i, t)t_{\text{op}}(t) \quad \forall i \in \text{RES} \quad (\text{B.5})$$

The total cost of the resources (\mathbf{C}_{op}) is calculated as the sum of the end-use over the different time-periods multiplied by the period duration (t_{op}) and the specific cost of the resources (c_{op}), Equation (B.5). To simplify the reading, we write the sum over typical days as $t \in T$ such as in Equation (B.5). The period T represents the sequence of hours and typical days over a year (8760h)². The full formulation is detailed in [52] or in the documentation [281].

$$\mathbf{GWP}_{\text{tot}} = \sum_{i \in \text{RES}} \mathbf{GWP}_{\text{op}}(i) \quad (\text{B.6})$$

$$\mathbf{GWP}_{\text{op}}(i) = \sum_{t \in T} gwp_{\text{op}}(i)\mathbf{F}_t(i, t)t_{\text{op}}(t) \quad \forall i \in \text{RES} \quad (\text{B.7})$$

The global annual GHG emissions are calculated using a LCA approach, i.e. taking into account emissions of the resources ‘from cradle to use’. It is based on the indicator ‘GWP100a-IPCC2013’ developed by the Intergovernmental Panel on Climate Change (IPCC) [282]. For climate change, the natural choice as indicator is the Global Warming Potential, expressed in ktCO₂-eq./year. In Equation (B.6), the total yearly emissions of the system ($\mathbf{GWP}_{\text{tot}}$) are defined as the emissions related to resources (\mathbf{GWP}_{op}). The total emissions of the resources are the emissions associated to fuels (from cradle to combustion) and imports of electricity (gwp_{op}) multiplied by the period duration (t_{op}), Equation (B.7). Thus, this version accounts only for operation without accounting for the GWP emitted during the construction of the technologies.

²The exception is storage level which is optimised over the 365 days of the year instead of typical days.

This makes the results comparable with metrics used in the reports by the European Commission and the International Energy Agency (IEA).

The above equations (Equations (B.1) - (B.7)) represent only a part of the formulation and illustrate the syntax that is used. Those representing the energy balance, network implementation, sectors representation, etc. are not presented in this work but are detailed in the latest version of the model, see [41] and in the documentation [281].

Finally, energy storage has two dimensions to be optimised: (i) the hourly power flow, encompassing both charging and discharging and, (ii) the stored energy quantity (also referred to as 'storage level'). EnergyScope TD optimises the former based on the hourly resolution of the typical days and the latter over the entire span of 8760 hours in a year. This formulation allows for the effective integration of a wide range of energy storage technologies, spanning short-term solutions like small thermal storage units and daily-use batteries, to longer-term options such as hydro-dam storage for seasonal storage, and even large-scale thermal storage for intra-week patterns. A previous study investigated the roles of various storage technologies, considering their sectoral applications and temporal aspects, within the context of the Swiss energy system [277].

B.2.2 Extending the model for pathway optimisation

In this section, we delve into the extension of EnergyScope TD from a static yearly snapshot model to a comprehensive pathway model. While snapshot models provide insights into the energy system for individual years, they lack the capacity to capture the dynamics inherent in investment strategies throughout a transition period. The proposed approach involves segmenting the transition into five-year intervals. This approach results in seven instances of EnergyScope TD – called representative years – spanning the 30-year transition period, covering the years from 2020 to 2050. To bridge these representative years, we introduce additional constraints that capture the investments changes between consecutive periods, accounting for societal inertia and evaluating both the cost implications and emissions of the transition (see Figure B.4). Overall, these constraints are integrated into a linear framework, ensuring computational efficiency, with an approximate computational time of 14 minutes on a personal laptop (2.4 GHz Intel Core i5 quad-core). Simplification and choices were necessary to implement linearly the problem while keeping a tractable computational time. In this section, the retained formulation is presented.

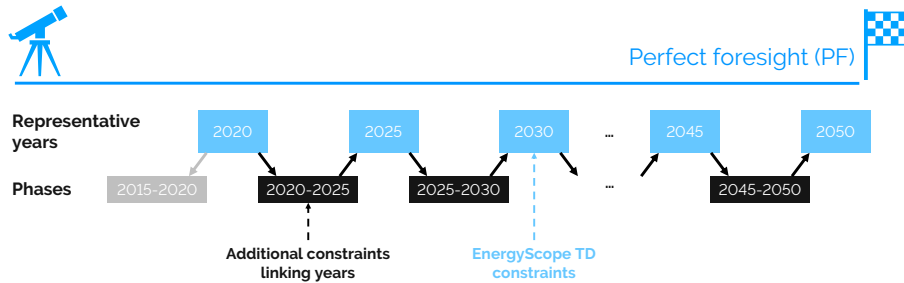


Figure B.4. The pathway methodology relies on 7 representative years (blue boxes) where the model ESTD is applied. Moreover, the formulation accounts for linking constraints (black boxes) and an initial condition (grey box). The overall problem is the pathway model.

The proposed formulation relies on representative years, selected every 5 years from 2020 to 2050. The period between two of them is called ‘*PHASE*’. For each of these 7 representative years, the EnergyScope TD model is run using the relevant data (such as energy demand, technology costs or GHG emissions constraints).

As a consequence, a new dimension ‘*year*’ is added to all **Variables** and parameters, except the discount rate (i_{rate}) assumed constant during the transition. This new dimension is necessary to represent the changes of technology and resource characteristics over the representative years. As an example, the investment cost (c_{inv}) of solar photovoltaic panels could drastically vary in the next decades (e.g. data used ranges between 1220 to 870 [€/kW] between 2020 and 2035).

Linking years

At this stage, all years are independent. In the following, we introduce new constraints to link representative years. The formulation allows to install new capacity (F_{new}), remove a capacity that has reached its lifespan (F_{old}) or decommission a technology prematurely (F_{decom}). These capacity changes occur during a phase, this implies that there is no capacity change during a representative year. Figure B.5 illustrates the concept.

$$F(y_{stop}, i) = F(y_{start}, i) + F_{new}(p, i) - F_{old}(p, i) - \sum_{p2 \in PHASE \cup \{2015_2020\}} F_{decom}(p, p2, i)$$

$$\forall p \in PHASE, y_{stop} \in Y_STOP(p), y_{start} \in Y_START(p), i \in TECH \quad (B.8)$$

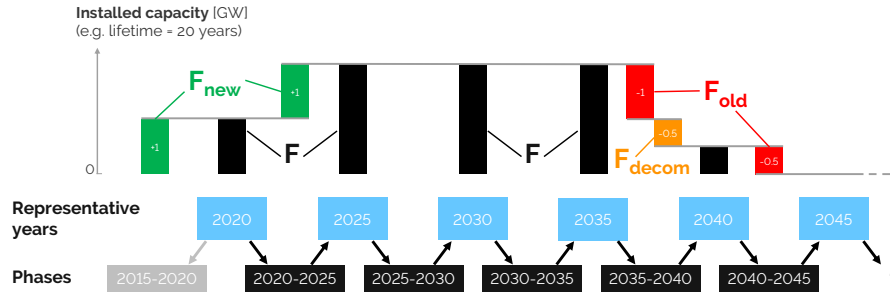


Figure B.5. Example of how the technology capacities and associated variables are evolving.

Similarly to a mass balance, Equation (B.8) is the technology capacity balance. The constraint forces the installation or withdrawing of capacities between two representative years: at the end of the phase (y_{stop}), the available capacity is the one used in the next representative year ($F(y_{stop})$). This capacity is equal to the one available in the previous representative year ($F(y_{start})$) plus the new installed capacity (F_{new}) minus the capacity that has reached its lifetime (F_{old}) minus the early decommissioned capacity (F_{decom}). One notices that the capacity available for each representative year depends on a year (y_{start} or y_{stop}), while the other capacity changes depend on a phase (p or $p2$). Moreover, the decommissioning term depends on another phase, which is the one when the technology decommissioned has been built. As an illustration, Figure B.5 gives an example where 0.5 GW of a capacity built in 2015_2020 is decommissioned in 2030_2035 ($F_{decom}(2030_2035, 2015_2020, i)$).

$$F_{decom}(p, p2, i) = 0$$

$$\forall i \in TECH, p \in PHASE, p2 \in PHASE \cup \{2015_2020\} | decom_{allowed}(p, p2) = 0 \quad (B.9)$$

$$F_{old}(p, i) = \begin{cases} \text{if}(age = 'STILL_IN_USE') \text{ then } 0 \\ \text{else } \left(F_{new}(age, i) - \sum_{p2 \in PHASE} F_{decom}(p2, age, i) \right) \end{cases}$$

$$\forall p \in PHASE, \forall j \in TECH | age \in AGE(p, j) \quad (B.10)$$

In linear programming, a solution might be mathematically correct, while not making sense in practice. As an example, a technology could be decommissioned before being built ($p < p_{built}$). Equations (B.9-B.10) allow preventing these non-sense while

keeping the formulation linear. Equation (B.9) forces the decommissioned capacity to zero when technology will be built after. To do so, a parameter ($decom_{allowed}$) is defined *a priori* and is equal to 0 or 1 when decommissioning is not possible or possible, respectively. Equation (B.10) defines the capacity reaching its lifetime limit at a certain phase, the concept is illustrated in Figure B.5. For each phase, a set (AGE) is calculated *a priori*. It relates, for a given phase and technology, when the technology was built. In the case the technology has already reached its lifetime limit, the set (AGE) returns the phase when the technology has been built. The first part of Equation (B.10) indicates that the technology is still available, and thus no capacity needs to be removed. The second part of the equation represents the capacity that reached its expected lifetime minus a part of the capacity that would have been decommissioned. As an example, Figure B.5 shows a 20 years lifetime technology with 1 GW of capacity installed before 2020. The ‘if’ in Equation (B.10) is linear as it is applied to a parameter and not a variable.

$$\mathbf{F}_{\text{new}}(2015_2020, i) = \mathbf{F}(YEAR_2020, i) \quad \forall i \in TECH \quad (\text{B.11})$$

To initialise the problem in 2020 with the existing design, an additional phase ‘2015_2020’ is created. Equation (B.11) requires that the capacity used in 2020 is installed in the previous phase.

Inertia of society

To avoid unrealistically fast changes in the system, additional constraints are needed during the phases for the mobility and low temperature heat sectors. Without the following constraints, the model would eliminate certain technologies in one phase, such as oil and gas decentralised boilers. Even if this result is mathematically and physically correct, (i.e., fuels are expensive and investing in more efficient technology is economically and environmentally more profitable), this swap of technology cannot occur in one phase (i.e., 5 years). Indeed, inertia of society to change, available manpower, supply chains and manufacturers limit the change.

$$\Delta_{\text{change}}(p, i) \geq \sum_{t \in T} (\mathbf{F}_t(y_{start}, i, t)) - \sum_{t \in T} (\mathbf{F}_t(y_{stop}, i, t)) \\ \forall j \in TECH, p \in PHASE, y_{start} \in Y_START(p), y_{stop} \in Y_STOP(p) \quad (\text{B.12})$$

$$\sum_{i \in TECH(HeatLowT)} \Delta_{\text{change}}(p, i) \leq lim_{LT,ren} \cdot (eui(y_{start}, HotWater) + eui(y_{start}, SpaceHeat))$$

$$\forall p \in PHASE, y_{start} \in Y_START(p) \quad (\text{B.13})$$

$$\sum_{i \in TECH(MobPass)} \Delta_{\text{change}}(p, i) \leq lim_{MobPass} \cdot eui(y_{start}, MobPass)) \quad \forall p \in PHASE, y_{start} \in Y_START(p) \quad (\text{B.14})$$

$$\sum_{i \in TECH(MobFreight)} \Delta_{\text{change}}(p, i) \leq lim_{MobFreight} \cdot eui(y_{start}, MobFreight) \quad \forall p \in PHASE, y_{start} \in Y_START(p) \quad (\text{B.15})$$

Equation (B.12) calculates the upper limit of change (Δ_{change}) in terms of supplied demand instead of installed capacity. Based on this quantification, the amount of change per phase is limited for low temperature heat ($lim_{LT,ren}$), Equation (B.13), passenger mobility ($lim_{MobPass}$), Equation (B.14) and freight mobility ($lim_{MobFreight}$), Equation (B.15). For instance, if the maximum allowable variation in supplied low temperature heat is set at 25%, it would restrict the technology-related changes in low temperature heat to 25% within a given phase. Consequently, if a technology supplies more than 25% of the low temperature heat, it would require multiple phases to replace it with a different technology.

Cost and emissions of the transition

To optimise the energy system, two key metrics must be adapted: the transition cost and the total Global Warming Potential (GWP). Concerning the first one, all costs are expressed in €₂₀₂₀ and an annualisation factor is used to distinguish investments over the transition. For the GWP, the metric used is based on the contributions of the gases over 100 years. It is assumed that the impact of emitting at the beginning or the end of transition are equivalent and thus no annualisation is used.

$$\min C_{\text{tot,trans}} = C_{\text{tot,capex}} + C_{\text{tot,opex}} \quad (\text{B.16})$$

$$C_{\text{tot,capex}} = \sum_{p \in PHASE \cup \{2015_2020\}} C_{\text{inv,phase}}(p) - \sum_{i \in TECH} C_{\text{inv,return}}(i) \quad (\text{B.17})$$

$$C_{\text{tot,opex}} = C_{\text{opex}}(2020) + t_{\text{phase}} \cdot \tau_{\text{phase}}(p) \cdot \sum_{p \in PHASE | y_{start} \in P_START(p), y_{stop} \in P_STOP(p)} \left(C_{\text{opex}}(y_{start}) + C_{\text{opex}}(y_{stop}) \right) / 2 \quad (\text{B.18})$$

$$\tau_{\text{phase}}(p) = 1 / (1 + i_{\text{rate}})^{\text{diff_2015_year}(p)} \quad (\text{B.19})$$

As an extension of Equation B.1, the objective function to be minimised is the total transition cost of the energy system ($C_{\text{tot,trans}}$), defined as the sum of the total CAPEX ($C_{\text{tot,capex}}$) and the OPEX ($C_{\text{tot,opex}}$), according to Equation (B.16). The total CAPEX ($C_{\text{tot,capex}}$) is the sum of the investment during each phase ($C_{\text{inv,phase}}$), Equa-

tion (B.17), to which the residual asset value in 2050 is withdrawn ($\mathbf{C}_{\text{inv,return}}$). Thus, the investments account for the installation and dismantlement costs of the technologies. The total OPEX ($\mathbf{C}_{\text{tot,opex}}$) is the sum of the OPEX in 2020 and the annualised sum of the OPEX during each phase (\mathbf{C}_{opex}), Equation (B.18). During a phase, the system OPEX is the product of the annualised phase factor, defined in Equation (B.19), and the arithmetic average of OPEX cost for the representative years before and after the phase. The annualised phase factor is defined based on an average discount rate during the transition.

$$\mathbf{C}_{\text{opex}}(y) = \sum_{i \in \text{TECH}} \mathbf{C}_{\text{maint}}(y, i) + \sum_{j \in \text{RES}} \mathbf{C}_{\text{op}}(y, j) \quad \forall y \in \text{YEARS} \quad (\text{B.20})$$

For each year, the yearly OPEX (\mathbf{C}_{opex}) is the sum of the operating and maintenance costs of technologies ($\mathbf{C}_{\text{maint}}$) and the operating cost of the resources (\mathbf{C}_{op}), Equation (B.20).

$$\mathbf{C}_{\text{inv,phase}}(p) = \sum_{j \in \text{TECH}} \mathbf{F}_{\text{new}}(p, j) \cdot \tau_{\text{phase}}(p) \cdot (c_{\text{inv}}(y_{\text{start}}, j) + c_{\text{inv}}(y_{\text{stop}}, j)) / 2 \quad \forall p \in \text{PHASE} | y_{\text{start}} \in P_START(p), y_{\text{stop}} \in P_STOP(p) \quad (\text{B.21})$$

The investment during a phase ($\mathbf{C}_{\text{inv,phase}}$) results from the multiplication of the newly built technologies (\mathbf{F}_{new}) with their annualised arithmetic averaged specific cost, Equation (B.21). The annualised phase factor (defined by Equation (B.19)) is used. The specific cost during the phase is defined as the average between the investment cost for the first and last year of the period.

$$\begin{aligned} \mathbf{C}_{\text{inv,return}}(i) = & \sum_{p \in \text{PHASE} \cup \{2015_2020\} | y_{\text{start}} \in Y_START(p), y_{\text{stop}} \in Y_STOP(p)} \tau_{\text{phase}}(p) \cdot (c_{\text{inv}}(y_{\text{start}}, i) + c_{\text{inv}}(y_{\text{stop}}, i)) / 2 \cdot \\ & \frac{\text{remaining_years}(i, p)}{\text{lifetime}(y_{\text{start}}, i)} \left(\mathbf{F}_{\text{new}}(p, i) - \sum_{p2 \in \text{PHASE}} \mathbf{F}_{\text{decom}}(p2, p, i) \right) \quad \forall i \in \text{TECH} \end{aligned} \quad (\text{B.22})$$

A part of the investment will remain after 2050. This residual investment, also called salvage value, can be calculated for each technology. A parameter, calculated *a priori*, gives for each technology and construction phase, the remaining amount of years (*remaining_years*). As an example, if a PV panel has been built in 2045 and has a 20 years lifetime, the parameter will equal to 15 years. Thus, the salvage value is a fraction of the investment cost of this technology when it has been built. This fraction is the ratio between the number of remaining years and the lifetime of the technology.

In the previous example, the residual investment of the PV built is 75%. Equation (B.22) computes, for each technology, the residual value that must be subtracted from the total cost. The residual value reflects the fact that the technology can still be used after the horizon of the model and is not fully amortised. The residual value is not applied to technologies that are removed prematurely. This is similar to the work of Prina et al. [58] but differs from other models, such as Plexos where a technology removed prematurely will benefit from its salvage value (see analysis of [256]).

In the work of Goffaux [50], we carried out a sensitivity analysis on the formulation of the salvage value. First and foremost, this analysis confirmed the need to account for the salvage value to avoid penalising the capital intensive technologies towards the end of the transition [38]. Then, the sensitivity analysis focused on two elements in the expression of the salvage value: $\tau_{phase}(p)$ and $\mathbf{F}_{decom}(p_2, p, i)$.

In Equation (B.22), τ_{phase} is the annualisation factor corresponding to the phase where the technology was built. With this expression, if a technology is still operational for half its lifetime after 2050, then half its initial investment is subtracted to the total transition cost. However, one could wonder if a technology that is still operational for half of its lifetime is not worth less than half of its initial investment cost, given the depreciation of the asset. In that case, the annualisation factor should account for the last phase of the optimisation (i.e., 2045_2050) when the residual value of the technologies are calculated and subtracted from the total transition cost.

On top of this, we also investigated the impact of accounting for the decommissioned technologies or not in the expression of the salvage value. In Equation (B.22), if a technology is decommissioned before 2050, then the salvage value of this technology will be 0. This is relevant since a technology decommissioned before 2050 would not be available after 2050. The issue is that the model could keep unnecessary technologies to subtract their salvage value from the total transition cost in order to decrease it. This would be done if the fixed OPEX of an unused technology is lower than its salvage value. Therefore, one could wonder if it would not be better to take into account the decommissioned technologies in the salvage value. In that case, a technology that would have been operational after 2050 but that had been prematurely decommissioned before 2050, would have a salvage value.

The overall conclusion of this sensitivity analysis was that the salvage value expression has little influence on the energy system at the end of the time horizon.

$$\mathbf{GWP}_{tot,trans} = \mathbf{GWP}_{tot}(2020) + t_{phase} \sum_{p \in PHASE | y_{start} \in Y_START(p), y_{stop} \in Y_STOP(p)} /2 (\mathbf{GWP}_{tot}(y_{start}) + \mathbf{GWP}_{tot}(y_{stop})) \quad (B.23)$$

$$\mathbf{GWP}_{\text{tot,trans}} \leq gwp_{lim,trans} \quad (\text{B.24})$$

The total Global Warming Potential (GWP) emissions during the transition ($\mathbf{GWP}_{\text{tot,trans}}$) are equal to the sum of the total emissions per period ($\mathbf{GWP}_{\text{tot}}$), Equation (B.23). The emissions during a phase is estimated as the arithmetic average of the representative years before and after the phase. Equation (B.24) limits the total GWP emissions during the transition by a maximum ($gwp_{lim,trans}$).

Appendix C

Case study: the Belgian energy system

C.1 Belgian energy system in 2020

The Belgian whole-energy system of 2020 was largely based (88.6% of the primary energy mix) on “conventional fuels” (i.e., oil and oil products (38.2%), natural gas (29.5%), uranium (16.3%) and solid fossil fuels (4.6%)) while the rest mainly accounts for 26.7 TWh of lignocellulosic and wet biomass, 12.8 TWh of wind and 5.1 TWh of solar [45]. Given the data available in the literature (mostly for the power sector) and, when not available, following the assumptions made by Limpens et al. [44], Table C.1 gives the major technologies used in 2020 to supply the different demands of Figure 2.2.

C.2 Belgian energy transition pathway towards carbon neutrality in 2050

This section presents the results of the deterministic (i.e., all parameters at their nominal value) perfect foresight optimisation of the Belgian energy transition pathway constrained to a linear decrease of the GHG emissions from 2020 (121 MtCO_{2,eq}) to carbon neutrality in 2050. After performing a technical investigation of the pathway by checking the greenhouse gas breakdown by energy sectors, the primary energy mix is analysed. To illustrate the sector coupling, a focus is made on the electrification of the sectors. Then, the cost implications in terms of investments and operations are discussed.

Table C.1. Major technologies used to supply the 2020-demands of Figure 2.2 in terms of share of production and installed capacity.

| End-use demand | Major technologies | Share of supply | Installed capacity |
|-----------------------------------|----------------------|-----------------|--------------------|
| Electricity | Nuclear | 39% | 5.9 GW |
| | CCGT | 21% | 3.9 GW |
| | Wind turbines | 14% | 5.0 GW |
| Heat High-Temp. | Gas boiler | 36% | 3.3 GW |
| | Coal boiler | 30% | 2.3 GW |
| | Oil boiler | 20% | 1.5 GW |
| Heat Low-Temp. (DEC) ^a | Oil boiler | 48% | 21.4 GW |
| | Gas boiler | 40% | 17.5 GW |
| | Wood boiler | 10% | 4.4 GW |
| Heat Low-Temp. (DHN) | Gas CHP | 59% | 0.3 GW |
| | Gas boiler | 15% | 0.3 GW |
| | Waste CHP | 15% | 0.1 GW |
| Private mobility ^b | Diesel car | 48% | 93.5 Mpass.-km/h |
| | Gasoline car | 49% | 94.7 Mpass.-km/h |
| | HEV | 2% | 5.9 Mpass.-km/h |
| Public mobility | Diesel bus | 43% | 3.6 Mpass.-km/h |
| | Train | 43% | 3.9 Mpass.-km/h |
| | CNG bus | 5% | 0.8 Mpass.-km/h |
| Freight mobility | Diesel truck | 74% | 62.7 Mt.-km/h |
| | Diesel boat | 15% | 10.8 Mt.-km/h |
| | Train | 11% | 2.5 Mt.-km/h |
| HVC | Naphtha/LPG cracking | 100% | 4.6 GW |
| Ammonia | Haber-Bosch | 100% | 1 GW |
| Methanol | Import | 100% | - |

^aThe decentralised heating units provide 98% of the low-temperature heat demand.

^bThe private mobility accounts for 80% of the passengers mobility.

C.2.1 Greenhouse gases and primary energy

Figure C.1 shows the Greenhouse Gases (GHG) per sector. The system reaches its upper bound (i.e., maximum emissions) every year.

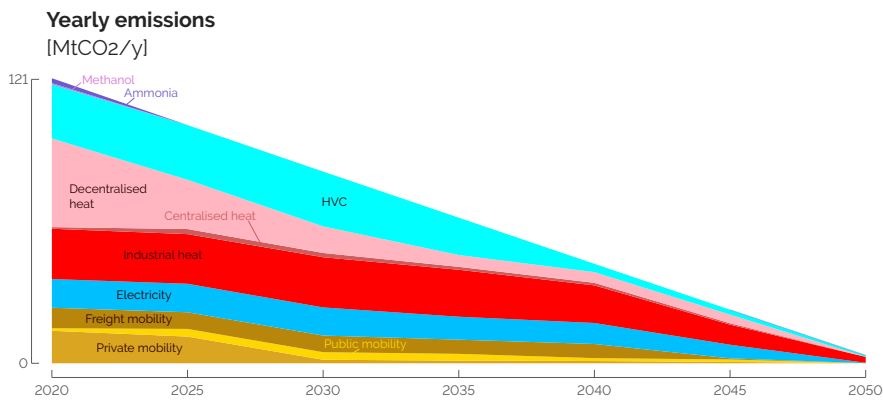


Figure C.1. Energy sectors have different rates to reduce GHG emissions over the transition. The system uses all the allowed GHG prescribed by the linear decrease from the emissions in 2020 until carbon neutrality in 2050.

The defossilisation of the different sectors are not performed at the same rate. The non-energy demand of methanol and ammonia are substituted by electrofuels. These are the first use of electrofuels as e-ammonia is the cheapest electrofuel thanks to the high maturity of the Haber-Bosch process. The decentralised heat and mobility sectors are also dropping first. This is a combination of efficiency and substitution of fossil fuels with electricity. In particular, the private mobility drops to near-zero emissions at early stages of the transition for two main reasons: (i) the switch of propulsion systems and, (ii) the modal shift. First, while accounting for the society inertia in this sector (see Equation (B.14)), battery electric vehicles (BEV) substitute ICE cars. This reduces the overall emissions of the private vehicles as electric motors are more efficient than ICE and they are driven by a less-emitting resource (i.e., electricity versus diesel and gasoline). On top of this, the model allows a modal shift from the private to the public mobility. From the current share of the passenger mobility provided by private vehicles (i.e., 80%), the model allows this share to go down to 50%. Efficiency comes mainly from district heating networks and electrical heat pumps for the heat sector, and public mobility and electric cars for the mobility sector. From 2040 onward, the decreases are mainly due to the substitution of the remaining fossil fuels by electrofuels as illustrated in Figure C.2.

Figure C.2 shows the primary energy mix for the different representative years. The pathway verifies five trends: (i) reduction of primary energy thanks to energy efficiency; (ii) massive integration of endogenous renewable energies; (iii) importance of electrification; (iv) the use of gas as the last fossil resource; and (v) the obligation to rely on renewable fuels to achieve carbon neutrality.

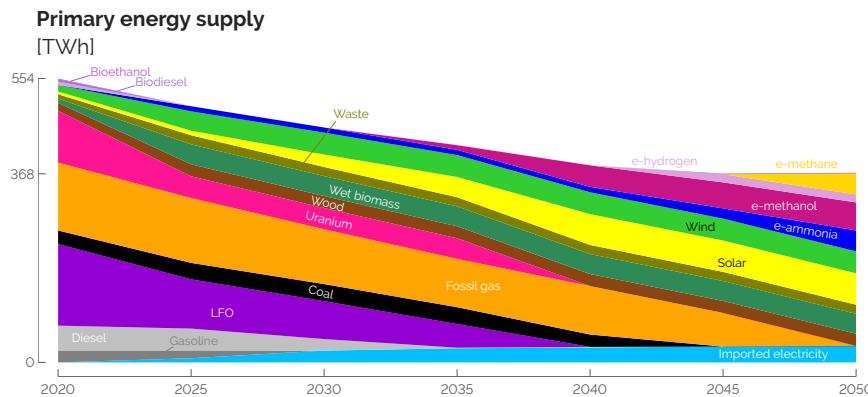


Figure C.2. Primary energy emitting GHG (below Uranium) are decreasing linearly with fossil gas remaining until 2045. A part of this energy is replaced by renewable ones and starting from 2040, a significant share of electrofuels. As end-use demands slightly increase (see Figure 2.2), the drop represents energy efficiency (i.e., providing the same services with less primary energy).

The energy supply decreases from 554 TWh/y in 2020 down to 368 TWh/y in 2050 (i.e., -34%) whereas, in the meantime, the demands have increased by 19%, on average. This drop of primary energy consumption reflects the penetration of efficient measures and technologies, such as the previously mentioned public mobility, DHN or heat pumps. The results in 2050 are aligned with other studies, such as Devogelaer et al. [283]¹ and My2050² [72] which estimates respectively a range of 305-417 TWh/y and 307-364 TWh/y for their central scenarios.

¹This study was ordered by the National Planning Bureau in 2013. Five scenarios are proposed.

²The Climate Change Service of the Federal Public Service Health launched an initiative in 2012 entitled ‘Low Carbon Belgium by 2050’. This initiative resulted in a report and a calculator in 2013 [284]. The Belgian calculator has been improved since then into a recent expert version called **My2050** [72]. From this study, the results of two scenarios will be used: one based on an optimistic evolution of technologies (Technology), and one focusing on an increased dependence on neighbouring countries (EU integration).

The first fossil energy to phase out is gasoline, which is exclusively used for private cars. Indeed, private mobility is partially replaced by public one³; and the cars are switching from gasoline and diesel to electricity. Then, diesel and LFO are decreasing. As diesel is used for trucks and buses mobility, it is harder to phase out compared to gasoline exclusively burned in cars. The first drop of LFO reflects the switch from oil boilers to other technologies: heat pumps and gas cogeneration mainly. Then, it is mainly used for the production of HVC, this reflects that HVC is a feedstock hard to defossilise. Finally, coal is kept mainly for industrial usage because it is a cheap fossil fuel (mainly for industrial usage). To phase it out beforehand, a penalty mechanism, such as a carbon tax, would be required, or its strict ban should be put in place. The last fossil energy present in the system is fossil gas, used for the production of electricity and heat, through cogeneration mainly. Indeed, gas plays a key role to balance the intermittency of solar and wind.

The consumption of uranium declines in 2025, dropping to 2 GW, primarily due to the political framework aimed at phasing out nuclear energy [285]. In the initial stages, significant deployment of endogenous energies takes place. This includes the utilization of wood, wet biomass, and wind energy, followed by the introduction of solar energy. However, solar energy is not fully deployed during this period due to higher integration costs. Starting from 2025, the importation of electrofuels begins, although their significant utilisation is observed from 2035 onwards. Initially, these fuels are predominantly employed as feedstocks in non-energy sectors. From 2040, e-methanol is additionally utilised for the production of High-Value Chemicals (HVCs), e-hydrogen is employed for mobility purposes, and both e-methane and e-ammonia are used for electricity generation through gas CHP and ammonia-based CCGT plants (see Figure C.3).

In 2020, Belgium has been a net-exporter of electricity, however with the shutdown of nuclear power plants and the increase of electricity consumption, Belgium will become a net importer of electricity. These imports reach their maximal allowed capacity by 2035 (i.e. 30% of electricity end use). This strong dependence on imported electricity illustrates the need for balancing intermittent renewables without relying on fossil fuels.

³Given the major role played by private cars in the Belgian passenger mobility nowadays (i.e., around 80% [114]), public transport (e.g., tramways, buses and trains) is assumed to be able to supply only half of it.

C.2.2 Electricity sector: Capacities and yearly balance

To better understand the electricity sector, the installed production capacities are given in Figure C.3, while the supply-demand yearly balance is illustrated in Figure C.4.

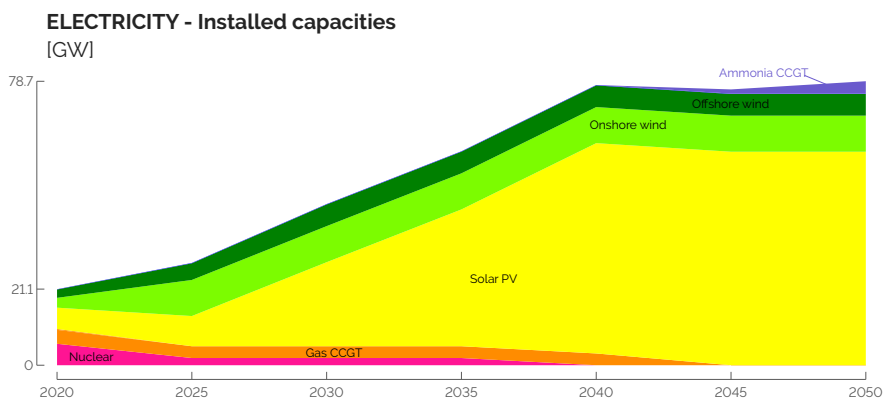


Figure C.3. The electrical production capacity will experience massive expansion of wind turbines (onshore and then offshore) and a soaring installed capacity of PV. Ammonia CCGT are installed at the end of the transition to provide a flexible capacity as gas CCGT are phased out.

As introduced in the primary energy analysis (see Figure C.2), renewable capacities soar. By 2050, wind and solar technologies deployments are 60 GW of PV, 10 GW of onshore wind turbines and 6 GW of offshore wind turbines. To compensate the intermittency, the system relies on imported electricity, gas CCGT, sector coupling and storage. This is in line with the work of Devogelaer [286] that ends up with about 80 GW of total installed power generation capacity by 2050, with less PV (i.e., 39 GW) and more wind capacities (i.e., 25 GW of which offshore takes 8.3 GW). As an illustration, in 2050, 176.8 TWh of electricity transit on the grid which includes 32.4 TWh of electricity imported and 15.4 TWh of electricity from CCGT. This result is aligned with other studies that estimates different ranges: 180-310 TWh/y [283], about 250 TWh/y [286], 126-140 TWh/y [72] and in a more recent study using the TIMES-BE model, 185-196 TWh/y [130]. Higher values from Devogelaer et al. [283] illustrate an almost exclusively electrified energy system. The differences between the study ranges reflect the different assumptions in terms of renewable potentials and availability of nuclear energy. A general trend is that Belgium should maximise its use of endogenous renewable resources, which Dubois et al. [183] identified as a cheaper option than importing additional renewable energies from abroad. Demand management reflects the flexible

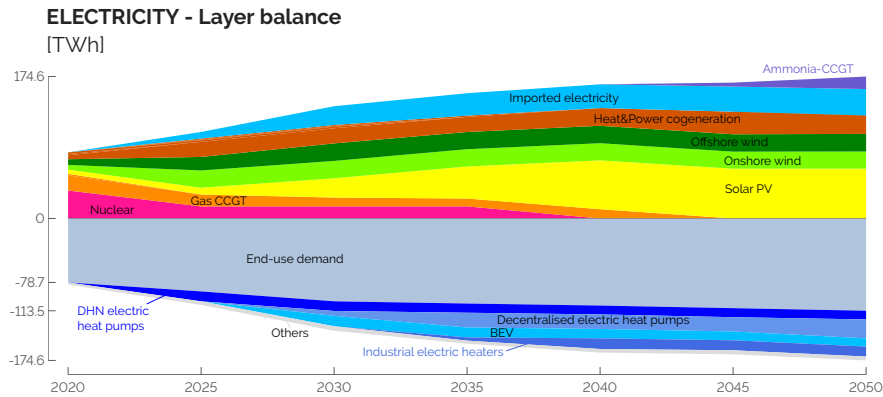


Figure C.4. The electricity supply (positive values) will remain a mix of different technologies where backup is first mainly provided by gas-CCGT and then imported electricity, heat and power cogeneration and later ammonia-CCGT. The electricity demand (negative values) is led by the electricity end-use demand, but the share used to electrify heat (heat pumps), vehicles (cars, trains, trams...) and industrial heaters drastically increases. This enables a flexible demand that can facilitate the integration of intermittent renewables.

use of electricity, mainly through heat pumps that uncouple the heat demand and the electricity consumption when combined with thermal storage. Gas CCGT is also a useful asset to compensate intermittent renewables. However, its capacity remains the same as the one installed in 2020. These results are verifying an hourly adequacy of the power demand. Moreover, in a previous study by Pavičević et al. [279], the snapshot version of the model has been coupled with Dispa-SET, a dispatch optimisation model. Results showed that the backup capacity was underestimated by less than 20% to respect reserve capacity, mainly due the lack of reserve capacity for grid stability.

From 2025, the electricity mix has a strong renewable share that rises up to 60% in 2050. The remaining 40% are mainly gas (or ammonia) in CCGT and cogeneration and imported electricity. From a demand perspective, the electrification first starts with DHN heat pumps, then electric cars, then decentralised heat pumps and finally industrial heaters. The latter reflects the usage of cheap PV production peaks.

C.2.3 Costs: Investments and operation

In the following paragraphs, the results are analysed from a cost perspective to decipher the choices made by the model, as the overall cost of the transition is 1004 b€ split unequally among the sectors.

Figure C.5 illustrates the cumulative investments made throughout the transition, amounting to a total of 377.8 b€. This makes 12.6 b€ on average per year, which represents 2.1% of the current Belgian GDP. This is in the range of other studies on climate-neutral scenarios concluding additional investment needs of the order of 2 to 3% of the GDP on a global scale [19, 287] or 2.7 to 3.8% at the European level [288].

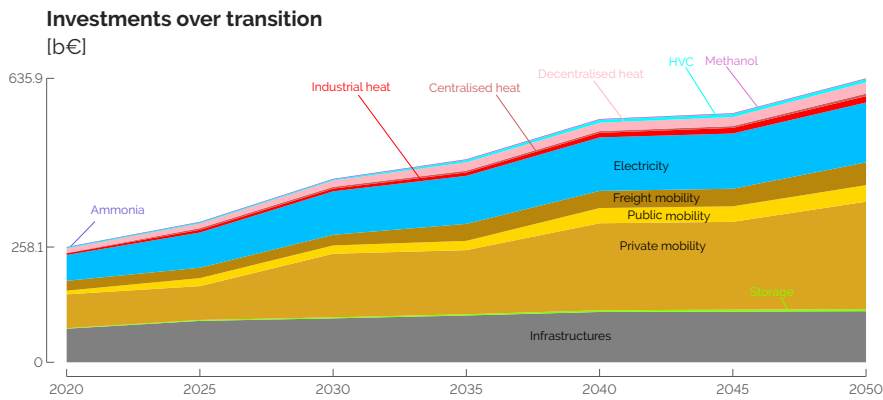


Figure C.5. The cumulative investments over the transition are unequally spread between the sectors. The energy system in 2020 is imposed as the existing energy system and its expenses are split in three main categories: mobility (mainly vehicles), infrastructure (mainly grids) and electricity (mainly thermal power plants). The investments required during the transition represents 150% the initial investment and mainly in the same three sectors.

Initially, the infrastructure, transport, and electricity sectors each account for approximately one-third of the investments. The investments in infrastructure are primarily driven by the electricity grid and the District Heating Network (DHN), representing a combined investment of 73 b€. The electricity sector's investment is led by power plants, totalling 31.5 b€. Notably, the investment costs in the mobility sector are primarily attributed to private cars, constituting 71% of the total. A rough estimation confirms the significant investment in cars, with an average of 500,000 vehicles registered annually in Belgium over the last decade [289] and assuming an average cost of 20 k€ per car, the funds allocated to private cars amount to 10 b€ per year. This

trend in private cars explains why the private mobility sector accounts for half of the investments required to achieve the transition by 2050. This finding aligns with other studies, such as Devogelaer et al. [283], which estimates cumulative investment expenditures of approximately 600 b€₂₀₀₅ for the transport sector between 2013 and 2050, which confirms our conservative approach in the estimation.

As a comparison, the investments required to fully deploy the PV and wind potentials from 2020 to 2050 amount to 74.4 b€, with an additional 22.2 b€ allocated to reinforce the grid. The electrification of the heating sectors necessitates investments of 29.2 b€, including 6.5 b€ for the deployment of the DHN infrastructure. Storage investments, primarily focused on DHN seasonal storage, amount to 3.6 b€. Apart from the investment required to replace all private vehicles (accounting for 44% of the overall investments), the remaining sectors represent a total of 212 b€. To mitigate the cost of the transition, My2050 suggests deploying a fleet of no more than one million vehicles and implementing a car sharing system, distinct from car-pooling, as an inevitable measure [72].

A part of the investment will be recovered at the end of the transition based on the remaining lifespan of the technologies after 2050. Figure C.6 illustrates the salvage value by sectors, calculated according to Equation (1.5). Out of the 114.4 b€ of investments in the infrastructure (i.e., mostly power grid and gas network), 55.9% remain available after 2050, due to their long lifetime. On the contrary, private mobility has a lower salvage value due to a major drop within the first four years and an average lifetime below 10 years [289].

In addition to investment decisions, the Operational Expenditure (OPEX), which accounts for resource utilisation and technology maintenance, are significant. Figure C.7 shows the yearly system cost for each sector except the OPEX related to resources that are grouped together. The latter dominates the OPEX, with a significant share of non-renewable resources (i.e., 63.6% in 2020) until 2040, followed by a steep increase in the share of renewable resources (i.e., 66.2% in 2050). The substantial reliance on non-renewable resources reflects the prevalent use of fossil fuels in our current energy system. The high cost-share of non-renewable fuels underscores the economic challenges of simply substituting fossil fuels with renewables, particularly evident when emphasizing that electrofuels are 2-3 times more expensive. Maintenance expenses in the private mobility sector rank second in terms of expenditure. On the other hand, maintenance expenses in other sectors are relatively small compared to the aforementioned sectors.

The annualised cost of the energy system in 2020 is estimated to 44.3 b€/y and increases by 5.5 b€/y to reach 49.8 b€/y by 2050. The work of Climact and VITO [72]

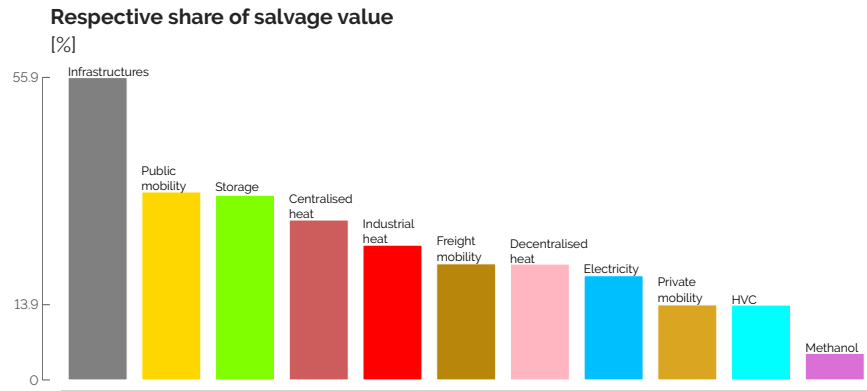


Figure C.6. By the end of the transition (i.e., in 2050), the ratio between the salvage value in a sector and its cumulative investment is unequal. Investments in infrastructures, public mobility, storage and other long-lifetime technologies experience an important salvage value on the contrary, investments in private mobility will not be recovered as vehicles have a short lifetime. All together, these salvage values represent 160.1 b€, 25% of the cumulative investment costs in 2050.

estimates the annualised cost in 2050 between 63 and 82 b€/y, while other studies just indicate the cost increase compared to 2015 (+11.7 to +21) [130, 283]. The differences come from the scope of the energy system: as an example Climact and VITO [72] also account for the agriculture sector. These differences highlight the difficulty to compare different studies due to difference of scope and partial availability of used data. Overall, comparing with existing studies shows the consistency of the results provided by EnergyScope Pathway.

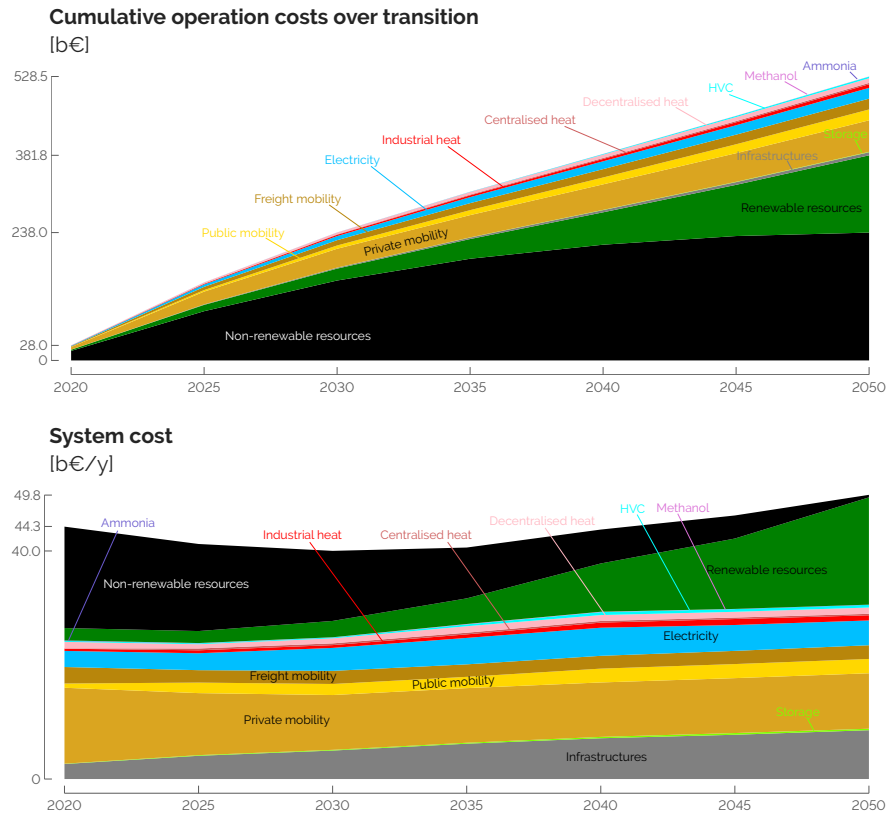


Figure C.7. The yearly system cost shows the shift from non-renewable to renewable resources (mainly electrofuels). Operation and maintenance costs represents almost 50% of the expenses.

C.3 Myopic versus perfect foresight pathway optimisation

This section aims at digging more into the details of the differences observed between the myopic approaches and the reference case, the hourly perfect foresight model (see Table C.2).

Similarly to Nerini et al. [63], Figure C.8 shows that myopic optimisation ends up with a slightly more expensive energy transition by 2050 (i.e., +3.2 b€), compared to the perfect foresight, despite the savings done at the early stages. Even though this over-cost is negligible compared to the overall cost of the transition (i.e., ~1000 b€), this is explained by the early investments in renewable technologies (i.e., PVs and

Table C.2. Comparison between the two different foresight approaches: Perfect foresight (PF) and Myopic (MY). Differences with the reference case (PF) below 1% are not shown (\simeq) and ones above 10% are in bold.

| | | PF | MY | Units |
|--------------------------------------|---------------------------------|-------|-------------|-------------------|
| Computational time ^a | | 830 | 373 | s |
| Costs in 2050 | Total transition ^b | 1004 | \simeq | b€ |
| | Cumulative opex | 528 | \simeq | b€ |
| | Cumulative capex | 636 | \simeq | b€ |
| | Salvage value | 160 | -1% | b€ |
| Primary energy mix in 2050 | Total | 368.0 | \simeq | TWh/y |
| | e-hydrogen | 15.6 | \simeq | TWh/y |
| | e-methane | 41.0 | +6% | TWh/y |
| | e-methanol | 54.8 | \simeq | TWh/y |
| | e-ammonia | 40.7 | -10% | TWh/y |
| Electrification in 2050 ^c | System ^d | 63.3 | \simeq | TWh _e |
| | Industrial heat ^e | 12.3 | -7% | TWh _{th} |
| | Decentralised heat ^e | 73.9 | \simeq | TWh _{th} |
| Year of full VRES-deployment | PV | 2045 | 2040 | - |
| | Wind-offshore | 2030 | 2025 | - |
| | Wind-onshore | 2025 | 2025 | - |

^aThese computational times were reached on a 2.4GHz 4-core machine.

^bAs detailed in Equation 1.1, the transition cost is the sum of the cumulative opex and capex, salvage value being deduced.

^cThe electrification of the other sectors (i.e., centralised heat (100%-heat pump), private (100%-BEV), public mobility (80%-train and tramway), freight mobility (25%-train) and non-energy demand (0%)) are identical between the three approaches and are, therefore, not presented in the table.

^dThe electrification of the system is computed as the difference between the total production of electricity and the end-use demand of electricity.

^eThe electrification of the industrial and decentralised heating sectors are expressed in terms of thermal energy (TWh_{th}) provided by electrified processes, respectively industrial resistors and decentralised electric heat pumps.

wind turbines) boosted by the significant salvage value retrieved from investing in the consequent reinforcement of the grid.

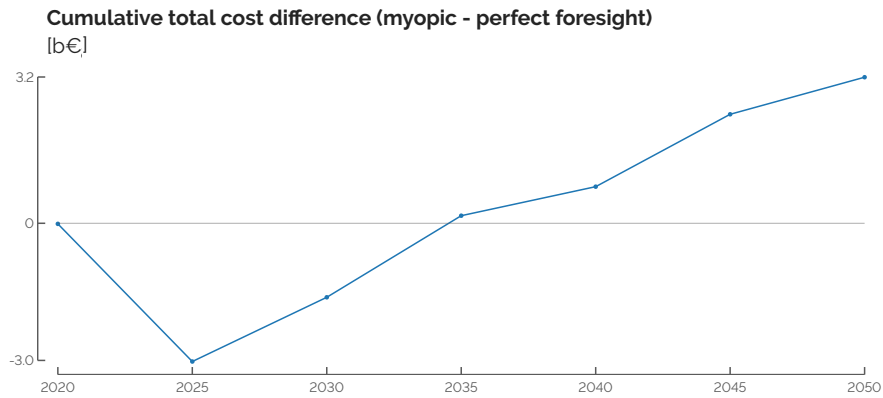


Figure C.8. Cumulative total cost (i.e. opex+capex-salvage value) difference between the myopic and perfect foresight (PF) approaches. Positive values mean that the myopic approach is more expensive than perfect foresight. Early savings of the myopic vision are overcompensated by late investments further on.

Figure C.9 highlights this as infrastructures and the electricity-technologies account respectively for 83.2 and 61.2 b€ in 2030 whereas the overall cumulative investments, so far, are 421.3 b€. The significant lifetime (e.g., 80 years) and investment cost (i.e., 368M€/GW_{VRES} [54]) of the power grid, and, on a smaller scale, the district heating network, explain why the myopic optimisation opts for a higher investment in these infrastructures, at early stages. Similarly to what Keppo and Strubegger [290] observed in their studies, these early investments consequently lead to more investments, later in the transition, to renew technologies that have become too old before 2050: during the phase between 2045 and 2050, the myopic approach needs to invest in 9.2GW of PVs that have been installed 25 years before whereas the perfect foresight, by smoothing its investments over the entire transition, has to renew only 2.5GW of PVs.

In 2050, the capacities installed in the different sectors, in other words the design of the system, are very similar between the two approaches. The passenger and freight mobility sectors are the same and differences smaller than 1GW are observed in other sectors. More interestingly, the myopic optimisation tends to postpone the decommissioning of capacities when the loss of salvage values at the end of an optimisation window would be bigger than the maintenance cost. For instance, in the myopic ap-

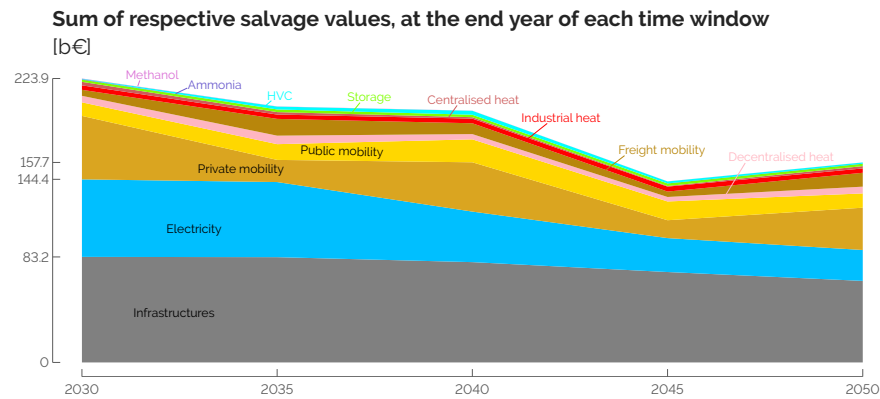


Figure C.9. Sum of the respective salvage values of each sector, per end year of each time window. All together, these salvage values represent 223.9 b€, 53% of the cumulative investment costs in 2030, and 157.7 b€, 24% of the cumulative investment costs in 2050.

proach, 0.8GW of industrial coal boilers will remain installed in 2045 and 2050 or 3.6GW of naphtha-crackers to produce HVC in 2040, whereas these technologies are not used. This could be compare to the “lock-ins” detailed in other studies [64, 290] where technologies installed at early stages of the transition remain in place. However, in our case, keeping in place unused technologies is due to the formulation of the salvage value. Indeed, to maximise the total transition cost, the model prefers recovering part of the salvage value of these assets rather than prematurely decommissioning them.

Highlighted in Figure C.10, the earlier availability of renewable (and intermittent) electricity accelerates the electrification of the other sectors. For instance, in 2035, 3.7GW (+75%) more of industrial electric heaters produce 5.1TWh/year (+130%) of additional industrial heat. In the low-temperature heat sector, decentralised and centralised electric heat pumps capacities are, respectively, 2.2GW (+19%) and 1GW (+8%) higher for each of the representative years between 2030 and 2045, to produce, around 7.8TWh/year (+23%) and 0.8TWh/year (+1%), at the expense of other technologies such as gas heat pumps. Finally, public trains substitute from 2035 a higher share of the CNG-buses.

In general, due to the formulation of the salvage value (see Equation (1.5)), the myopic approach is more techno-oriented as investing more in technologies is beneficial, especially at the early stages of the transition. Therefore, before converging to a simi-

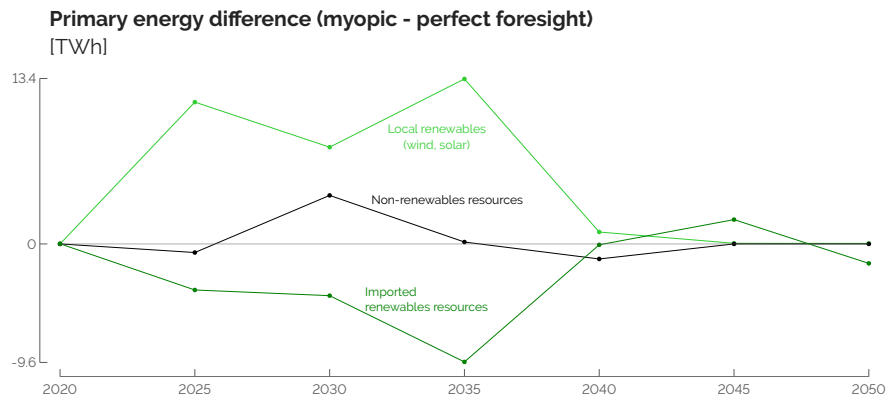


Figure C.10. Difference of primary energy resources between the myopic and perfect foresight (PF) approaches. Positive values mean that the myopic approach is higher than perfect foresight.

lar energy mix in 2050, the myopic system relies more on local renewables (e.g., solar and wind) than on importing renewable energy carriers (e.g., e-ammonia, e-methanol, e-hydrogen or e-methane), see Figure C.10. In parallel, in the near term, the system relies on average slightly more on conventional/non-renewable sources, like observed in other studies [290–292].

C.4 Assessment of different emissions-trajectories

This section compare results of the optimisation subject to different emissions-trajectories with the case where the emissions are constrained to decrease linearly from the level in 2020 to carbon neutrality in 2050. The first comparison is done with the trajectory subject to respect the CO₂ budget prescribed in the RL-based pathway optimisation, i.e., 1.2 Gt_{CO₂,eq} (Section 2.5). Then, to assess the impact of the myopic approach on the optimisation of the transition, it is compared to perfect foresight results, removing the constraint on the emissions-trajectory.

C.4.1 CO₂ budget versus linear decrease of emissions

Figure C.11 shows the yearly emissions attributed to each sector in the REF case (i.e., imposed CO₂ budget) and a case where the CO₂-trajectory is constrained instead. Interestingly, these two transition pathways end up in a similar carbon-neutral whole-energy system in 2050. The two main sectors that significantly reduce their emissions

in the REF case are the production of HVC and the high-temperature heat. In the former, this is linked to the earlier phase-out of oil products through naphtha-cracking. In the latter, it is the use of coal in industrial coal boilers that is phased-out. Overall, ending up to the same level of emissions in 2050, the REF case represents a 60% reduction of the cumulative emissions compared to the linear decrease, for a 7.5% more expensive transition.

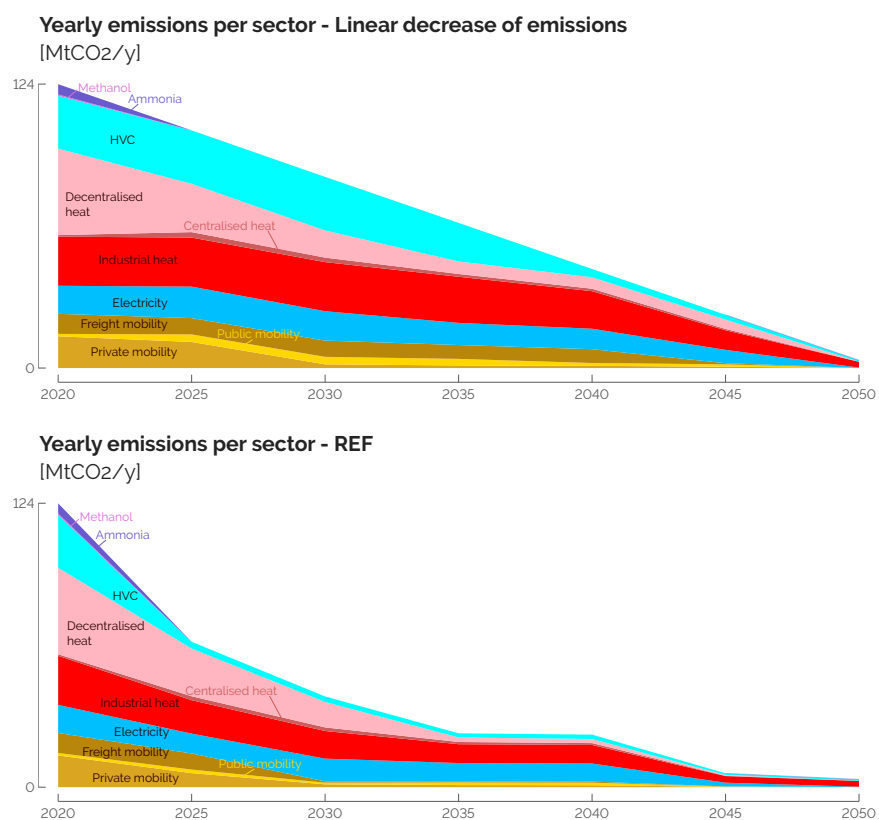


Figure C.11. Respecting the CO₂ budget imposed in the REF case drastically cuts the emissions of the system, especially in the production of High-Value Chemicals (HVC) and the high-temperature heating sector.

C.4.2 Comparison without restriction on GHG

The outcomes of a model could be limited when the case study is too restrictive. Indeed, one could argue that the comparison between myopic, monthly and perfect foresight are very similar as the energy system is strongly constrained in terms of GHG emissions.

In the following, we perform a similar comparison of the transition pathway without restricting the GHG emissions.

Reference case

Figure C.12 illustrates the transition taken by Belgium without restriction on the GHG emissions.

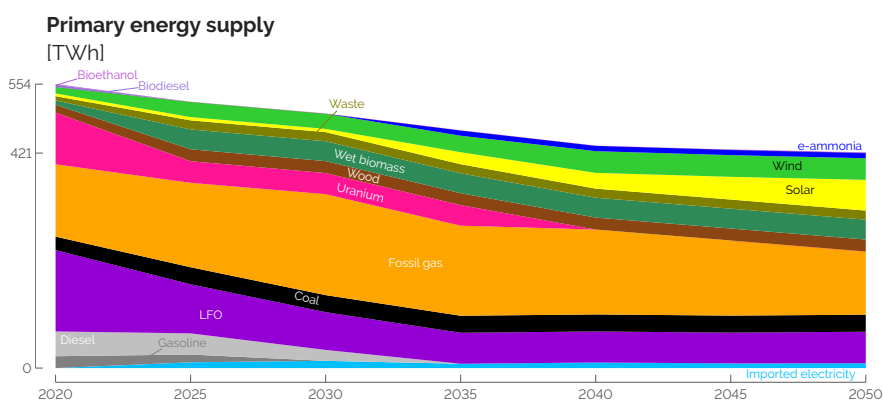


Figure C.12. Primary energy mix of a non-constrained energy transition. In this results, carbon neutrality is not reached in 2050. Some fossil fuels remain used.

Similar trends that for the defossilisation are observed: primary energy mix reduces, renewable energy integration rises and an electro-fuel is imported. However, some changes reflects the cheapest option that the system could utilise such as using as little electrofuels as possible. In this case, only e-ammonia is used for its end use demand.

Instead of analysing the energy system in details, the following paragraphs will investigate if the comparison findings are consistent on a different case study.

Comparison with Myopic approach

Several key messages of the comparison have been summarised in Table C.2. In the following paragraphs, we analyse how these conclusions are affected when the constraint on the GHG-emissions trajectory is removed.

First, considering the overall transition cost, the myopic approach keeps on making limited short-term savings, i.e., down to -0.2%, before ending up with a slightly more expensive transition by 2050, i.e., +0.2%. Similarly to the case with an imposed GHG-emissions trajectory, myopic optimisation invests more, compared to the perfect foresight, at early stages into VRES technologies to benefit from the significant salvage values of the related grid infrastructures. In 2030, the salvage value of the infrastructures and electricity-generation technologies account for 80.2 and 56.2 b€, respectively, whereas the overall CAPEX are 404.8 b€ by then.

Then, in the case with a prescribed GHG-emissions trajectory, the myopic approach invests more by the end of the transition to renew PV installed more massively at early stages and that reached the end of their lifetime before the end of the transition. In the case without this emissions trajectory, there is less urgency/need for integrating renewables in the system. Consequently, in the latter case, there is not such an extra-investment to make to renew too old renewable assets. On top of this, the slower uptake of VRES in the case without emissions trajectory leads to a smaller difference of electrification of the other sectors between the perfect foresight and myopic approaches.

Finally, even though the way to get there differs between the perfect foresight and the myopic approaches, the system designs by 2050 are very similar between these two in most of the sectors. The main observed difference is in the freight transport where diesel boats are preferred to gas boats. This can be looked as a result of the lock-in effect where choices made at early stages, due to the limited foresight, remain in place in the longer term.

In essence, when comparing perfect foresight and myopic approaches, distinctions arise in minor aspects, while the fundamental conclusions of Table C.2 were verified. These variances have been elucidated in the preceding enumerated points and can primarily be attributed to the changes in the case study, rather than reflecting limitations inherent to the model or the comparative analysis itself.

C.5 Monthly versus hourly pathway optimisation

This section compares the perfect foresight optimisation based on a monthly time resolution with the reference case (hourly time resolution). The main advantage of the monthly approach is its computational time, i.e., a reduction of 99.8% compared to the hourly resolution (see Table C.3). This tractability represents a significant advantage

when several thousands of runs are necessary, e.g., for uncertainty quantification as it has been performed in [49].

Table C.3. Comparison between the two different time resolutions: Hourly (PF) and Monthly (MO). Differences with the reference case (PF) below 1% are not shown (\approx) and ones above 10% are in bold.

| | | PF | MO | Units |
|--------------------------------------|---------------------------------|-----------|-------------|-------------------|
| Computational time ^a | | 830 | 2 | s |
| Costs in 2050 | Total transition ^b | 1004 | -2% | b€ |
| | Cumulative opex | 528 | -3% | b€ |
| | Cumulative capex | 636 | -2% | b€ |
| | Salvage value | 160 | -5% | b€ |
| Primary energy mix in 2050 | Total | 368.0 | +2% | TWh/y |
| | e-hydrogen | 15.6 | +2% | TWh/y |
| | e-methane | 41.0 | +51% | TWh/y |
| | e-methanol | 54.8 | \approx | TWh/y |
| | e-ammonia | 40.7 | +55% | TWh/y |
| Electrification in 2050 ^c | System ^d | 63.3 | -27% | TWh _e |
| | Industrial heat ^e | 12.3 | -98% | TWh _{th} |
| | Decentralised heat ^e | 73.9 | -13% | TWh _{th} |
| Year of full VRES-deployment | PV | 2045 | 2040 | - |
| | Wind-offshore | 2030 | 2025 | - |
| | Wind-onshore | 2025 | 2025 | - |

^aThese computational times were reached on a 2.4GHz 4-core machine.

^bAs detailed in Equation 1.1, the transition cost is the sum of the cumulative opex and capex, salvage value being deduced.

^cThe electrification of the other sectors (i.e., centralised heat (100%-heat pump), private (100%-BEV), public mobility (80%-train and tramway), freight mobility (25%-train) and non-energy demand (0%)) are identical between the three approaches and are, therefore, not presented in the table.

^dThe electrification of the system is computed as the difference between the total production of electricity and the end-use demand of electricity.

^eThe electrification of the industrial and decentralised heating sectors are expressed in terms of thermal energy (TWh_{th}) provided by electrified processes, respectively industrial resistors and decentralised electric heat pumps.

However, averaging time series of end-use demands and renewable productions brings some discrepancies. First and foremost, VRES loose their intrinsic power intermittency [268]. This has a series of consequences. Overall, this overestimates the uptake and emergence of solar and wind power generation and, consequently, overestimate their share in the primary electricity mix, especially at intermediate stages of

the transition [268, 293] (see Figure C.13). In line with these studies, the more there is VRES in the primary electricity mix, the higher is the error⁴ with lower time resolution. In 2025 and 2050, where the share of VRES in the electricity primary mix is 46% and 66%, respectively, this error goes from 10% to 18%.

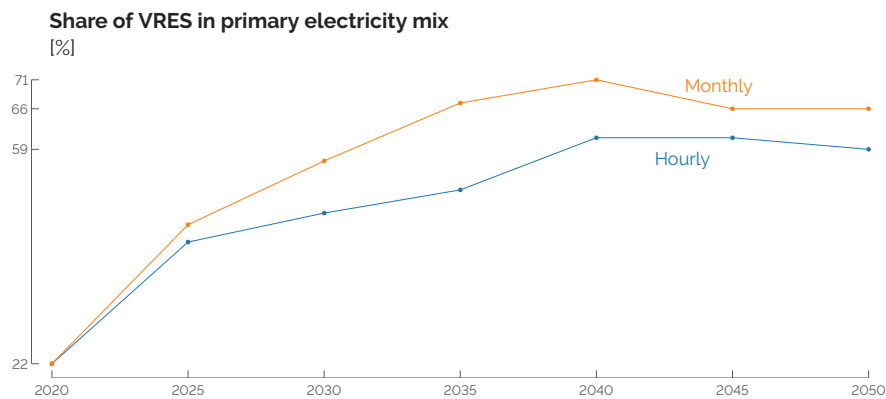


Figure C.13. Share of VRES (i.e., solar and wind) in the electricity primary mix for the monthly and hourly time resolutions.

When considering the system overall, this averaged time-variability requires a more limited sector-coupling in the monthly model to absorb the intermittency of renewables. Industrial and decentralised heat demands are less electrified (see Table C.3). This leads to 30% electrification of the overall system versus 36% for the hourly approach. This smaller production of electricity is done to the detriment of direct import of electricity, completely removed from the primary mix, as assumed to keep on having a higher global warming potential than conventional assets (e.g., CCGT running on gas and, later on, renewable gas and ammonia). Then, the generation mix in heating sectors or non-energy demands is less diversified, leading the sharper and later switch of resources and technologies. For instance, lignocellulosic biomass is “cannibalised” by industrial boilers to the detriment of biomass-to-methanol or HVC. Besides this, in general, we observe an overestimation of conventional technologies (e.g., running on gas or oil) generation, either by installing more capacities or having a higher load factor for similar capacities. In line with Poncelet et al. [293], this leads to an overall underestimation of the operational (and investment) costs (see Table C.3).

⁴Like Poncelet et al. [293], this error is defined as: $\sum_i \frac{|\text{supply share}_i^{MO} - \text{supply share}_i^{PF}|}{2}$, where index i runs over all technologies and import of electricity and the supply shares are expressed as a percentage.

Finally, in the mobility sectors, there is no difference between low and high time resolutions. This is due to the fact that these demands are assumed to stay the same over the different hours of the year (i.e., freight mobility) or have a favorite technology to supply them (e.g., BEV for private mobility).

Appendix D

Pathway optimisation under uncertainties

D.1 Total transition cost

Table D.1 gives the ranking and total Sobol index over the total transition cost of each of the 34 parameters listed in Table 2.2. The first column shows these indicators for the GSA applied on the hourly pathway model. For information, the second column gives the same indicators but for an uncertainty quantification carried out on the monthly pathway model that has some limitations [40] but has the main advantage to run much faster. Given the similar rankings of the parameters between these two, this comparison shows that the monthly model can be a computationally efficient proxy to quantify the uncertainties of the actual hourly model and point out the key parameters on optimisation-driving objective, the total transition cost.

Besides the top-4 parameters, rankings are slightly different. The main difference in terms of ranking relates to the import of electricity from abroad, i.e., its cost of purchasing and its availability. Indeed, as observed by Limpens et al. [40], the monthly model does not require this import given the easier integration of monthly-averaged local VRES. However, this does not jeopardize the comparative analysis given the similar Sobol' indices. Given their wide range of uncertainty [-64.3%; 179.8%] and their significant role to meet the CO₂ budget, the cost of purchasing electrofuels is the first, by far, impacting parameter. Next, comes, naturally, the industrial EUD, representing, at the nominal value, 60% of the total demands by 2050. The top-3 is completed by the variation of the discount rate, directly impacting the annualisation and the salvage values of the assets. Finally, since the current Belgian whole-energy system deeply

relies on fossil resources, and would still do in the near future, the cost of purchasing fossil fuels is part of the impacting parameters. On the contrary, due to the very low annualised, cost, long lifetime leading to a significant salvage value and a low-emitting fuel, the parameters related to SMR barely impact the total transition cost.

Table D.1. Total Sobol' indices of the uncertain parameters over the total transition cost in the hourly and monthly (see Appendix C.5) pathway models. The similar rankings (and indices) show the validity of using the faster (even though less accurate) monthly model to assess uncertainties.

| Parameter | Ranking (Sobol' index) | |
|---------------------------------------|------------------------|---------------|
| | Hourly model | Monthly model |
| Purchase electrofuels | 1 (46.8%) | 1 (47.4%) |
| Industry EUD | 2 (23.2%) | 2 (23.5%) |
| Discount rate | 3 (12.0%) | 3 (11.0%) |
| Purchase fossil fuels | 4 (5.7%) | 4 (6.9%) |
| Variable OPEX of technologies | 5 (3.1%) | 5 (2.9%) |
| Purchase biofuels | 6 (2.6%) | 6 (2.6%) |
| CAPEX electric motor | 7 (2.1%) | 8 (1.9%) |
| Purchase electricity | 8 (1.5%) | 34 (<0.1%) |
| Hourly load factor wind turbines | 9 (1.1%) | 9 (1.3%) |
| Hourly load factor PV | 10 (1.1%) | 7 (1.9%) |
| Potential capacity SMR | 11 (0.9%) | 11 (0.9%) |
| CAPEX car | 12 (0.8%) | 13 (0.7%) |
| Available local biomass | 13 (0.7%) | 12 (0.8%) |
| Passenger mobility EUD | 14 (0.7%) | 14 (0.7%) |
| Modal share change LT-heat | 15 (0.5%) | 15 (0.5%) |
| Max capacity PV | 16 (0.5%) | 10 (1.1%) |
| Households EUD | 17 (0.5%) | 16 (0.5%) |
| Services EUD | 18 (0.5%) | 17 (0.4%) |
| Max share of public transport | 19 (0.3%) | 19 (0.3%) |
| Max capacity onshore wind | 20 (0.3%) | 18 (0.3%) |
| CAPEX PV | 21 (0.2%) | 20 (0.2%) |
| Efficiency electric motor | 22 (0.2%) | 22 (0.1%) |
| Max capacity offshore wind | 23 (0.2%) | 21 (0.2%) |
| Available electricity import | 24 (0.1%) | 33 (<0.1%) |
| CAPEX ICE | 25 (0.1%) | 24 (0.1%) |
| CAPEX fuel cell engine | 26 (0.1%) | 23 (0.1%) |
| Efficiency fuel cell engine | 27 (0.1%) | 25 (<0.1%) |
| Modal share change freight mobility | 28 (0.1%) | 26 (<0.1%) |
| Modal share change passenger mobility | 29 (<0.1%) | 27 (<0.1%) |
| CAPEX grid reinforcement | 30 (<0.1%) | 30 (<0.1%) |
| CAPEX efficiency measures | 31 (<0.1%) | 28 (<0.1%) |
| CAPEX bus | 32 (<0.1%) | 29 (<0.1%) |
| CAPEX SMR | 33 (<0.1%) | 32 (<0.1%) |
| CAPEX power grid | 34 (<0.1%) | 31 (<0.1%) |

D.2 Imported renewable electrofuels

Table D.2. Comparison of the quantities of imported renewable electrofuels, in TWh, between the REF case, the SMR case and the statistical features from the GSA (i.e., Q1, median and Q3). 2020 is not in the table as, per assumption, no renewable electrofuel is imported for this year. For the sake of clarity, zeroes are replaced by “-”.

| Year | Case | e-methane | e-hydrogen | e-ammonia | e-methanol |
|------|--------|-----------|------------|-----------|------------|
| 2025 | REF | - | - | 10 | 52 |
| | SMR | - | - | 10 | 29 |
| | Q1 | - | - | 9 | 2 |
| | Median | - | - | 10 | 47 |
| 2030 | Q3 | - | - | 11 | 55 |
| | REF | - | 1 | 10 | 52 |
| | SMR | - | 1 | 10 | 52 |
| | Q1 | - | - | 9 | 43 |
| 2035 | Median | - | - | 10 | 50 |
| | Q3 | - | 1 | 12 | 57 |
| | REF | - | 17 | 10 | 53 |
| | SMR | - | 17 | 10 | 53 |
| 2040 | Q1 | - | - | 9 | 42 |
| | Median | - | 5 | 11 | 51 |
| | Q3 | - | 16 | 33 | 58 |
| | REF | - | 16 | 23 | 54 |
| 2045 | SMR | - | 16 | 10 | 54 |
| | Q1 | - | - | 10 | 41 |
| | Median | - | 12 | 26 | 51 |
| | Q3 | 8 | 16 | 68 | 60 |
| 2050 | REF | 40 | 16 | 42 | 54 |
| | SMR | - | 16 | 11 | 54 |
| | Q1 | - | - | 12 | 42 |
| | Median | - | 12 | 37 | 52 |
| 2050 | Q3 | 35 | 17 | 71 | 60 |
| | REF | 39 | 16 | 44 | 55 |
| | SMR | 7 | 16 | 11 | 55 |
| | Q1 | - | - | 11 | 43 |
| 2050 | Median | 1 | 13 | 31 | 53 |
| | Q3 | 36 | 17 | 66 | 61 |

Figures D.1, D.2, D.3 and D.4 give the distribution of the different routes of supply and consumption of methane, hydrogen, ammonia and methanol, resulting from the 1260 samples of the GSA.

Given its lower cost of purchasing than its renewable equivalent (Figure 2.3) and lower GWP than other fossil fuels (i.e., $gwp_{op,NG} = 0.27 \text{ kt}_{\text{CO}_2,\text{eq}}/\text{GWh}$ versus $gwp_{op,LFO} = 0.31 \text{ kt}_{\text{CO}_2,\text{eq}}/\text{GWh}$ or $gwp_{op,coal} = 0.40 \text{ kt}_{\text{CO}_2,\text{eq}}/\text{GWh}$), fossil NG remains the main source of gas in the system until 2040. Besides bio-hydrolysis as the main consumer of wet biomass to consistently produce gas, e-methane eventually substitutes fossil natural gas by 2045-2050 in order to respect the CO₂ budget for the transition. As a versatile energy carrier, gas is used by a wide variety of technologies in the different sectors. Initially, in 2020, decentralised gas boilers, CCGT and industrial gas boilers represent the biggest consumers of gas with 39%, 21% and 16% of the total consumption, respectively. Progressively, in line with the rest of the system shifting towards more efficiency in the mid-term, industrial CHP represent the lion's share, next to other usages in the transport or LT-heating sectors.

On the contrary, import of fossil-based hydrogen, largely produced from steam-methane-reforming [294], is rarely part of the solution due to the emissions related to the consumption of natural gas. E-hydrogen is the consistent source of hydrogen in the system, next to local production (i.e., steam-methane-reforming, electrolysis or ammonia-cracking) in some rare cases where low industrial EUD coincides with more abundant electricity from SMR or PV. In terms of consumption, FC-trucks are the more consistent player. FC-cars are also at stake but in specific cases where their CAPEX and the CAPEX of electric vehicles are in the bottom and the top of their respective uncertainty ranges.

Becoming cheaper than its fossil equivalent at early stages of the transition (i.e., from 2030 onward), e-ammonia is the exclusive stream of ammonia in the system, except rare cases. Then, on top of its consistent NED, the largest consumption of ammonia is CCGT as flexible power generation units, to substitute their e-methane equivalents that have a higher LCOE (see Figure 2.4).

Similarly to ammonia, on top of local production in rare cases, e-methanol is the key source for methanol. Besides its own NED, methanol is mostly consumed to produce HVC via the MTO process instead of naphtha-cracking, in order to respect to CO₂ budget for the transition.

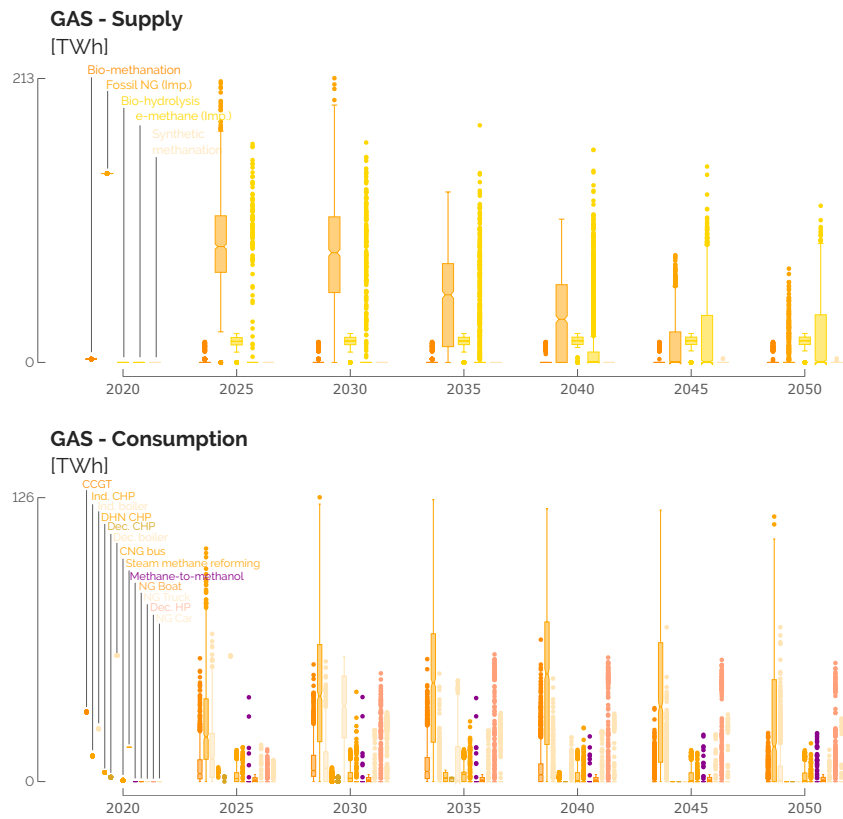


Figure D.1. Distribution of the different streams of supply (top) and consumption (bottom) of methane from the Global Sensitivity Analysis (GSA).

D.3 Installed capacities

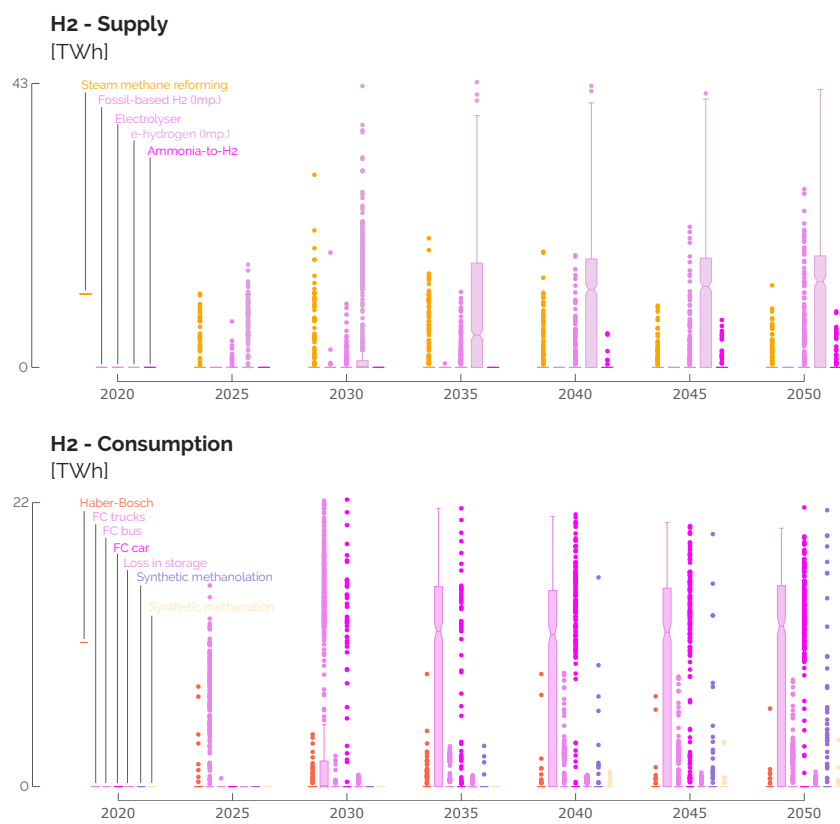


Figure D.2. Distribution of the different streams of supply (top) and consumption (bottom) of hydrogen from the Global Sensitivity Analysis (GSA).

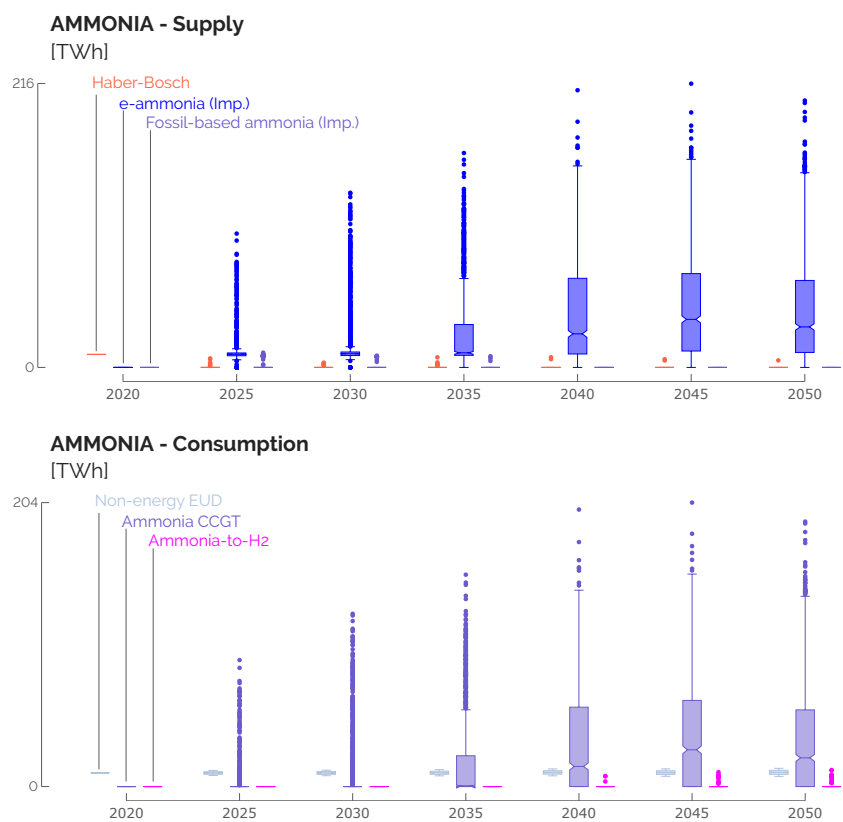


Figure D.3. Distribution of the different streams of supply (top) and consumption (bottom) of ammonia from the Global Sensitivity Analysis (GSA).

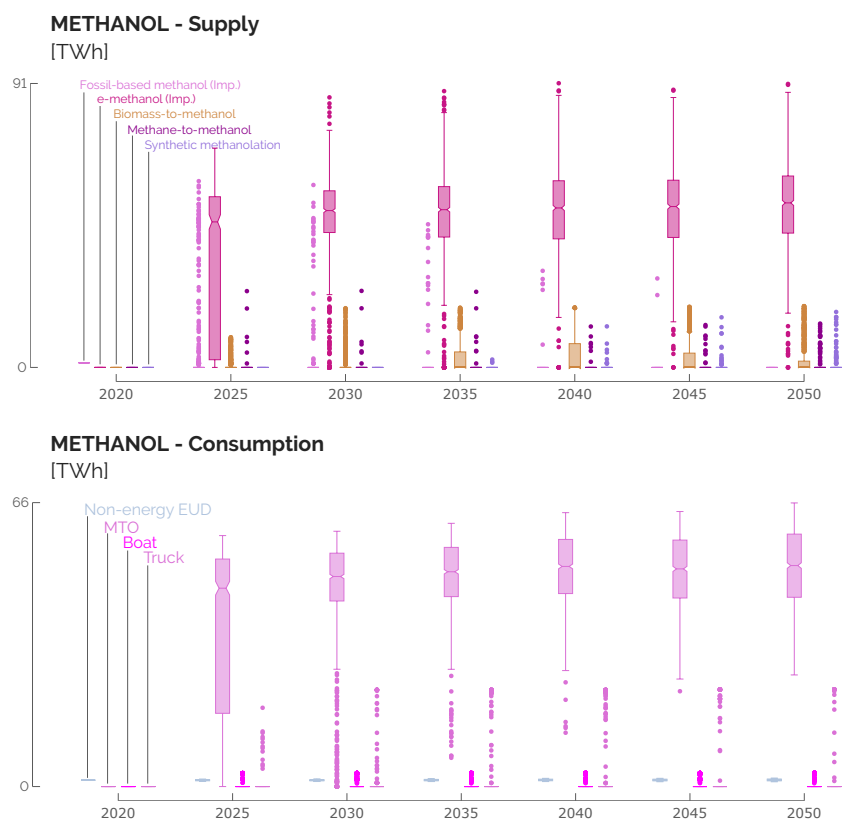


Figure D.4. Distribution of the different streams of supply (top) and consumption (bottom) of methanol from the Global Sensitivity Analysis (GSA).

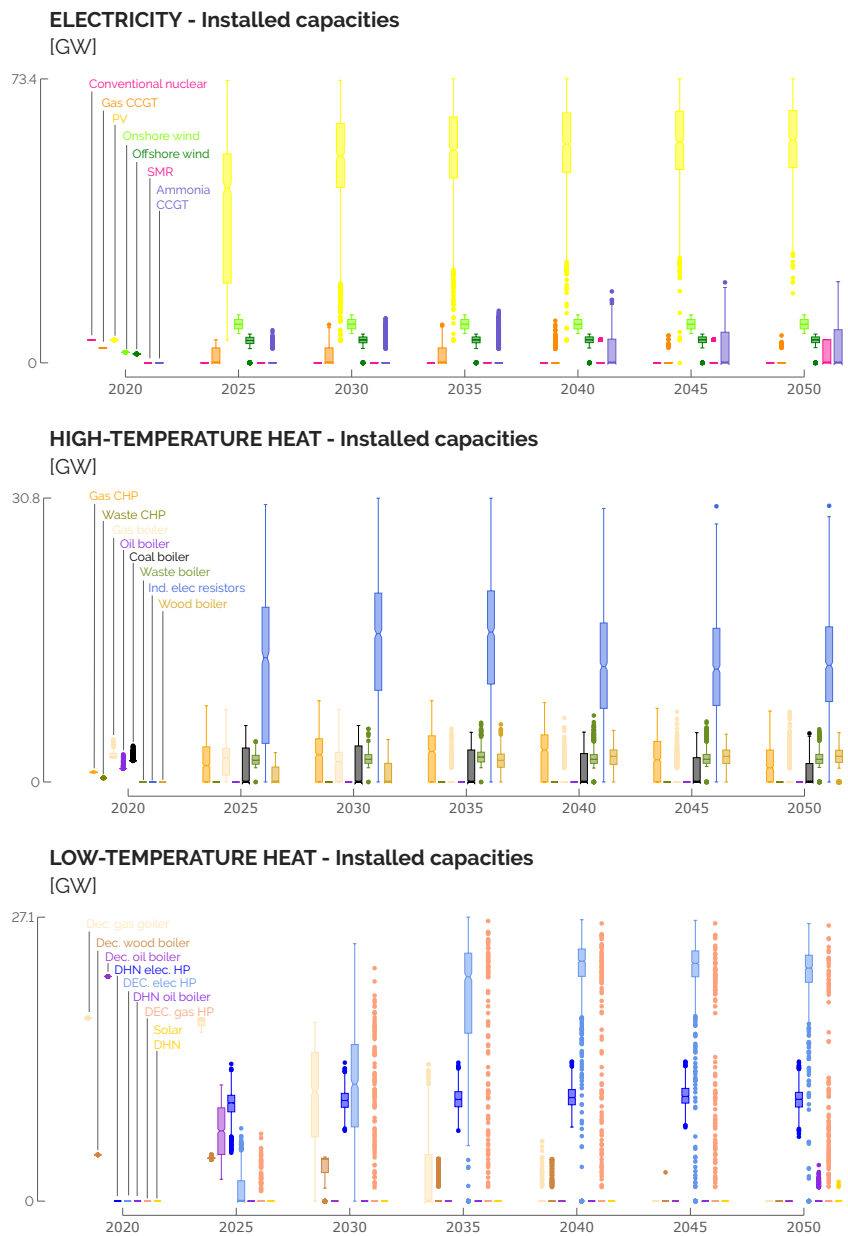


Figure D.5. Distribution of the installed capacities among the end-use sectors of electricity, HT and LT heat from the Global Sensitivity Analysis (GSA).

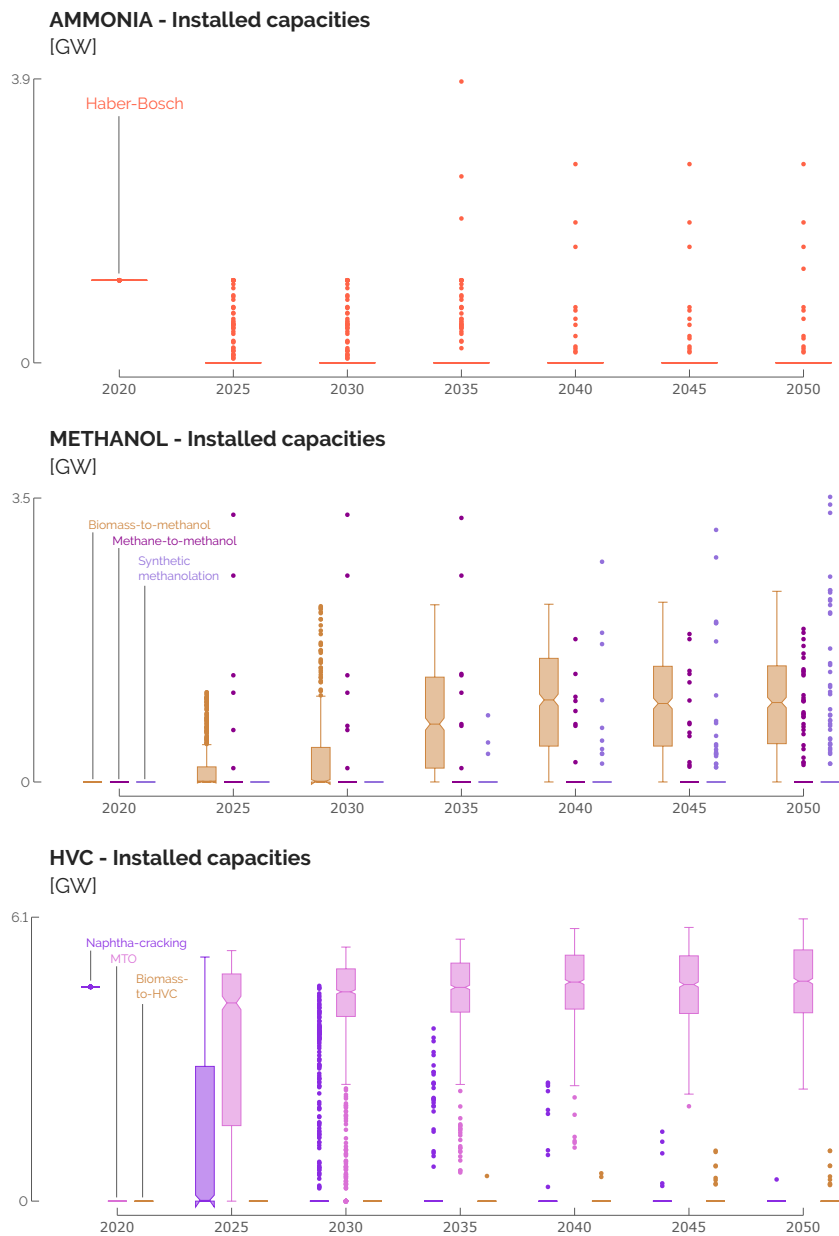


Figure D.6. Distribution of the installed capacities among the end-use sectors of ammonia, methanol and HVC from the Global Sensitivity Analysis (GSA).

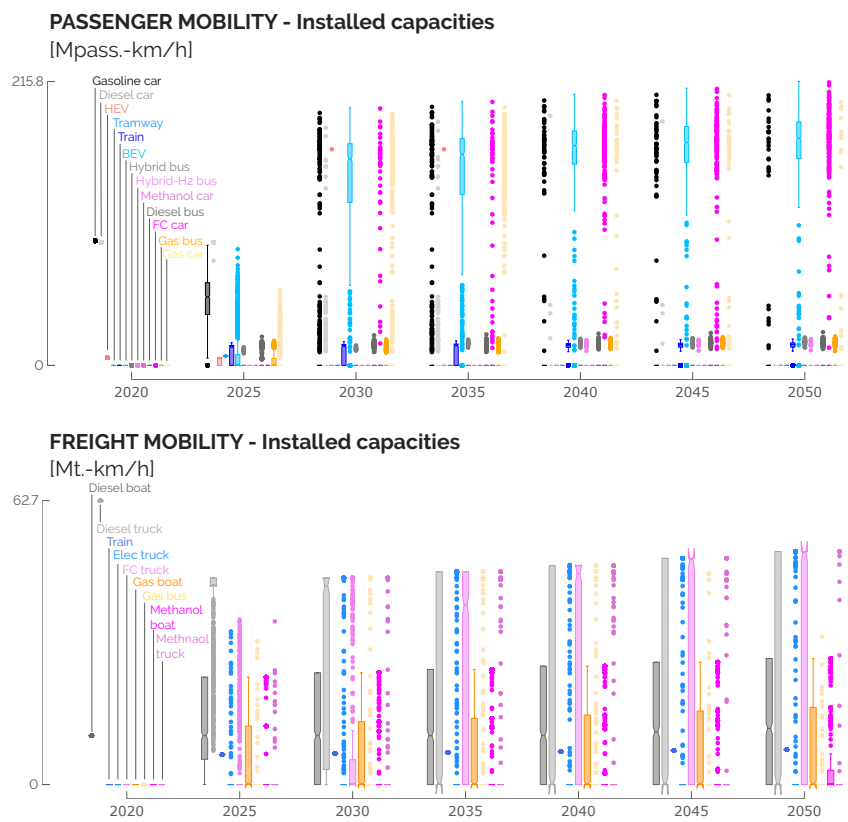


Figure D.7. Distribution of the installed capacities among the end-use sectors of passenger and freight mobility from the Global Sensitivity Analysis (GSA).

Appendix E

Reinforcement Learning on hourly and monthly models

The Reinforcement Learning (RL)-based exploration of myopic transition pathways can require thousands of runs to converge. To reduce the computational burden and maximise this exploration, the learning phase of the agent could start on the monthly model before being refined on the one with an hourly time resolution, the so-called transfer learning [185]. Even though averaging time series of end-use demands and renewable productions brings some discrepancies (i.e., faster emergence of local VRES and smaller electrification of the system), the main advantage of the monthly approach is its computational time, i.e., couple of seconds versus 15 min for the hourly model (see Appendix C.5). This section aims at comparing results from the learning process on the monthly model with the one on the hourly model. The monthly learning has been carried out by applying the same rules (see Section 4.1). The purpose is to assess the capacity of the monthly model to be a good proxy of the hourly myopic transitions.

Considering the actions taken by the agent and their binding effect on the environment with a monthly resolution, we see similar trends as in the hourly model (see Figure E.1). Limiting the consumption of coal is always binding where LFO is “naturally” removed from the mix by the cost-minimisation. Where limiting the consumption of fossil gas has a major impact at the early stages, limiting the system emissions up to carbon neutrality becomes more crucial at the end of the transition.

Besides the sharper decrease of emissions early in the transition, the monthly myopic pathways fit with the trend provided by RL optimisation on the hourly model. The difference in the early drop of emissions between the monthly and hourly models comes

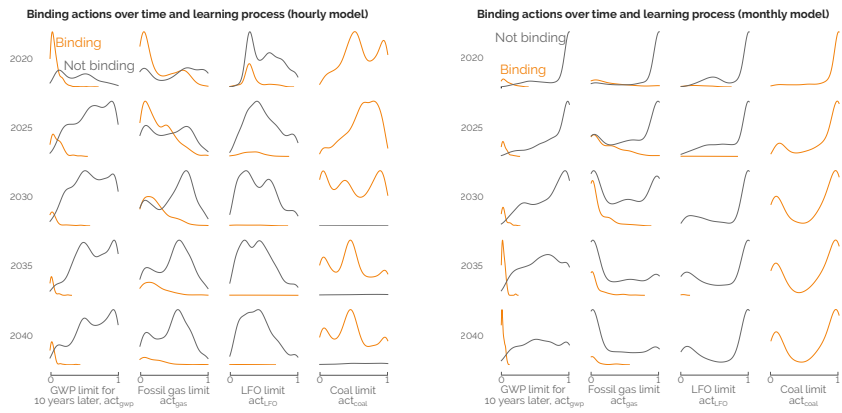


Figure E.1. Binding versus non-binding constraints on the hourly and monthly models: distribution of occurrences. When the agent learns on the monthly model, the actions are binding in the similar timing and similar ranges as when learning on the hourly model.

from the easier integration of local VRES as the hourly intermittency is averaged over a month (see Appendix C.5).

Even more than for the emissions, the monthly model is a good proxy to assess the pathways of annual system cost as well as cumulative costs such as CAPEX, OPEX and salvage value by 2050 (see Figures E.2 and E.3).

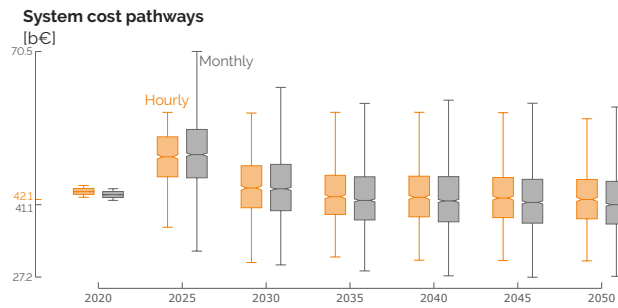


Figure E.2. Comparison of annual system cost pathways from the RL-based myopic optimisation on the hourly and monthly models.

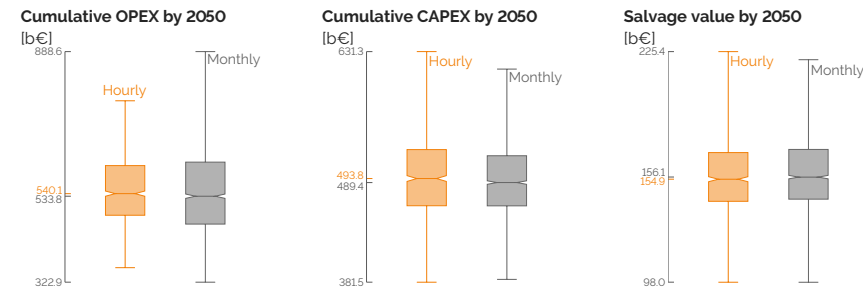


Figure E.3. Comparison of cumulative OPEX (left), CAPEX (right) and salvage value (right) in 2050 from the RL-based myopic optimisation on the hourly and monthly models.

The monthly model also captures the need to import more electrofuels by 2050 in the myopic transitions (see Figure E.4). The other main difference concerns the import of electricity from neighbouring countries. As detailed in Appendix C.5, this comes from the averaging of the hourly times series of VRES that can provide electricity in a more constant way.

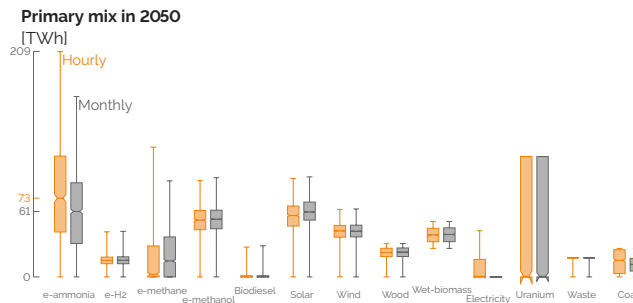


Figure E.4. Comparison of the primary energy mix in 2050 from the RL-based myopic optimisation on the hourly and monthly models. To a lesser extent that the hourly model, the monthly optimisation also captures the need to import more electrofuels when the foresight is limited.

In conclusion, with the advantage of the smaller computational burden, the monthly model myopic model is found to be a good proxy with its equivalent based on hourly time resolution.